2007

Experimental methodology for measuring combustion and injector coupled responses

Ryan C. Cavitt

EXPERIMENTAL METHODOLOGY FOR MEASURING COMBUSTION AND INJECTOR COUPLED RESPONSES

by

RYAN C. CAVITT

A THESIS

Submitted in partial fulfillment of the requirements
for the degree of Master of Science in Engineering
in
The Department of Mechanical and Aerospace Engineering
to
The School of Graduate Studies
of
The University of Alabama in Huntsville

HUNTSVILLE, ALABAMA

2007

In presenting this thesis in partial fulfillment of the requirements for a master's degree from The University of Alabama in Huntsville, I agree that the Library of this University shall make it freely available for inspection. I further agree that permission for extensive copying for scholarly purposes may be granted by my advisor or, in his/her absence, by the Chair of the Department or the Dean of the School of Graduate Studies. It is also understood that due recognition shall be given to me and to The University of Alabama in Huntsville in any scholarly use which may be made of any material in this thesis.

(student signature: Ryan C. Cavitt) 5/22/07 (date)

THESIS APPROVAL FORM

Submitted by Ryan C. Cavitt in the partial fulfillment of the requirements for the degree of Master of Science in Engineering in Mechanical Engineering and accepted on behalf of the Faculty of the School of Graduate Studies by the thesis committee.

We, the undersigned members of the Graduate Faculty of The University of Alabama in Huntsville, certify that we have advised and/or supervised the candidate of the work described in this thesis. We further certify that we have reviewed the thesis manuscript and approve it in partial fulfillment of the requirements for the degree of Master of Science in Engineering in Mechanical Engineering.

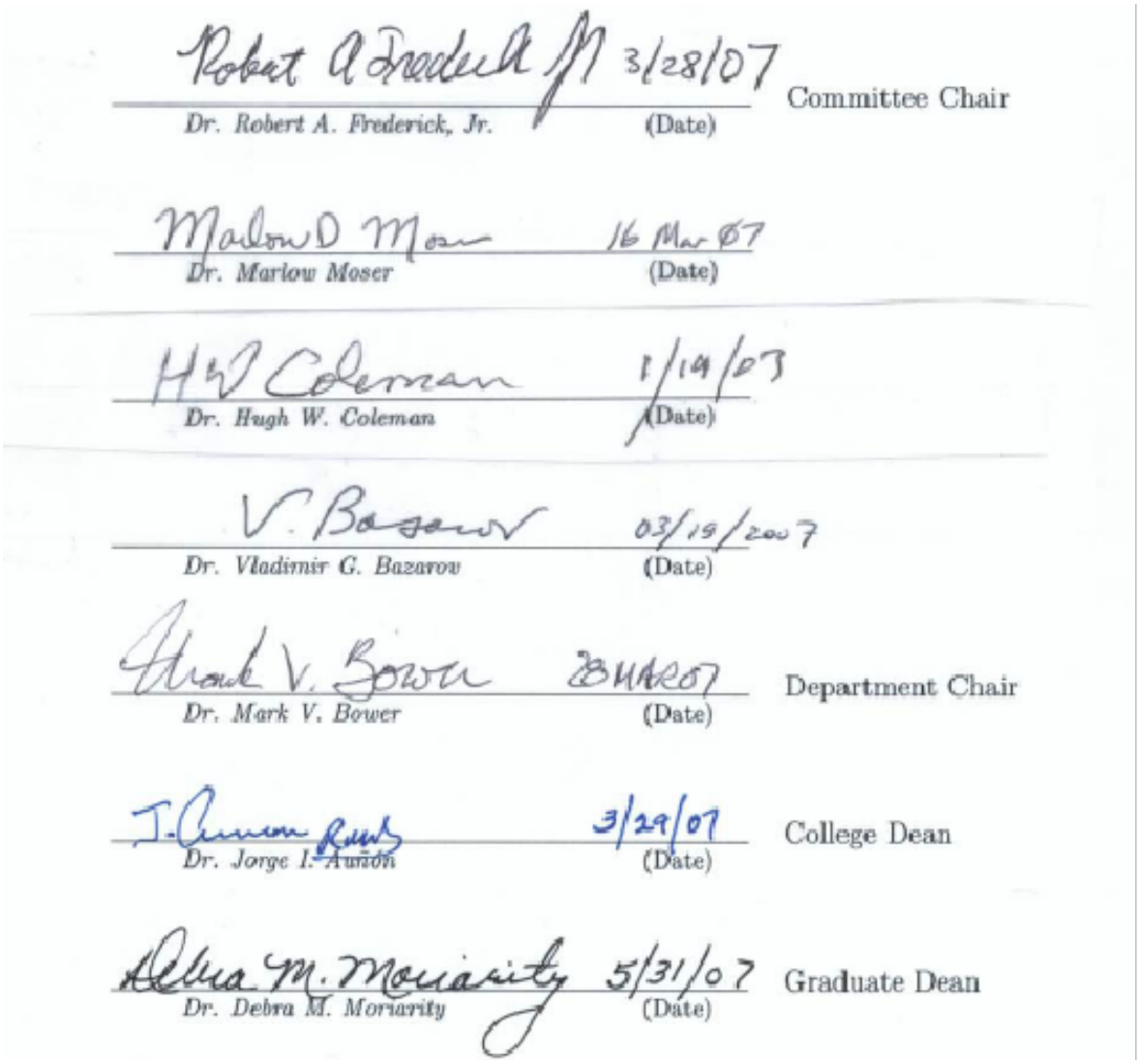

ABSTRACT

School of Graduate Studies
The University of Alabama in Huntsville

Degree Master of Science in Engineering College/Dept. Engineering/Mechanical and Aerospace Engineering

Name of Candidate Ryan C. Cavitt

Title Experimental Methodology for Measuring Combustion and Injector Coupled Responses

The objective of this research was to design, build and test a laboratory scale liquid propellant rocket injector stability characterization test facility. The design of the experiment is based on a Russian scaling methodology that employs gaseous propellants to simulate supercritical full scale propellants at atmospheric pressures. The preliminary objective of the experimentation was to determine if the methodology was capable of creating high frequency combustion instability. The maximum fundamental mode pressure fluctuations were 17 % peak to peak of the mean chamber pressure. Russian pentad impinging jet injectors with impingement angles of thirty, forty-five, or sixty degrees showed significantly different combustion stability characteristics using this methodology. The studies were run with gaseous methane and gaseous oxygen as the propellants. The excited modes of instability were the first radial mode and a combined mode of the first radial and second tangential modes.

Abstract Approval: Committee Chair

Department Chair

Graduate Dean

ACKNOWLEDGMENTS

This work was made possible through NASA CUIP funding. I would like to thank my advisor, Dr. Robert Frederick, for his guidance on the project as well as for teaching me about developmental foresight and management. I would also like to thank Dr. Clark Hawk for hiring me as a graduate research assistant at the Propulsion Research Center.

I would also like to acknowledge my committee for their individual expertise; Dr. Marlow Moser, for rocket test stand assistance, and to Dr. Hugh Coleman, for his uncertainty analysis aid. I would like to express my deep gratitude to Dr. Vladimir Bazarov for the endless injector wisdom and inspiring me to apply creativity in engineering design.

I would also like to thank Royal Ritchey for the prompt and precise fabrication of all the custom hardware as well as for teaching me practical design specifications. Additional thanks to Erik Lee for facing the unknown DIAdem, and conquering as well as to Tony Hall, JRC Facility Engineer, for answering my endless questions.

Most of all, I would like to thank my beautiful bride, Keri, for all of her support while I was facing seemingly insurmountable research challenges and understanding endless work nights. Also to all of my family, especially my mother for her encouragement and support since before kindergarten as well as my brother for his support and edits. Last, but certainly not least, to the Bearcats who were always able to make me forget about any work related problems.

TABLE OF CONTENTS

LIST OF FIGURES

LIST OF TABLES

LIST OF SYMBOLS

SYMBOL	DEFINITION
A	Area
a_{mn}	Transverse Bessel Function Zero
c*	Characteristic Velocity
τ	Characteristic Delay
ρ	Density
d	Diameter
Φ	Equivalence Ratio
f	Frequency
df	Frequency Increment
L	Length
Q	Longitudinal Bessel Function Zero
$\dot{m}$	Mass Flow Rate
MW	Molecular Weight
η_{peak}	Percentage of Power Above Threshold
Ω	Phase
η	Power Density

Π	Power Density Above Threshold
P	Pressure
γ	Ration of Specific Heats
c	Speed of Sound
$R\#$	Universal Gas Constant
v	Velocity
$\dot{Q}$	Volumetric Flow Rate

Subscripts

air	Air
c	Chamber
$sector$	Chamber Sector
$prod$	Combustion Product
d	Discharge
full scale	Full Scale Condition
inj	Injector
model	Sub Scale Condition

Superscripts

$'$	Dynamic

To Keri Sue

One test result is worth one thousand expert opinions.

—Werner von Braun

CHAPTER 1

INTRODUCTION

1.1 Problem Formulation

High frequency combustion instability continues to hinder the development of liquid rocket engines. The phenomenon is characterized by pressure fluctuations at distinct frequencies in a combustion vessel. These chamber pressure oscillations result from a coupling of the combustion process and the fluid dynamics [1]. In particular, it can occur when the acoustic characteristics of the hardware (chamber, injector, feed lines, turbine, etc.) are on the same order of magnitude as the combustion process. This temporal similarity allows the oscillations to grow rapidly if they are in phase. The observable signs of high frequency combustion instability are regular, high amplitude chamber pressure pulsations, increase in heat release and oscillations in manifold pressure. These factors occurring simultaneously creates an extremely dangerous condition. The increased heat transfer can melt or decrease the mechanical strength of materials while the forces acting on the hardware are increased. The most common damage from combustion instability is fire face erosion. In extreme cases, chamber pressure oscillations can lead to catastrophic hardware failure. This destructive phenomenon can appear and destroy an engine in fractions of a second [2].

A higher-order problem is trajectory control. An unstable engine will produce thrust variations, which can impede proper vehicle attitude control.

There are two main branches of high frequency combustion instability: intrinsic and injection coupled. Intrinsic instability refers to the the phenomena being directly coupled to the subprocesses between injector discharge and combustion. Injector coupled instability is directly linked to the injector acoustics. Specifically, the combustion is unstable due to mass flow rate variations in response to the pressure drop fluctuations that the injector experiences [3].

1.2 Historical Background

Combustion instability was first discovered in the late 1930s [4]. Until combustion instability manifested itself as audible noise in a test situation, researchers struggled to find the reason for failures without specialized instrumentation. In all likelihood, combustion instability has been around just as long as chemical rocket propulsion.

Rocket failures were common during development in the 1950s. Toward the end of the decade, combustion instability had already been split into the present day categories: low frequency (chug), intermediate (buzz), and high frequency (screech) [5]. To better understand these phenomena, theories were developed by such famous scientists as Penner [6,7] and Crocco [8]. Experimental investigations were also taking place to verify analytical theories. Advances such as combustor windows, developed at the National Advisory Committee for Aeronautics Lewis Research Center, allowed the first experimental evaluation of combined modes of combustion instability. Through

the years high frequency transducers, continuously variable length chambers, and 2D combustion chambers aided in the understanding of the combustion process. During the 1960s, the development of large thrust engines was underway. These engines were more susceptible to instability than the smaller engines of the past. Passive and active methods of suppression were implemented to reduce the pressure oscillations and are described in Section 1.3. One of the most influential engine components, with respect to stability, was found to be the injector. Injector design was highlighted as a crucial component in the design process through the development of the F-1 engine and was the key to stability in the final design.

Development of the F-1 engine occurred from the mid 1950s to the early 1970s. This engine was developed to meet the heavy launch requirements of the Apollo program. Five F-1 engines make up the first stage of the Saturn V launch vehicle. The engine is a gas generator cycle with liquid oxygen (LOX) and Rocket Propellant 1 (RP-1) as the propellants. The final design of the engine boasts an impressive sea level thrust and specific impulse of $1,522,000\,lbf$ and 265.4 seconds, respectively [9]. Presently, this engine provides the greatest thrust of any single chamber engine.

Oefelein and Yang [9] have compiled a thorough description of the F-1 development with respect to combustion instability. At the onset of development, the injector design was adapted from the E-1 Air Force engine. Between January 1959 and May 1960, forty-four full scale tests were run. Twenty of the forty four tests resulted in spontaneous instabilities with amplitudes greater than 100 % of the mean chamber pressure. In response to this problem, a committee was formed to develop

new injector designs. Focus was set on the injector due to the confidence of chamber and nozzle geometry performance characteristics. Some of these injectors were more successful, but others exhibited oscillation amplitudes exceeding 400 % of mean chamber pressure. In all cases, the first tangential mode of instability was present near 500 Hz. High frequency combustion instability had shown that it was a formidable opponent.

Full scale testing between October 1962 and June 1963 led to the development of the preliminary flight rating test (PFRT) injector configuration which utilized an impinging doublet for the RP-1 and an impinging triplet for the LOX. These tests were successful in improving jet displacement sensitivity and eliminating injection coupling, which drove the spontaneous onset of high frequency combustion instability. However, these improvements in stability came at the expense of decreased performance. Hydraulic modification kits were implemented into the manifold system which, in turn, added engine weight. The impinging jet sensitivity was improved by moving the combustion zone farther from the injector face, resulting in decreased combustion efficiency. During this design period, multiple passive suppression devices such as chamber divergent rings, manifold flow diverters and isolation tabs were essential to achieve dynamic stability.

With a PFRT injector configuration established, full scale testing between June 1963 and January 1965 aimed to further improve stability as well as engine performance. Multiple injector impingement angles and orifice diameters were tested and optimized. The problem of resurging oscillation was suppressed by decreasing the fuel film cooling flow by a factor of two. This modification was unique in that it

increased performance and stability simultaneously. By June 1964, the flight rating test injector was selected. The full scale tests conducted in the following years further optimized the stability and performance to the impressive flight qualification injector.

As depicted by the F-1 development engine history, the injector plays a principal role in engine stability. The initial design was wildly unstable in contrast to the final design which could suppress a 100 % chamber pressure oscillation in 13 milliseconds . The development of the engine, which spanned across three decades, called for over two thousand full scale tests to overcome instability. This is a crucial example which demonstrates that an initial injector design which provides stable operation will save excessive time and resources in the development and qualification of a liquid rocket engine.

1.3 Common Solutions

Significant progress has been achieved in improving engine stability utilizing both experimental and numerical results. Although the whole picture eludes researchers, many trends have been identified in order to design stable engines. The common methods to deal with instability can be categorized into three groups: passive control, active control, and design modifications.

Passive control commonly employs geometric barriers or voids in the combustion chamber. The most generic form of passive control is the baffle. A baffle is a protrusion from the injector face which breaks up the initial volume near the injector. The baffle is broken into compartments to section the chamber volume. In most

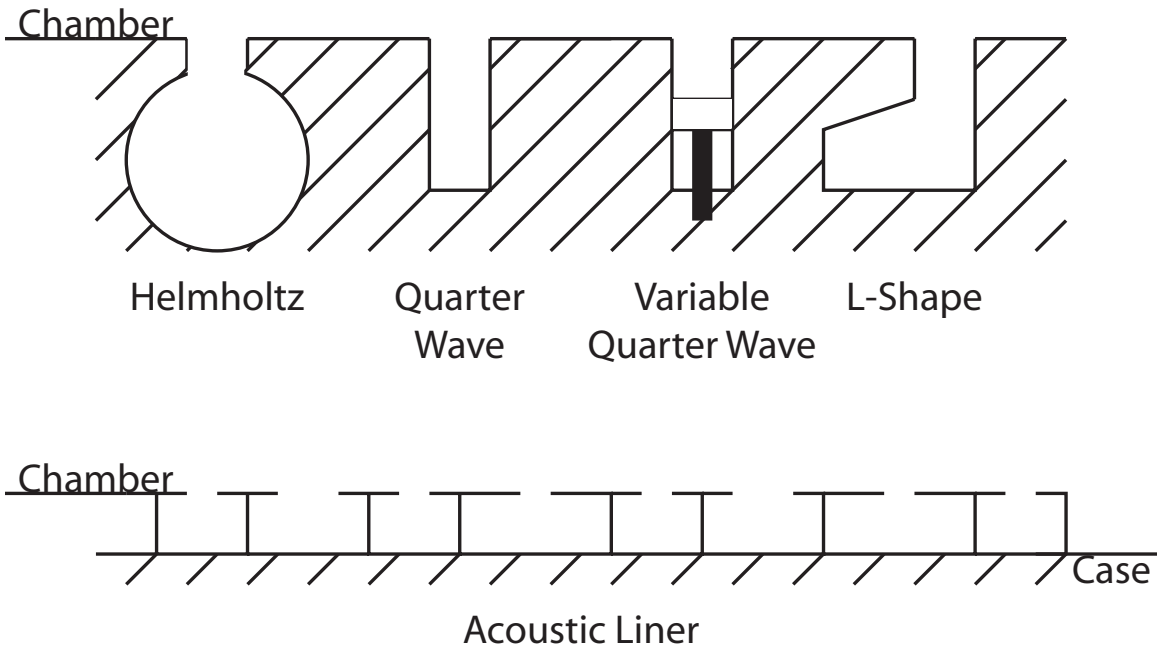

Figure 1.1: Common Acoustic Cavities

modern engines, the number of compartments is odd in order to avoid placing the protrusions at nodes, which would enhance standing modes of instability [10].

Another way to passively dampen instabilities is through the use of acoustic absorption cavities. A graphic depiction of some commonly used acoustic cavities can be seen in Figure 1.1. The most popular cavity is the Helmholtz resonator. This resonator is a cavity commonly placed near the chamber wall on the injector face. This placement is ideal since it is at the antinode of all acoustic modes as well as being convenient for fabrication. Quarter wave resonators are also used with some regularity. The purpose for designing cavities into a combustion chamber is that the resonators can be tuned to absorb certain frequencies. An experienced rocket designer would be familiar with which modes of instability are most likely to appear. The frequencies of the modes are then calculated and the resonators are designed to

absorb those natural frequencies. Baffles are almost always employed in an initial design and resonators are also quite common. A recent numerical analysis has shown that of the mentioned passive suppression devices, the Helmholtz resonator with rounded corners is the most effective absorber [11].

Active control is a much more difficult means of instability suppression. Historically, this approach has been limited to the research field. Active control works on the principle of destructive interference. The general scheme is to sense the pressure fluctuations in the combustion chamber and impose an anti-signal to cancel the fluctuation. To accomplish this, a feedback loop is required between the sensing instrument and the reaction forcing instrument. Usually, the feedback loop is a mathematical transfer function applying fuzzy logic control. A research team at the Georgia Institute of Technology performs extensive work on this field of control. Within the research team, a working model has been developed. The model is a small chemical thruster which can be throttled unstable and returned to stable operation via the control system which applies an anti-pressure signal [12]. This is a promising option, but power requirements would be tremendous on a real engine. Since small engines do not typically experience high frequency combustion instability, this specific control method does not have any direct applications at this time.

The previously described methods of instability suppression focus on counteracting unstable chamber pressure waves. Design modifications aim for the proper engine component design to avoid the appearance of combustion instability altogether. For low frequency combustion instability, it is customary to design the pressure drop across the injector at or above 10 % of the chamber pressure or increase damping in

the feed lines. This design factor separates the vibrations of both the vehicle and the engine. High frequency combustion instability is much more difficult to resolve with proper design. Most of the components of the engine, such as the chamber, feed lines, and throat diameter, have strict regulations based on the engine performance requirements. With these requirements, the injector must allow proper mass flow and reasonable characteristic velocity (c*) values. The means of injection are broad within the required performance. This fact, coupled with the reality that the most common mechanisms are directly related to the injection process, leads to an extensive library of injector designs. The most common types are impinging jet (F-1), shear coaxial (Space Shuttle Main Engine), jet-swirl (Russian RD-170), pintle (Lunar Descent Module Engine) and swirl-swirl. Each injector design has inherent advantages and disadvantages; therefore, the different types are used in different applications and with different propellants. Typically, a designer will have the experience and references to fabricate an initial injector design. After the initial design and fabrication, the engine is tested and the injector geometric parameters can be changed to find the most stable configuration.

Historically, Russian engine designers have focused on design modification as opposed to hardware addition for passive suppression. Specifically, the focus has been on injector and feed system dynamics. In effect, this approach is natural active control through proper design of injector dynamic characteristics.

1.4 High Frequency Combustion Instability Testing

The most straightforward approach to determine the stability of a liquid rocket engine is to test the full scale engine. Unfortunately, this is usually not a feasible nor efficient approach. Full scale testing is extremely expensive and time consuming. If this method of testing is to be used solely, the liquid rocket engine designer is forced to rely entirely on previous designs and experience for the initial design. In the event of unstable operation, modifications are required. Passive suppression methods such as baffles and resonators are commonly employed, but can prove insufficient. In these cases, more extreme changes may be necessary at the cost of excessive time and resources. Engine stability considerations must be implemented early in the design process to avoid modifying designed hardware to obtain stable combustion. Subscale testing can be implemented to avoid such a problematic cycle. A successful subscale experimental program will never substitute for full scale testing, but can aid in reducing the chances of experiencing high frequency combustion instability in the final design. Some subscale engine combustors can be seen in Figure 1.2. These chambers and injectors are designed to create similarity to the full scale engine.

Scaling procedures were heavily developed in the 1950's [6,7]. Many techniques are based on the dimensional analysis of fluid dynamic and combustion criteria such as Reynolds number, Prandtl number and Damköhler number. To derive the scaling procedures, assumptions and limitations must be invoked. These assumptions and limitations make certain techniques incompatible with unique engines. Achieving similarity can be difficult or even impossible with an appropriate methodology

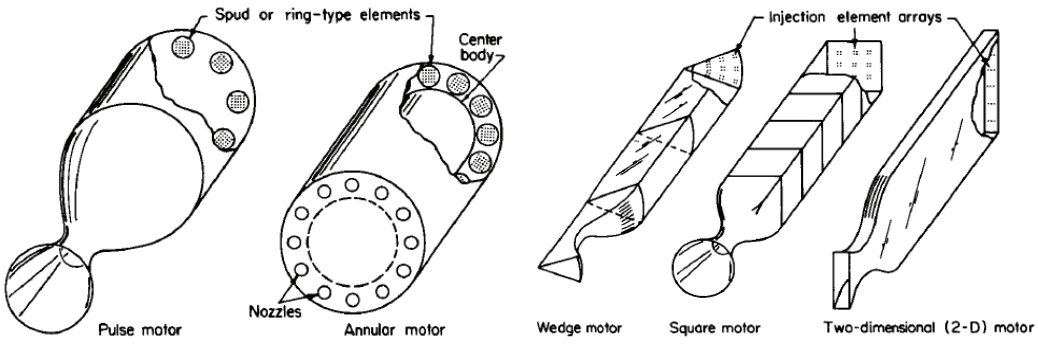

Figure 1.2: Model Combustion Chambers (Coultas and Kesselring 1972)

in practice. To put these theories to the test, laboratory scale experimentation is required.

Many different approaches to subscale testing exist. Single element injector testing is obviously the simplest form of scaling. However, the use of only one injector limits the information that can be extracted from experiments. Intra-element phenomena such as injector flow and combustion characteristics are the only characteristics that can be represented by this single element technique. In the event of stable combustion at nominal operating conditions, stability rating can be used by the varying operating conditions to identify the boundaries of instability and subsequently, how far the operating conditions are from unstable operation. For instance, fuel mass flow rate can be throttled to change the mixture ratio to isolate feed system dynamic affects. Also, chamber pressure variations can aid in scrutinizing atomization and vaporization influences [13].

As with any scaling procedure, there are limitations. The single injector method neglects inter-element influences. The influence of neighboring sprays can

have a significant affect on the overall stability of the system which must be investigated by other means. Similarity matching is of utmost importance not only for the injector, but also the combustion chamber conditions. Modeling the full scale chamber conditions is not simple and certain assumptions about the full scale chamber conditions must be applied. One such assumption is that the uniform temperature of the chamber is the temperature of the combustion products. This, however, may not be an accurate assumption.

The most dangerous modes of instability, from a catastrophic failure standpoint, are the tangential modes. In this instance, the maximum pressure fluctuations are occurring near the injector fire face, where the temperature can be influenced by heat loss through the injector face and recirculation flow, creating a complex temperature field. Some engines employ a fire face which is fabricated from a porous material, *i.e.*, Rigimesh, to inject fuel for cooling. This factor will also add to the local temperature gradient. If the combustion product temperature is used to determine the speed of sound of the full scale combustion chamber, an inaccurate condition is supplied to the model.

Experimentally determining an engine's stability can be a difficult task. The appropriate methodology must be selected and followed in a logical manner. There are two types of stability testing, but the specialized instrumentation is similar for both. Customarily, high frequency pressure transducers or accelerometers are placed in the combustion chamber walls and the propellant manifolds. In order to experimentally determine the mode of instability through data analysis, there are two options. The first method is to experimentally determine or make assumptions about the chamber

thermal environment, calculate the expected natural frequencies and compare them to the experimental data. The other is to place the chamber transducers in specific angular positions. By ascertaining the phase shifts between transducers, the mode of instability can be determined. If available, accelerometers can be used in conjunction with the pressure transducers to quantify the engine vibrations. Certain combustors are designed with optical access to the thrust chamber. Optical diagnostics can be implemented to view the combustion process and quantify otherwise calculated parameters in the chamber. All of the listed instruments are in addition to steady state measurements normally monitored.

1.4.1 Spontaneous Instability Testing

Stability rating can be split into two categories: spontaneous testing and bomb or dynamic testing. Spontaneous testing can be achieved in multiple ways such as temperature ramping or flow rate throttling. The nominal flight conditions are tested as well as the operating conditions surrounding the nominal operating conditions. By systematically changing the operating conditions of the engine, a stability boundary map can be created. Knowing the boundaries where the engine will become unstable is advantageous for the designer. Ideally, the flight condition would be as far way from the boundary as possible on the stable side. A perturbation that could push the parameters toward the unstable regime might be a single unexpected pressure pulsation in the chamber. With such a case, it is important to know how far the engine is from unstable operation to quantify the threshold of deviation from nominal operating conditions that can be tolerated.

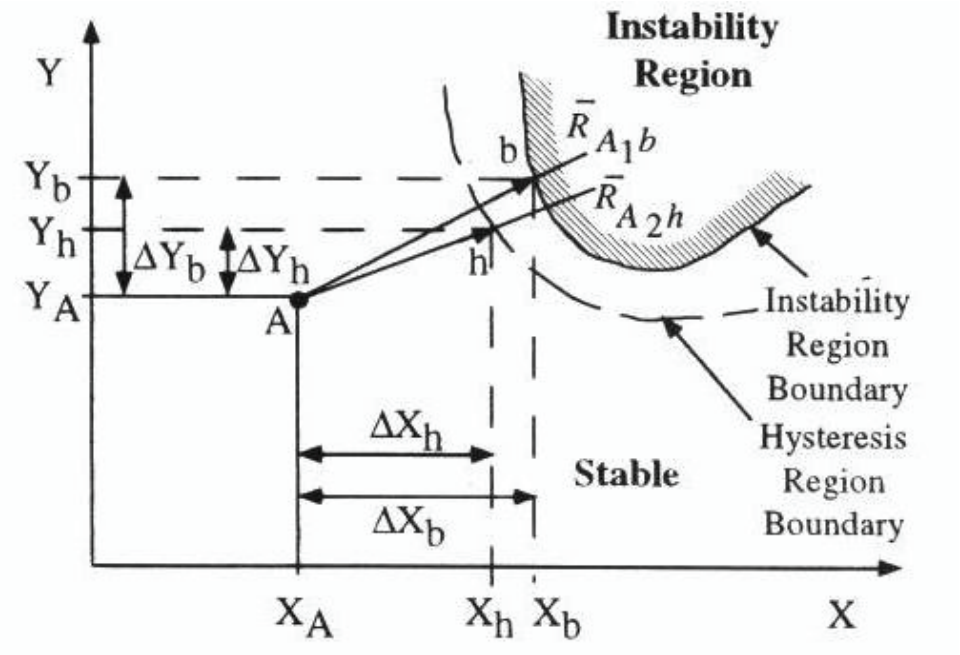

Figure 1.3: Spontaneous Instability Quantification (Fisher et al. 2004)

Figure 1.3 shows a generic example of instability mapping. The X and Y axes can be any parameter under investigation that may give insight to the stability trend such as propellant flow rate or injector pressure drop. Multiple maps can be created for various injectors and compared. Point A on the graph indicates the nominal operating conditions of the full scale engine. $\overline{R}$ is the "distance" from the nominal operating conditions to either the hysteresis or instability boundary. When comparing multiple maps, the configuration with the largest $\overline{R}$ value is the most stable configuration.

1.4.2 Dynamic Testing

Similar to spontaneous testing, bomb testing is used to determine the chamber response to off nominal conditions. Combustion, as a steady process, is turbulent

and noisy with inherent fluctuations which can induce instability. The pressure spikes that can excite instability can result from a multiplicity of processes. The usage of a chamber bomb simulates the unspecified source of pulsation. These simulated pulsations can be either singular or repeated. For singular bomb tests, an explosive charge is placed in a specific position inside the chamber. The explosive strength and directionality are chosen according to the mode of instability under investigation. There are also positions in the chamber that can induce multiple pure or combined modes of instability. A typical pressure plot from a bomb test can be seen in Figure 1.4.

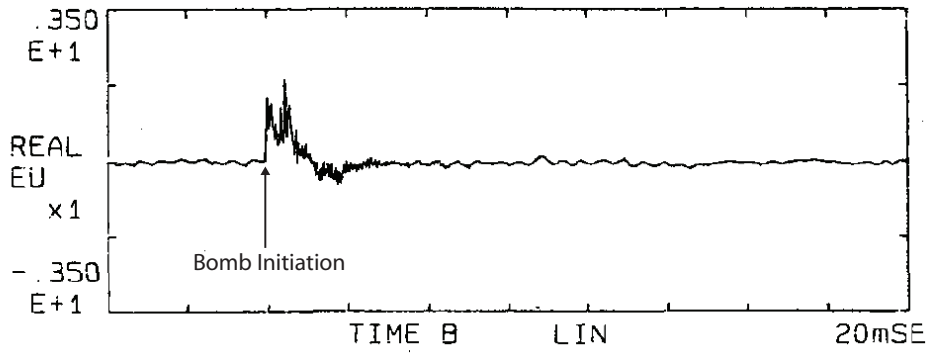

Figure 1.4: Dynamic Stability Pressure Plot (Sasaki et al. 1998)

Traditionally, the bombs are enclosed Cyclotrimethylenetrinitramine (RDX). In order to repeatedly bomb a chamber, extra heavy duty equipment is required unless the flight hardware has sufficient strength to withstand the repeated over pressurization blast. A typical bomb test follows this sequence: main ignition, steady state operation, detonation of bomb (thermally or electrically), and shut down. By analyzing the chamber pressure trace, the stability can be quantified. The relaxation time, or the time for the chamber pressure to return to near steady state operation, can be

determined. The necessary relaxation time is usually set as an engine requirement, and many common standards exist.

Pulsed bombing is very similar to singular bomb tests. Instead of a singular bomb inside the chamber, a passage is drilled into the chamber wall to allow pulsations to enter. The source of the pulsation charges can be gun powder, explosive charges or neutral gas. Similar to the bomb tests, the charges are released to excite certain modes of instability. The most common application is stability rating for spinning tangential modes of instability. In this test scenario, the barrel is mounted tangentially. Perhaps the most interesting characteristic of this testing method is the potential for variation in pulse strength of sequential charges in a single test. This simulates a pressure wave increasing in intensity. Bomb testing is a necessary method to ensure that the engine will run stably in the event of unforeseen pressure disturbance triggers.

1.5 Role of the Injector in High Frequency Combustion Instability

The injector is responsible for preparing the combustible mixture for combustion. Therefore, propellant injection is a critical component in the system with regard to stability. There are a plethora of theories on the complex processes responsible for engine stability. Traditional and contemporary theories point to three major factors directly responsible: atomization, mixing and vaporization.

Atomization is the process of propellant droplet formation, dispersion and break up. This process can be broken down into multiple stages. Primary atomization refers to the droplet sizes, which are attributed to the injector spray formation itself. Secondary atomization is the interaction between neighboring injector element sprays.

With respect to the combustion process, this interaction is correlated to a combustion delay directly after injection. This requirement necessitates the injector to create optimally atomized sprays.

Vaporization is the process of changing the state of the propellant from a liquid to a gas. Many textbooks represent this process as a liquid droplet with an encapsulating flame. The surrounding flame and thermal environment supply the heat to gasify the droplet. Assuming that there are no liquid combustion processes, some energy must be absorbed into the liquid droplets in order to react. This process represents a delay in the combustion process as well, represented by a finite amount of time for a droplet to vaporize after injection. When combustion instability is occurring, a wave of pressure and heat is present in the chamber. Each droplet will experience this wave travel through, and the vaporization will be enhanced by this increase in temperature and pressure. This enhanced vaporization will occur after a finite delay. If the next wave comes through in phase with the delay, the oscillation will gain energy and grow [14]. This process can be an explanation for the rapid appearance and growth of combustion instability. This view of instability is consistent with the Rayleigh criterion.

The final leading process is propellant mixing. Mixing occurs in various ways depending on the propellant and injector types. Liquid propellants can mix prior to vaporization. Similarly, gaseous propellants must mix prior to combustion. If oxidizer and fuel liquid droplets are in close proximity while vaporizing, the delay to reaction can be greatly reduced. Injector design must be heavily scrutinized in order to optimize the delay for propellants to mix.

In reality, all of these process are occurring simultaneously under steady state operation. One can see how these processes are closely intertwined and dependent upon one another. To properly analyze a system, assumptions must be made to simplify the complex processes. Usually, a single process with the longest delay will be identified as the slowest or rate limiting factor. In the United States, it has been customary to assume vaporization or atomization as the most important time factor prior to the combustion process. Russian engineers view the combustion process much differently. They claim mixing is the dominant process, because in modern engines, the propellants are introduced to the chamber near or above supercritical conditions after staged combustion or from regenerative cooling [15]. This difference has led to decades of opposing research paths for the United States and Russia.

The few mentioned mechanisms listed certainly do not exhaust the realm of possibilities of potential origins for the onset of unstable combustion. They are simply the factors which have been repeatedly investigated and upon which multiple theories have been based. In order to understand and simulate the phenomena, more unit physics research is required. The peculiarities of a liquid rocket engine under steady state conditions are extensively complex. An accurate solution to a realistic steady combustion process would be an excellent first step. In order to replicate reality, the analysis would need to simulate the liquid interactions, heat transfer, recirculation and the detailed combustion mechanisms, to mention a few. Once a steady state solution is found, the perturbations can be applied to the system to determine the dynamic characteristics of the system.

Although many years of work have been applied to the problem of combustion instability, there are no strict solutions. Low frequency instability is the easiest to suppress. Intermediate frequency instability is rarely encountered and is usually a stepping stone to high frequency combustion instability.

High frequency combustion instability continues to be a hinderance in solid rocket, liquid rocket and air breathing engine development. As the flight requirements become more demanding, propulsion systems will be required to be more powerful with high efficiencies. This is pushing the limits of materials, while calling for further optimization of flight hardware. In order to meet this present day requirement, a more thorough understanding of high frequency combustion instability must be developed. While computational simulations become more sophisticated, a rational scaling technique to determine injector stability would be extremely useful to the present day liquid rocket engine designer.

Recent publications describe a scaling methodology developed at the Russian NIICHIMMASH Design Bureau [15]. While having the attractive qualities of time savings and monetary efficiency, this scaling technique could serve as the missing tool that liquid rocket engine designers have been searching for.

This methodology has been heavily utilized at the Korean Aerospace Research Institute (KARI). One such publication is on the methodology fundamentals. Sohn [16] describes the individual aspects of the scaling criteria. The article also includes sample calculations required to create similarity between a full scale engine and the laboratory scale experiment.

Researchers at KARI have subsequently utilized the described Russian methodology [17]. One study investigated the effect of oxidizer post recess ratio in a coaxial double swirl injector. The results exhibit that the decrease in post recess increases stability. This is a common aspect of fundamental injector studies with coaxial injectors. The application of this technique was to scrutinize the injector design for a developmental engine. Another study scrutinized the effect of impinging angle on a split triplet injector [18]. Therefore, it has been implemented as a useful design tool.

CHAPTER 2

RUSSIAN METHODOLOGY

2.1 Overview

The objective of this project is to apply and evaluate a Russian injector scaling technique in order to determine the stability of liquid rocket engine injectors. Although many scaling techniques have been derived, there has yet to be a dominant, successful subscale technique used in practice. At the initial conception of an engine, there is no limit as to which type of injector to utilize. Presently, the best tool that a liquid rocket engine designer has is experience from previous engine development programs, which may or may not be similar to the new engine. Testing and analysis of the Russian methodology will give liquid rocket engine designers an experimental tool to use in the early stages of the design process to drive the injector design toward the stable regime.

2.2 Test Facility and Operation Description

Following the rules of the methodology, a test facility has been designed in Russia. Figure 2.1 shows a general apparatus scheme that has been in operation in Russia.

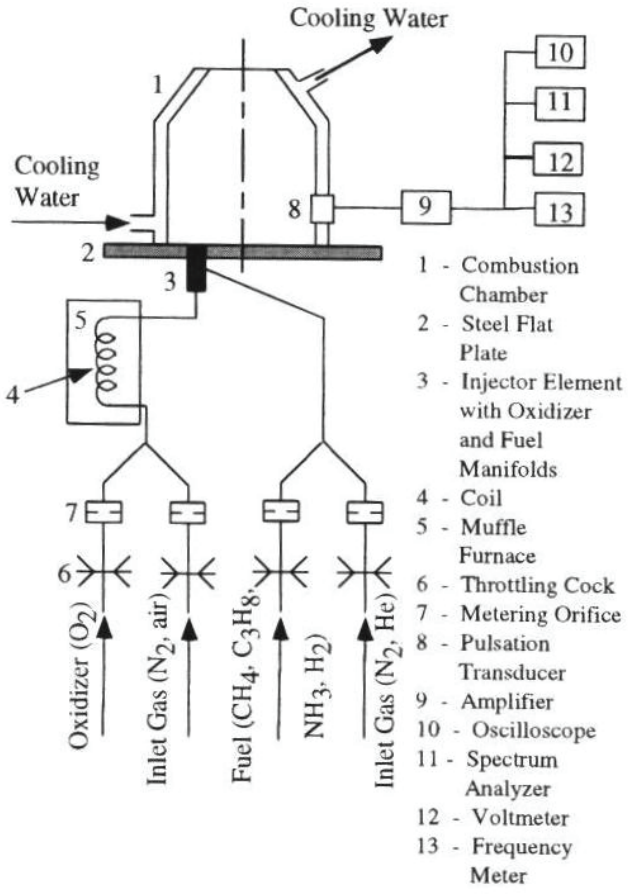

Figure 2.1: General Russian Methodology Test Apparatus (Fisher et al. 2004)

As depicted in Figure 2.1, the atmospheric pressure chamber (1) is water cooled to allow long duration firings. Since the chamber is operated at atmospheric conditions, its main function is to act as a resonator. The chamber may have a nozzle to decrease acoustic damping. Although supersonic flow is not possible without the use of a vacuum chamber, longitudinal waves will be more prevalent with a nozzle. Also, the chamber may have a transparent window for optical diagnostics. The fire face (2) is a flat, steel plate with the injector (3) mounted near the wall to fire vertically. A heating element (4,5) is present in the oxidizer line to aid in matching speed of sound

and further enhance the volumetric flow rate capability. Mass flow control is required to throttle the propellants, in this case shown as a valve (6) and a pressure orifice (7) for flow measurement. Instrumentation requirements are modestly described. A single pulsation transducer (8) is necessary to measure chamber pressure oscillations. Although accelerometers are customary, the low mean chamber pressure may experience extremely low pressure chamber oscillations and therefore small accelerations. Typical data acquisition equipment (9-13) conditions, analyzes, and records the transducer signal. All of these components will most likely be included in a modern data acquisition system.

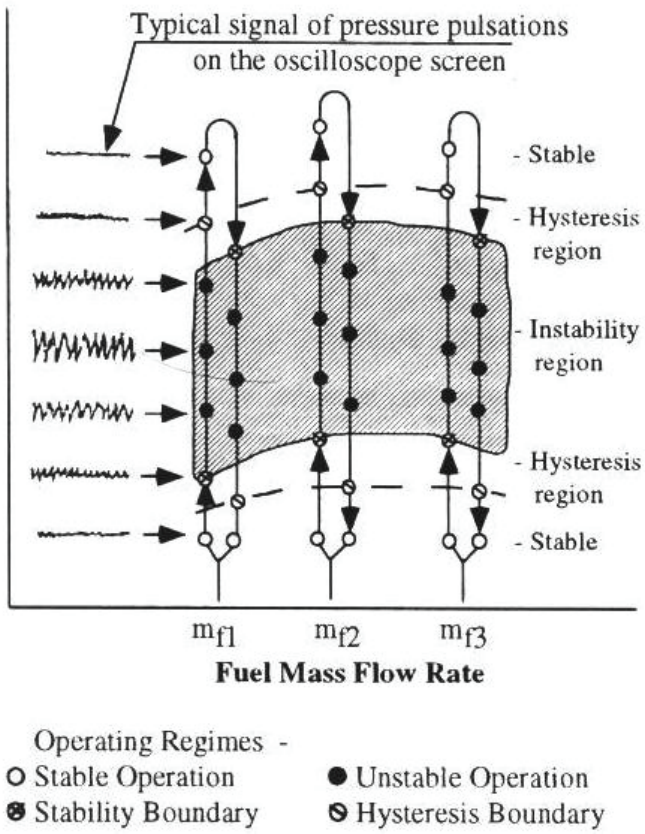

Figure 2.2: Boundary of Instability Map (Fisher et al. 2004)

The test strategy for this experiment can be seen in Figure 2.2. For this test procedure, one firing consists of a single fuel mass flow rate. The oxidizer flow rate is then throttled from minimum to maximum and back down to the minimum. By returning to the minimum flow rate, the hysteresis region can be defined. Once instability is encountered, the hysteresis is defined by the position at which the oscillations decrease below a set amplitude. If the position is not where the instability begins on the way back down, there is a hysteresis region present. While throttling, the dynamic pressure is monitored and recorded. This procedure is repeated for a sufficient number of fuel flow rates until a satisfactory mesh is created. The operating conditions of the full scale engine should be near the center of the instability map to ensure that the engine's response to any off nominal conditions is known.

To determine the stability map, a dynamic pressure amplitude must be defined which is considered unstable (the boundary of the shaded region in Figure 2.2). This threshold is usually a percentage of the relative dynamic amplitude (p'/p_c). An engine is considered to operate stably if there are no sustained chamber pressure oscillations exceeding 10 % peak to peak of mean chamber pressure. Although for certain cases, this amplitude limit may be 5 % or 3 % [19]. Therefore, the definition of the threshold is largely dependent on the application. Once an amplitude threshold is defined, the map can be created.

2.3 Similarity in Scaling

The scaling techniques discussed up to this point have been techniques that keep full scale engine operating conditions consistent. This is usually implemented

by taking a portion of the full scale engine. For example, a subscale wedge combustor is simply an angular slice of the full scale chamber. This method implements a need for boundary condition matching. With a subscale wedge combustor, the chamber acoustics are significantly different from the full scale cylindrical chamber. This can make a correlation of stability data to the full scale impossible. Another similar subscale technique is to reduce the dimensions of all of the engine components and the appropriate operating conditions. This technique sounds quite simple, but is actually rather complex in determining similar conditions in the subscale facility. When linear dimensions decrease, areas and volumes decrease logarithmically. With this change, it is difficult to find operating condition and boundary condition similarity.

The Russian methodology that will be described is a combination of the previous scaling techniques. This methodology is a form of subscale testing, but is more specifically a component test, namely for the injector. The technique is focused on matching the boundary conditions and governing dimensionless parameters and relations from full scale to subscale conditions.

To achieve similitude between full scale and subscale systems, three types of similarity must be satisfied: geometric, kinematic and dynamic [20]. For the application at hand, geometric similarity is matched by using full scale injectors. The kinematic similarity is achieved by producing similar fluid flow. This implies that the fluid flow stream lines must be the same. Dynamic similarity describes the forces present in the systems. The relative ratios of the forces must the same, which includes pressures and accelerations. The Buckingham Pi theorem is applied to find the dimensionless criteria for scaling. Typical non-geometric criteria for the methodology to

be described are Reynolds number, Euler number, Strougal number and Mach Number. Another facet of the system to be studied is that there are multiple components, fuel and oxidizer. This adds significant complexity in matching similarity criteria. The ratios of different fuel to oxidizer properties must be carefully considered such as mixture ratio density ratio and viscosity ratio.

It is fundamentally impossible to achieve complete similarity between full scale and subscale. Therefore, it is of utmost importance to identify and match the controlling similarity parameters with respect to the phenomena under investigation.

2.4 Assumptions and Requirements

A brief description of the Russian methodology was written by Denisov, Shibanov and Agarkov and published in 2004 [15]. Section 2.2 and Section 2.4 are largely taken from the publication.

As described in Section 1.4, any subscale program requires assumptions about the full scale operating conditions in order to enable useful correlation. The following list of assumptions and scaling requirements describes the Russian methodology.

1. Partial modeling must be employed. The processes in the full scale combustion chamber and feed system are far too complex to be completely simulated. A number of important parameters must be identified prior to scaling. This allows similarity to exist for the most important parameters that are assumed to be controlling the phenomena. In fact, for different types of injectors, there may be different sets of primary parameters. In this case, it is crucial to select the

governing parameters to be scaled in order to gain maximum results from the subscale testing.

2. Full scale bipropellant injectors are employed. This is a convenient rule in order to match similarity criteria as well as compare full scale and subscale results. A single element is required, but may not be sufficient for all engines. If the full scale chamber employs multiple injector designs, a cluster must be used with representative spacing. Similarly, monopropellant injectors may be used, but care must be taken to correctly represent the full scale chamber acoustics.

3. Neighboring sprays in a combustion chamber play a negligible role in the stability of the system. The bipropellant injector is assumed to function independently in the propellant mixing zone. This assumption leads to the use of a single element injector in the subscale test. In order to bypass the assumption, a cluster of injectors can be used.

4. Spontaneous instability boundary mapping is employed as described in Section 2.2. The mapping is achieved by throttling the propellant flow rates.

5. The phases of the combustion chamber acoustics and combustion process must be similar.

$$\Omega = (\tau f)^{-1}_{model} = (\tau f)^{-1}_{full\,scale}\,. \tag{2.1}$$

Ω is the phase between the chamber acoustics and characteristic combustion delay (τ). In this methodology, the fuel and oxidizer mixing time (τ), and

f is the chamber oscillation frequency. The values of these parameters are determined experimentally or from analytical models if available.

6. The transverse acoustic mode of the chamber must be matched.

$$f_{model} = f_{full\,scale} \tag{2.2}$$

$$\frac{d_{model}}{c_{model}} = \frac{d_{full\,scale}}{c_{full\,scale}}. \tag{2.3}$$

In this case d is the diameter of the circular chamber and c is the speed of sound in the chamber. The full scale diameter will be known and the speed of sound can be estimated from the adiabatic combustion temperature minus any heat extraction. Therefore, the remaining parameter to be determined is the speed of sound in the model chamber. This parameter can be difficult to estimate with a large temperature gradient existing in the model chamber due to the single element. The speed of sound can be determined by placing temperature probes in the combustion chamber to map a temperature field and estimate an overall average chamber temperature.

7. The next phase that must be matched is the phase between the injector manifold acoustics and the injection process.

$$\Omega_{inj} = (\tau_{inj}\, f)^{-1}_{model} = (\tau_{inj}\, f)^{-1}_{full\,scale}\,. \tag{2.4}$$

In this instance, τ_{inj} is the time required for the pressure oscillation to pass through the injector and f is assumed to be the chamber oscillation frequency, which is already matched due to Equation 2.2. By using the full scale injector one can see that the speed of sound must be equal for full scale and subscale conditions with the following relation.

$$\tau_{inj} \approx \frac{L_{inj}}{c_{inj}}. \tag{2.5}$$

With the length of the injector (L_{inj}) equal, matching the speed of sound (c_{inj}) is required to satisfy this scaling rule, which can be difficult in the subscale facility.

8. Mean chamber pressure (p_c) has no significant influence on the chamber acoustic field, the important parameter is the ratio of dynamic pressure amplitude (p') to mean chamber pressure p'/p_c.

9. The single injector element must be placed close to the wall in order to excite the tangential mode of instability, which is often the most dangerous. The pressure anti-node for the tangential mode is at the chamber wall. This condition creates the most likely occurrence of the tangential mode.

10. Mixing is the rate limiting factor in modern liquid rocket engine combustion chambers. Large boost engines require high chamber pressures to meet performance requirements. In many cases, the pressure can exceed the critical pressure of the propellants. The propellant temperature is also elevated at the

injector inlet. The popularity of regenerative cooling and staged combustion can create propellant temperatures above the critical point. If the propellant temperature and pressure are above critical, the propellant is considered supercritical. Supercritical fluid lacks surface tension; therefore, the propellant resembles a dense gas more closely than a liquid. This condition leads to an absence of atomization and vaporization prior to combustion, leaving mixing to control the rate of combustion. In fact, if the propellants are injected into the combustion chamber near the critical points, the atomization and vaporization may be negligible.

11. The subscale propellants must be gaseous. The previous assumption about the supercritical state specifies that the propellants are more near gaseous than liquid. Under low pressure conditions, this is the most accurate simulant of the full scale propellants.

12. Dilution of the fuel and oxidizer is not required but can aid in creating volumetric flow rate similarity. This allows more flexibility of the test facility. The mixing process is largely affected by the discharge velocity (v_d) of the propellants. By matching the volumetric flow rate ($\dot{Q}$) of the propellant with a full scale injector, the discharge velocity is automatically matched, due to identical injectors with identical flow areas (A_{inj}). By diluting the reactive gases with a neutral gas, a greater discharge velocity can be achieved while maintaining similar combustion chemistry.

$$v_d = \left(\frac{\dot{Q}}{A_{inj}}\right)_{model} = \left(\frac{\dot{Q}}{A_{inj}}\right)_{full\ scale} \tag{2.6}$$

$$\dot{Q} = \left(\frac{\dot{m}}{\rho}\right)_{model} = \left(\frac{\dot{m}}{\rho}\right)_{full\ scale}. \tag{2.7}$$

Equation 2.7 highlights one of the convenient simplicities of the methodology. While matching volumetric flow rate, mass flow rate and density need to be in similar ratios. The propellant density in the full scale engine under high pressure is two or three orders of magnitude greater than in the ambient pressure subscale chamber. This difference allows similarity to be achieved with mass flow rates orders of magnitude lower than in the full scale. This greatly simplifies the requirements for test facility setup and operation.

13. The fuel and oxidizer lines may be reversed if appropriate or necessary. If scaling can be achieved by swapping the propellant feed lines, the mixing process will be changed. This can cause a different combustion response.

Although there is no mention of combustion chemistry in the methodology, it obviously plays an important role in creating similarity. There is also no detail on the similarity requirement for simulant fuels, *i.e.*, if it is possible to simulate RP-1 with a mixture of hydrocarbons or hydrogen. With respect to mixing, the subscale molecule should be the same or near the same size as the full scale molecule. When simulating a fuel that is unavailable in the subscale apparatus, it is more important to match the equivalence ratio than the mixture ratio.

2.5 Case Studies

In order to verify that the proposed scaling methodology truly simulates the full scale engine, a subscale program must be implemented to compare full scale and subscale results. If the results are similar for properly scaled conditions, the scaling technique is verified as a useful experimental tool. Unfortunately, full scale instability data is difficult to procure, but there has been some publication on full scale unstable results. The following sections are case studies of two injectors with available published full scale data.

2.5.1 RD-170 Main Chamber Injector

The RD-170 engine is a Russian engine used for heavy launch vehicles such as the Zenit and Energia. The engine operates on an oxidizer rich preburner staged combustion cycle using LOX/RP-1. The engine boasts performance characteristics of sea level thrust and specific impulse of $1,632,000\,lbf$ and 309 seconds, respectively. The performance exceeds that of the F-1 engine, but the RD-170 utilizes four chambers operating from a single turbopump. While being very powerful, the thrust can be throttled from 50 % to 105 % [21].

The RD-170 development experienced instability but was overcome through testing. Impressively, the main chamber does not employ any classic baffles or resonators. However, there are injectors that protrude from the fire face, which are aligned to create six separate sections around the chamber circumference similar to a baffle. The main chamber of this engine has multiple injector designs. There are

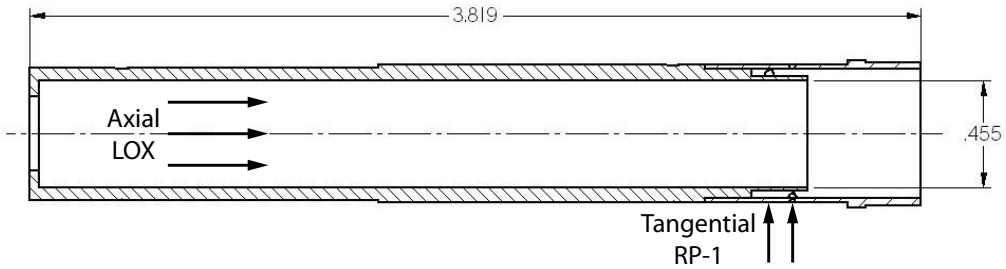

Figure 2.3: RD-170 Main Combustion Chamber Injector (dimensions in mm)

multiple designs for the fire face surface injectors and the baffle injectors. One such injector, coaxial with annulus swirling flow, can be seen in Figure 2.3. Even though there are multiple injector designs, the fuel mass flow rates for the different injector groups differ by no less than 3 % and no more than 10 % [22].

The overall operating conditions of this engine are well known. Unfortunately, the detailed operation of the engine is not documented in open literature by the developers. A method of liquid rocket engine cycle analysis was created by Goertz [23]. The analysis method was applied to multiple engines including the RD-170 engine by Manski, et al. [24]. This analysis is the basis of the full scale operating conditions for the case study. The necessary parameters were taken from the injector inlet and chamber, depicted in Figure 2.4. These parameters were taken and averaged over the sum of all injectors (271) to determine the flow rates for a single injector. This assumption is not precise, but since there are small percentages in fuel flow rate variation from injector to injector, it is a fair approximation.

The manifold conditions of the propellants can be seen in Table 2.1. The high manifold pressures of this staged combustion cycle engine exceed the critical pressure

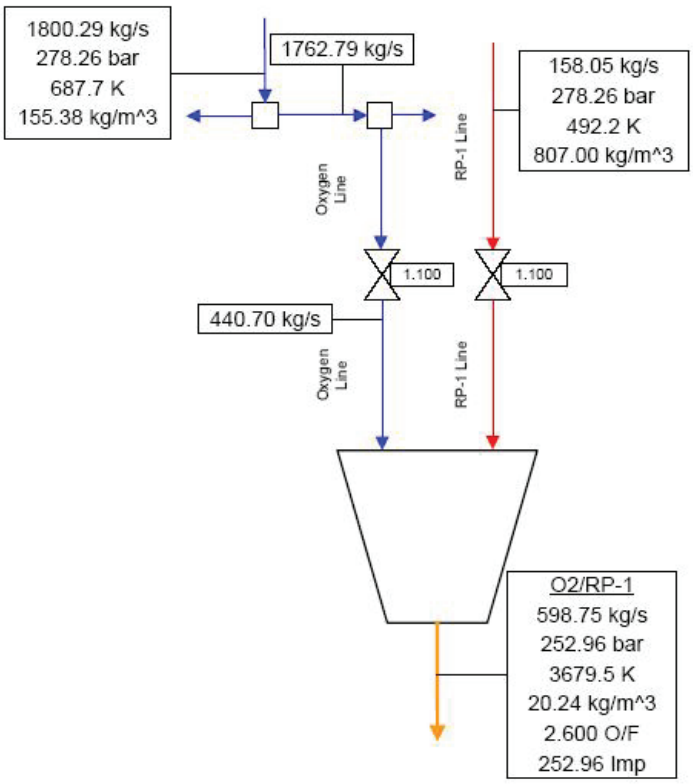

Figure 2.4: RD-170 Main Chamber Operating Conditions

for both the Rocket Propellant 1 and liquid oxygen. The LOX manifold temperature is far beyond critical, which makes the LOX supercritical. The earth storable RP-1 does not meet the critical temperature, but it is assumed that the vaporization and atomization are negligible if present in the chamber.

There is no published data on the stability of the full scale engine. It is assumed that the engine is stable at the conditions that are available. Scaling the flight conditions and showing that the injector runs stable will be a first step to show that the technique is accurate. Strictly speaking, a true scaling scheme would employ all different injector elements to accurately represent the acoustic field of the full scale

Table 2.1: RD-170 Injector Manifold Conditions

	RP-1	LOX
$P_{critical}\ [MPa]$	2.17	5.04
$P_{manifold}\ [MPa]$	27.83	27.83
$T_{critical}\ [K]$	676	155
$T_{manifold}\ [K]$	492	688
$\dot{Q}\ [cc/s]$	723	10470

chamber. A detailed set of drawings of the propellant manifolds in order to match the manifold acoustics would also be required.

To approximately scale the operating conditions, two major requirements must be fulfilled. The first is volumetric flow rate similarity for both the fuel and oxidizer. The second is similar stoichiometry. Parametric studies were conducted with oxygen, air and nitrogen diluent to constitute the oxidizer while propane, methane, hydrogen and nitrogen diluent combinations were explored for the fuel. Temperature was also varied in attempts to converge on a solution. Through the studies, many trends were determined. By using pure oxygen, it is impossible to match stoichiometric conditions simultaneously with volumetric flow rate. As a side note, with oxidizer rich gas generator or preburner injectors, it would be possible to scale by using pure oxygen at such lean conditions. The combination of air as the oxidizer, and propane, methane, and nitrogen fuel diluent was found to be a successful combination. In fact, since RP-1 is a blend of hydrocarbons and additives, it may be the best simulant propellant. Multiple solutions were found by employing dilution as well as heating. Appendix C includes the detailed code used to solve the set of equations. These

conditions only scale the propellant conditions, the chamber diameter must be sized according to Section 2.4.

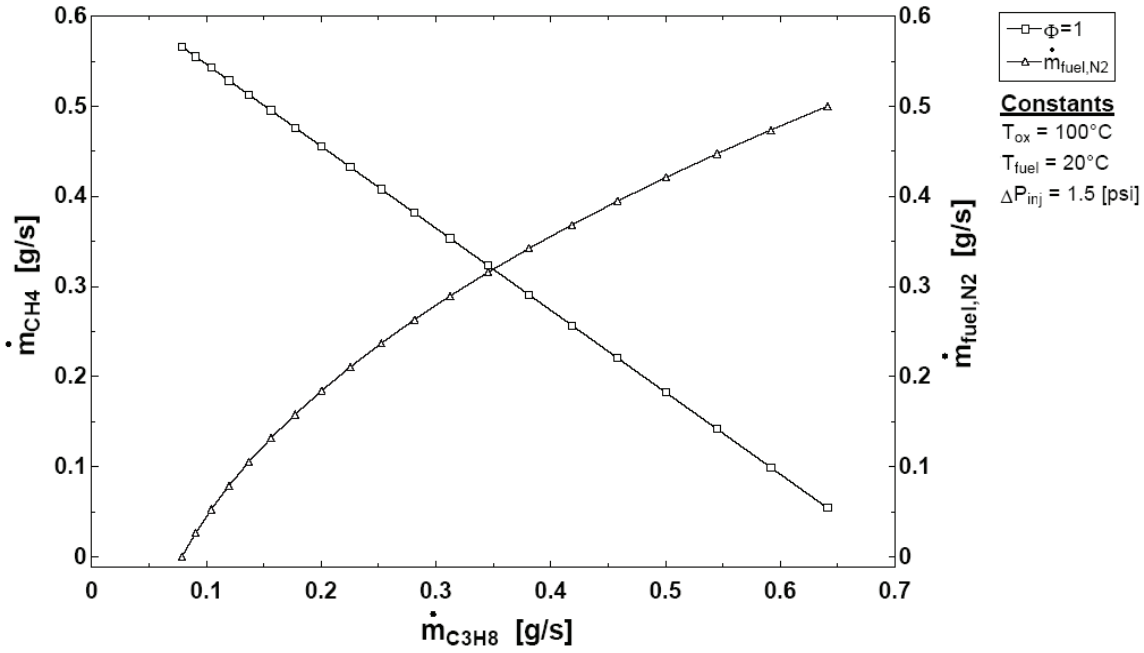

Figure 2.5: RD-170 Dilution Scaled Conditions to Match $\dot{Q}$ and Stoichiometry

Figure 2.5 shows a set of solutions that match volumetric flow rate and stoichiometry. The solutions listed are for a matched oxidizer volumetric flow rate and temperature of air at 10.91 g/s and 100 C, respectively. The curve listed as $\phi = 1$ shows the proportion of methane and propane at stoichiometric and similar fuel volumetric flow rate conditions. As the ratio of methane mass flow to propane mass flow changes, the stoichiometric mixture ratio shifts between 3.6 (pure propane) and 4 (pure methane), which is taken into account in the analysis code. The $\dot{m}_{fuel,N2}$ curve shows the amount of nitrogen fuel diluent required to maintain the correct fuel volumetric flow rate. An interesting study would be to run a single throttling test

that spans all of the set points listed to see if there were any significant differences in stability. Any variation may expose the absence of a scaling requirement or inaccurate assumption.

Table 2.2: RD-170 Injector Scaling by Temperature Ramping to Match $\dot{Q}$ and Stoichiometry

T_{fuel} [C]	T_{ox} [C]	$\dot{m}_{CH4}$ [g/s]	$\dot{m}_{C3H8}$ [g/s]	$\dot{m}_{fuel,N2}$ [g/s]	$\dot{m}_{Air}$ [g/s]	$\dot{m}_{ox,N2}$ [g/s]	$\dot{m}_{O2}$ [g/s]	$\left(\frac{O}{F}\right)_{stoich}$
20	100	0.566	0.0786	0	10.91	0	2.543	3.945
25	100	0.5585	0.08686	0	10.91	0	2.543	3.941
30	100	0.551	0.09515	0	10.91	0	2.543	3.936
35	100	0.5434	0.1035	0	10.91	0	2.543	3.931
40	100	0.5358	0.1119	0	10.91	0	2.543	3.927
45	100	0.5281	0.1203	0	10.91	0	2.543	3.922
50	100	0.5204	0.1287	0	10.91	0	2.543	3.918
55	100	0.5127	0.1372	0	10.91	0	2.543	3.913
60	100	0.5049	0.1458	0	10.91	0	2.543	3.908
65	100	0.4971	0.1544	0	10.91	0	2.543	3.904
70	100	0.4893	0.163	0	10.91	0	2.543	3.899
75	100	0.4814	0.1717	0	10.91	0	2.543	3.894
80	100	0.4734	0.1804	0	10.91	0	2.543	3.89
85	100	0.4655	0.1891	0	10.91	0	2.543	3.885
90	100	0.4575	0.1979	0	10.91	0	2.543	3.88
95	100	0.4494	0.2068	0	10.91	0	2.543	3.875
100	100	0.4413	0.2157	0	10.91	0	2.543	3.871
105	100	0.4332	0.2246	0	10.91	0	2.543	3.866
110	100	0.425	0.2336	0	10.91	0	2.543	3.861
115	100	0.4168	0.2426	0	10.91	0	2.543	3.856

Table 2.2 is a list of another set of scaled solutions. This set of operating conditions uses no diluents in the propellants. The temperature of the fuel is increased, while the fuel proportions are changing in order to meet the scaling requirements of volumetric flow rate, as in Table 2.1, and stoichiometric conditions. In this instance,

the column $\dot{m}_{O2}$ represents the amount of oxygen in the air. This table would also be an interesting test matrix to search for any differentiation.

2.5.2 Rocketdyne LOX/Methane Coaxial Injector

An experimental program was developed in the late 1980s at Rocketdyne's Santa Susanna Field Laboratory in support of the National Aerospace and Space Administration (NASA) Lewis Research Center. The aim of the investigation was to determine if there was a correlation between hydrogen and hydrocarbon fuels with respect to stability. Historically, hydrogen temperature ramping tests have been successful in displaying repeated transition from stable to unstable conditions at a specific hydrogen temperature. The hydrocarbon selected for the study was the mild cryogen, methane. The testing procedures include spontaneous instability, via temperature ramping and dynamic instability, via bomb testing. The data of interest from this report are the steady state spontaneous instability occurrences and the temperature ramping test results [25].

The hardware employed in this test program was an 82 element combustor design, based on a thrust chamber used for LOX/Methane performance testing at NASA Marshall Space Flight Center. All 82 elements are an identical coaxial configuration, which can be seen in Figure 2.6. The original manuscript is of poor quality, but an enlarged image can be referenced in Appendix A. In this assembly, the injector face orifices comprise the sleeve of the fuel annulus. The diameter of the cylindrical chamber is 5.66 inches.

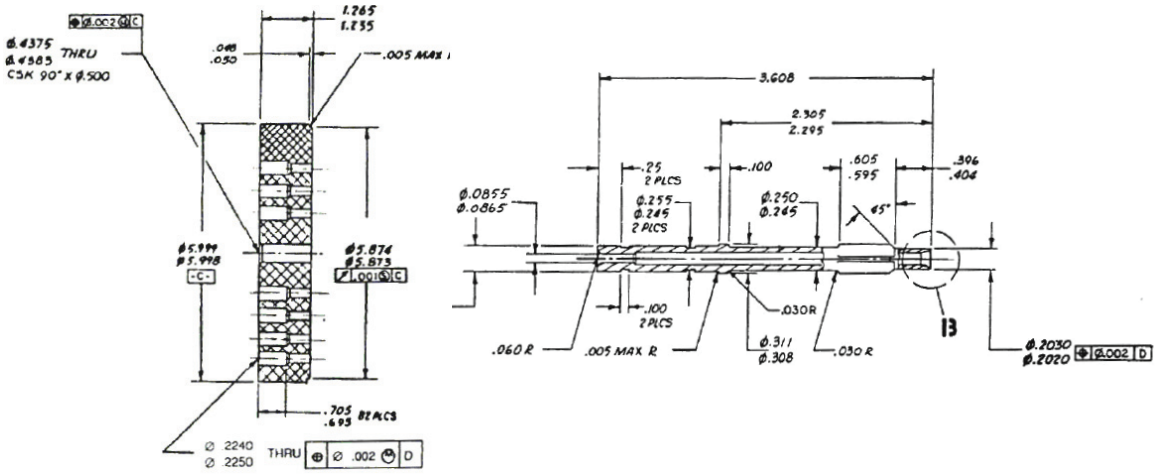

Figure 2.6: Rocketdyne Shear Coaxial Injector (Jensen 1989)

Of the seventeen tests, three tests were temperature ramping tests, which all experienced an injector coupled instability at 14.0 kHz. Other tests were aimed at determining performance, but resulted in spontaneous high frequency combustion instability. Tests 014-004, 014-019, and 014-022 were all unstable at the first tangential mode (4.2 kHz). Test 014-022 was selected to scale for this Russian laboratory scale method. The entire test matrix is available to determine the scaled conditions.

Table 2.3: Rocketdyne Coaxial Injector Manifold Conditions (Test 014-022)

	Methane	LOX
$P_{critical}\ [MPa]$	4.60	5.04
$P_{manifold}\ [MPa]$	19.43	17.35
$T_{critical}\ [K]$	191	155
$T_{manifold}\ [K]$	283	109
$\dot{Q}\ [cc/s]$	881	334

Table 2.3 lists the manifold conditions of Test 014-022. The pressure in the manifolds for both the LOX and methane exceeds the respective critical pressures.

The methane temperature is above the critical point; therefore, the fuel is a supercritical fluid. The LOX is just below the critical temperature. Again, since there is little deviation from the critical temperature, it is assumed that negligible LOX vaporization and atomization exist in the chamber.

Jensen, et al. [25] have included multiple waterfall plots of the test results. These plots can be compared to any subscale data that would be created. The RD-170 analysis code was modified and implemented to run parametric studies. Since the LOX was relatively cold, scaling the LOX volumetric flow rate was straightforward with pure oxygen. The obvious fuel of choice for this study was methane. Due to the stoichiometric restrictions, nitrogen and heat are required to model the full scale conditions.

Table 2.4 shows a list of scaled volumetric flow rate and stoichiometric conditions. As can be seen, a balance between fuel temperature and fuel diluent exists. Increased heat applied to the methane decreases the need for fuel diluent. These conditions would be interesting to run as a temperature ramping test.

2.5.3 Case Study Summary

Table 2.5 is a summary of the scaled conditions presented in Section 2.5. This table represents the operating conditions required to run all three specified solution sets.

Table 2.4: Rocketdyne Coaxial Injector Scaled Conditions

T_{fuel} [C]	T_{ox} [C]	$\dot{m}_{CH4}$ [g/s]	$\dot{m}_{fuel,N2}$ [g/s]	$\dot{m}_{O2}$ [g/s]	$\Phi_{full\,scale}$	Φ_{model}
20	20	0.1613	0.8962	0.4902	0.7619	0.7619
30	20	0.1613	0.8587	0.4902	0.7619	0.7619
40	20	0.1613	0.8236	0.4902	0.7619	0.7619
50	20	0.1613	0.7906	0.4902	0.7619	0.7619
60	20	0.1613	0.7596	0.4902	0.7619	0.7619
70	20	0.1613	0.7304	0.4902	0.7619	0.7619
80	20	0.1613	0.7029	0.4902	0.7619	0.7619
90	20	0.1613	0.6768	0.4902	0.7619	0.7619
100	20	0.1613	0.6521	0.4902	0.7619	0.7619
110	20	0.1613	0.6287	0.4902	0.7619	0.7619
120	20	0.1613	0.6065	0.4902	0.7619	0.7619
130	20	0.1613	0.5854	0.4902	0.7619	0.7619
140	20	0.1613	0.5652	0.4902	0.7619	0.7619
150	20	0.1613	0.546	0.4902	0.7619	0.7619
160	20	0.1613	0.5277	0.4902	0.7619	0.7619
170	20	0.1613	0.5102	0.4902	0.7619	0.7619
180	20	0.1613	0.4935	0.4902	0.7619	0.7619
190	20	0.1613	0.4775	0.4902	0.7619	0.7619
200	20	0.1613	0.4621	0.4902	0.7619	0.7619

Table 2.5: Summary of Capabilities Required to Run Case Studies

	$\dot{m}_{ox}$ [g/s]	$\dot{m}_{ox,N2}$ [g/s]	$\dot{m}_{CH4}$ [g/s]	$\dot{m}_{C3H8}$ [g/s]	$\dot{m}_{fuel,N2}$ [g/s]	T_{fuel} [C]	T_{ox} [C]
min	0.49	0.00	0.00	0.00	0.00	20	20
max	11.00	0.00	0.57	0.65	0.50	100	200

2.6 Assessment

This scaling technique has been developed and applied in Russia, but remains untested in the United States. The fact that the two case studies examined here were successful in finding multiple subscale operating conditions is encouraging, due to the fact that thermodynamic and combustion chemistry could have restricted a realistic solution.

As a first investigation, multiple injectors that are classically associated with unstable operation should be tested at generic operating conditions to determine if the proposed methodology can indeed create unstable combustion. If unstable combustion occurs, the phenomena can be explored further by adhering to added scaling rules. Once the methodology is fully applied to a full scale injector, such as those investigated, the full scale data could be compared to the subscale results to find any correlation. If successful, this methodology would be a valuable tool that liquid rocket engine designers could use before designing full scale hardware with confidence of stable combustion.

CHAPTER 3

EXPERIMENTAL APPROACH

3.1 Test Strategy

An experiment was designed to recreate and investigate the Russian methodology. The method of boundary mapping was strictly adhered to by setting a fuel mass flow rate and throttling the oxidizer. For the first set of experiments on this machine, the propellants were chosen as gaseous oxygen and methane with no diluents. The heating capability was also not included in the experimental design.

There are multiple objectives to the proposed set of experiments. The first is to determine if the test facility is capable of creating unstable combustion. Secondly, a parametric study of one injector variable was conducted, namely, the angle at which the fuel is injected to the oxygen flow.

3.1.1 Test Matrix

A table of set point ranges can be seen in Table 3.1. The detailed matrix can be referenced in Appendix C.

The test matrix employs only oxygen as the oxidizer and methane as the fuel, with no diluents or heating. There are nine fuel mass flow rates to map each

Table 3.1: Test Matrix Summary

Test	Number of Set Points	$\dot{m}_{CH4}$ [g/s]	Φ	$\dot{m}_{O2}$ [g/s]	$\dot{m}_{total}$ [g/s]	$\dot{Q}_{CH4}$ [cc/s]	$\dot{Q}_{O2}$ [cc/s]
1.0	13	0.11	2-0.5	0.21 - 0.87	0.32 - 0.98	166	166 - 667
1.5	13	0.16	2-0.5	0.32 - 1.31	0.49 - 1.47	250	250 - 1001
2.0	13	0.22	2-0.5	0.43 - 1.74	0.65 - 1.96	333	333 - 1335
2.5	13	0.27	2-0.5	0.54 - 2.18	0.81 - 2.45	416	417 - 1669
3.0	13	0.33	2-0.5	0.65 - 2.62	0.98 - 2.94	500	500 - 2002
3.5	13	0.38	2-0.5	0.76 - 3.05	1.14 - 3.44	584	583 - 2336
4.0	13	0.44	2-0.5	0.87 - 3.49	1.31 - 3.93	666	667 - 2670
4.5	13	0.49	2-0.5	0.98 - 3.93	1.47 - 4.42	750	750 - 3003
5.0	13	0.55	2-0.5	1.09 - 4.36	1.63 - 4.91	833	834 - 3337

injector, which is a sufficient number to create a representative stability map for the baseline testing. The mass flow rate of methane is near the maximum range at 20 % to 100 % of full scale. For each fuel mass flow rate, there are thirteen oxidizer set point increments. The set points vary from equivalence ratio 0.5 to 2: six lean, six rich and one stoichiometric. The test matrix was applied to all of the injectors in order to have instability data at the same test conditions. A graphical representation of the test matrix for the experiments can be seen in Figure 3.1.

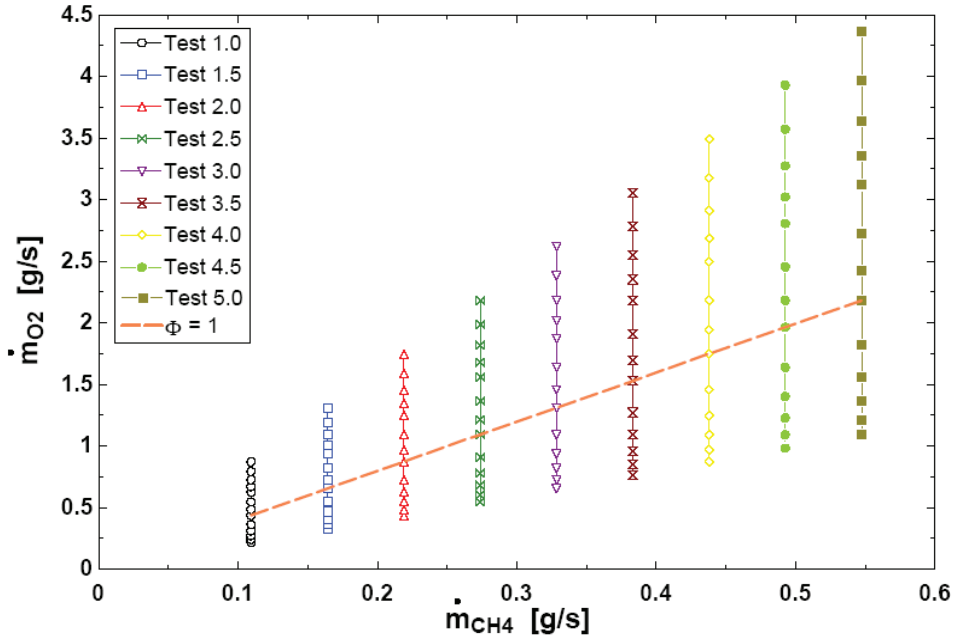

Figure 3.1: Experimental Test Matrix

3.1.2 Injector Design

The main objective of the experiment was to determine if the methodology was successful in creating unstable combustion. This is a byproduct of all of the experiments. The secondary objective of the experiments was to investigate the differences in impingement angle on stability with an impinging jet injector. The three impinging jet injectors can be seen in Figure 3.2. As shown in Figure 3.2, the injectors are not a typical pentad configuration. In traditional impinging jet injectors, the sprays are injected through a flat fire face, where they intersect a finite distance from the fire face. This design is typical of Russian medium thrust hypergolic engines where the propellants mix in the injector post.

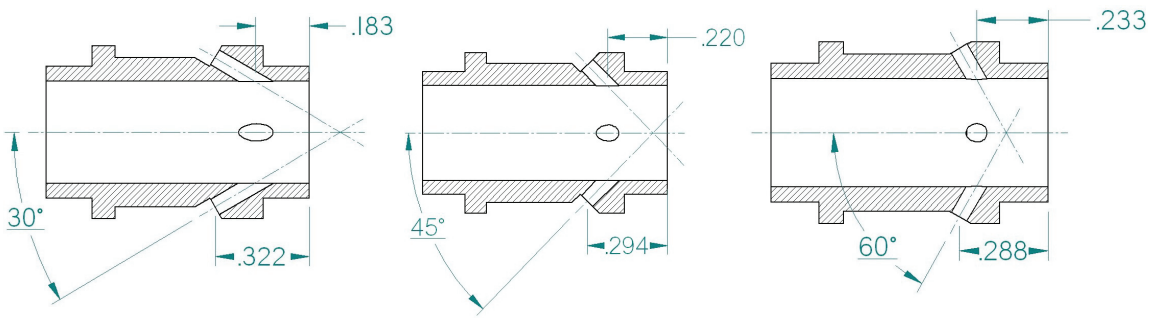

Figure 3.2: Impinging Jet Injectors

The naming scheme used throughout Chapter 4 will have up to four parts. The first section corresponds to the degree of fuel impingement, *i.e.*, 30, 45 or 60 degree. The second is the test session date which can be referenced in Table E.4. The third is the test number, *i.e.*, Test 2.5 from the test matrix. The test name also immediately corresponds to the single fuel mass flow rate. The final part is the equivalence ratio of the set point. Therefore, a test session can be specified by the first two parts, a specific test number can be specified with three parts, and a specific set point can be specified by all four naming parts. For example, Set Point 30-1-1.5-1.0 would signify a thirty degree impinging jet run on the first test session (February 5^{th}), at Test 1.5, or 0.16 g/s, and the seventh set point, or stoichiometric set point.

3.2 Apparatus Design

To assess and refine the Russian methodology, a test facility was designed. A generalized design approach was adopted to create capabilities of typical liquid rocket engines, namely, volumetric flow rate capabilities. Therefore, in the initial design phase, there were no specific injectors planned for testing. The facility was

designed to have a wide range of capabilities to accommodate various injectors. The main oxidizer chosen was oxygen with nitrogen as the oxidizer diluent. Methane and propane were chosen as the fuels with nitrogen as the fuel diluent. Although the methodology does not call for multiple fuel feed lines, the capability was designed into the system to enable fuel mixing if necessary. Another additional feature that was designed into the facility is heating of all propellants and diluents. The methodology schematic (Figure 2.1) shows that the oxidizer is heated, but the fuel is not. Due to the scaling criteria that calls for matching propellant speed of sound, it is important to heat both fuel and oxidizer. With these criteria in mind, an initial design was formulated. A list of flow and heating design parameters can be seen in Table 3.2.

Table 3.2: Initial Test Facility Design Parameters

	Mass Flow Rate [g/s]	Manifold Temperature Range [K]
Oxygen	2.0	300 - 450
Oxidizer Nitrogen	1.0	300 - 450
Methane	0.5	250 - 450
Fuel Nitrogen	1.0	250 - 450
Propane	0.5	250 - 450

Another difference between the published methodology test facility and the University of Alabama in Huntsville (UAH) test facility is the use of an open, uncooled chamber. This chamber is simply a resonator since it does not have a converging nozzle. Water cooled chambers have been designed from typical Russian heritage hardware that incorporate a converging nozzle. It was decided that for baseline testing, an uncooled chamber was sufficient.

All of the required equipment to house the injector was custom designed. The injector manifold and oxidizer collector were designed by Dr. Vladimir Bazarov. Each of the parts has been fabricated at the UAH Research Machine Shop. A detailed assembly of the injector manifold can be seen in Figure 3.3 and all component drawings are included in Appendix A.

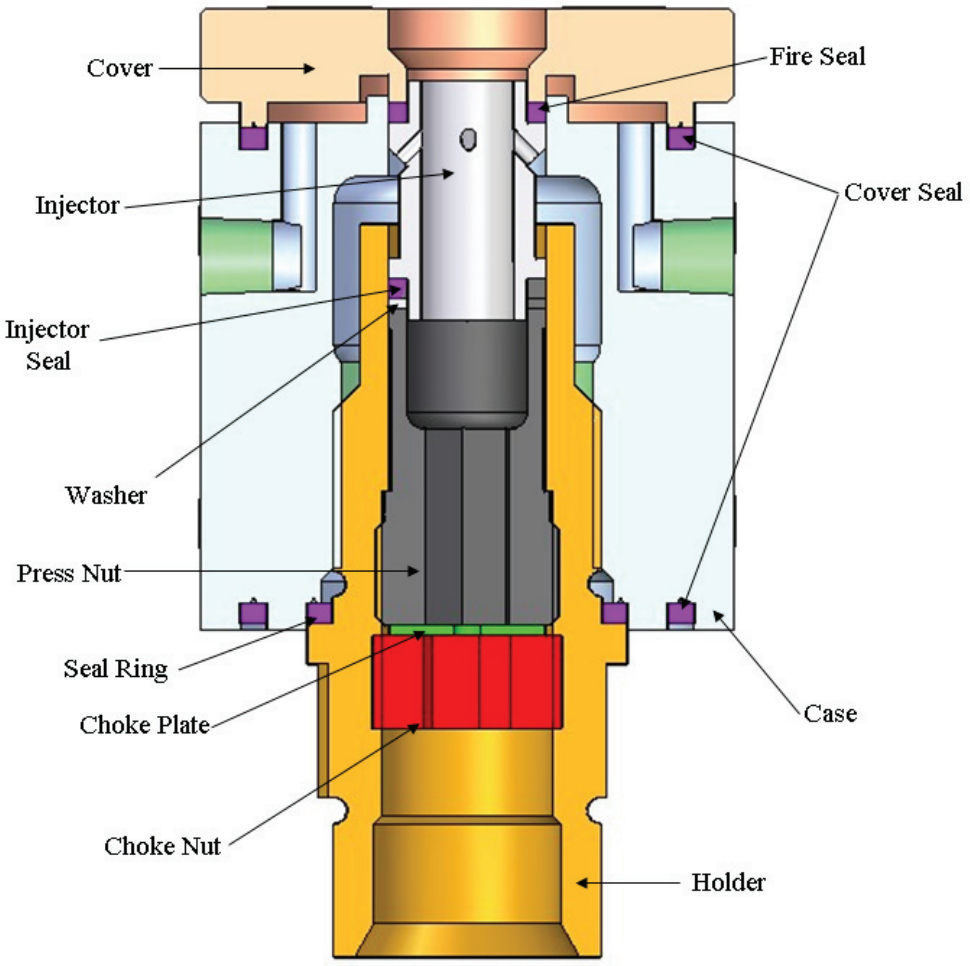

Figure 3.3: Impinging Jet Injector Assembly

The oxidizer is supplied axially through the holder and the fuel manifold is the volume inside the case. The interface between the case and cover employs a gap

to cool the manifold assembly. The supply and return for this cooling channel are shown as green case holes in Figure 3.3. The holder houses the injector, which is secured into place by the press nut. All washers and seals were also custom designed and fabricated. The choke plate shown is not a requirement for proper installation but can be used to change the pressure drop dependence of the injector. In this case, the injector is an impinging jet, but the hardware is compatible with many injector designs. This identical configuration is also capable of holding swirl injectors of similar external dimensions. There is sufficient length to allow long injectors such as shear coaxial or the RD-170 main chamber injectors that have long oxidizer posts. These larger injectors have a separate holder, press nut and cover design. The oxidizer collector, which is the location where the oxygen and nitrogen mix, has a flange fixed to the bottom of the case. The fuel collector, where fuels and diluent mix, is an external piece of hardware which is piped to the fuel manifold. A damping section is employed in the fuel collector, which can damp any oscillations that penetrate through the injector. The damping section is comprised of two perforated discs separated by a spacer with stainless steel wool inside.

The instrumentation and common test equipment were selected based on the specifications of Table 3.2. The most important piece of instrumentation is the PCB 106B high frequency pressure transducer. The calibration sheet and specifications can be seen in Appendix F. Selecting a pressure range was based on typical instability ratios of peak to peak over chamber pressure. A transducer was selected with a range of $0-8\,\text{psi}$. This transducer would reach the limit of operation at a ratio of $55\,\%$. The mass flow controllers were selected for their robust design. These electronic controllers

function on a laminarization principle. The attractive characteristics of the controller are the internal proportional-integral-derivative (PID) control of mass flow and the internal calibration for over forty types of gas. The heating requirements dictated that the most effective heater design was an inline heater. All of these heaters have the heating element in the flow. The oxygen heater has a larger heating element to avoid localized temperatures, which could induce auto ignition of the stainless steel casing.

3.3 Facility Description

The test facility is housed at the UAH Johnson Research Center. All of the experimental equipment is mounted on a cart which is supplied with propellants by the rocket test stand.

A schematic of the experimental feed system can be seen in Figure 3.4. The propellant and purge pressures which are supplied to the cart are regulated by pre-existing test stand pressure regulators and dome loaders. The reactive gas lines from the test stand are plugged directly into actuated fire valves to control passage into the cart feed system. A downstream pressure regulator ensures that the pressure upstream of the mass flow controller (Omega FMA-2609 / FMA-2613) does not exceed the rated pressure of the controller. Between the regulator and controller is a pressure relief valve, which has multiple functions. The first function is to alleviate excessive pressure into the mass flow controller. The second is a manual override handle to alleviate pressure on the cart in case of electrical failure. Downstream of the mass flow controller is an inline heater (Omega AHP-3741 / AHP-5150), which is controlled

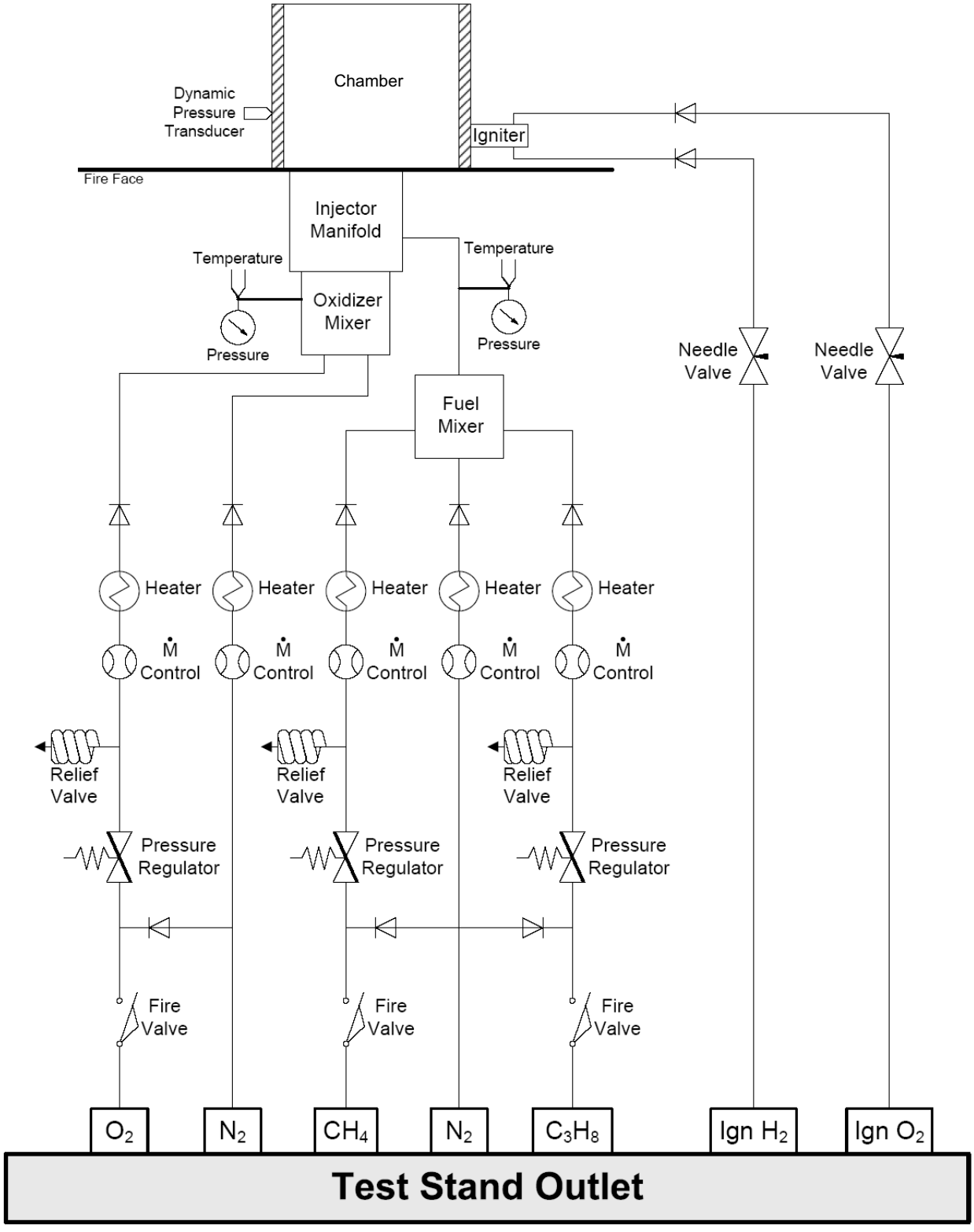

Figure 3.4: Piping Schematic

by an Omega CNi853-C24 PID temperature controller and Omega SCR19P-12-040-S9 phase angle rectifier. The propellants pass through a check valve to restrict reverse flow and are subsequently mixed in the respective collectors. The nitrogen lines also have dual functionality. The nitrogen lines are the rocket test stand main purge lines, which can only be regulated up to 100 psi. Therefore, there are no pressure regulators on these feed lines. Each nitrogen line is branched to a check valve and to a reactive gas line. These branches are the cart feed system purge lines. The pressure of the reactive gases entering the fire valves must be sufficiently high to ensure that the check valve is not cracked open to allow nitrogen flow. As a safety precaution, the reactive gas pressure should be three times that of the nitrogen. This purge piping scheme completely separates the fuel and oxidizer lines on the cart which makes reverse flow and mixing impossible. The nitrogen mass flow and temperature are regulated similarly to the reactive gases. Each manifold has a pressure and temperature reading before the gases enter the injector.

The injector manifold with its mounting equipment can be seen in Figure 3.5. The case and cover are placed into a 5 inch disk with a tapered, square hole. The brackets on the side of the case are slid onto the countersunk cap screws. This design allows the case to be elevated or dropped down to ensure that the injector surface is flush to the fire face surface. The assembly is set into a large steel plate, which acts as the injection face.

The injector is ignited by a gaseous oxygen (GOX), gaseous hydrogen (H_2) igniter supplied by the rocket test stand. Again, the pressure is regulated by pre-existing test stand equipment and needle valves are located downstream to throttle

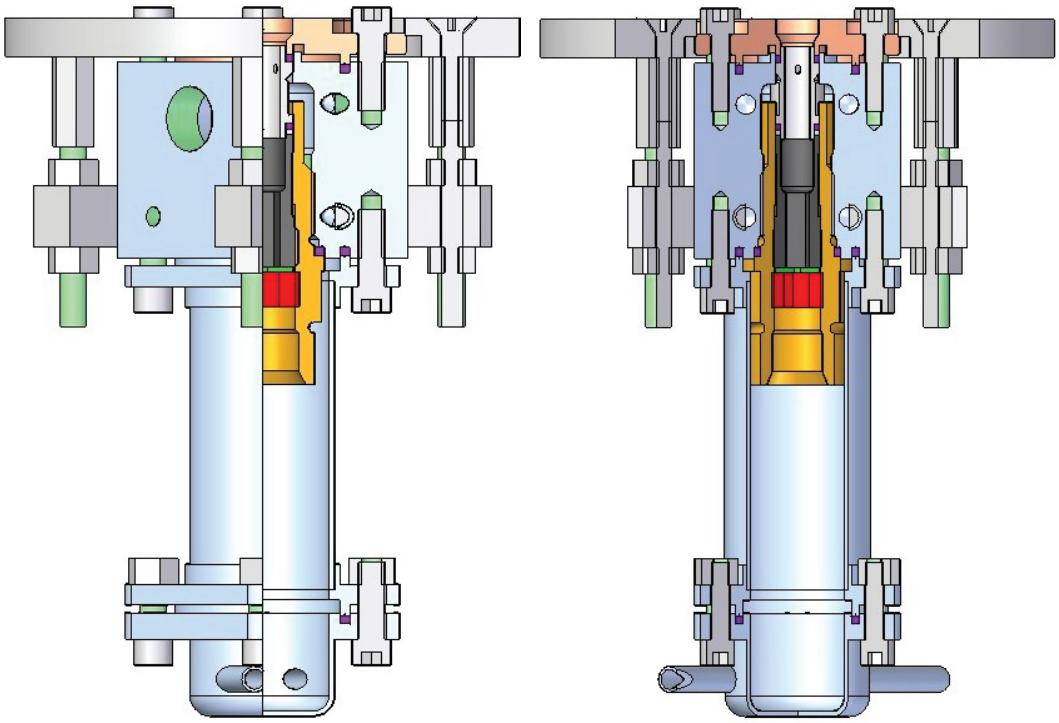

Figure 3.5: Injector Manifold with Mounting Equipment

the flow rate. The igniter is run in the rich regime to bring down the temperature of the ignition flame. The chamber has a port for the dynamic pressure transducer. This transducer is mounted into a PCB 064B06 water cooled jacket to ensure that there is no excessive heating to the instrument.

The existing test capabilities can be seen in Table 3.3. The maximum mass flow rates of the oxidizers are an order of magnitude higher than the initial design specifications. This is due to a design change applied after calculations of the requirements to scale the RD-170 injector. The high oxidizer mass flow rate will also allow scaling of oxidizer rich gas generator or preburner injectors. However, a degree of precision is lost due to the increased range. The other capabilities are similar, although the propane is above the initial design specification. This is due to the fact that the

Table 3.3: Test Facility Capabilities

	Mass Flow Rate Range [g/s]	Manifold Temperature Range [K]
Oxygen	0.02181 - 21.81	300 - 450
Air	0.01973 - 19.73	300 - 450
Oxidizer Nitrogen	0.0002 - 0.95	300 - 450
Methane	0.0001 - 0.55	250 - 450
Fuel Nitrogen	0.0002 - 0.95	250 - 450
Propane	0.0002 - 0.763	250 - 450

controllers are exactly the same, but the densities differ by a factor of three, as well as the increased propane viscosity. The temperature ranges remain to be tested except for air. The air was capable of exceeding the specified temperature with a nitrogen heater which is lower power. Therefore, there is reason to believe the temperature capabilities will exceed those specified. Upon further review of Section 2.5.1 and Section 2.5.2, it can be seen that the test facility is able to achieve volumetric flow rate and stoichiometric similarity for both case studies.

3.4 Data Acquisition and Experimental Control

Due to the fact that the experiment is supplied by the rocket test stand, control and data acquisition for both systems are required. A dual control system has been implemented to control the test stand and experiment simultaneously. The test stand is controlled by a programmable logic controller (PLC), and the experiment is controlled with National Instruments LabVIEW v8.0 software. The PLC is ideal

for test stand control due to the robust, reliable operation. LabVIEW is used for mass flow control and acquisition of all measurements.

3.4.1 Data Acquisition

The data acquisition system monitors all pertinent test stand pressures. Sixteen test stand pressure measurements are monitored and recorded. Each feedline (oxidizer main, fuel main, oxidizer ignition, and fuel ignition) has four pressure measurements: tank, dome loader, purge, and line (downstream of dome loader). Each measurement is displayed in the control room during testing to ensure proper test stand functionality. The readings are also recorded to file for subsequent troubleshooting, if necessary.

A multiplicity of readings are taken on the experiment. The first set of measurements comes from the mass flow controllers. These controllers are communicated with via RS-232 serial connection. Each controller sends five readings which include outlet pressure, outlet temperature, volumetric flow rate, actual mass flow rate and mass flow rate set point. With all five controllers, there are twenty five measurements. The next measurements are at the outlet of each heater. These temperature probes actually have two thermocouples inside of a single sheath. All thermocouples used on the experiment are K-Type. This allows a temperature reading to be sent to the data acquisition system as well as the temperature controller. Downstream of the heaters are manifold pressure and temperature measurements for both the oxidizer and fuel. The dynamic pressure transducer is located in the chamber wall two inches from the fire face. A Radio Shack 33-3026 computer microphone with a range of $30 - 15,000\,\mathrm{Hz}$

is located at the top edge of the chamber. This instrument is used as a check to ensure that the transducer is reading correctly by spectral analysis comparison. All of the steady state readings are monitored and recorded during testing. Unfortunately, the RS-232 readings are only recorded once per set point.

3.4.2 Experimental Control Sequence

The test stand and the fire valves on the cart are controlled by the PLC. A specialized program was created to control the experimental sequence. All timing values are entered prior to testing and can be ensured of proper functionality by running a test sequence with unpressurized feed lines.

A LabVIEW virtual instrument has been developed to control the mass flow controllers in addition to acquiring all measurements. The program is flexible with respect to altering the timing values. The following steps comprise the experimental sequence. The operator inputs all mass flow rate set points into an external spreadsheet. All inputs, such as injector type, propellants and injector distance from the wall, are then entered into the LabVIEW front panel. These inputs are written to the file properties, which are compatible with the National Instruments DIAdem v10.0 data analysis software developed. This data mining technique vastly decreases the data analysis time. It is also useful to future users unfamiliar with the data sets. The program is started and the filename is input as the set point spreadsheet is read in. The test stand pressure readings are displayed to ensure that the pressures are at the set values. The PLC is then activated to begin the firing sequence. A digital signal is sent from the PLC to the LabVIEW program to inform the program that the PLC

has been activated. Data recording is then enabled. Based on the timing sequence, a delay is added before setting the mass flow controllers to the ignition set points. Once the injector flow is initialized, the igniter is fired by the PLC. A typical timing sequence can be seen in Figure 3.6.

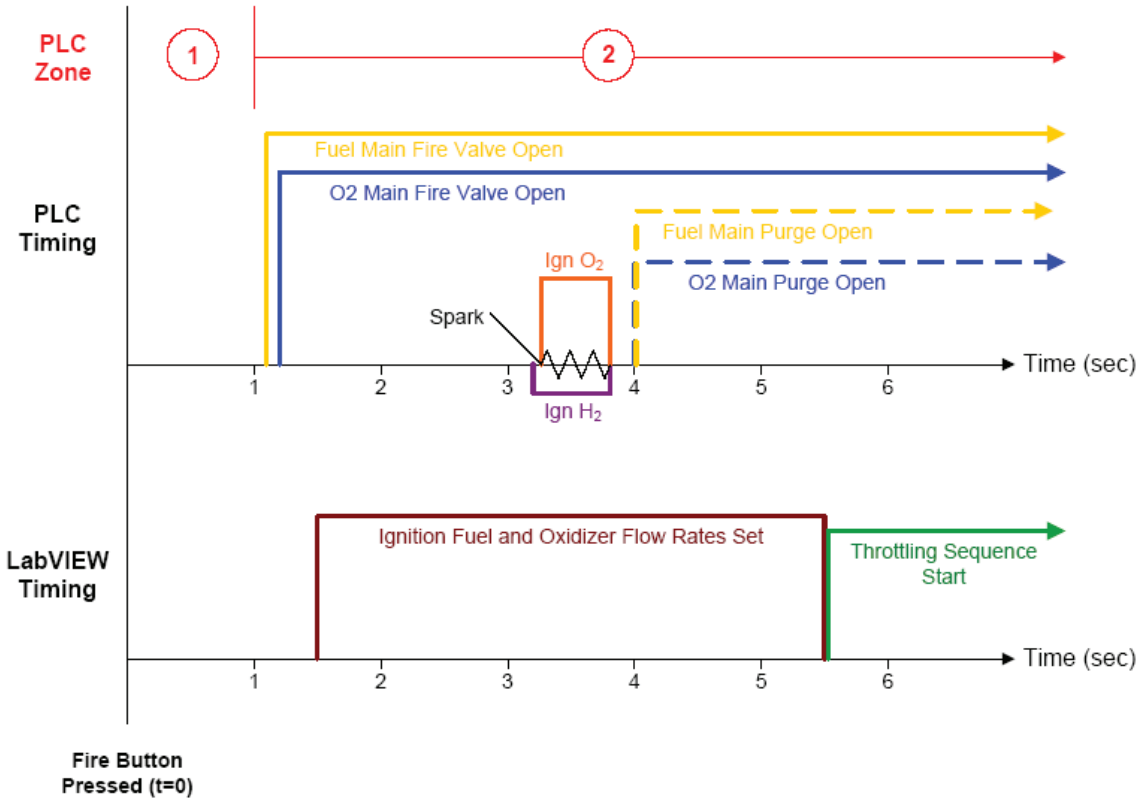

Figure 3.6: LabVIEW and PLC Ignition Timing Sequence

After an additional delay, the first throttling point is sent to the mass flow controllers. The program then checks if the actual oxidizer mass flow rate is within a set threshold of the set point. Once the set point is reached, all of the measurements are taken from each controller. The data acquisition card must then be switched from steady state to high frequency. The high frequency data is then taken from the

chamber transducer and microphone at a customizable rate and number of samples. Once the high frequency data acquisition is complete, the card is switched back to steady state reading. This throttling sequence is repeated until the final set point is complete. The program then notifies the operator that the experimental sequence is complete and it is ready for the PLC to be deactivated, which initiates the purge sequence. The program then checks for all mass flow controllers to approach zero mass flow and the set points are then returned to zero.

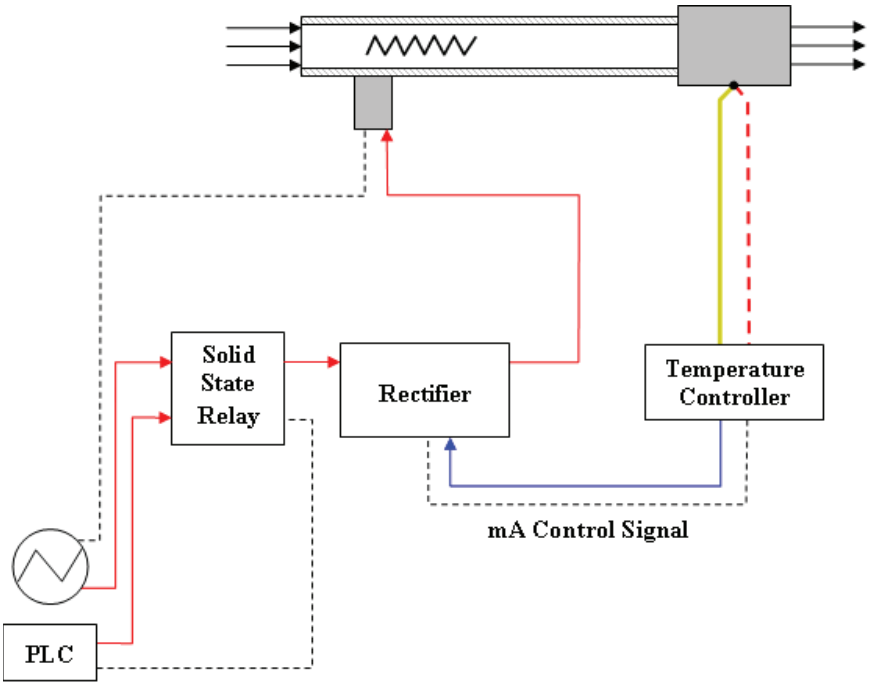

Figure 3.7: Heater Control Schematic

The heater control system operates independently from the data acquisition and described control system. A schematic of the system can be seen in Figure 3.7. The voltage for the heater is supplied through an Omega SSRL240DC25 solid state relay. The control signal for the solid state relay is the same digital signal that informs

the LabVIEW program that the PLC is active. Therefore, the heaters can only be powered while the test sequence is functional to avoid overheating with no flow. The voltage is regulated by a phase angle fired rectifier which takes the 120 volt supply voltage and allows a portion of the voltage through to the heater. The amount of voltage is regulated by the temperature controller. The controller has internal, configurable PID settings, which are optimized for an average flow rate. A 4 mA to 20 mA signal tells the rectifier what voltage is required. One of the dual thermocouples at the outlet of the heater is input to the controller to dictate the feedback. Although this is a stand alone system, set point temperatures are input to the controllers prior to firing and the rest is automated. The temperature probes at the heater outlet that go to the data acquisition system are for troubleshooting as well as an indication of how much heat is lost from the heater outlet to the manifold.

3.5 Chamber Temperature Determination

The chamber is only equipped with a single, high frequency pressure transducer; therefore, determining the mode of instability via multiple transducer phase shift is impossible. Upon analysis of the preliminary experiments, a correlation between the experimental chamber frequencies and calculated natural frequencies was not found. This problem arises from not knowing the temperature distribution of the gases in the chamber. An array of thermocouples was added to the chamber to collect data on the chamber temperature during testing. An estimate of the chamber natural frequencies can be performed by determination of the chamber temperature profile and gas composition profile. The most significant factor is chamber gas tempera-

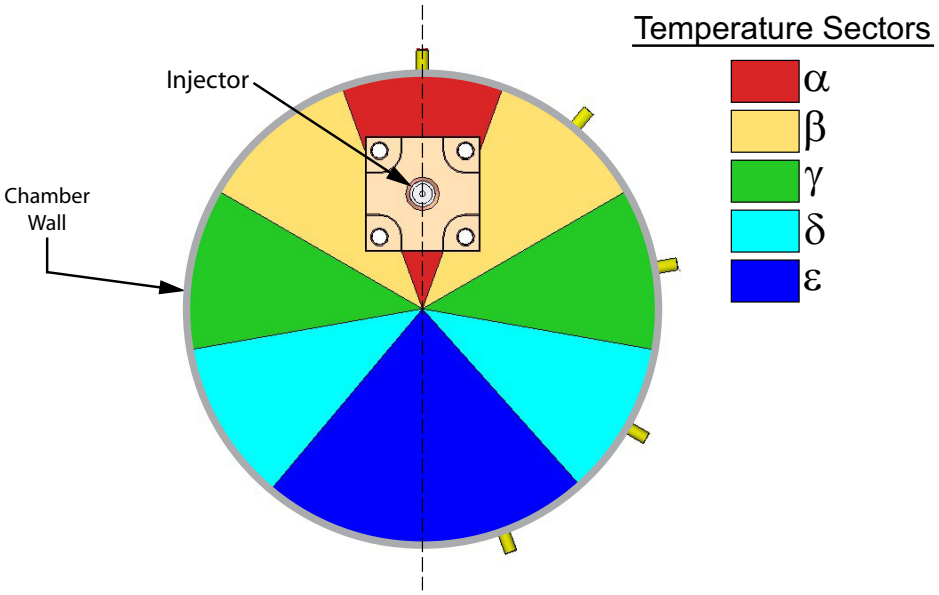

Figure 3.8: Chamber Temperature Sectors (Top View)

ture. To determine the chamber temperature, five thermocouples were systematically placed approximately 0.1 inch through the chamber wall.

The chamber was split into the five sectors shown in Figure 3.8. Each sector encompasses 80 degrees except for the α sector which is 40 degrees. K-Type thermocouples were installed 20 degrees from the boundary of each sector, which are represented as yellow posts around the right hand side periphery of the chamber in the figure. As indicated in the schematic, the chamber is assumed to be symmetric across the dashed axis.

CHAPTER 4

EXPERIMENTAL RESULTS

Following the test matrix set out, a preliminary round of experiments was conducted. All three impinging jet injectors were run. After initial data analysis, repeatability studies of the impinging jet injectors were run.

Data analysis has shown that the test apparatus is successful is creating high frequency combustion instability. The experimentation has also shown that the test method is sensitive enough to exploit stability differences in the injector fuel impingement angle.

4.1 Data Analysis Technique

Creating the data files compatible with National Instruments DIAdem v10.0 significantly reduced analysis time. The software package is ideal for repetitive analyses with report generation.

4.1.1 Operating Condition Analysis

The DIAdem operating condition analysis package manipulates all of the experimental steady state readings including mass flow rates, fuel manifold pressure

and temperature, oxidizer manifold pressure and temperature as well as the chamber sector temperatures. Mass flow rate is only sampled once per set point, so there is no manipulation of the data in the DIAdem package. The feed system readings are averaged over one second preceding the high frequency measurement. The standard deviation is also calculated over the same period. Therefore, the statistics are calculated at each set point. The random uncertainty is calculated from the standard deviation of each measurement. To determine the mass flow rate variability, video was recorded of the controller display and analyzed to estimate the random component of uncertainty in mass flow rate. The systematic uncertainty components were taken from the calibration or specification for each piece of instrumentation. Propagation of error analysis according to Coleman and Steele was applied to all parameters of interest based on a 95 % confidence interval [26]. The uncertainty analysis code developed can be see in Appendix D.

For a single test, there are thirteen values of each measurement. Similarly for the chamber sector temperatures, a temperature average is taken over the same period preceding the high frequency measurement. There is no calculation of the standard deviation of the chamber temperatures due to the approximations applied to the natural frequency analysis. This allows each mode of interest to be calculated at each set point. The data sets are then formatted to be compatible with the next operating condition analysis step.

These data sets are imported to Engineering Equation Solver (EES), which runs the flow parameter calculations to determine the possibly significant operating conditions such as momentum ratio, Reynolds numbers, propellant velocities and

volumetric flow rate. This analysis package also calculates the uncertainty with every input and output parameter. The detailed flow parameter and uncertainty algorithm can be referenced in Appendix D.

This algorithm also uses the chamber temperatures to determine the chamber natural frequencies. The following computational method was created for the experimental set up. To determine the natural frequencies, the speed of sound is fundamentally important. Equation 4.1 calculates the speed of sound in an ideal gas.

$$c = \sqrt{\gamma \frac{R\#}{MW} T}, \tag{4.1}$$

where c is the speed of sound in the gas, γ is the ratio of specific heats, $R\#$ is the universal gas constant, MW is the molecular weight of the gas and T is the temperature. The thermal environment in the chamber is quite complex. The flame is not placed symmetrically inside of the chamber and the velocity of the flame and combustion products create recirculation zones as well as entrain air. Therefore, multiple assumptions about the gas composition had to be input to the algorithm. Each sector is composed of combustion products as well as air. Percentages of combustion products were assigned to each sector. The assumed sector combustion product composition percentages can be seen in Table 4.1.

Table 4.1: Chamber Gas Composition Percentage of Combustion Products

α	β	γ	δ	ϵ
100	60	30	10	5

To obtain the molecular weight and ratio of specific heats for the combustion products, GasEQ iterations were run. GasEQ is a combustion equilibrium code that solves various propellant combinations including dissociation. The inputs to the model were a refined mesh of mixture ratios from the test matrix with methane and oxygen. A plot of the molecular weight as a function of mixture ratio was created and a polynomial was fit. The same was done for the ratio of specific heats. Weighted averages of γ and MW were then calculated based on the percentage of combustion products and air in each sector as seen in Equations 4.2 and 4.3.

$$\gamma_{sector} = (Gas\%)\gamma_{prod} + (1 - Gas\%)\gamma_{air}. \tag{4.2}$$

$$MW_{sector} = (Gas\%)MW_{prod} + (1 - Gas\%)MW_{air}. \tag{4.3}$$

The speed of sound of each sector was then calculated with the corresponding temperature and gas composition characteristics. To obtain the average speed of sound in the entire chamber, the individual speeds were averaged based on the sector portion of the chamber. For example, the β sector is 80 degrees; therefore, it comprises 22.2 % of the chamber. The detailed code can be referenced in Appendix D.

4.1.2 Frequency Analysis

The second DIAdem analysis algorithm manipulates the chamber dynamic pressure measurements. The key aspects of the analysis sequence can be seen in Figures 4.1 and 4.2.

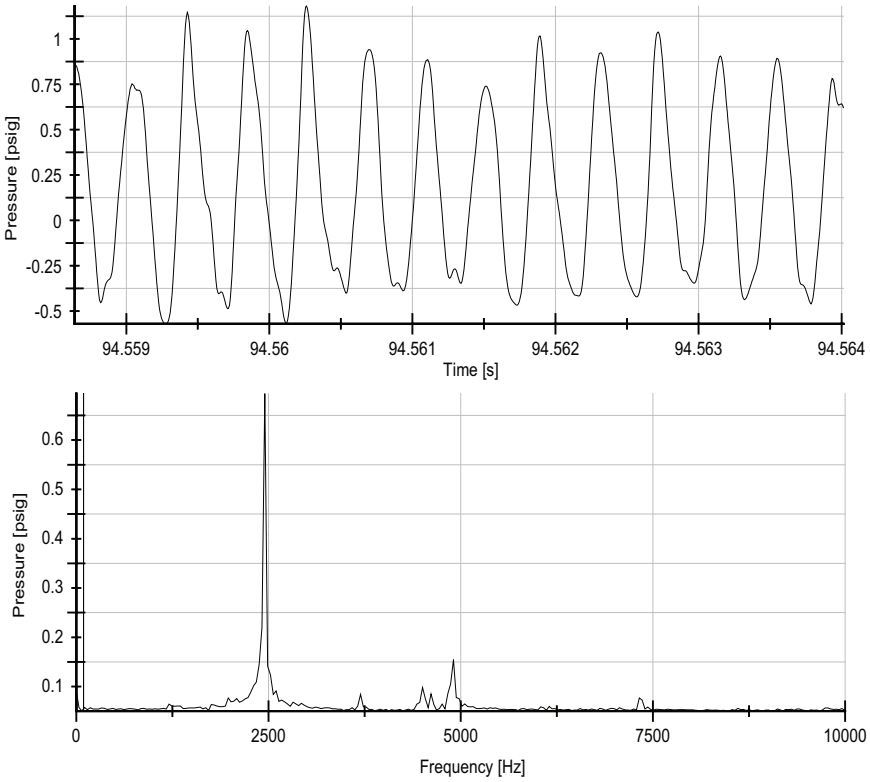

Figure 4.1: Time Domain to Frequency Domain Conversion

The first script of the program loads all nine test data files to a single data set. This allows a complete test session or test matrix for a single injector to be analyzed at the same time. The second script performs a Fast Fourier Transform (FFT) on every set point time domain dynamic pressure measurement as in Figure 4.1. The built in DIAdem FFT function performs the time domain to frequency domain conversion. The frequency domain amplitude is converted as peak amplitude, not peak to peak or logarithmic. Each high frequency set point measurement is five thousand samples, at a sampling frequency of 150 kHz. The data acquisition system also employs an anti-aliasing Butterworth filter with a cutoff frequency of 20 kHz. The conversion is a true FFT; therefore, only 4096 of the 5000 samples are taken into account.

The third script creates waterfall plots for each test run as well as an FFT plot of each set point. The data mining capabilities allow the plots to be customized with injector type, injector location in chamber, the test date, experimental operator, and the mass flow rates of the fuel and oxidizer. The final function of this algorithm is searching for peaks. A frequency range is input into the program, and the maximum amplitude for each set point is output. These amplitudes are necessary for stability mapping. All of the preceding frequency analysis scripts are included in the RUSKIE analysis package created by Erik Lee.

The final DIAdem program looks at the energy associated with the FFTs as well as further peak searching capability. A diagram of the key parameters can be seen in Figure 4.2.

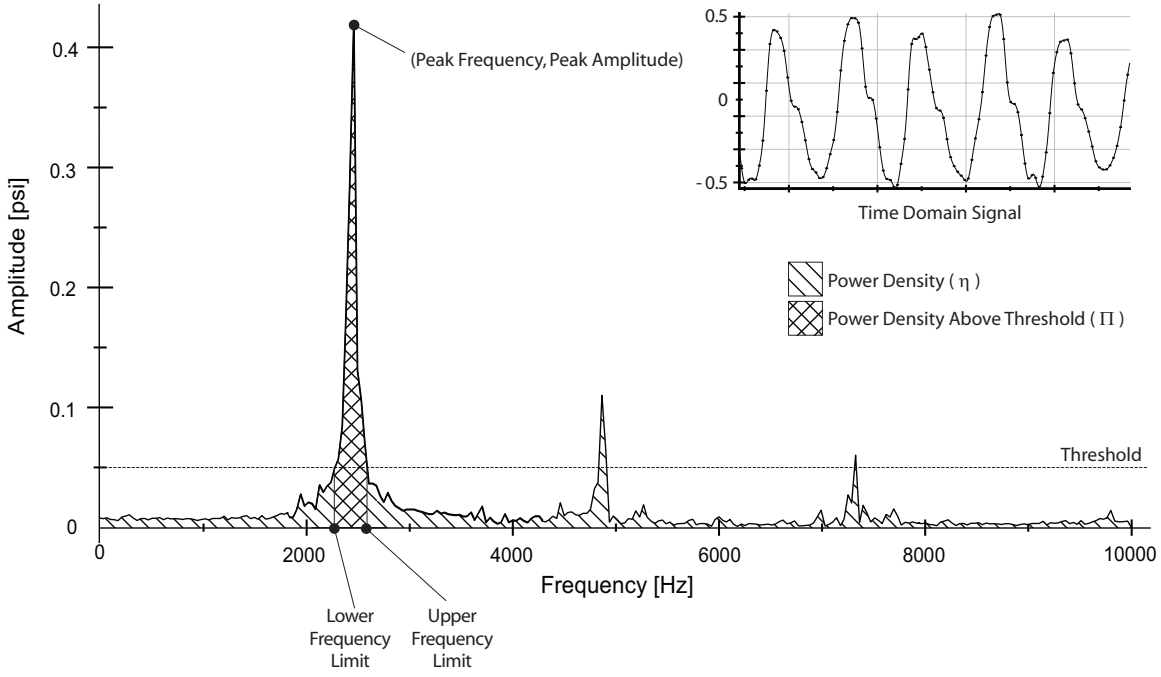

Figure 4.2: Frequency Analysis Example

First, the algorithm integrates across each FFT as in Equation 4.4.

$$\eta = \int P \cdot df, \tag{4.4}$$

where η is the power density $\left[\frac{kW}{m^3}\right]$, P is the FFT pressure magnitude $[Pa]$, and df is the frequency increment $[Hz]$. The indefinite integral is evaluated from 0 Hz to 20,000 Hz, or the cutoff frequency. This integration gives the power density associated with each set point. The program also outputs the maximum peak frequency which corresponds to the peak frequency from the previous code. An additional feature searches for peaks that are above a user defined threshold. As shown in Figure 4.2, the threshold is set at 0.05 psi. The dominant peak at 2400 Hz is considered to be a peak, and the area is integrated as in Equation 4.4 between the lower frequency limit and upper frequency limit. The harmonics at 4,800 Hz and 7,200 Hz are not considered to be above the threshold in this case. This is due to the definition of a peak with respect to the threshold. The algorithm scrutinizes each frequency/amplitude index by evaluating the relationships between the current point, the surrounding three points and the threshold. The application of such a peak criteria is to avoid picking up noise or avoiding peaks that are only above the threshold for a single point. The outputs of the script are number of peaks above a user defined threshold, the upper and lower frequency limits for each peak above the threshold, the power total power (η), the power within the peaks above the threshold (Π), and the percentage of power in the peaks (η_{peak}) given by Equation 4.5.

$$\eta_{peak} = \frac{\Pi}{\eta}. \tag{4.5}$$

All of the script files can be referenced in Appendix G.

4.1.3 Stability Mapping Analysis

With the amplitudes and operating conditions determined, the ultimate analysis goal of the methodology can be realized via stability mapping. The advantage to stability mapping lies in the graphic representation of the chamber response as a function of important operating parameters. A stability map is a graphical depiction of the stability of the system with respect to two system parameters. Either axis can be an independent or dependent variable. The third axis is the chamber response, typically the dynamic chamber pressure with respect to a set threshold. Figure 2.2 is a stability map with a set threshold to define the unstable region from the stable region. This threshold is dependent upon the application. To improve upon this, the use of color mapping allows the user to define the threshold level. A MATLAB code was created to plot the stability maps. The plotting code can be referenced in Appendix G. A refined mesh was created and the data points are linearly interpolated between. The surface is forced to go through each real data point.

4.2 High Frequency Combustion Instability

As stated in Chapter 1, there are three signature characteristics of high frequency combustion instability. The three factors are manifold pressure fluctuations,

increased heat release, and chamber pressure oscillations. Firing of the impinging jet injectors was successful in displaying all three characteristics. The data presented in this section is from Test Session 30-3.

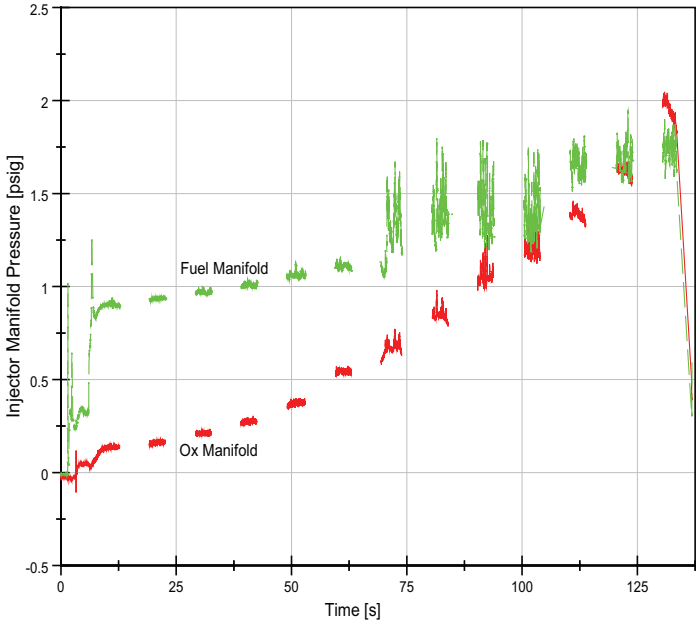

Figure 4.3: Typical Manifold Pressure Variation (Test 30-3-4.0)

An example of typical injector manifold pressure spikes can be seen in Figure 4.3. The data is taken from Test 30-3-4.0. The pressure traces show many interesting factors. As described by the test matrix, the fuel mass flow rate is held constant at 0.44 g/s. The graph shows that the pressure is increasing as the oxygen is being throttled. This is due to the non-traditional impingement position of the fuel. In customary impinging jet injectors, the streams meet in the chamber, where the pressure is nearly constant. In this case, the fuel is injected into the oxidizer post.

Therefore, as the pressure drop of the oxidizer increases, the fuel pressure must also increase to ensure constant fuel mass flow rate.

The gaps in the pressure curves are due to the data acquisition card switching. This inconvenience will be addressed in Section 5.2. The interesting aspect of Figure 4.3 is in the pressure fluctuation that occurs during oxygen throttling. As the oxidizer mass flow rate increases from the initially rich conditions, the manifold pressures show negligible fluctuation on the order ± 0.05 psig. Once the mixture ratio becomes stoichiometric, the pressure in the manifold widely varies. The fuel manifold fluctuations are nearly 0.5 psig, which is 33 % of the total pressure drop. The three subsequent mass flow rate set points vary similarly in amplitude. Unfortunately, the static pressure transducers are unable to pick up any coherent frequencies, if indeed they exist. The last three lean set points have smaller amplitudes, but are significant in comparison with the rich conditions. This will later be shown to correlate with the excited chamber frequency.

The second sign of high frequency combustion instability is increased heat release. The chamber temperature profile from Test 30-3-4.0 can be seen in Figure 4.4. The first three seconds show the temperature profile before ignition, which are in the order one would expect: α sector as the hottest and decreasing around the chamber to ϵ sector as the lowest. The igniter is activated at 3.3 seconds and increases the temperature. By the second set point, the temperatures have leveled off to a nearly steady temperature. The rich set point temperatures are above the initial temperatures which indicates that the gas temperature is higher than the chamber wall temperature. As previously shown with manifold pressure, there is a significant

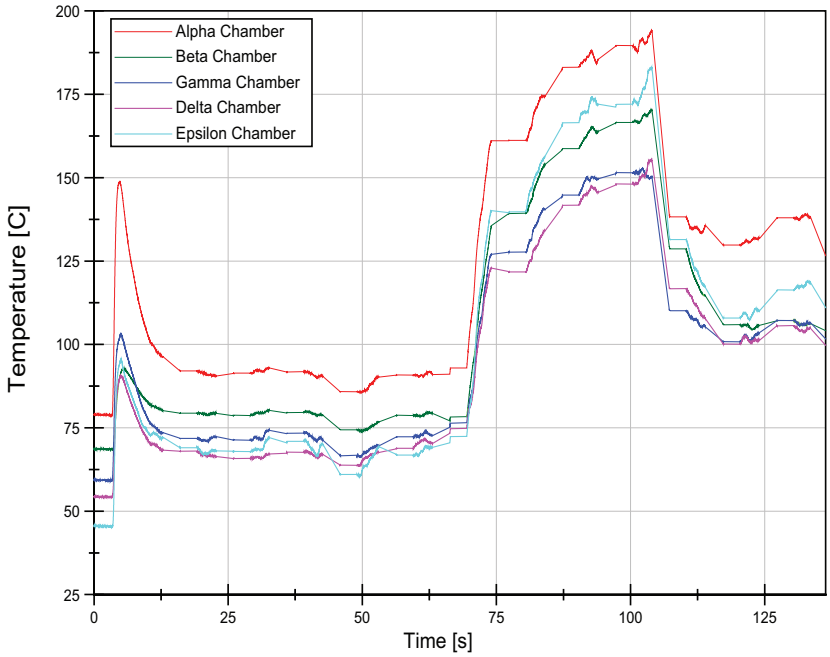

Figure 4.4: Typical Chamber Temperature Profile

deviation at the stoichiometric set point. The temperatures nearly double from the rich temperature. With this transition comes a change in order. The farthest sector away from the flame quickly becomes the second highest temperature. This phenomenon is a function of the flame action as well as the instability mode the chamber is experiencing. Again, as in the pressure manifold variation, the system transitions to a new regime for the final three lean set points. The temperatures are above those in the rich region, but not as extreme as the previous four set points.

The third, and most important factor, with respect to identifying high frequency combustion instability is the dynamic chamber pressure. A portion from the high frequency pressure transducer recording at the stoichiometric set point can be seen in Figure 4.5. Each circular marker indicates a data point. The peak to peak

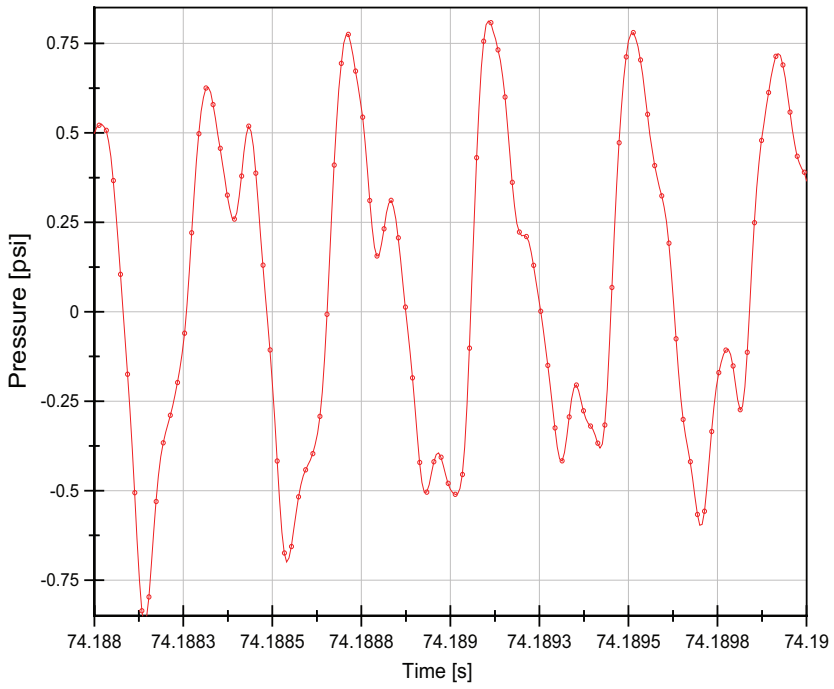

Figure 4.5: Typical Chamber Pressure Fluctuation (Test 30-3-4.0-1.0)

pressure is roughly 1.5 psi. This gives a ratio of peak to peak pressure to mean chamber pressure of 10 %. This percentage is beyond the instability thresholds suggested by the Chemical Propulsion Information Agency [19]. The chamber pressure trace has many interesting aspects. The waves are relatively smooth, but not sinusoidal. The shapes of the waves are due to an excited fundamental frequency as well the harmonics associated with that natural frequency.

By applying Fast Fourier Transform (FFT), the components of the wave can be determined. A waterfall plot of Test 30-3-4.0 can be seen in Figure 4.6. The fuel rich set points all have relatively low amplitudes near 2,500 Hz. At the stoichiometric set point, the amplitude increases with the same frequency. This frequency is sustained at the next two set points with different amplitudes. Then, there is a distinct shift

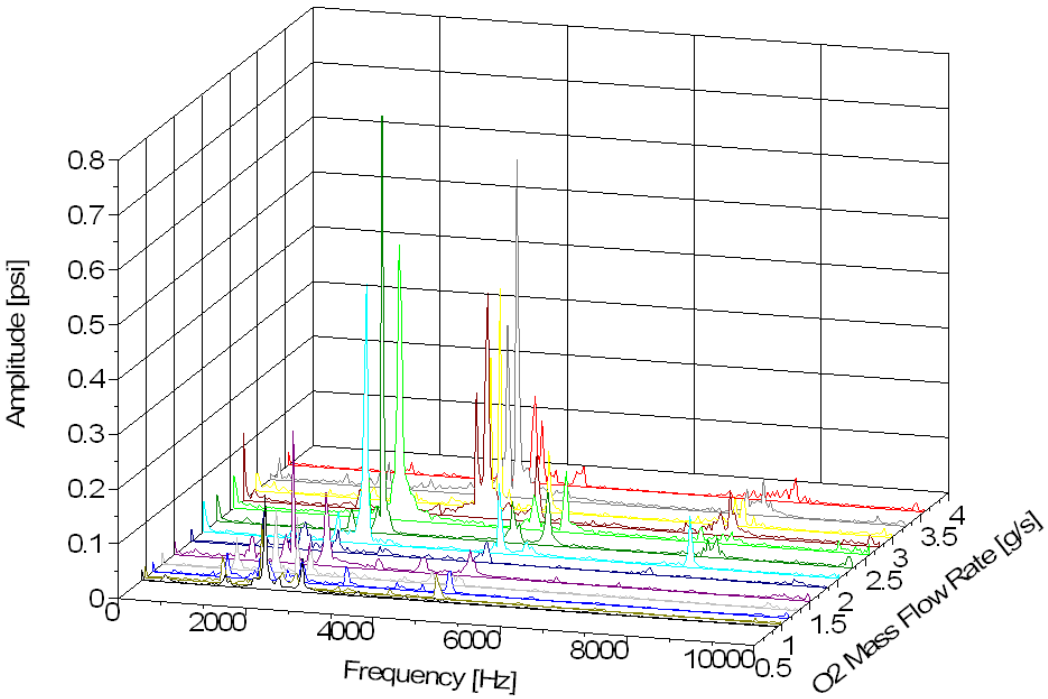

Figure 4.6: Test 30-3-4.0 Waterfall Plot

in frequency from 2,500 Hz to 4,000 Hz. The effect of this frequency shift has been noted with the manifold pressure and chamber temperature traces.

This example of high frequency combustion instability is typical of any test that encountered instability. The maximum fundamental mode dynamic pressure to mean pressure ratio from all testing was found to be 17 %.

4.3 Repeatability and Variation

Due to the unsteady nature of the phenomena under investigation, repeatability has been a significant challenge in instability research throughout history. This fact promotes necessity of any instability testing to be repeated. The entire test matrix was run on each impinging jet injector on four separate occasions. The following

graphs are stability maps for the forty-five degree impinging jet injector each day of testing. The amplitude criterion is the maximum amplitude between 100 Hz and 20,000 Hz. All uncertainty bars shown are consistent with a 95 % confidence interval from propagation of error analysis with systematic and random uncertainty components, which was described in Section 4.1.1. This is true for all stability plots shown in the subsequent sections. The four following stability maps are from each of the four test sessions.

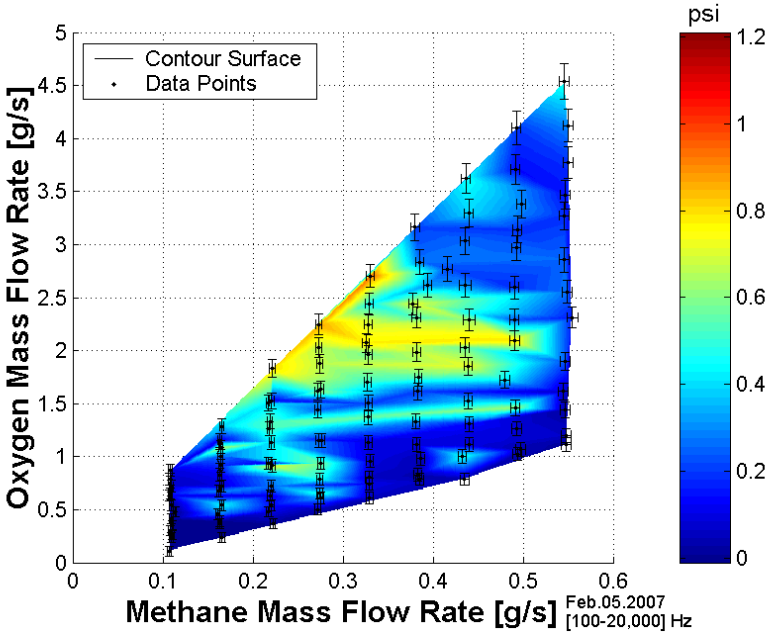

Figure 4.7: 45-1 Amplitude Stability Map

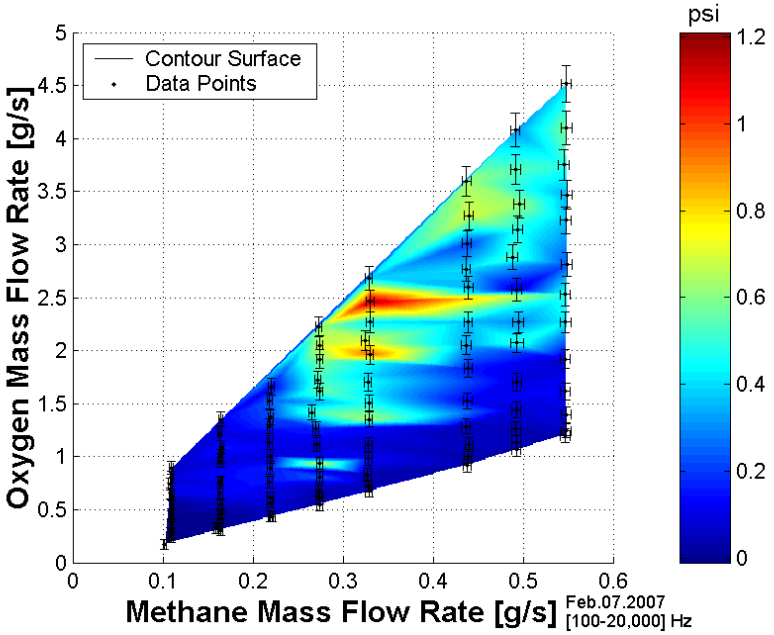

Figure 4.8: 45-2 Amplitude Stability Map

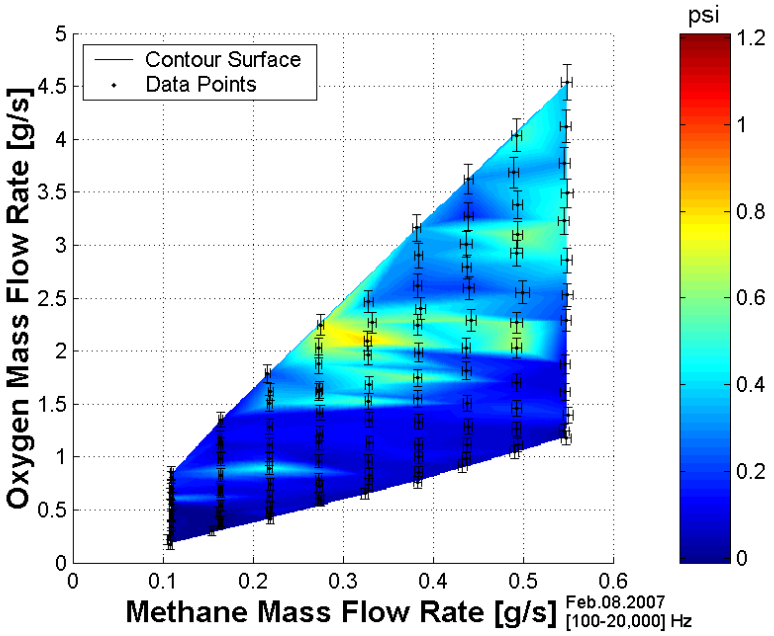

Figure 4.9: 45-3 Amplitude Stability Map

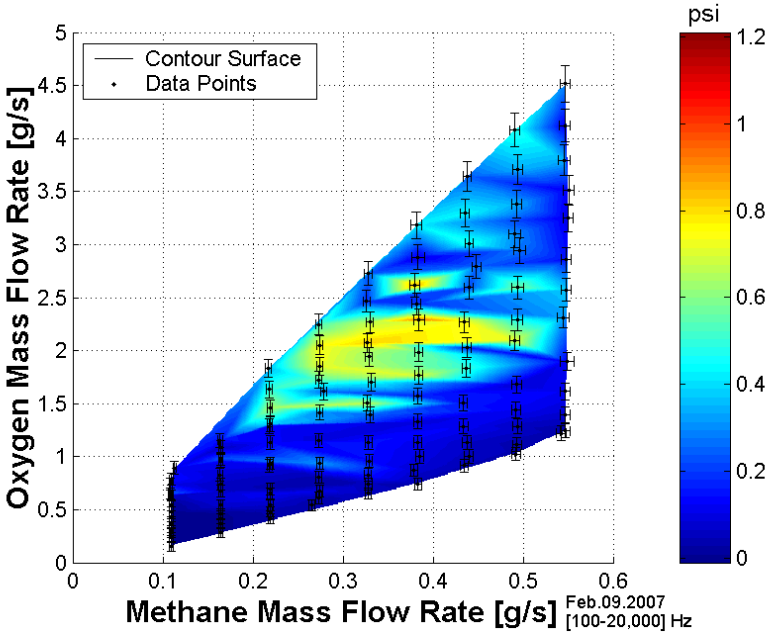

Figure 4.10: 45-4 Amplitude Stability Map

By visual comparison of all four maps, it is apparent that the troublesome area is consistently in the same general region. A box between 1.25 g/s and 2.50 g/s of oxygen and 0.2 g/s and 0.5 g/s of methane covers the high amplitude instability area of each test session. There is marginal instability near 0.5 psi which exists in the lean portions of the highest fuel mass flow rates except on February 5th. It should also be mentioned that all four maps have identical color scales. Therefore, the amplitude magnitudes were relatively consistent from test to test.

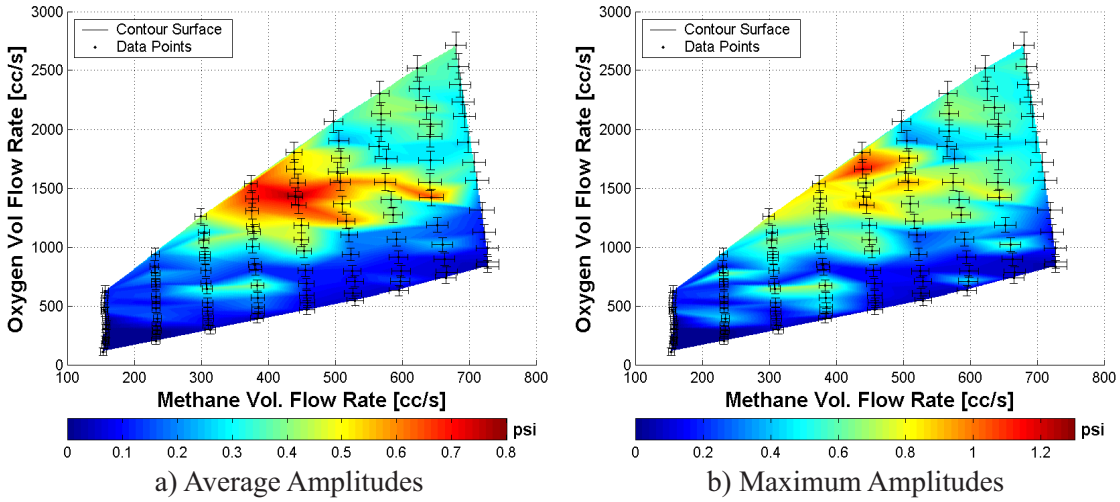

Figure 4.11: Forty-Five Degree Impinging Jet Stability Maps (All Frequencies) [a)Four Test Session Average, b)Four Test Session Maximum]

Figure 4.11 shows the average and the maximum amplitude maps for the four test sessions. The maximum values indicate the worst case scenario for the forty-five degree injector. In comparing the two maps, it is apparent that the regions are quite similar in location and relative amplitude. However, the scales of the two maps are different, the average magnitudes must increase 150 % to match the maximum amplitude map.

The variation in location, appearance and strength of the instability regions is an indication of the variability of the process itself. The test footage shows flame structure bifurcation. The bifurcation is apparent in the audible signal, and therefore will add uncertainty in the data since high frequency chamber pressure measurements are sampled for only 0.0333 seconds per set point. Therefore, the small sampling time will only capture a portion of the bifurcation and cannot show that there are multiple modes of instability present or a single mode and stable operation at a single set point. In an attempt to help quantify this, a map of the amplitude deviation was created, shown in Figure 4.12.

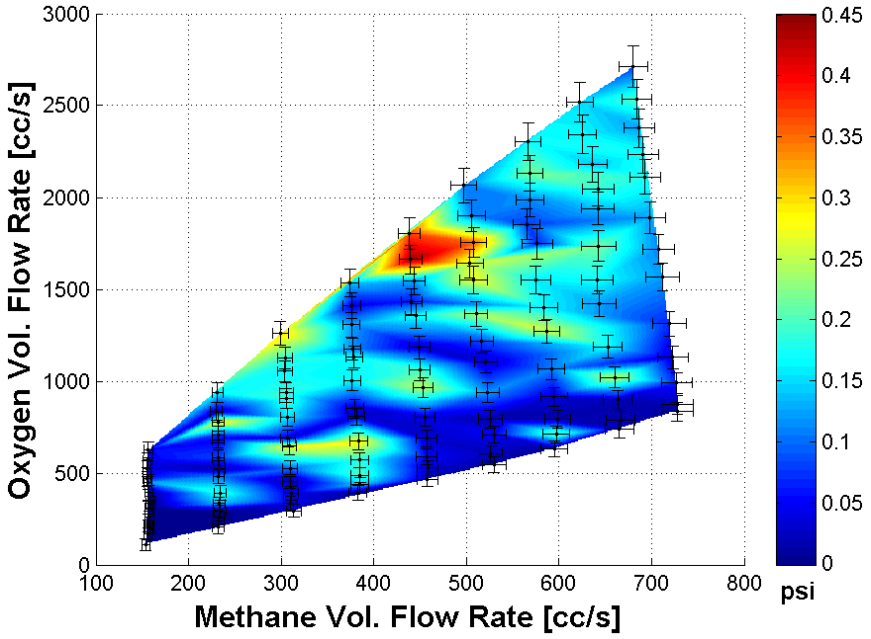

Figure 4.12: Forty-Five Degree Impinging Jet Deviation Stability Map

The highest deviation region is in the high amplitude region which specifies that the amplitude varied from session to session. If the region of high standard deviation encompassed the high amplitude region from the maximum amplitude map,

it would be apparent that the onset of instability or transition to instability was shifted from day to day. This is not the case, the deviation amplitudes seem to be largely randomly located. Therefore, it is impossible to determine from this graph if the deviation is from the unstable amplitudes differing or from the session to session appearance of instability. One point to be taken from the graph is the relatively low deviation amplitude scale.

4.4 Impinging Jet Injector Stability

This section describes the similarities and differences among the three impinging jet injectors. The first section specifies the accuracy of determining the modes of instability present in the chamber. The following sections describe the results of the stability mapping as well as flame peculiarities.

4.4.1 Identification of the Modes of Instability

By matching the observed peak frequencies to the calculated frequencies, it is possible to determine the mode of instability present in the chamber. Predicting the mode of instability is essential to understanding the processes occurring in the chamber. Barrere's equation was applied to calculate the various acoustic modes and can be seen in Equation 4.6.

$$f_{m,n,q} = \frac{c}{2}\sqrt{\left(\frac{2a_{mn}}{d}\right)^2 + \left(\frac{Q}{L}\right)^2} \tag{4.6}$$

$m \neq 0 \quad n = 0 \quad Q = 0$ radial mode
$m = 0 \quad n \neq 0 \quad Q = 0$ tangential mode
$m = 0 \quad n = 0 \quad Q \neq 0$ longitudinal mode.

This equation incorporates the Bessel function zeroes (Q and a_{mn}) [27]. The testing displayed consistent results with respect to when certain modes were excited.

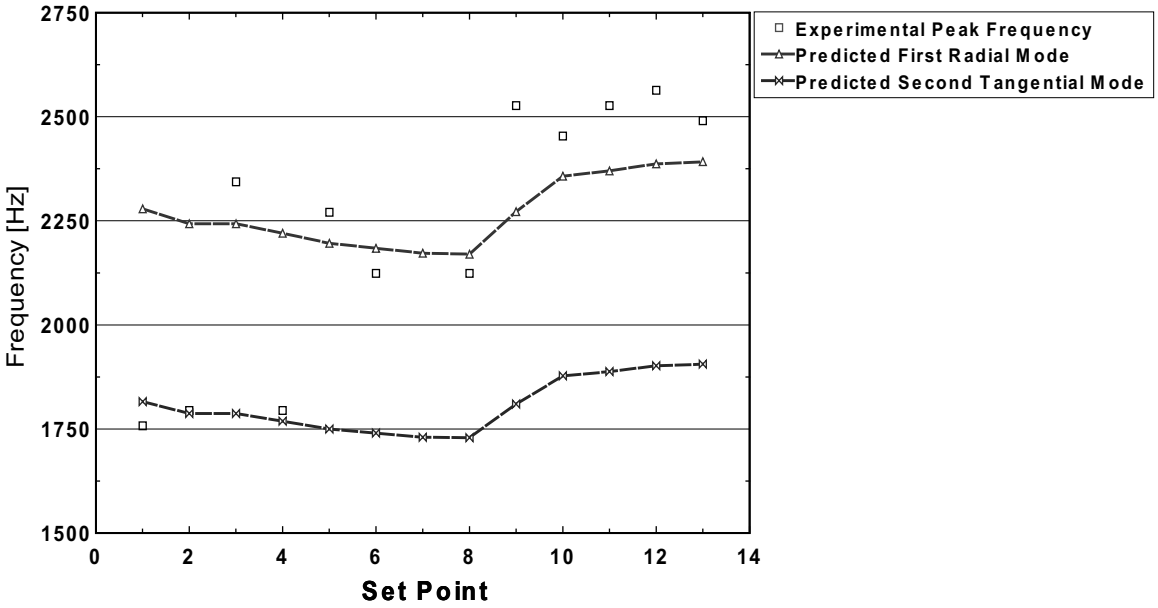

Figure 4.13: Test 30-3-3.0 Mode Prediction

Figure 4.13 shows the comparison of experimental peak frequencies to the chamber natural frequencies calculated for Test 30-3-3.0. In looking at the experimental and predicted data points, it is possible to determine which modes of instability are excited. At set points one, two and four, the experimental peak frequency matches the second tangential mode. Although, at set point three the frequency transitions to the first radial mode. After the fourth set point, the radial mode is steadily present except for the stoichiometric set point. The temperature shift is also evident, and in agreement with predicted and experimental data points. The first radial mode decreases up to set point eight and increases sharply. There is excellent agreement between the experimental peak frequencies and calculated values with respect to mode

frequency shift. It should also be noted that it is anticipated that the temperature probe position give a low representation of the sector temperature; therefore, the low estimation of frequency is acceptable.

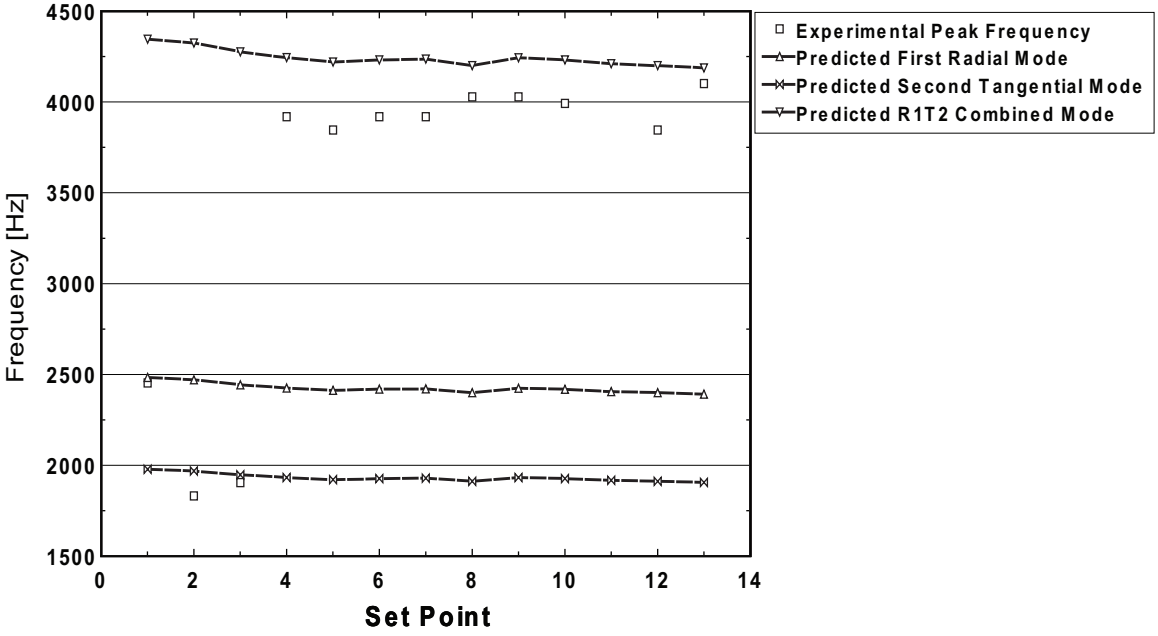

Figure 4.14: Test 30-3-5.0 Mode Prediction

Figure 4.14 is from the same data set, but at the maximum methane mass flow rate (Test 30-3-5.0). The first set point excites the first radial mode and transitions to the second tangential mode for set point two and three. Beyond the third set point, the two modes are combined, besides the outlier point at 11. This case has two differences in the mode prediction from Test 30-3-3.0. The frequency shifts are not predicted by the model and the frequencies are consistently over predicted. The flow conditions are certainly different from the pure mode case, which could transfer the heat differently. Another cause would be the nature of the experimental combined mode. The combined mode manifests itself as a broad peak, in fact, much like

two peaks competing at nearly the same frequency. For this case, the experimental peak frequency may be represented by a small range rather than a single point. By taking the wide peak into consideration, it may be possible to match the frequency shift. Another consideration to be taken into account is the fact that the low amplitude pulsations, which are generally present in the rich conditions, are well matched. Therefore the model works well for all pressure amplitudes, not only the well defined, high amplitude peaks. Overall, there is satisfactory agreement and consistency to be a practical model to determine the excited chamber mode.

The results may be surprising due to the fact that the methodology is proclaimed to excite the tangential mode of instability. After analyzing the injector position in the chamber, it is apparent that the expected modes were excited. Without the use of a radiative or water cooled chamber, the risk of burning through the chamber wall needed to be minimized. Therefore, the injector was placed 2.5 inches from the chamber wall. When taking into account the diameter of the chamber, 8 inches, it is apparent that the injector is closer to the pressure antinode of the radial mode. This injector placement is the reason for exciting the first radial mode of instability as opposed to the first tangential mode. This shift in mode has been shown in the frequency spectrum in Figure 4.6.

The modes of instability presented here represent the typical transitions experienced with the other impinging jet angles. In general, the thirty degree impinging jet sharply transitioned to the combined mode, the forty-five degree impinging jet transitioned roughly, and the sixty degree impinging jet was extremely rough. This transition occurred with increasing fuel mass flow rate, and therefore increased heat

release and volumetric flow rate. It must be mentioned that the complex temperature gradient in the chamber is capable of creating abnormal acoustics. The mode shapes may be distorted, and the calculations are for a uniform temperature. Therefore, the predicted results are the most likely modes present. The only way to truly determine the modes is with multiple dynamic pressure transducers in the chamber.

4.4.2 Stability Mapping - All Frequencies

The data presented in this section is derived from four individual test sessions for each injector. The operating conditions and amplitude components were all averaged and searched for maximums. The averaging function creates a more continuous surface and the maximum map represents the worst case scenario. The color scales are properly bounded to allow comparison between injectors as well as to give sufficient detail of the instability region. The frequency range that was searched through to determine maximum amplitudes was 100 - 20,000 Hz. This range is near the minimum frequency and up to the Butterworth filter cutoff frequency.

The first set of maps can be seen in Figure 4.15. Graph a) is the average amplitude values, and b) is the maximum amplitude values, which is consistent for all maps in this section. The average map shows that there is a well-defined region of high amplitude instability in the lean, central region. The lean region between Tests 4.0 and 5.0 is consistently near 0.4 psi. In comparing the average and maximum amplitudes, the regions are very similar, which shows that the trends from test to test are not erratic.

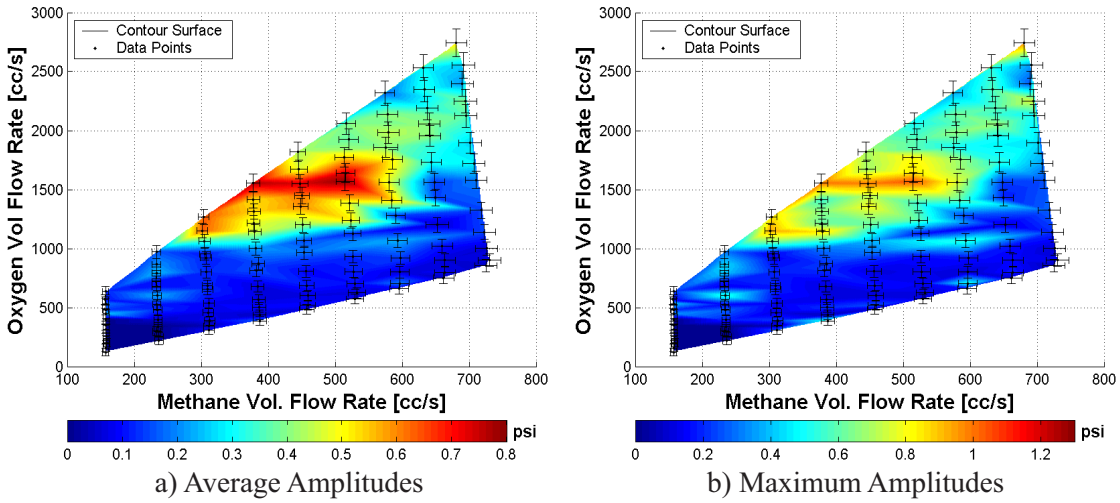

Figure 4.15: Thirty Degree Impinging Jet Stability Maps (All Frequencies) [a)Four Test Session Average, b)Four Test Session Maximum]

The stability maps for the forty-five degree impinging jet can be seen in Figure 4.16. These maps show similar results to the thirty degree impinging jet injector. The high amplitude region is in the same position and similar in size. The lower amplitude region in the upper right hand corner is also present and consistent. There are two significant differences between the two injectors. The first is the spreading of the central instability region with the forty-five degree injector. This spreading is not only in the maximum, but also the average. The spreading could be due to two different mechanisms. The first is a hard transition whose position is inconsistent from run to run. The other possible mechanism is a smoother transition to high amplitude pulsations in comparison to the thirty degree impinging jet injector, which has a much harder transition near stoichiometric conditions. In review of Section 4.3, the later explanation is most likely. The second difference is in the moderate instability

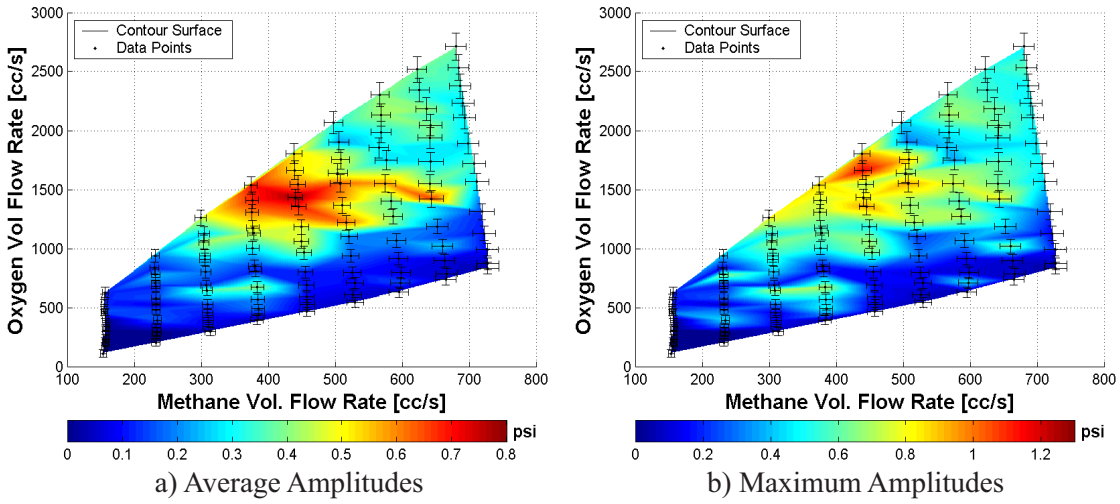

Figure 4.16: Forty-Five Degree Impinging Jet Stability Maps (All Frequencies) [a)Four Test Session Average, b)Four Test Session Maximum]

amplitude present in the rich region of operation. The thirty degree impinging jet has a well-defined boundary, which is absent in the forty-five degree impinging jet.

The sixty degree impinging jet injector shows a different picture than the previous impingement angles. The stability maps for the sixty degree impinging jet can be seen in Figure 4.17. In this case, the most troublesome region is concentrated in the lean, high fuel flow rate portion of the test matrix. The high amplitude region has merged with the moderate amplitude region common from the past two injectors. The spreading present in the forty-five degree impinging jet is also apparent in the sixty degree impinging jet, even into the fuel rich operating conditions.

The stability mapping technique has shown that there are obvious differences in the impingement angle of the fuel with respect to the combustion chamber response. These maps show the region of severe stability and allow any user to define the threshold of instability individually. There is a limit to how this large bandwidth can

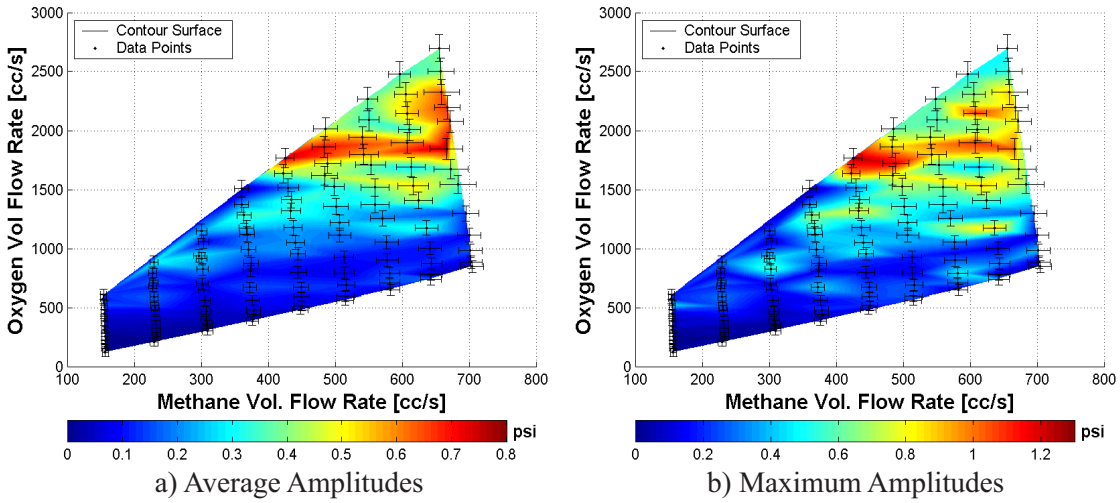

Figure 4.17: Sixty Degree Impinging Jet Stability Maps (All Frequencies) [a)Four Test Session Average, b)Four Test Session Maximum]

be used as a design tool. If the designer is only concerned about the quantitative amplitude, this presentation of the data is sufficient. Although, further application of the stability mapping technique can offer much more insight into the modes of instability.

4.4.3 Stability Mode Mapping

In order to scrutinize the modes of instability that are excited, it is possible to apply mapping with a smaller frequency bandwidth. By calculating the natural frequencies of the chamber, it is possible to segregate the regions of instability from the complete bandwidth to a narrow bandwidth centered on the particular mode of instability that is of interest. The comparison of the overall bandwidth map to the narrow bandwidth map will show where instability mode transitions exist. In

this case, the most prevalent modes, first radial and combined first radial, second tangential are investigated.

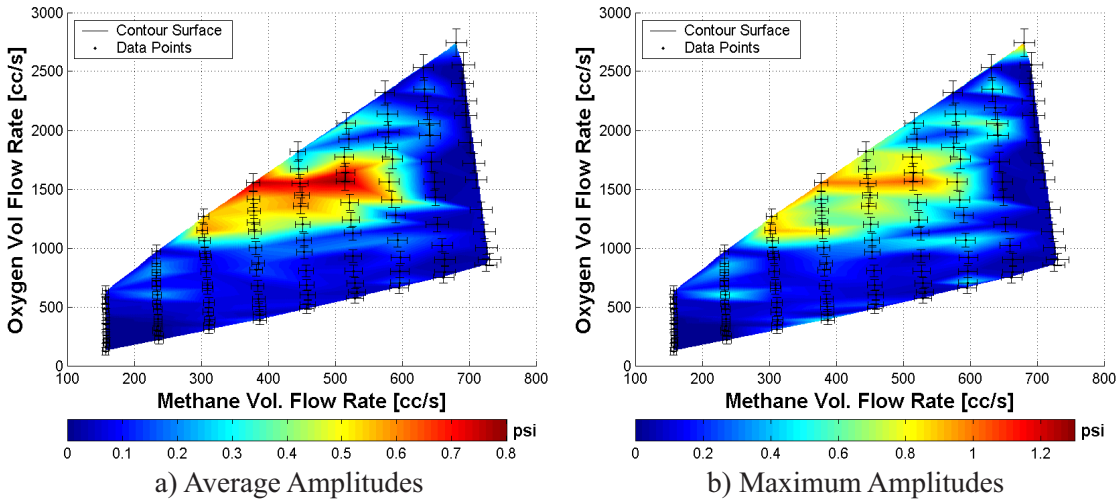

Figure 4.18: Thirty Degree Impinging Jet Stability Maps (radial) [a)Four Test Session Average, b)Four Test Session Maximum]

Figure 4.18 is the stability map created by amplitude searching between 2,000 Hz and 3,000 Hz. This bandwidth was selected due to the radial mode of the chamber. The range is relatively large due to the fact that the temperature of the chamber varied and therefore so did the radial frequency. Figure 4.18 shows that the radial region is the highest amplitude area.

Figure 4.19 shows that the combined mode is present in the lean, high methane mass flow rate region. To ensure that these are the only dangerous modes, comparison of the radial and combined modes with Figure 4.15 is required. All regions of significant instability are accounted for. These results are consistent with the waterfall plots of the individual tests.

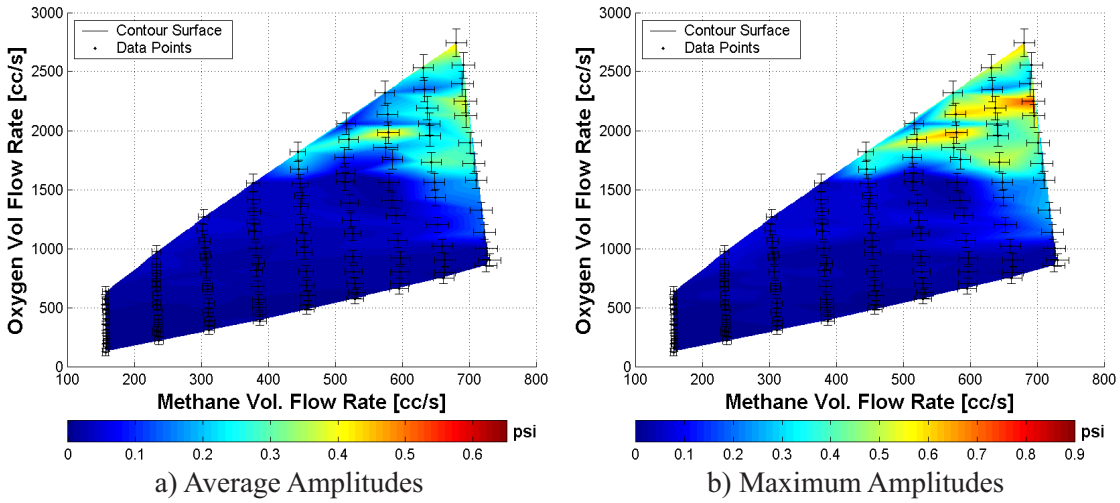

Figure 4.19: Thirty Degree Impinging Jet Stability Maps (combined) [a)Four Test Session Average, b)Four Test Session Maximum]

Figure 4.20 is the radial map for the forty-five degree impinging jet injector. Again, this figure shows that the same region exists from the thirty degree impinging jet injector. There is significantly more spreading especially in the maximum map.

The first radial, second tangential mode can be seen in Figure 4.21. This map definitively shows that the instability region is in the lean, high fuel mass flow rate region. The results for the thirty degree impinging jet and forty-five degree impinging jet show similar trends.

The sixty degree impinging jet injector mapping shows a much different picture. Figure 4.22 is the map of the radial mode. It is obvious that the radial mode is not as prevalent in this injector. In comparing the maximum and average maps, it is seen that the one instance on high amplitude instability near the end of Test 3.0 and 3.5 on the right has been significantly averaged down on the left. This indicates that

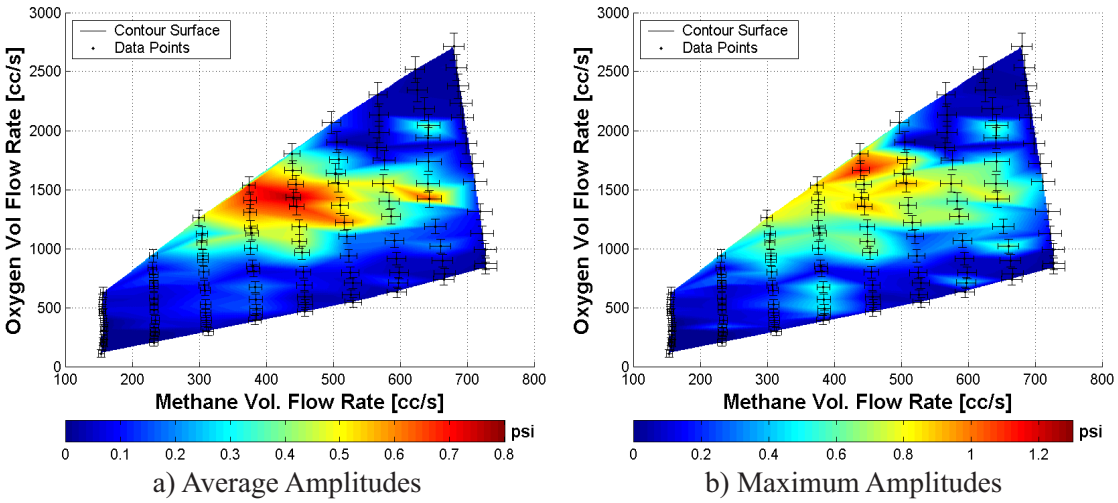

Figure 4.20: Forty-Five Degree Impinging Jet Stability Maps (radial) [a)Four Test Session Average, b)Four Test Session Maximum]

out of the four test sessions, the radial mode appeared above 1 psi only once. This is also supported in the review of individual test session maps.

The combined mode of the sixty degree impinging jet injector can be seen in Figure 4.23. It is apparent from this graph that the combined mode of instability appears in the same region for all injectors. Although, the sixty degree impinging jet injector has significantly higher amplitudes.

The application of the mode stability mapping has multiple advantages. If the nominal operating condition is near a region of instability, the mode can be identified. The second is if there are multiple modes present, the transition regions can be identified. This is important if the nominal flight operation is near an area of transition. If the injector design is already finalized, acoustic absorption devices may be required. This technique will show if the devices need to be tuned to a single frequency or multiple. Using the forty five degree impinging jet as an example, if the

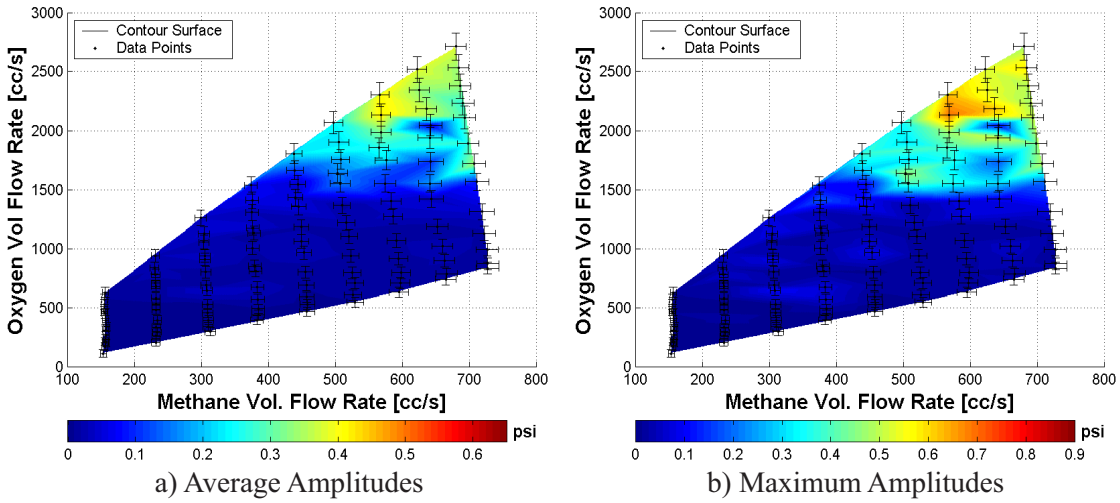

Figure 4.21: Forty-Five Degree Impinging Jet Stability Maps (combined) [a)Four Test Session Average, b)Four Test Session Maximum]

designed flight conditions are at 400 cc/s of fuel, and 1000 cc/s of oxidizer, acoustic cavities would only need to be designed at the radial mode. A design point at 500 cc/s of fuel, and 1500 cc/s of oxidizer would require damping devices tuned to both the first radial mode and the first radial, second tangential mode.

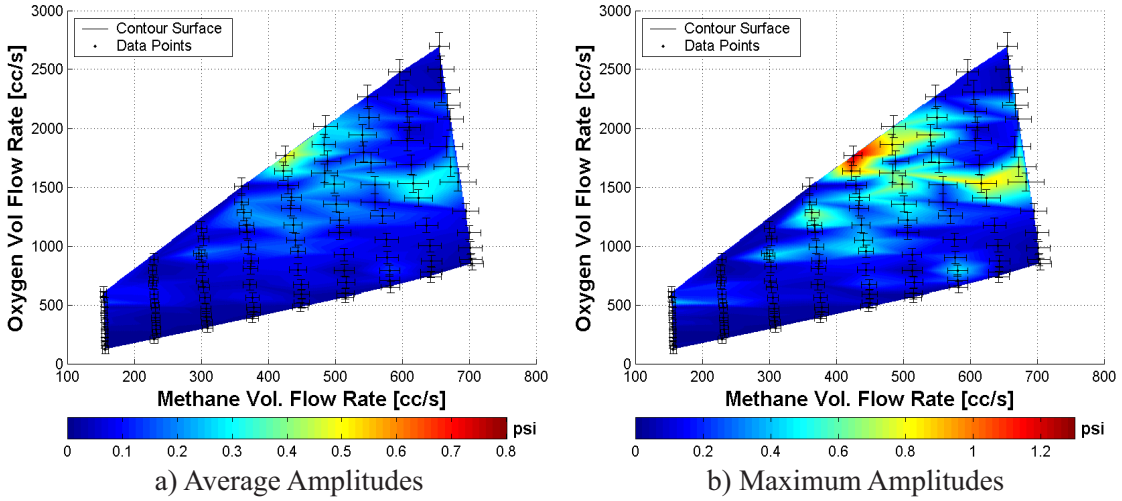

Figure 4.22: Sixty Degree Impinging Jet Stability Maps (radial) [a)Four Test Session Average, b)Four Test Session Maximum]

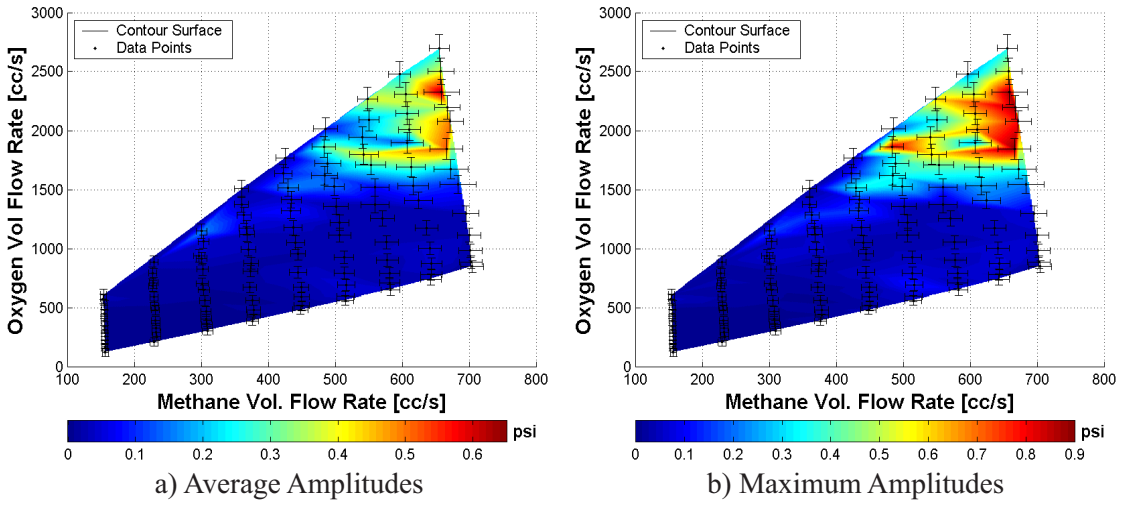

Figure 4.23: Sixty Degree Impinging Jet Stability Maps (combined) [a)Four Test Session Average, b)Four Test Session Maximum]

4.4.4 Stability Mapping - Energy Considerations

Stability mapping of the maximum amplitudes does not capture the whole picture of the system. It may be the most important factor to some engine developers, but the acoustic energy must also be considered. The energy being released by the chemical reaction is dissipated in many ways: heat release, kinetic energy, radiation and acoustic energy. The important component for this study is the acoustic energy. By integrating across the frequency domain spectrum, it is possible to determine the power density of each operating condition set point. The advantage of this mapping is to determine not only where the largest peaks exist but, also to include any harmonics that may have significant energy that could be a potential danger. All of the maps in this section were created to express the worst case scenario, via the energy maximums, not the averages.

The thirty degree impinging jet injector power density map can be seen in Figure 4.24. This map shows that the energy is fairly evenly distributed above the stoichiometric set point (Mixture Ratio of 4). This aspect is interesting due to the fact that the combined mode was not as significant in maximum amplitude. The map reveals that the energy found in the combined mode harmonics is larger than that of the harmonics of the radial mode.

The energy map for the forty-five degree impinging jet can be seen in Figure 4.25. This map shows less acoustic energy present in the 2 g/s area, but larger maximums.

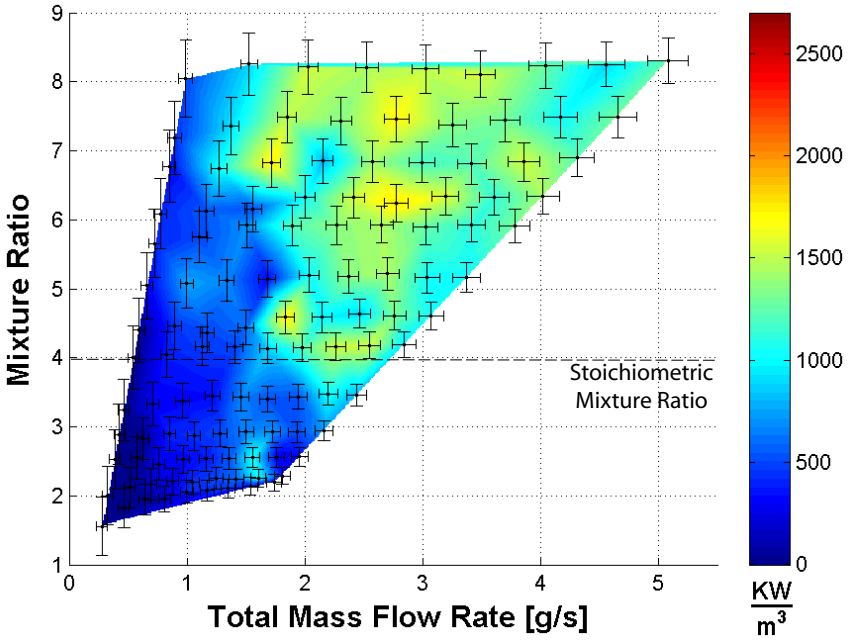

Figure 4.24: Thirty Degree Impinging Jet Injector Total Energy Map

The sixty degree impinging jet injector energy map in Figure 4.26 displays severe energy content in the lean conditions above 2.75 g/s of total mass flow rate. The combined mode, which was dominant with this injector, has significantly more energy than the other injectors. Upon review of the waterfall plots, it is apparent that the peaks exist, but are broad and jagged.

More acoustic energy should be expected with more turbulence and therefore noise, so the energy should certainly increase with the total mass flow rate. As depicted, the trend is evident, but there is no steady increase. The energy flattens out in areas which proves that the instability component is displayed, not just the background combustion noise.

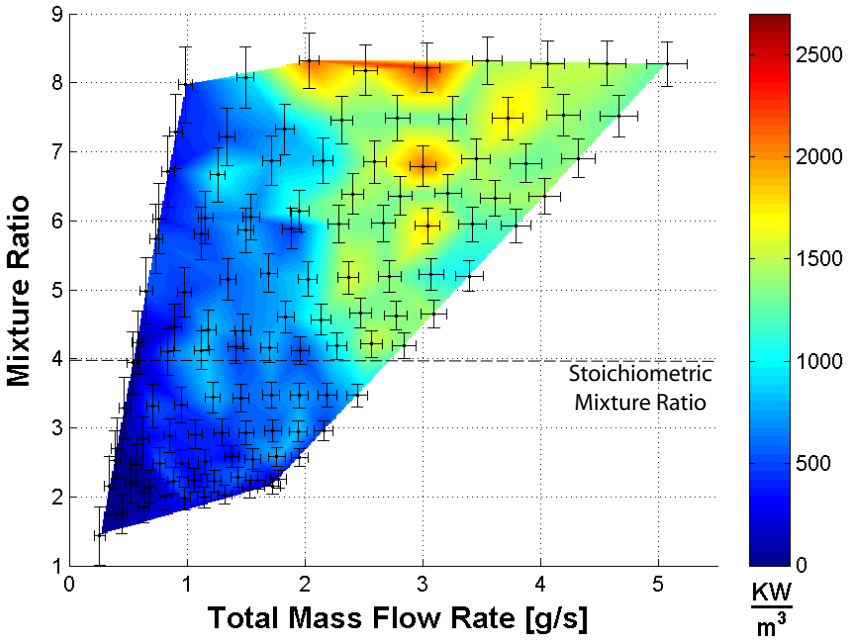

Figure 4.25: Forty-Five Degree Impinging Jet Injector Total Energy Map

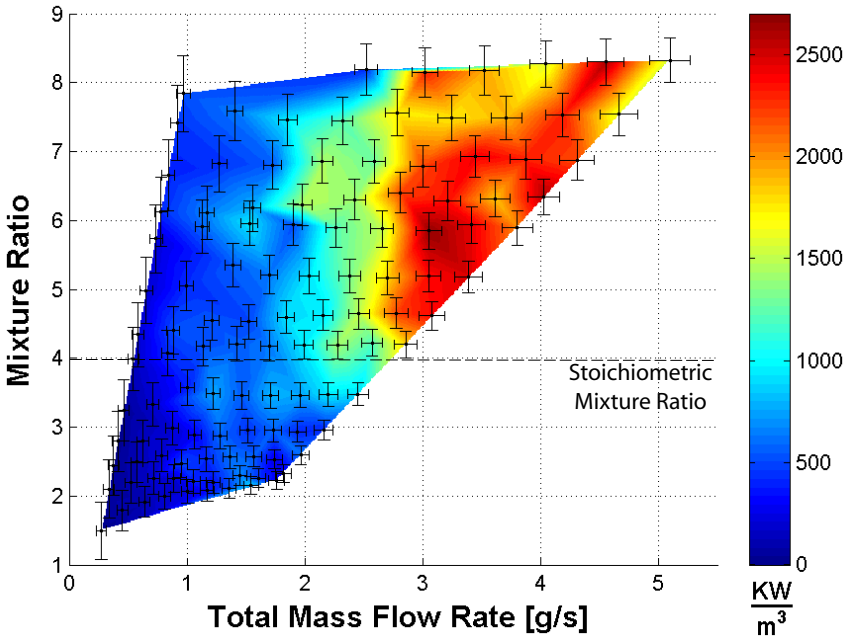

Figure 4.26: Sixty Degree Impinging Jet Injector Total Energy Map

4.4.5 Flame Instability

An additional feature of the methodology is the ability to monitor the flame behavior during testing. By using a chamber with no nozzle, video was taken during all test sessions. In rich, low methane mass flow rate conditions (Tests 1.0 and 1.5), the flame had the visual appearance of a pure diffusion flame. This condition was as expected by producing soot. As the oxygen was throttled, the flame became shorter due to the increased supply of oxygen. At rich, higher methane mass flow rates, the flame did not have the appearance of a diffusion flame. The flame can be seen in the upper left hand corner of Figure 4.27. The high velocity of the propellants enhanced the mixing and there is an orange tinted volume surrounding the flame, but not nearly as much soot formation as in the low fuel mass flow rates.

Figure 4.27 shows the typical flame reaction to throttling at Test 5.0 conditions. The photographs show the sequence from rich (upper left) to lean (lower right). As the oxygen mass flow rate is increased, the flame length decreases. It is approximated that the flame length ranges from 14 inches to 3 inches. The interesting factor to note from Figure 4.27 is that the flame never appears to detach from the fire face. The flame structure is prone to attachment. This fact is an important consideration in some of the flame behavior to be described.

Certain unexpected flame phenomena were consistently experienced during experimentation. The first phenomena was flame bending. Figure 4.28 has two photographs taken during steady operation (left) and with a bent flame (right). The appearance of this phenomenon is always in conjunction with the first radial mode of

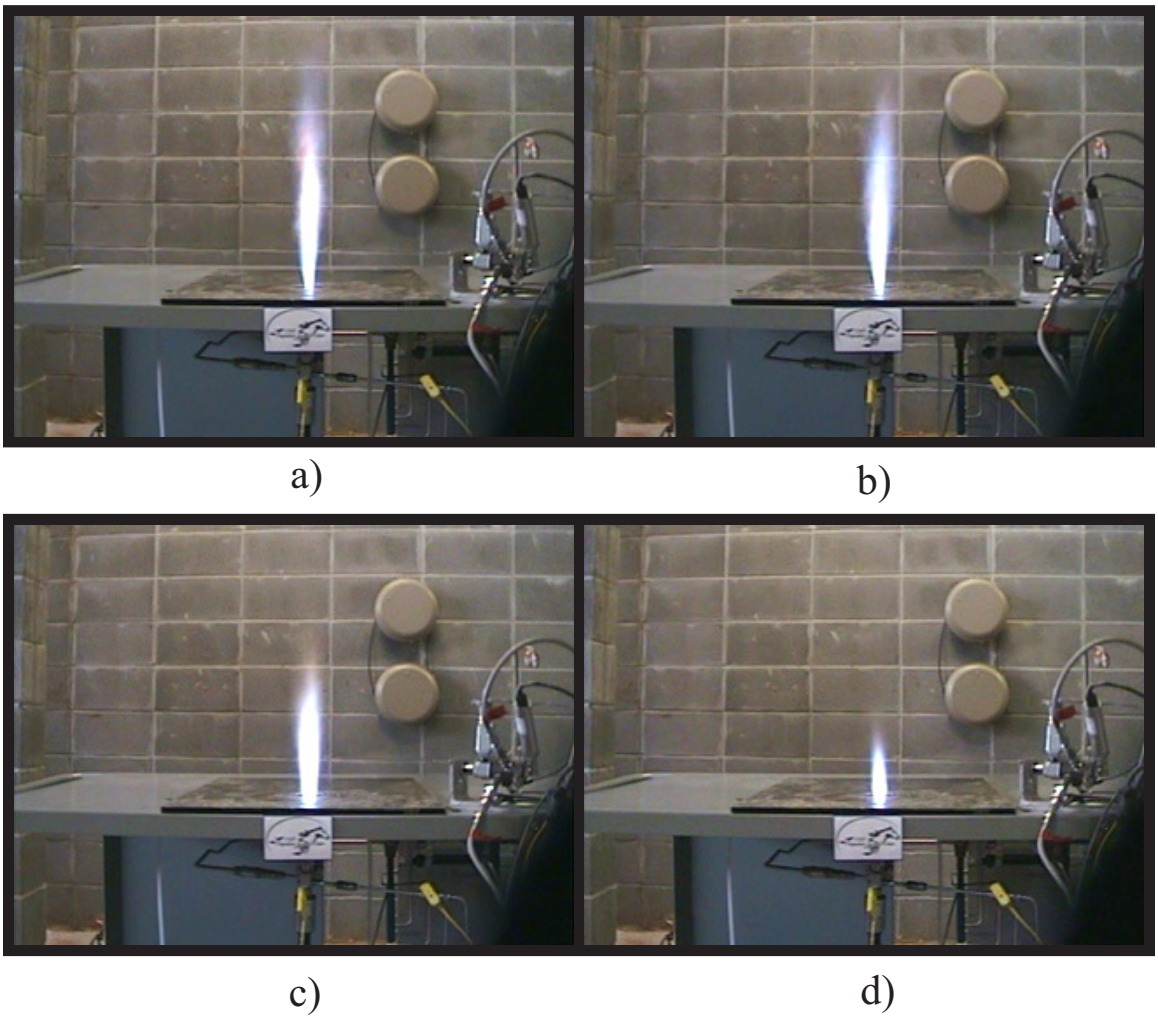

Figure 4.27: Flame Length and Attachment

instability. The flame also always bends in the same direction, toward the chamber axis. The mixing zone of the injector is created by four impinging fuel jets all aimed at the injector axis. With sufficient momentum, the fuel is able to reach the center of the injector. As the narrow mixing zone forms, it is easily disturbed by the pressure pulsations. If sufficiently strong pressure waves exist, the mixing zone can be shifted far enough to attach the initial flame section to the cover lip.

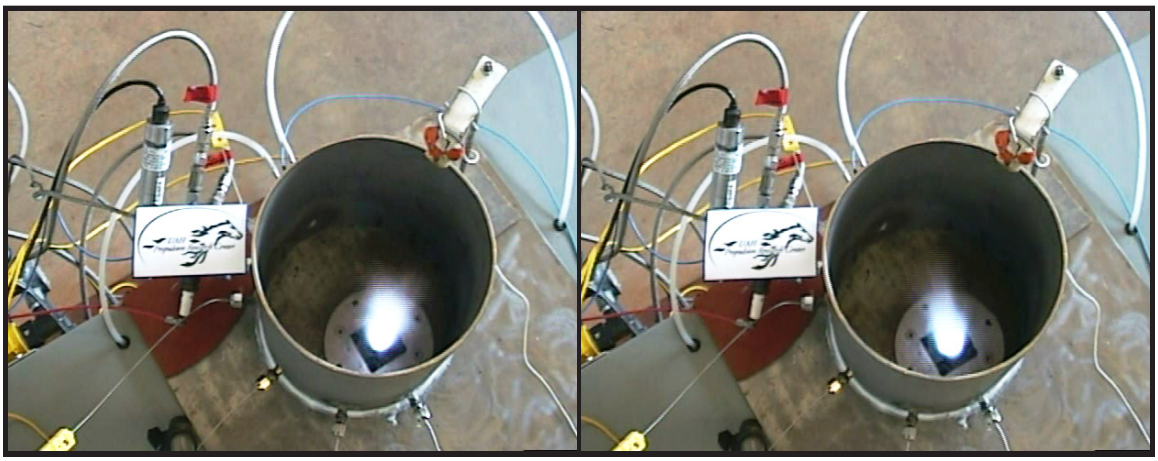

a) Vertical Flame b) Bent Flame

Figure 4.28: Flame Bending

This phenomena was also apparent in the chamber thermocouple readings. The α section is always the highest temperature. As the radial mode was excited, the ϵ chamber section quickly went from coldest to the second hottest. With this flame bending present, heat is released in the ϵ sector direction. This fact, coupled with the fact that the radial mode transfers the heat across the chamber, is the reason for the unexpected ϵ temperature increase.

The most unexpected and severe flame property was flame surging in the sixty degree impinging jet. This phenomenon was only experienced with the sixty degree impinging jet injector. There are two experimental signatures of the onset of surging. The first is the regular manifold pressure pulsations. Pressure spikes were present in the manifolds for all injector designs under unstable operation. However, the thirty and forty-five degree injector manifold pressure pulsations showed no regularity. The measurements were sampled at 250 Hz, and the obviously limited response time of a general purpose pressure transducer makes it impossible to determine otherwise. A

pressure trace of the manifold pressures of the sixty degree impinging jet can be seen in Figure 4.29. The pressure spikes are fluctuating near 1.5 Hz.

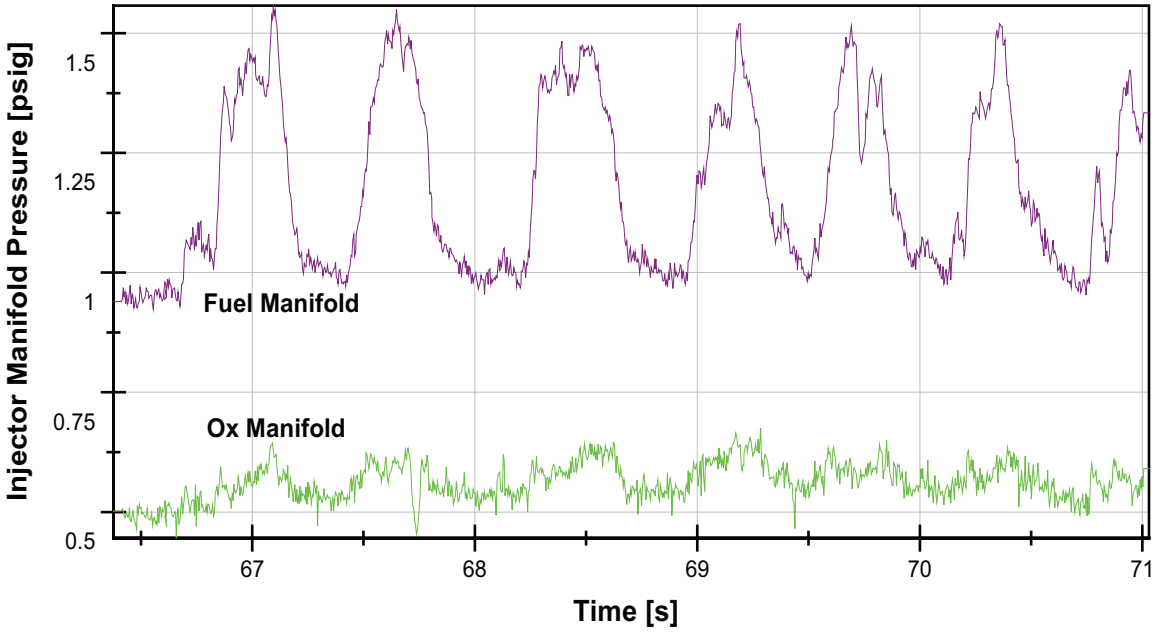

Figure 4.29: Manifold Pressure Surging

The second sign of flame surging is the audible and visual pulsations. The left hand picture of Figure 4.30 is the flame on the minimal part of the pulsation, the right hand picture is the maximum part of the pulsation. The size of the flame and the illumination intensifies. The audio component of the video is in phase with this visual display. Sound from the test footage indicates that the frequency of sound pulsation is near 1.5 Hz as well. At the intensified part of the pulsation, the sound increases in frequency and amplitude. The operation is similar to a pulsating siren.

This frequency is too low to be considered low frequency combustion instability which is normally on the order of 100 Hz. The possibility of injector coupling seems reasonable, but again, the frequency is not on the order of the acoustic phenomena.

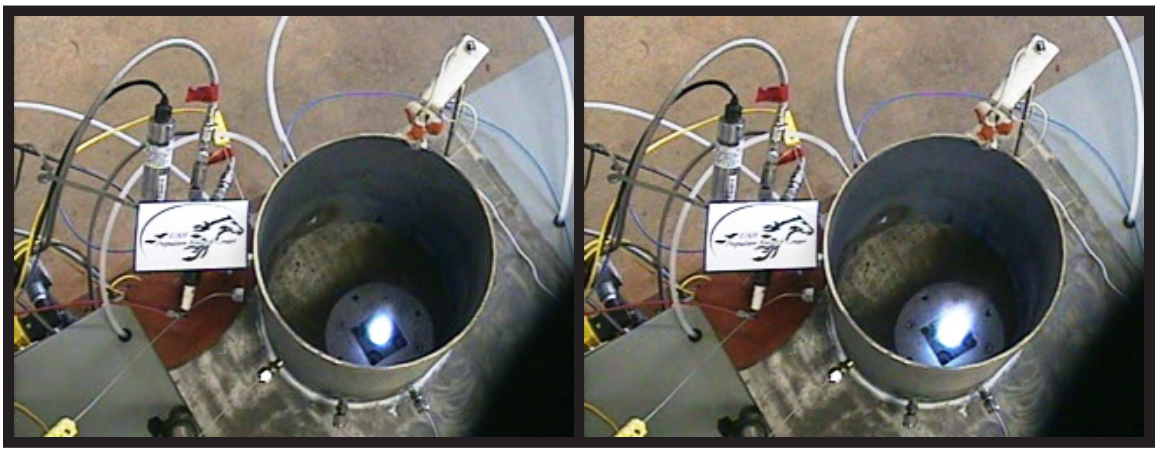

a) Low Illumination b) High Illumination

Figure 4.30: Flame Effects From Surging

The phenomenon is not attributed to any acoustic factor. In looking at the design of the sixty degree impinging jet, the fuel sprays are most likely to intersect inside of the injector. This geometrical characteristic would create a larger recirculation zone downstream of the fuel spray than the other impinging designs. Once sufficient combustible mixture is created in the zone, the heat is available to combust. This secondary combustion process within the combustion process would account for all of the factors present: manifold pulsations, an increase in flame size and illumination as well as the heat release increase that intensifies combustion to push the injector toward high frequency combustion instability which is manifested as the audible component. As the recirculation zone fills again, the chamber returns to nominal conditions only to occur with the 1.5 Hz frequency.

This phenomena is extremely dangerous with respect to high frequency combustion instability. It is the ideal trigger to push the combustion process into the unstable regime. Running the test matrix with this injector proved difficult. At the

leanest conditions, the flame had the tendency to blow out. The blow out would be attributed to the detonation of the recirculation zone, and with the fuel in low supply, the flame was unable to sustain itself.

4.4.6 Impinging Jet Injector Summary

The stability mapping presented here has shown that there are significant differences between the three impinging jet injectors. To highlight the trends between the injectors, the following sets of plots have been created. Figure 4.31 is two plots from the average amplitude data from all of the injectors. The left hand plot is at a equivalence ratio of 0.95. The thirty degree injector (Imp30) is fairly steady across the mass flow rate range. This indicates that the injector is not susceptible to instability near the stoichiometric set points. The sixty degree injector increases near the end of the total mass flow rate range. This indicates that near the stoichiometric set points, there is negligible pressure fluctuations until the upper portion of the total mass flow rate range, where the combined mode exists. The forty-five degree impinging jet injector is quite erratic. This has been documented from the stability mapping as the slower transition to unstable operation.

The right hand plot is for an equivalence ratio of 0.58, in the lean region where there was more unstable behavior. The thirty and forty-five degree injectors show the same trend, which was apparent from the mapping. The amplitude increase in the middle of the total mass flow rate range is from the high amplitude radial instability. The sixty degree injector increases and levels out for the last three set points, again

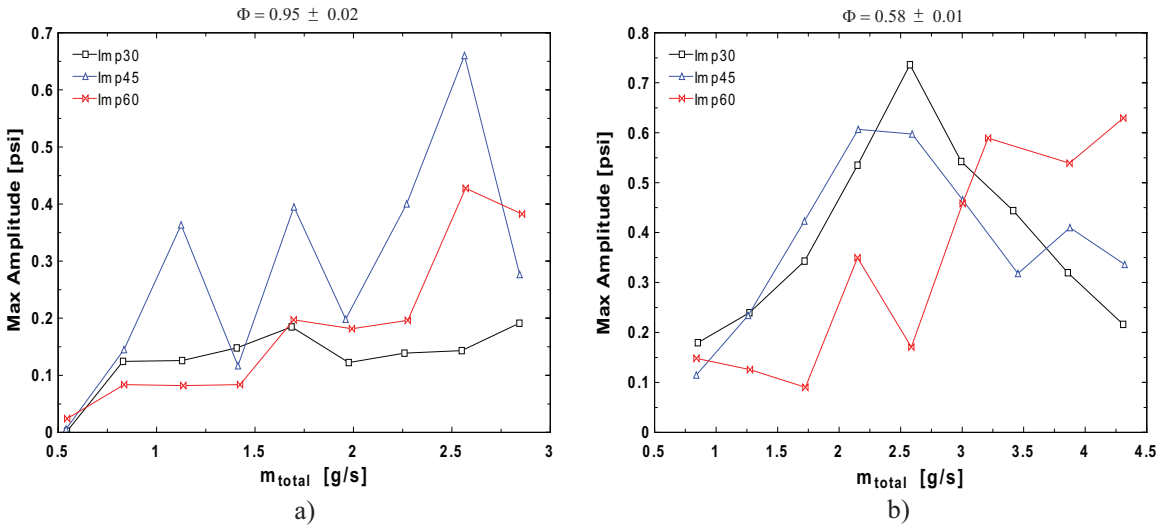

Figure 4.31: Constant Equivalence Ratio Amplitude Comparison [a)$\Phi = 0.95$, b)$\Phi = 0.58$]

where the combined mode is present which was most prevalent in the sixty degree injector.

By looking at the average energy content of each injector in Figure 4.32, comparisons can be made. The left hand plot is near the stoichiometric set point. All injectors show the same trend: there is fairly steady increase as the total mass flow rate increases. In fact, it would be impossible to differentiate between the different injectors. This energy increase is simply from the increase in energy into the chamber from the fuel mass flow rate. The lean plot on the right shows a different picture. The thirty degree injector has the sharpest increase, is jagged and slowly increases. The forty-five degree injector reaches a much higher maximum energy level. The sixty degree injector increases to a steady maximum. This leveling is where the combined mode is present.

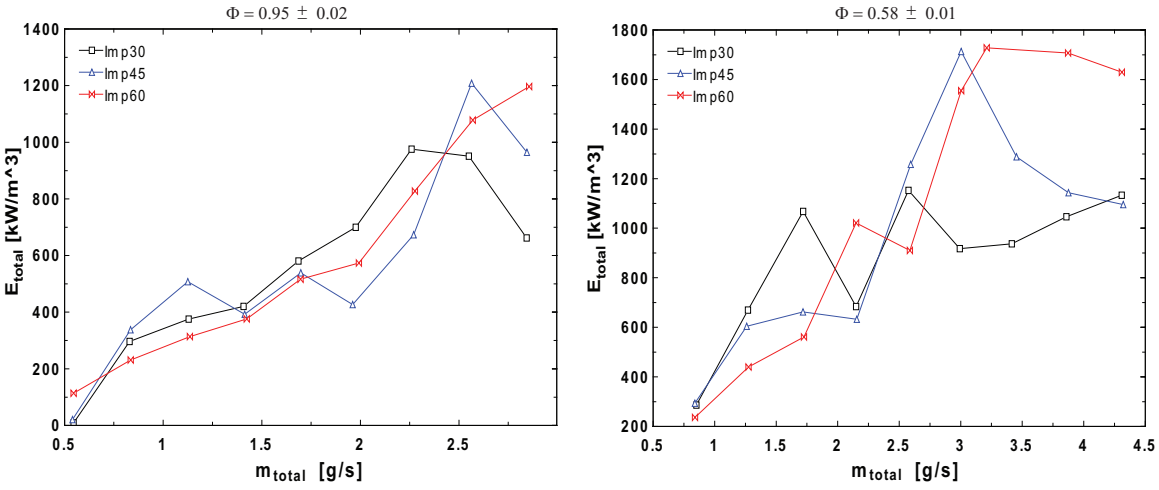

Figure 4.32: Constant Equivalence Ratio Energy Comparison [a)$\Phi = 0.95$, b)$\Phi = 0.58$]

The presence of the instability is thought to be from the vigorous mixing that is inherent to the injection technique. From examination of the flame at various equivalence ratios in Section 4.4.5, it is apparent that the flame was not detached from the injector tip. This indicates that the propellants were sufficiently mixed to combust immediately in the chamber or possible sustained in the injector tip itself. The mechanisms most likely to induce instability are represented as a delay between injection and combustion, in this case the mixing time. The mixing time is so short that there is always combustible mixture available to enhance pressure oscillations. This fact makes sense when evaluating the typical use of the injector, hypergolic propellants that do not mix as easily as the gaseous methane and oxygen.

From combustion chamber length considerations, it is better to have no flame liftoff and combustion should take place as close to the injector face as possible. Unfortunately, this study has shown that such a condition is susceptible to high

frequency combustion instability. This has been a consistent trend in the history of liquid rocket engine development, in that the most efficient liquid rocket engines are most likely to experience high frequency combustion instability. The location of combustion in reference to the injector face is similar to many other engineering problems. If no other means are available, the distance must be optimized. The proper distance will allow pressure waves to traverse the fire face with little to no combustible mixture present to enhance the dynamic pressure amplitude.

CHAPTER 5

CONCLUSIONS

5.1 Summary

This work sought to create a liquid rocket engine injector test facility as well as baseline testing of the facility. The single element Russian methodology test facility for injector stability characterization has been successfully demonstrated and implemented. The advantage of time efficiency is apparent from the amount of data that was recorded in five days. In summary, the research was successful in both main objectives. The results from the tests conducted lead to the following conclusions:

1. The baseline experimentation has shown that the scaling technique is capable of fundamental mode pressure fluctuations up to 17 % $\frac{P'}{P_c}$. Instabilities were observed at radial and tangential modes of the chamber dependent upon the injector and operating conditions. Since the chamber had no nozzle, the acoustic damping was much higher than that of a real chamber.

2. The method can make relatively repeatable distinctions of the stability characteristics of different injector designs. The variability of the process is apparent

in the session to session deviation. Flame bifurcation is a major component of the phenomena and must be addressed in analysis.

3. The sensitivity of the test facility operation and sensing capability is sufficient in differentiating injector design modifications. In this study, the fuel impingement angle had a major influence on the stability of the combustion process. In comparison from average and maximum amplitudes for four test sessions, the mean amplitude scale must be increased by 50 %.

4. The testing has shown excitation of non-traditional modes of instability as the first radial and combined first radial, second tangential mode. Tangential modes of instability are customarily studied, but any transverse mode can be excited with the test facility.

5. The throttling test procedure is successful at creating a coherent idea of the system stability in a wide range of conditions. Using stability mapping is ideal for conveying large amounts of data to easily make conclusions and recommendations for injector design.

6. Matching the volumetric flow rate and stoichiometry of full scale injectors has been shown to be possible with the laboratory scale facility. This is an important step in determining the feasibility and usefulness of the test methodology.

7. The impinging jet injector displays poor stability in a non-hypergolic configuration. The thirty and forty-five degree impinging jet injectors have major susceptibility to the radial mode.

8. The sixty degree impinging jet injector experiences the first radial, second tangential combined mode, as well as the flame surging problem.

5.2 Recommendations

With the test facility working well, there are many interesting studies and modifications that could be made in order to investigate and apply the scaling procedures described by the Russian methodology. The following list of ideas has been generated during analysis of the collected data.

1. **Experimental Control.** The mass flow controllers are now controlled via serial port. By controlling them with analog output and continuously sampling the actual mass flow rate, the uncertainty in the mass flow readings could be estimated better. The manifold pressure transducers should be switched to the BNC-2090 to allow continuous monitoring and avoid the DAQ card switching for the important data. As a matter of convenience and expanded test capability, the heater controllers should be controlled via RS-485. Although the LabVIEW program functions in a safe and reliable manner, the sequence could be improved, especially with the analog output control of the mass flow controllers. A state machine skeleton would be preferable to the sequence currently coded.

2. **Instrumentation.** To improve the frequency mode determination, five dynamic pressure transducers should be placed within the chamber to define the phase shift and therefore the excited mode. An added feature would be to im-

plement dynamic pressure transducers into the injector manifolds which would help with analyzing injector coupling.

3. **Case Studies.** The most important goal of the overall study is to determine if the methodology actually scales to full scale conditions. Therefore, the case studies described should be carried out with the following methodology rules applied: volumetric flow rate and stoichiometry.

4. **Injector Coupling.** Although injector coupling was not found in these studies, the use of the fabricated choke plates would promote injector coupling. Using an impinging jet injector with an oxidizer choke plate would change the injector acoustics closer to an open/closed end tube as opposed to the open/open tube of the injector oxidizer post. A modeling effort could be added in conjunction with the code presented by Hutt and Rocker [3].

5. **Chamber.** A new chamber or set of chambers must be fabricated. A water cooled chamber is necessary to place the injector near the chamber wall. Another option would be to make the chamber from an alloy with an extreme melting temperature. Materials such as columbium, titanium or an alloy would be ideal for radiative heat transfer. With the new chamber, a new variable could be studied, the injector placement. With a set operating condition, the chamber could be traversed along the fire face to excite different modes. Another chamber idea would be to create a rectangular chamber to study standing tangential modes. The walls could be heat resistant or could be gun drilled to allow coolant to pass. This capability would allow one of the chamber walls to

be traversed to change the chamber natural frequency. It would be easy to set up a stepper motor for remote control of the chamber width. A truly unique capability would be to write a simple algorithm that continuously monitors the chamber temperatures and hence the natural frequency and send the stepper motor a command to keep the frequency constant by traversing the chamber wall.

APPENDICES

APPENDIX A

HARDWARE COMPONENT DRAWINGS

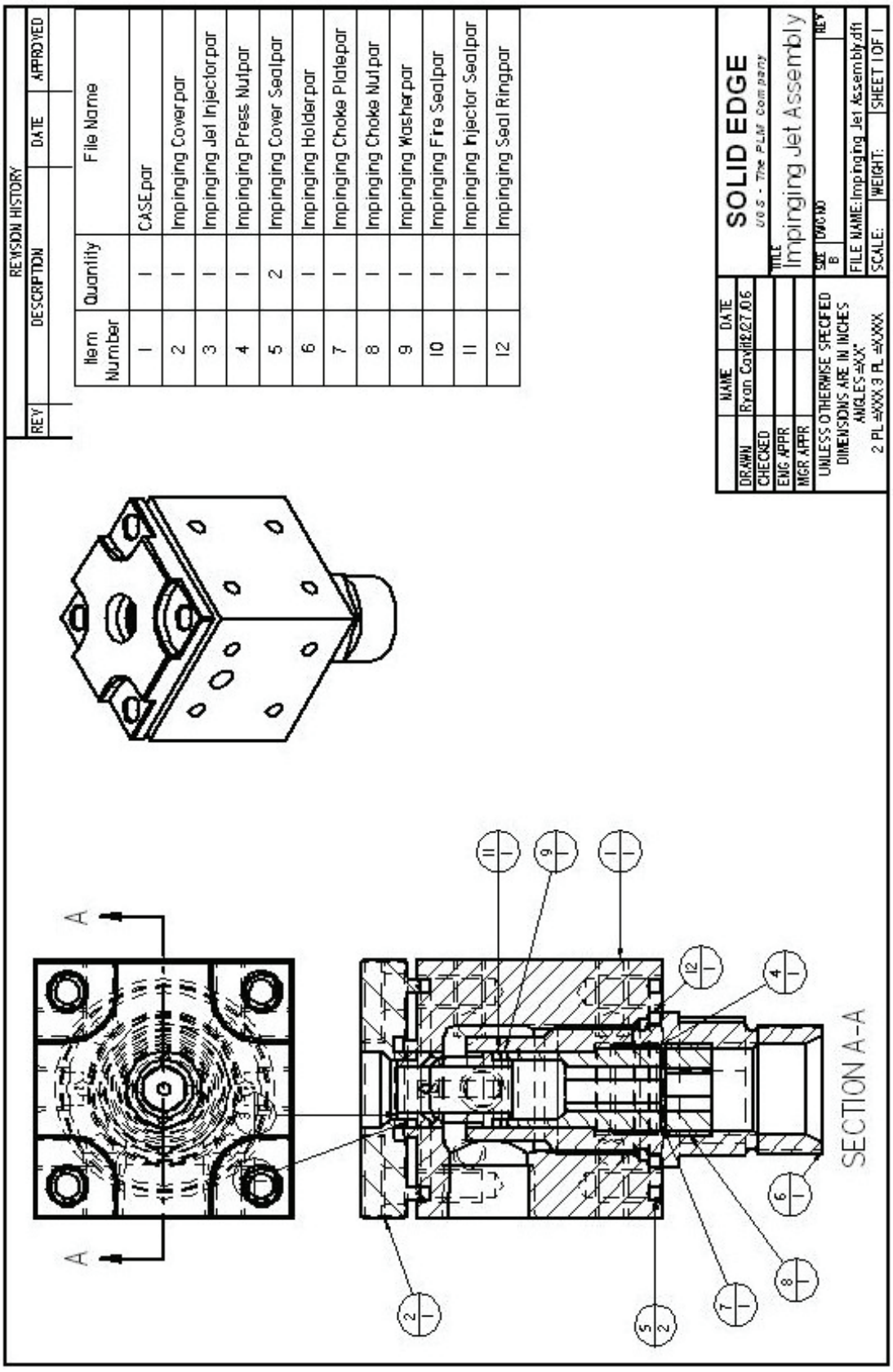

Figure A.1: Impinging Jet Injector Assembly

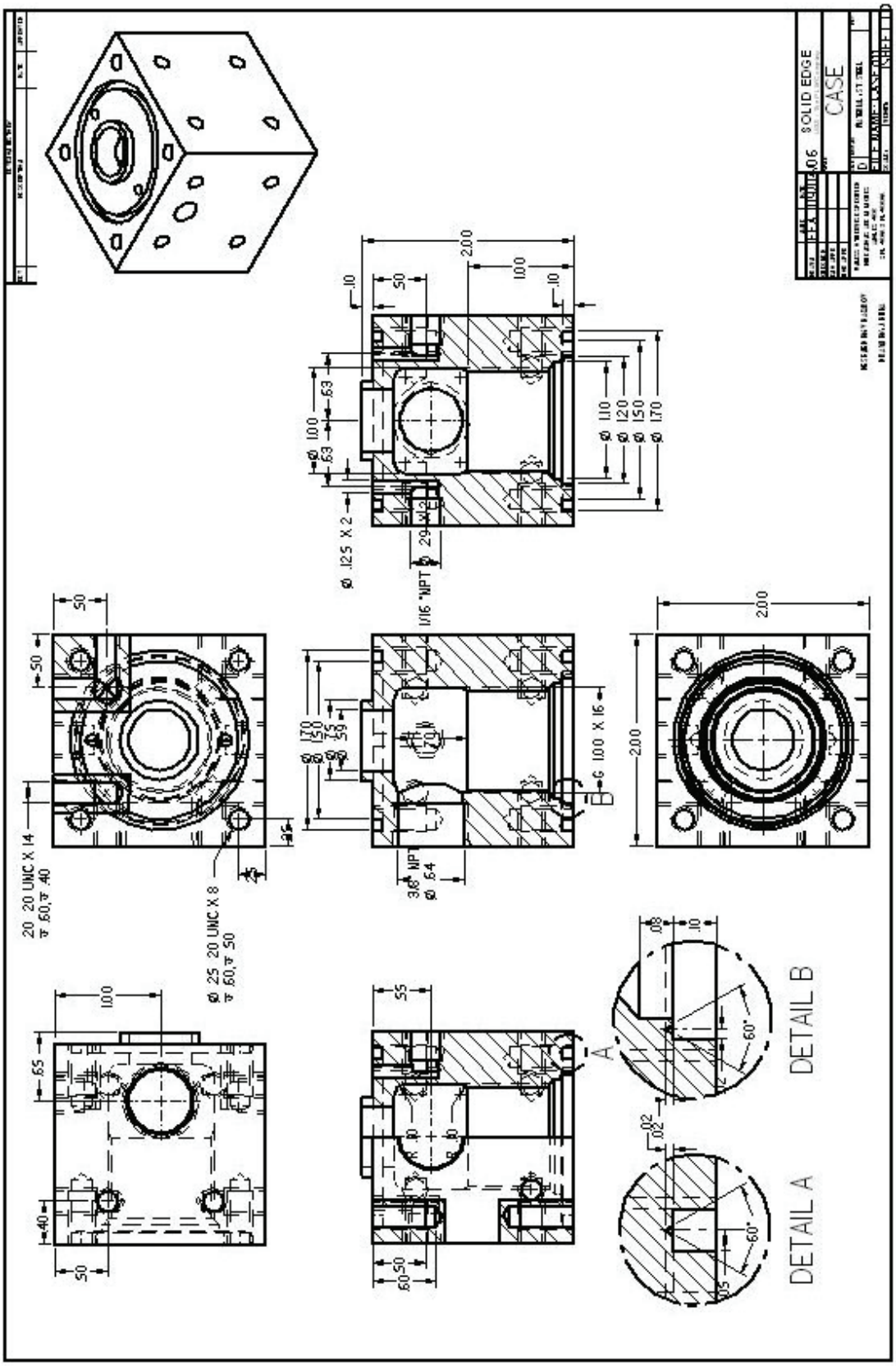

Figure A.2: Injector Manifold Case

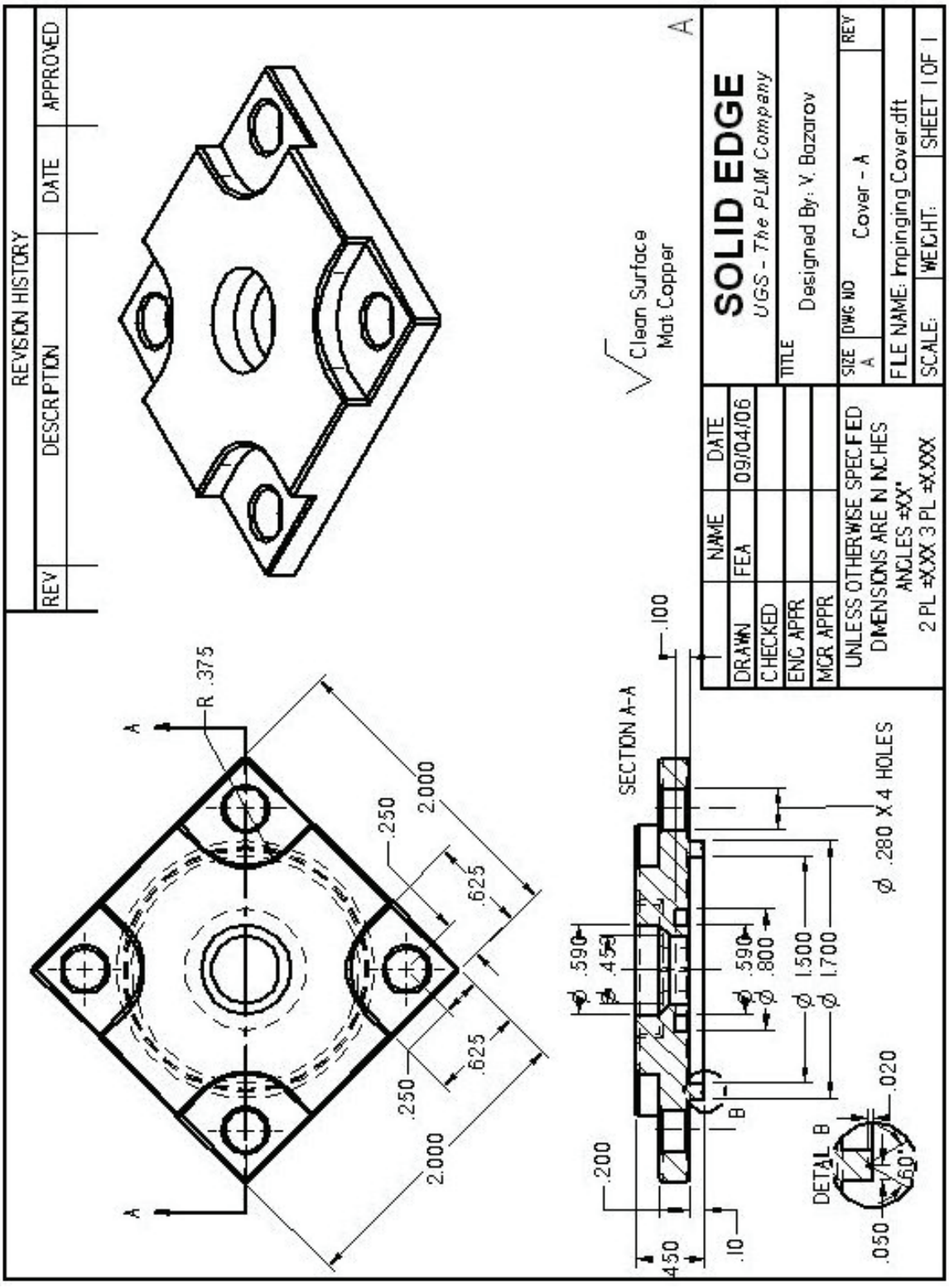

Figure A.3: Impinging Jet Injector Cover

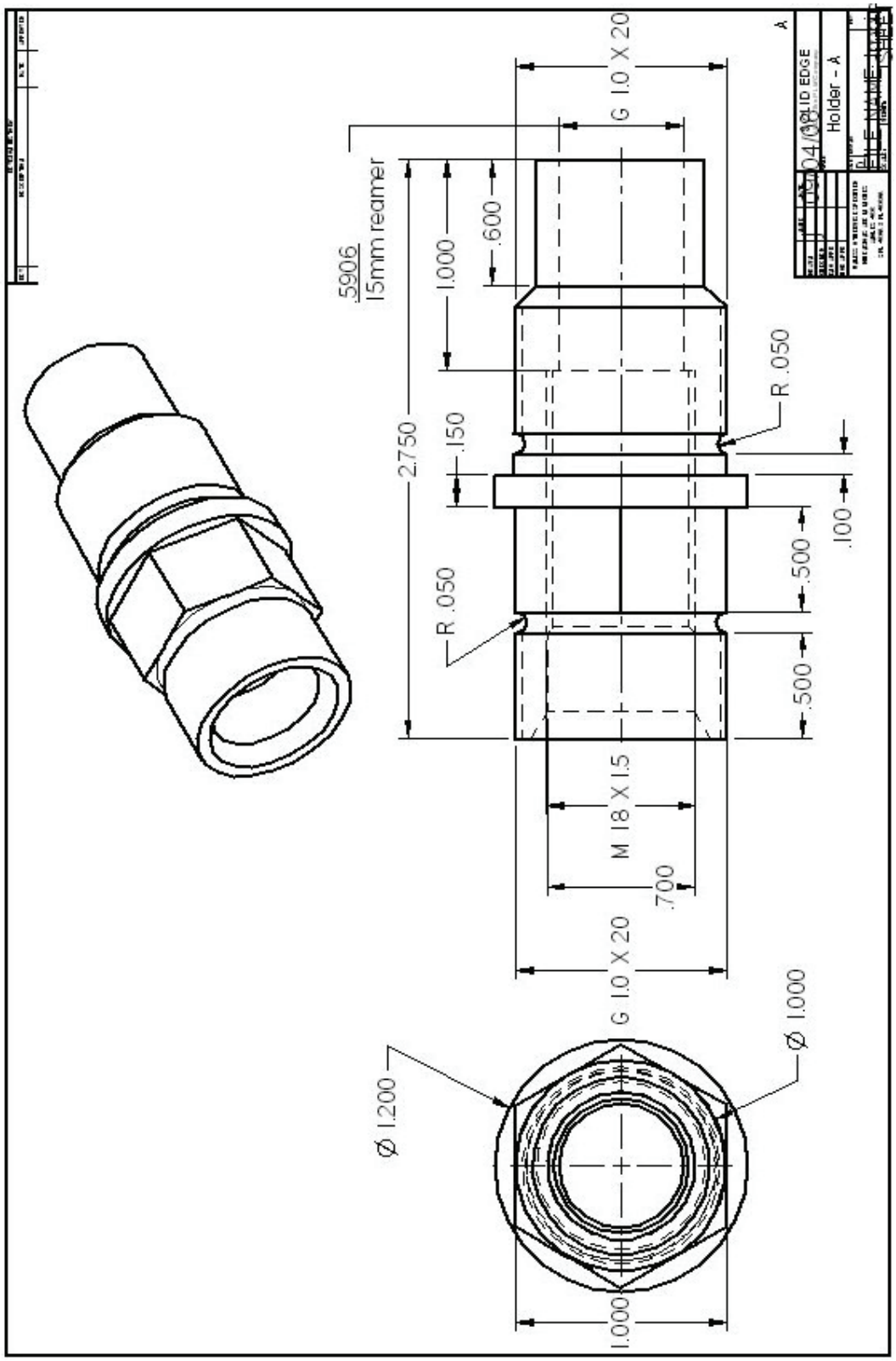

Figure A.4: Impinging Jet Holder

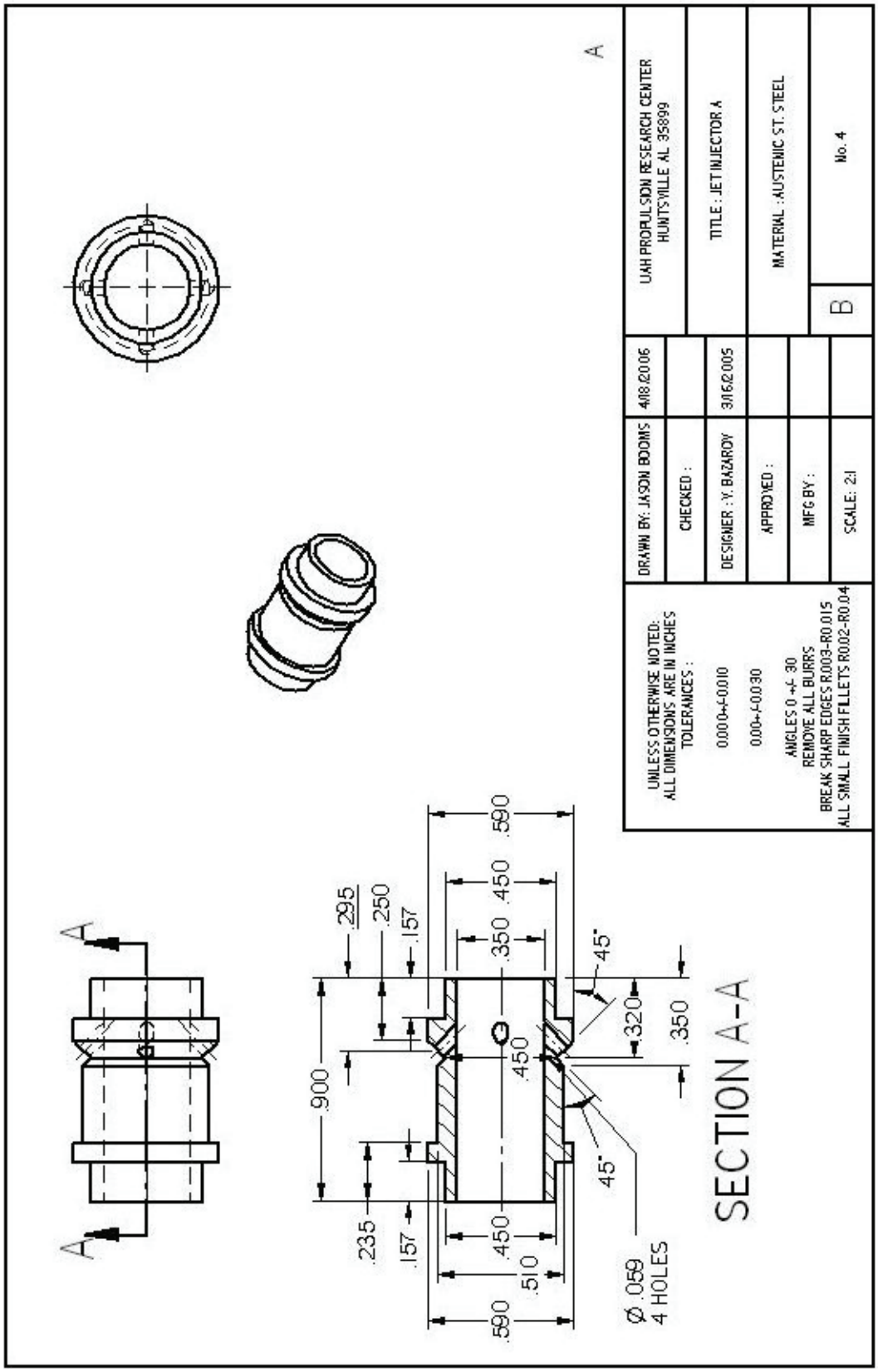

Figure A.5: Impinging Jet Injector

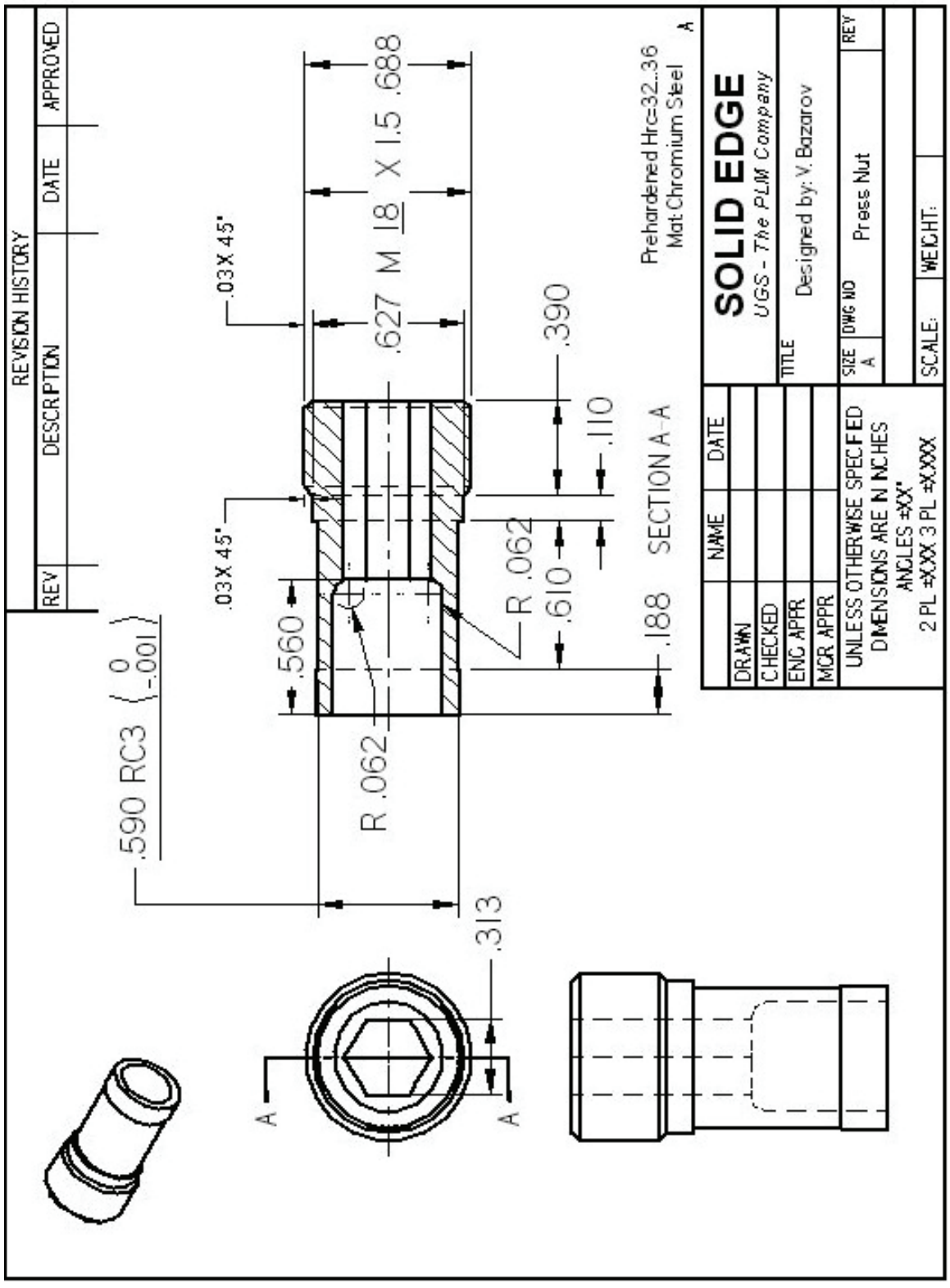

Figure A.6: Impinging Jet Injector Press Nut

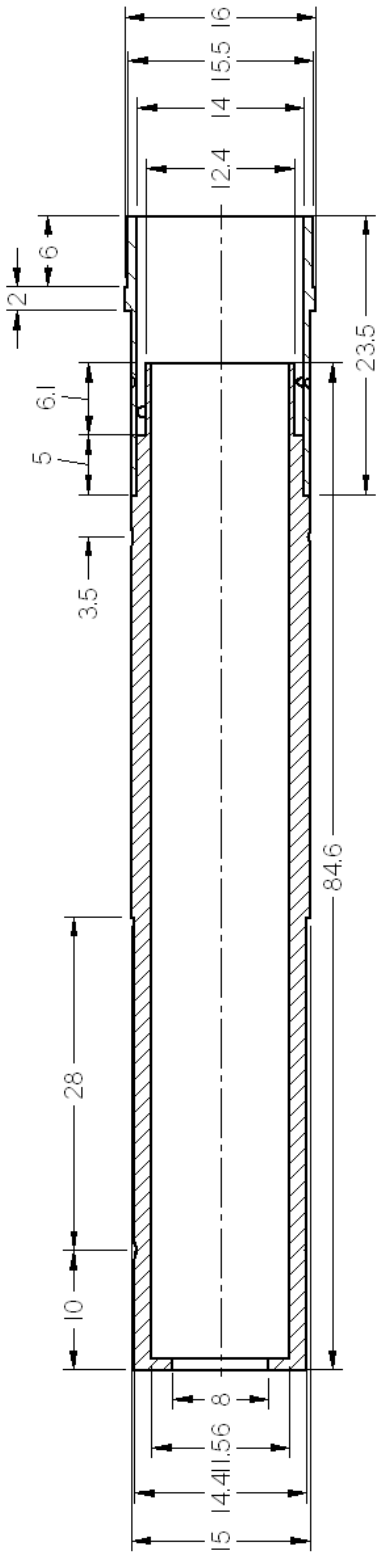

Figure A.7: RD-170 Main Chamber Injector (measurements in mm)

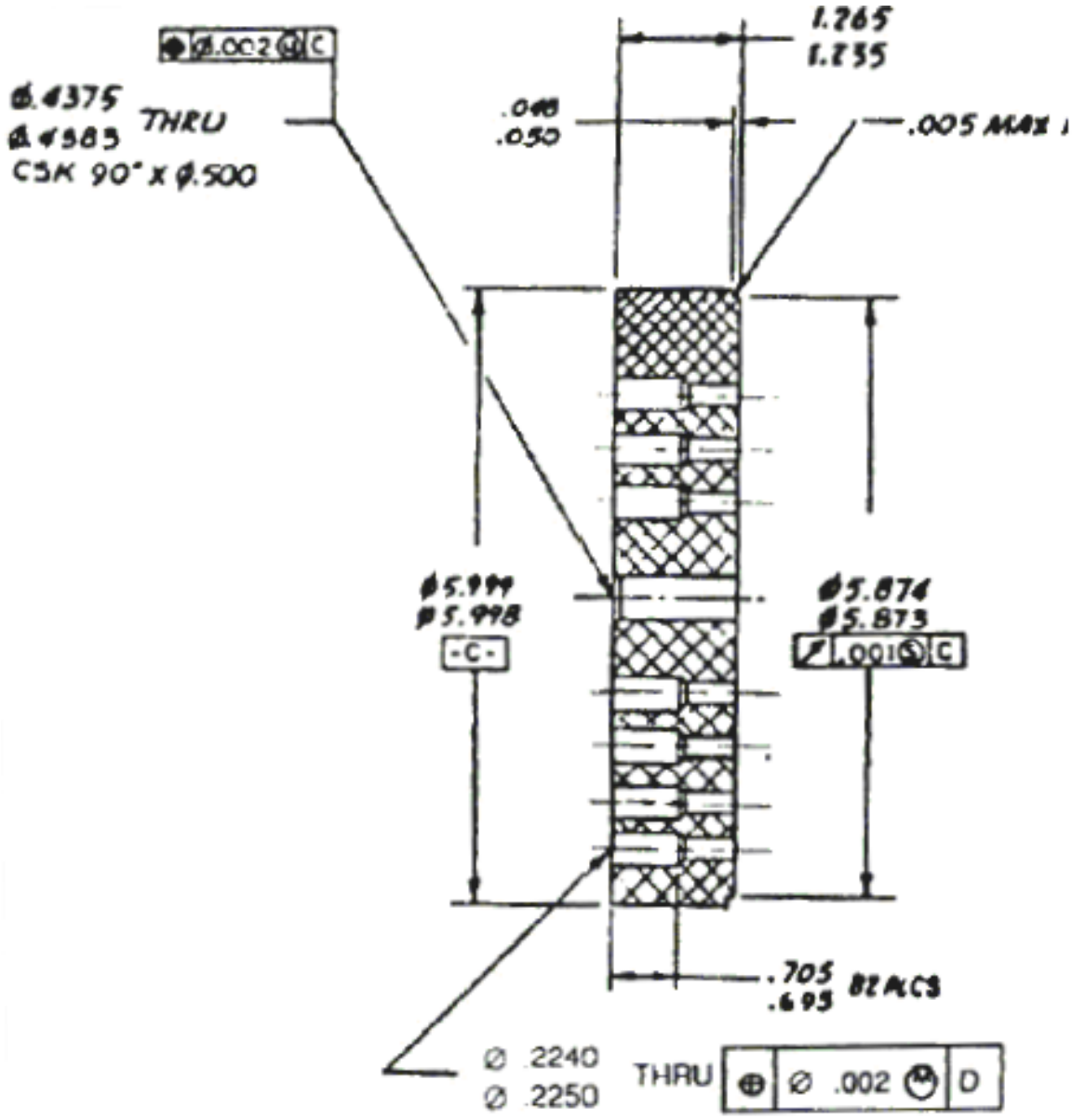

Figure A.8: Rocketdyne Coaxial Injector Sleeve (Jensen 1989)

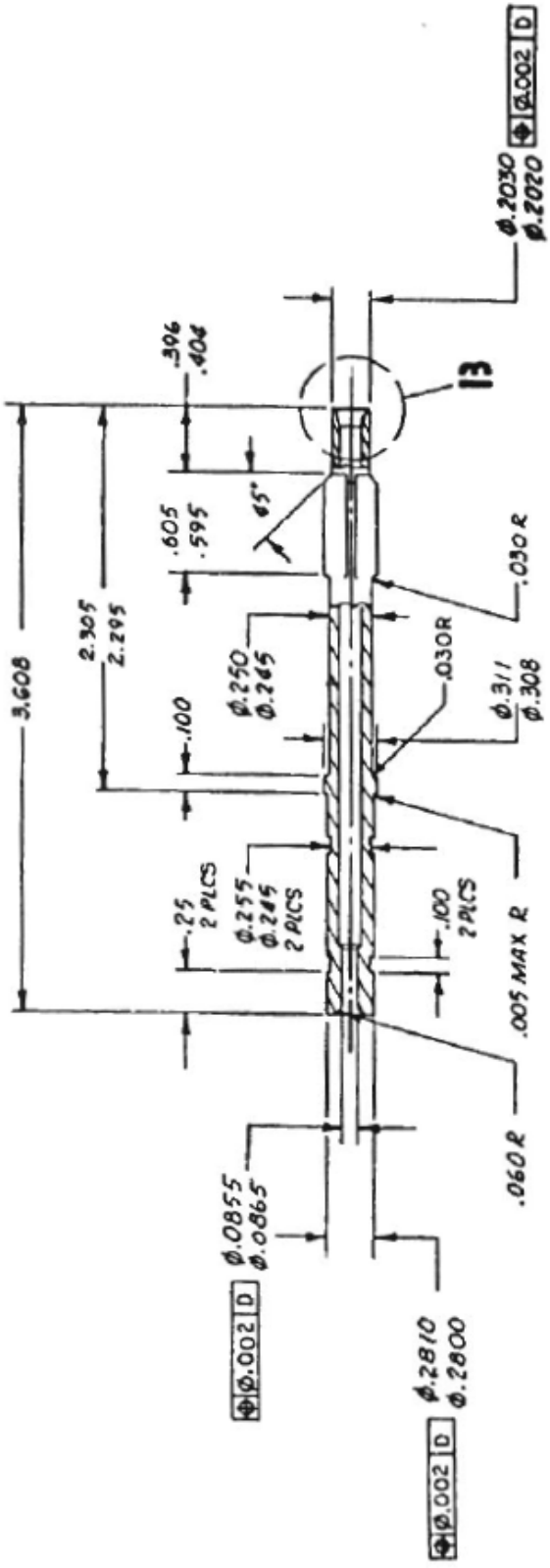

Figure A.9: Rocketdyne Coaxial Injector Post (Jensen 1989)

APPENDIX B

TEST PROCEDURES

Russian Methodology Test Procedure

Date:_____
Red Team Members:_____
Propellants:_____
Injector:_____

Table 1. Experimental Mass Flow Settings and Ranges

Test #	Oxidizer Mass Flow Rate [g/s]	Fuel 1 Mass Flow Rate [g/s]	Fuel 2 Mass Flow Rate [g/s]	Ox Diluent Mass Flow Rate [g/s]	Fuel Diluent Mass Flow Rate [g/s]

High Frequency Measurements
Sampling Rate:_____
Number of Samples per Measurement:_____

Author (Ryan Cavitt):
Dr. Moser:
Dr. Frederick:
Dr. Lineberry:
Tony Hall: **(Test Engineer)**

Other operators or Red Team Members not shown on this document must be certified by the Test Engineer

Rev06

Figure B.1: Page 1 of the procedure manual

Injector Manifold Assembly (follow these steps sequentially)

1. Attach the mounting plate to the table with short head hex cap screws (black oxide) and apply Fire Barrier Silicone
2. Assemble Injector Assembly as in Figure 2 with the following steps
   I. Screw press nut, washer and injector seal into holder to the end of threading
   II. Screw the holder and seal ring fully into the case
   III. Push the injector and fire seal down into the case until contact and alignment with press nut
   IV. Unscrew the press nut 2 rotations, so that the lip of the injector clears the lip of the case (this step ensures that the cover seal will seal the cover and case)
   V. Place the cover onto the case and fasten with short head hex cap screws (black oxide)
   VI. Tighten the press nut to seal the assembly
   VII. Put in choke nut and choke plate if applicable
3. Slide case with brackets onto mounting plate with fuel inlet facing the fuel collector, not fully flush
4. Attach case cooling lines
5. Push cover flush with plate and fasten with nuts (apply Fire Barrier silicone)
6. Mount oxidizer collector onto the case with hex cap screws
7. Attach fuel line and oxidizer line to injector assembly

Test Stand Preparation

- ☐ Roll cart into test cell
- ☐ Attach pressurization air to actuated fire valve air manifold (plastic tubing)
- ☐ Attach the pressurization air to the compressor in the instrumentation room and make sure that the compressor is on auto compress
- ☐ Attach power to actuated fire valve control line
- ☐ Attach main air/oxygen line to the oxidizer fire valve
- ☐ Attach main fuel line to the fuel fire valve
- ☐ Attach fuel purge line to the fuel purge cross (see plumbing schematic appendix for fuel purge tee location)
- ☐ Attach oxidizer purge line to oxidizer purge tee (see plumbing schematic appendix for oxidizer purge tee location)
- ☐ Attach the methane drain line to the dome loader fuel vent line
- ☐ Attach the oxygen drain line
- ☐ Close the water manifold valves
- ☐ Attach the water line from the instrumentation room to the quick disconnect fitting on the water manifold

Igniter Setup

- ☐ Attach blue igniter ground to actuator grounding post
- ☐ Attach oxygen line to the igniter
- ☐ Attach hydrogen line to the igniter
- ☐ Attach red spark plug connection to the spark plug tip on the igniter

Figure B.2: Page 2 of the procedure manual

- ☐ Clamp grounding clamp to the copper plate behind the thrust stand
- ☐ Set the secondary oxygen needle valve to the correct setting
- ☐ Set the secondary hydrogen needle valve to the correct setting

Instrumentation

- ☐ Attach the Sensotec serial #768094 pressure transducer to the igniter and plug into A3 in the DAQ
- ☐ Place the omega fuel collector static pressure transducer inline and plug into A2 in the DAQ (see piping schematic appendix for transducer location)
- ☐ Place Omega oxidizer static pressure transducer inline and plug into A1 in the DAQ(see piping schematic appendix for transducer location)
- ☐ Assemble the dynamic pressure transducer into the cooling jacket on the chamber, hook up the power system and plug the signal into unpowered BNC channel 1
- ☐ Turn on microphone, place on mount and plug into unpowered BNC channel 2 (see piping schematic appendix for microphone location)
- ☐ Input the oxidizer collector K-type thermocouple to thermocouple input #8
- ☐ Input the fuel collector K-type thermocouple to thermocouple input #7
- ☐ Input the oxidizer nitrogen K-type thermocouple (marked B) to thermocouple input #2
- ☐ Input the methane K-type thermocouple (marked C) to thermocouple input #3
- ☐ Input the fuel nitrogen K-type thermocouple (marked D) to thermocouple input #4
- ☐ Input the propane K-type thermocouple (marked E) to thermocouple input #5
- ☐ Input the chamber farside K-type thermocouple to thermocouple input #6
- ☐ Input the chamber nearside K-type thermocouple to thermocouple input #1
- ☐ If using the heaters
    - Input unpowered BNC #2 to the PLC plug on the electrical enclosure face
    - Plug in the SCRs and Contollers and turn on the controller switch
    - Input the desired setpoints
    - Turn on the SCR switch
- ☐ Plug in the color coded mass flow controller terminal block into the serial line (black-green-white wire) and attach power to the mass flow controllers
- ☐ Make sure mass flow controllers have the correct settings (gas type, baud rate, serial control, etc.)
- ☐ Set up video camera on the cart and hook up RCA cables and power plug (see piping schematic appendix for video camera location)
- ☐ Ensure that the DAQ patches are correct in the instrumentation room, documented in D:/Russian Methodology/Sensor Info and Locations.xls on the control room computer

Control Room Settings

- ☐ Ensure PLC times are correct in RUSSIAN2.SWP, referencing D:/Russian Methodology/Russian PLC times.xls
- ☐ Upload PLC timing values to PLC (RUSSIAN2.SWP)
- ☐ Make sure test facility area is clear

Figure B.3: Page 3 of the procedure manual

- With all Red Team members in the control room, use the control board to switch on the ox main, ox primary dome, ox secondary dome, fuel main, fuel primary dome, fuel secondary dome
- Insert enable plug
- Press Reset on the
- Press FIRE on the control board
- Ensure the actuators are functioning properly
- When zone 2 is complete press the BRB button to enter zone 4
- Run RUSKIE_10.vi with the title "PLC check" to ensure the transducers are connected correctly and are reading approximately zero

ONLY Red Team allowed in test cell area from this point forward

Leak Check

Cooling Lines

- Attach the cooling lines on the cart top to the dynamic pressure transducer cooling jacket
- Place the drainage line on the tee and the other end in the drain
- Open water main line in the instrumentation room
- Open the cooling jacket and injector assembly cooling line manifold valves
- Ensure that there is no leakage from the H2O system
  - In the event of leakage, reassemble the manifold strictly adhering to the assembly instructions
- Remove electrical tape from injector face
- Put up all blockades around the test facility

See Appendix A for Propellant Line Leak Check Procedures if needed

Propellant Line Fill

- Remove the key from the control board
- Ensure that the water manifold valves are open and water is running into the drain, and electrical tape is removed from injector face
- Slowly open the nitrogen tanks to the nitrogen manifold
- Slowly open the nitrogen manifold ball valves
- Ensure that there is sufficient pressure in the manifold
- Adjust the pressure settings to the appropriate pressures, according to the Pressure Board Settings Table below

Oxygen Ignition	Fuel Ignition	Oxygen Main	Fuel Main
60 psi	60 psi	300 psi	300 psi
Oxygen Ignition Purge	**Fuel Ignition Purge**	**Oxygen Main Purge**	**Fuel Main Purge**
30 psi	30 psi	50 psi	50 psi

Pressurized Lines – Safety Glasses

Figure B.4: Page 4 of the procedure manual

Pressurized Lines – Safety Glasses Required

☐ Commence Purge Check Sequence

Table 2. Purge Check Sequence

Step	Control Room	Test Cell
1	Replace key and turn on board	
2	Communication check with the intercom	
3		When ready, tell the control room to start the purge check sequence
4	Switch on fuel primary purge, initiate mass flow controller (.3g/s)	
5		Confirm injector purge flow
6	Switch off fuel primary purge, set mass flow controller to zero, switch on fuel secondary purge	
7		Confirm igniter purge flow
8	Switch off fuel secondary purge, switch on ox primary purge, initiate mass flow controller (1g/s)	
9		Confirm injector purge flow
10	Switch off ox primary purge, set mass flow controller to zero, switch on ox secondary purge	
11		Confirm igniter purge flow
12	Switch off ox secondary purge	

☐ Slowly open the main fuel tanks
☐ Slowly open the main fuel manifold ball valves
☐ Ensure that there is sufficient pressure in the manifold
☐ Slowly open the hydrogen tank to the secondary fuel manifold
☐ Slowly open the secondary fuel manifold ball valve
☐ Ensure that there is sufficient pressure in the manifold
☐ Slowly open the oxygen tank to the secondary oxygen manifold
☐ Slowly open the secondary oxidizer manifold ball valve
☐ Ensure that there is sufficient pressure in the manifold
☐ Slowly open the oxygen tank to the primary oxygen manifold
☐ Slowly open the primary oxygen manifold ball valves
☐ Ensure that there is sufficient pressure in the manifold
☐ Make sure that the pressure settings are correct on the pressure regulator board and record

NEVER go out to the test stand without the control board key when propellants are present in the lines

Figure B.5: Page 5 of the procedure manual.

Pressurized Lines – Safety Glasses Required

Firing Sequence*

- Open LabVIEW virtual instrument and set all the settings in the appropriate input locations
- Make sure test facility area is clear
- With all Red Team members in the control room, use the control board to switch on the ox main, ox primary dome, ox secondary dome, fuel main, fuel main dome, fuel secondary dome
- For the first firing
  - Fill the cart propellant lines with propellant using the mass flow control.vi and the manual fire valves
- Input test matrix into D:/Russian Methodology/Test Matrix.txt
- Run LabVIEW program
- Ensure that all test stand pressures are correct
- Hit record on the DVD recorder
- Announce the Test Number
- Press Reset
- Insert enable plug
- Cross fingers
- Press FIRE on the control board
- When experimental sequence is complete LabVIEW will say it is ready to purge, then manually purge the lines with the big red button
- The LabVIEW program will automatically stop when the purge flow is zero

*Familiarize yourself with failure mode solutions before firing sequence

Shut-Down Sequence

- Close main fuel tanks
- Vent main fuel manifold
- Close main oxygen manifold ball valves
- Close main oxygen tanks
- Vent main oxygen manifold
- Close main fuel manifold ball valves
- Close igniter fuel tank
- Vent igniter fuel manifold
- Close igniter fuel manifold ball valves
- Close igniter oxygen tank and vent
- Vent igniter oxygen manifold
- Close igniter oxygen manifold ball valves
- Close nitrogen manifold nitrogen tanks
- Vent nitrogen manifold
- Close nitrogen manifold ball valves
- Ensure all pressures are back to ambient with LabVIEW
- Turn off water

Figure B.6: Page 6 of the procedure manual

Pressurized Lines – Safetv Glasses Required

- ☐ Close nitrogen manifold ball valves
- ☐ Ensure all pressures are back to ambient with LabVIEW
- ☐ Turn off water
- ☐ Detach water line and blow out with actuator air line
- ☐ Detach actuator air line from the compressor
- ☐ Detach propellant lines from cart
- ☐ Place chamber on the thrust stand
- ☐ Detach instrumentation and store
- ☐ Tuck cart into air breathing room to rest, kiss goodnight

Figure B.7: Page 7 of the procedure manual

Failure Analysis

FAILURE MODE	SOLUTION	EFFECT
Gas leaks in supply lines	Leak Check	
Power failure	Fuel vent valve releases fuel to drainage	Shut-down sequence when power returns
Missed ignition	Press BRB on the test stand control box and the reset button on the LabVIEW program	Try sequence once more or adjust PLC timing/ injector ignition operating conditions
Inadvertent Burning of Experiment	Press BRB on the test stand control box and the reset button on the LabVIEW program	Shut-down sequence and assess damage
Over Pressurization	Press BRB on the test stand control box and the reset button on the LabVIEW program	Shut-down sequence and assess failure location and possible damage
Mass Flow Control Failure	Press BRB on the test stand control box and the reset button on the LabVIEW program	Check controller settings and LabVIEW program settings
No Cooling Water	Press BRB on the test stand control box and the reset button on the LabVIEW program	
Accidental ignition or start of gas flow	Key ignitions, normally closed valves	
Experiment will not stop	Press BRB on the test stand control box and the reset button on the LabVIEW program, manual shut-off at K-bottle	
Gas leaks in supply lines	Leak check, hydrocarbon meter, forced ventilation	

Figure B.8: Page 8 of the procedure manual

Piping Schematic Appendix

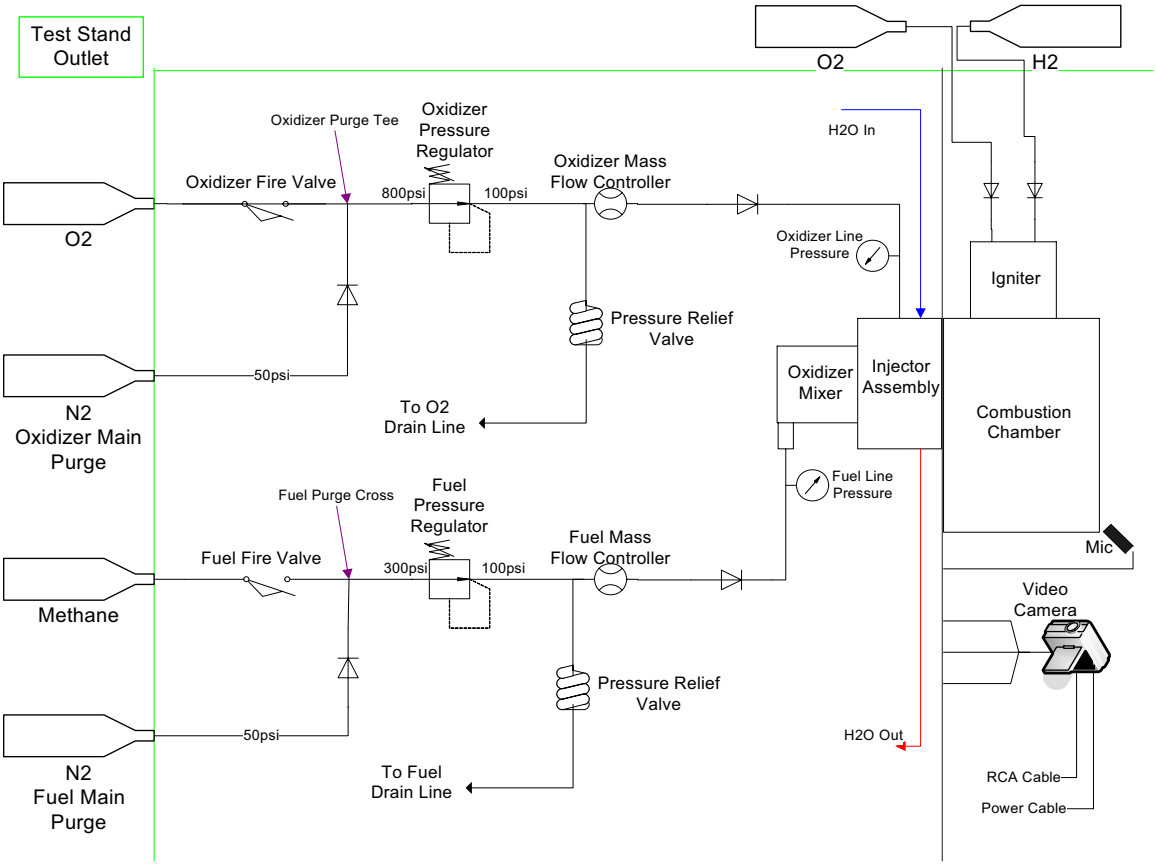

Figure 1. Experimental Piping Schematic

Figure B.9: Page 9 of the procedure manual

Appendix A – Propellant Line Leak Check

Table 3. Experimental Pressure Settings

Oxygen Ignition	Fuel Ignition	Oxygen Main	Fuel Main
60 psi	60 psi	300 psi	300 psi
Oxygen Ignition Purge	**Fuel Ignition Purge**	**Oxygen Main Purge**	**Fuel Main Purge**
30 psi	30 psi	50 psi	50 psi

- Tighten all fittings and components from the test stand connection to the injector for each line

Pressurized Lines – Safety Glasses Required

Fuel Main Line

- Turn on the control board
- Turn on the fuel main, oxidizer main, oxidizer primary dome, fuel primary dome, oxidizer secondary dome, and fuel secondary dome
- Turn on the primary fuel dome switch
- Go outside to the fuel and nitrogen storage area
- Slowly open nitrogen bottles to the nitrogen manifold
- Slowly open manifold ball valves to nitrogen manifold
- Check to make sure there is sufficient pressure in the manifold using the analog gauges
- Set the Experimental Pressure Settings on the pressure regulator board
- Slowly open the nitrogen bottle on the fuel main manifold
- Slowly open the fuel main manifold valve
- Check to make sure there is sufficient pressure in the manifold using the analog gauges
- One red team member must return to the control room, the others go to the test cell

Table 4. Fuel Main Leak Check Procedure

Step	Control Room	Test Cell
1	Replace key and turn on board	
2	Communication check with the intercom	
3		When ready, tell the control room to actuate the fuel main fire valve
4	Switch on the fuel main fire valve, initiate mass flow controller (.3g/s)	
5		Set cart regulator to 90 psi with flow through the mass flow controller
6		Find leaks with bubble solution
7	Turn off ox main fire valve, set mass flow controller to zero	
8		Tighten the appropriate fittings
9	Iterate Steps 3-8 until no leaks are present	

Figure B.10: Page 10 of the procedure manual

Pressurized Lines – Safety Glasses Required

- Depressurize fuel main manifold

Oxidizer Main Line

- Move the nitrogen tank to the oxidizer main manifold
- Slowly open the nitrogen bottle to the oxidizer main manifold
- Slowly open the oxidizer main manifold valve
- Check to make sure there is sufficient pressure in the manifold using the analog gauges

Table 5. Oxidizer Main Leak Check Procedure

Step	Control Room	Test Cell
1	Replace key and turn on board	
2	Communication check with the intercom	
3		When ready, tell the control room to actuate the ox main fire valve
4	Switch on the ox main fire valve, initiate mass flow controller (1g/s)	
5		Set cart regulator to 90 psi with flow through the mass flow controller
6		Find leaks with bubble solution
7	Turn off ox main fire valve, set mass flow controller to zero	
8		Tighten the appropriate fittings
9	Iterate Steps 3-8 until no leaks are present	

- Depressurize oxidizer main manifold

Igniter Fuel Line (skip this leak check if the igniter has not been disassembled since the previous experimental session)

- Attach nitrogen to fuel igniter manifold
- Slowly open nitrogen tank
- Slowly open manifold ball valve to fuel igniter manifold
- Check to make sure there is sufficient pressure in the manifold using the analog gauge (≈ 200 psi)
- One red team member must return to the control room, the others go to the test cell
-

Table 6. Igniter Fuel Leak Check Procedure

Step	Control Room	Test Cell
1	Replace key and turn on board	
2	Communication check with the intercom	
3		When ready, tell the control room to actuate the fuel secondary fire valve
4	Switch on the fuel secondary fire valve	
5		Find leaks with bubble solution

Figure B.11: Page 11 of the procedure manual

Pressurized Lines – Safety Glasses Required

6	Turn off fuel secondary fire valve	
7		Tighten the appropriate fittings
8	Iterate Steps 3-7 until no leaks are present	

Igniter Oxygen Line (skip this leak check if the igniter has not been disassembled since the previous experimental session)

- Attach nitrogen to oxygen igniter manifold
- Slowly open nitrogen tank
- Slowly open manifold ball valves to oxygen igniter manifold
- Check to make sure there is sufficient pressure in the manifold using the analog gauge (≈ 200 psi)
- Set the oxygen igniter pressure on the pressure regulator board
- One red team member must return to the control room, the others go to the test cell

Table 7. Igniter Oxygen Leak Check Procedure

Step	Control Room	Test Cell
1	Replace key and turn on board	
2	Communication check with the intercom	
3		When ready, tell the control room to actuate the oxidizer secondary fire valve
4	Switch on the oxidizer secondary fire valve	
5		Find leaks with bubble solution
6	Turn off oxidizer secondary fire valve	
7		Tighten the appropriate fittings
8	Iterate Steps 3-7 until no leaks are present	

Figure B.12: Page 12 of the procedure manual

APPENDIX C

CASE STUDY CODE

Rocketdyne Injector Scaling

ROCKETDYNE LOX/Methane Coaxial Injector Investigation (Test 022)

$$N_{inj} = 82$$

Full Scale Methane Conditions (Test 022)

$$\dot{m}_{Methane} = 21.69 \ \text{[lbm/s]} \quad \text{Data from Jensen reference}$$

$$\rho_{Methane} = 8.5 \ \left[\text{lbm/ft}^3\right] \quad \text{Data from Jensen reference}$$

$$\dot{Q}_{Methane,US} = \dot{m}_{Methane} / \rho_{Methane}$$

$$\dot{Q}_{Methane} = \frac{\dot{Q}_{Methane,US} \cdot \left| 0.028317 \ \frac{\text{m}^3}{\text{ft}^3} \right|}{N_{inj}}$$

Full Scale LOX Conditions (Test 022)

$$\dot{m}_{LOX} = 65.92 \ \text{[lbm/s]} \quad \text{Data from Jensen reference}$$

$$\rho_{LOX} = 68.1 \ \left[\text{lbm/ft}^3\right] \quad \text{Data from Jensen reference}$$

$$\dot{Q}_{LOX,US} = \dot{m}_{lox}/\rho_{LOX}$$

$$\dot{Q}_{LOX} = \frac{\dot{Q}_{LOX,US} \cdot \left|0.028317 \ \frac{\text{m}^3}{\text{ft}^3}\right|}{N_{inj}}$$

Overall Full Scale Conditions

$$OF_{fs} = \dot{m}_{LOX}/\dot{m}_{Methane}$$

$$\Phi_{fs} = OF_{fs}/OF_{stoich}$$

$$CH_4 + 2\,O_2 = CO_2 + 2\,H_2O$$

$$OF_{stoich} = \frac{2 \ \text{[g/gmol]} \cdot \text{MW}\,(Oxygen)}{1 \ \text{[g/gmol]} \cdot \text{MW}\,(Methane)}$$

Subscale Methane Conditions

$$P_{inj} = 1.5 \ \left[\text{lbf/in}^2\right]$$

$$P_{fuel} = \left(14.7 \ \left[\text{lbf/in}^2\right] + P_{inj}\right) \cdot \left|6.89476 \ \frac{\text{kPa}}{\text{lbf/in}^2}\right|$$

$$\rho_{CH4} = \rho\left(CH4,\ \mathrm{T} = T_{fuel},\ \mathrm{P} = P_{fuel}\right)$$

$$\rho_{fuel,N2} = \rho\left(N2,\ \mathrm{T} = T_{fuel},\ \mathrm{P} = P_{fuel}\right)$$

$$Y_{CH4} = \frac{\dot{m}_{CH4}}{\dot{m}_{CH4} + \dot{m}_{fuel,N2}}$$

$$Y_{fuel,N2} = 1 - Y_{CH4}$$

$$\rho_{fuel} = Y_{fuel,N2} \cdot \rho_{fuel,N2} + Y_{CH4} \cdot \rho_{CH4}$$

$$\dot{Q}_{fuel} = \dot{Q}_{Methane}$$

$$\dot{Q}_{fuel} = \frac{\dot{m}_{CH4} + \dot{m}_{fuel,N2}}{\rho_{fuel} \cdot \left|1000\ \frac{\mathrm{g}}{\mathrm{kg}}\right|}$$

Subscale Oxygen Conditions

$$P_{ox} = \left(14.7\ \left[\mathrm{lbf/in^2}\right] + P_{inj}\right) \cdot \left|6.89476\ \frac{\mathrm{kPa}}{\mathrm{lbf/in^2}}\right|$$

$$\rho_{O2} = \rho\left(O2,\ \mathrm{T} = T_{ox},\ \mathrm{P} = P_{ox}\right)$$

$$\rho_{ox} = \rho_{O2}$$

$$\dot{Q}_{ox} = \dot{Q}_{LOX}$$

$$\dot{Q}_{ox} = \frac{\dot{m}_{O2}}{\rho_{ox} \cdot \left|1000\ \frac{\mathrm{g}}{\mathrm{kg}}\right|}$$

Overall Subscale Conditions

$$OF_{model} = \dot{m}_{O2}/\dot{m}_{CH4}$$

$$\Phi_{model} = OF_{model}/OF_{stoich}$$

$$\Phi_{model} = \Phi_{fs}$$

RD-170 Main Chamber Scaling

Equations

RD-170 Main Chamber Oxidizer

$$N_{inj} = 271$$

Full Scale LOX Manifold Conditions

$$P_{LOX} = 278.26 \text{ [bar]} \quad \text{Data from Manski reference}$$

$$T_{LOX} = 687.7 \text{ [K]} \quad \text{Data from Manski reference}$$

$$\dot{m}_{LOX,total} = 440.7 \text{ [kg/s]} \quad \text{Data from Manski reference}$$

$$\rho_{LOX} = 155.38 \left[\text{kg/m}^3\right] \quad \text{Data from Manski reference}$$

$$\dot{m}_{LOX} = \dot{m}_{LOX,total}/N_{inj}$$

$$\dot{Q}_{LOX} = \dot{m}_{LOX}/\rho_{LOX}$$

S

Subscale Oxidizer Conditions

$$P_{ox,US} = 1.5 \text{ [psi]}$$

$$P_{ox} = (14.7 \text{ [psi]} + P_{ox,US}) \cdot \left| 6.89476 \frac{\text{kPa}}{\text{psi}} \right|$$

$$Y_{Air} = \frac{\dot{m}_{Air}}{\dot{m}_{Air} + \dot{m}_{oxN2}}$$

$$Y_{oxN2} = 1 - Y_{Air}$$

$$\rho_{Air} = \rho\left(Air,\ \mathrm{T} = T_{ox},\ \mathrm{P} = P_{ox}\right)$$

$$\rho_{oxN2} = \rho\left(N2,\ \mathrm{T} = T_{ox},\ \mathrm{P} = P_{ox}\right)$$

$$\rho_{ox} = Y_{Air} \cdot \rho_{Air} + Y_{oxN2} \cdot \rho_{oxN2}$$

$$\dot{Q}_{ox} = \frac{(\dot{m}_{Air} + \dot{m}_{oxN2}) \cdot \left| 0.001 \ \frac{\text{kg}}{\text{g}} \right|}{\rho_{ox}}$$

$$\dot{Q}_{ox} = \dot{Q}_{LOX}$$

$$\dot{m}_{O2} = .233 \cdot \dot{m}_{Air}$$

RD-170 Main Chamber Fuel

Full Scale RP-1 Manifold Conditions

$$P_{RP1} = 278.26 \text{ [bar]} \quad \text{Data from Manski reference}$$

$$T_{RP1} = 492.2 \text{ [K]} \quad \text{Data from Manski reference}$$

$$\dot{m}_{RP1,total} = 158.05 \ [\text{kg/s}] \quad \text{Data from Manski reference}$$

$$\rho_{RP1} = 807.00 \ \left[\text{kg/m}^3\right] \quad \text{Data from Manski reference}$$

$$\dot{m}_{RP1} = \dot{m}_{RP1,total}/N_{inj}$$

$$\dot{Q}_{RP1} = \dot{m}_{RP1}/\rho_{RP1}$$

Subscale Fuel Conditions

$$P_{fuel,US} = 1.5 \ [\text{psi}]$$

$$\dot{m}_{total} = \dot{m}_{C3H8} + \dot{m}_{fuel,N2} + \dot{m}_{CH4}$$

$$P_{fuel} = (14.7 \ [\text{psi}] + P_{fuel,US}) \cdot \left| 6.89476 \ \frac{\text{kPa}}{\text{psi}} \right|$$

$$Y_{CH4} = \dot{m}_{CH4}/\dot{m}_{total}$$

$$Y_{C3H8} = \dot{m}_{C3H8}/\dot{m}_{total}$$

$$Y_{fuel,N2} = 1 - Y_{CH4} - Y_{C3H8}$$

$$\rho_{CH4} = \rho\left(CH4, \ \text{T} = T_{fuel}, \ \text{P} = P_{fuel}\right)$$

$$\rho_{fuel,N2} = \rho\left(N2, \ \text{T} = T_{fuel}, \ \text{P} = P_{fuel}\right)$$

$$\rho_{C3H8} = \rho\left(C3H8, \ \text{T} = T_{fuel}, \ \text{P} = P_{fuel}\right)$$

$$\rho_{fuel} = Y_{CH4} \cdot \rho_{CH4} + Y_{fuel,N2} \cdot \rho_{fuel,N2} + Y_{C3H8} \cdot \rho_{C3H8}$$

$$\dot{Q}_{fuel} = \frac{(\dot{m}_{total}) \cdot \left| 0.001 \ \frac{\text{kg}}{\text{g}} \right|}{\rho_{fuel}}$$

$$\dot{Q}_{fuel} = \dot{Q}_{RP1}$$

$$OF = \frac{\dot{m}_{O2}}{\dot{m}_{CH4} + \dot{m}_{C3H8}}$$

Stoichiometric Determination Calculation

$$X\,CH_4 \ + \ Y\,C_3H_8 \ + Z\,O_2 \ = \ A\,CO_2 \ + \ B\,H_2O$$

$$MW_{O2} = \text{MW}\,(Oxygen)$$

$$MW_{C3H8} = \text{MW}\,(Propane)$$

$$MW_{CH4} = \text{MW}\,(Methane)$$

$$\dot{m}_{CH4} = X \cdot MW_{CH4}$$

$$\dot{m}_{C3H8} = Y \cdot MW_{C3H8}$$

$$\dot{m}_{O2,st} = Z \cdot MW_{O2}$$

Hydrogen Balance

$$4 \cdot X + 8 \cdot Y = 2 \cdot B$$

Carbon Balance

$$X + 3 \cdot Y = A$$

Oxygen Balance

$$2 \cdot Z = 2 \cdot A + B$$

$$OF_{stoich} = \left(\frac{\dot{m}_{O2,st}}{\dot{m}_{C3H8} + \dot{m}_{CH4}} \right)$$

$$\Phi = OF/OF_{stoich}$$

$$\Phi = 1$$

APPENDIX D

UNCERTAINTY ANALYSIS

PARAMETERS OF INTEREST AND UNCERTAINTY CALCULATIONS

All uncertainty analyses follow the propagation of error technique by Coleman and Steele [26].

Mass Flow Rate

$\dot{m}_f$ random uncertainty was based on the video of the instrument display. The finding was that the flow rate was largely effected by the manifold pressure pulsations. The following relation was defined based on the magnitude of the pressure standard deviation, fuel mass flow rate and a scaling factor to ensure the proper magnitude.

$$O_{Factor} = .06 \ \ [1/\text{psi}]$$

$$P_{m,f} = \dot{m}_f \cdot \sigma_{P,f} \cdot O_{Factor}$$

Omega FMA-2609A

$$B_{m,f} = 0.008 \cdot \dot{m}_f + .002 \cdot (0.547 \ \text{[g/s]})$$

$$U_{m,f} = \sqrt{\left(B_{m,f}^2 + P_{m,f}^2\right)}$$

$\dot{m}_o$ random uncertainty was based a similar video. The random variation was much more steady, and scaled with O2 mass flow rate, therefore, a curve was fit.

$$F_{Factor} = 0.0334$$

$$P_{m,o} = F_{Factor} \cdot \dot{m}_o$$

Omega FMA-2613A

$$B_{m,o} = 0.008 \cdot \dot{m}_o + .002 \cdot (21.81 \ \text{[g/s]})$$

$$U_{m,o} = \sqrt{\left(B_{m,o}^2 + P_{m,o}^2\right)}$$

Temperature

K-Type Thermocouple

$$B_T = 2.2 \ \text{[K]}$$

Special Limits of Error K-Type Thermocouple

$$B_{T,sle} = 1.1 \ \text{[K]}$$

$$U_{T,f} = \sqrt{\left(B_T^2 + \left(2 \cdot \sigma_{T,f}\right)^2\right)}$$

$$U_{T,o} = \sqrt{\left(B_T^2 + \left(2 \cdot \sigma_{T,o}\right)^2\right)}$$

Pressure

Omega PX313 Series

$$B_P = .075 \ \text{[psi]}$$

Estimated Ambient Pressure Bias

$$B_{amb} = 0.3 \ \text{[psi]}$$

$$P_f = (14.7 \ \text{[psi]} + P_{f,US}) \cdot \left|6894.76 \ \frac{\text{Pa}}{\text{psi}}\right|$$

$$U_{P,f} = \sqrt{\left(B_{amb}^2 + B_P^2 + \left(2 \cdot \sigma_{P,f}\right)^2\right)} \cdot \left|6894.76 \ \frac{\text{Pa}}{\text{psi}}\right|$$

$$P_o = (14.7 \ \text{[psi]} + P_{o,US}) \cdot \left|6894.76 \ \frac{\text{Pa}}{\text{psi}}\right|$$

$$U_{P,o} = \sqrt{\left(B_{amb}^2 + B_P^2 + \left(2 \cdot \sigma_{P,o}\right)^2\right)} \cdot \left|6894.76 \ \frac{\text{Pa}}{\text{psi}}\right|$$

Mixture Ratio Calculations

$$OF = \frac{\dot{m}_o}{\dot{m}_f}$$

$$U_{OF} = \sqrt{OF^2 \cdot \left[\left(\frac{U_{mo}}{\dot{m}_o} \right)^2 + \left(\frac{U_{mf}}{\dot{m}_f} \right)^2 \right]}$$

Total Mass Flow Rate Calculations

$$\dot{m}_{total} = \dot{m}_f + \dot{m}_o$$

$$U_{m,total} = \sqrt{\left(U_{m_f}^2 + U_{m_o}^2 \right)}$$

Oxidizer Density

Assume Negligible uncertainty in molecular weight and universal gas constant

$$MW_o = \mathrm{MW}\left(Oxygen\right)$$

$$T_o = \mathrm{ConvertTemp}(C,\ K,\ T_{o,C})$$

Real Gas Solution

$$\rho_o = \rho\left(Oxygen,\ \mathrm{T} = T_{o,C},\ \mathrm{P} = P_o\right)$$

$$U_{\rho,o} = \sqrt{\rho_o^2 \cdot \left[\left(\frac{U_{P,o}}{P_o} \right)^2 + \left(\frac{U_{T,o}}{T_o} \right)^2 \right]}$$

Fuel Density

Assume Negligible uncertainty in molecular weight and universal gas constant

$$MW_f = \mathrm{MW}\left(Methane\right)$$

$$T_f = \text{ConvertTemp}(C,\ K,\ T_{f,C})$$

Real Gas Solution

$$\rho_f = \rho\left(Methane,\ \text{T} = T_{f,C},\ \text{P} = P_f\right)$$

$$U_{\rho,f} = \sqrt{\rho_f^2 \cdot \left[\left(\frac{U_{P,f}}{P_f}\right)^2 + \left(\frac{U_{T,f}}{T_f}\right)^2\right]}$$

Oxidizer Velocity

$$D_{o,US} = .35\ \ [\text{in}]$$

$$D_o = D_{o,US} \cdot \left|0.0254\ \frac{\text{m}}{\text{in}}\right|$$

$$U_{D,o,US} = .003\ \ [\text{in}]$$

$$U_{D,o} = U_{D,o,US} \cdot \left|0.0254\ \frac{\text{m}}{\text{in}}\right|$$

$$V_o = 4\left(\frac{\dot{\text{m}}_\text{o}\left|0.001\ \frac{\text{kg}}{\text{g}}\right|}{\pi \cdot \rho_\text{o} \cdot \text{D}_\text{o}^2}\right)$$

$$U_{V,o} = \sqrt{V_o^2 \cdot \left[\left(\frac{\dot{U}_{mo}}{\dot{m}_o}\right)^2 + \left(\frac{U_{\rho,o}}{\rho_o}\right)^2 + 4 \cdot \left(\frac{U_{D,o}}{D_o}\right)^2\right]}$$

Fuel Velocity

$$D_{f,US} = .059\ \ [\text{in}]$$

$$D_f = D_{f,US} \cdot \left|0.0254\ \frac{\text{m}}{\text{in}}\right|$$

$$U_{D,f,US} = .003\ \ [\text{in}]$$

$$U_{D,f} = U_{D,f,US} \cdot \left| 0.0254 \ \frac{\mathrm{m}}{\mathrm{in}} \right|$$

$$V_f = \frac{\dot{m}_f \cdot \left| 0.001 \ \frac{\mathrm{kg}}{\mathrm{g}} \right|}{\pi \cdot \rho_f \cdot D_f^2}$$

$$U_{V,f} = \sqrt{V_f^2 \cdot \left[\left(\frac{\dot{U}_{mf}}{\dot{m}_f} \right)^2 + \left(\frac{U_{\rho,f}}{\rho_f} \right)^2 + 4 \cdot \left(\frac{U_{D,f}}{D_f} \right)^2 \right]}$$

Velocity Ratio

$$V_{ratio} = \frac{V_f}{V_o}$$

$$U_{V,ratio} = \sqrt{V_{ratio}^2 \cdot \left[\left(\frac{U_{V,f}}{V_f} \right)^2 + \left(\frac{U_{V,o}}{V_o} \right)^2 \right]}$$

Reynold's Number - Oxidizer

Assume Negligible uncertainty in viscosity

$$\mu_o = \mu \left(Oxygen, \ \mathrm{P} = P_o, \ \mathrm{T} = T_{o,C} \right)$$

$$Re_o = \frac{\rho_o \cdot V_o \cdot D_o}{\mu_o}$$

$$U_{Re,o} = \sqrt{Re_o^2 \cdot \left[\left(\frac{U_{\rho,o}}{\rho_o} \right)^2 + \left(\frac{U_{V,o}}{V_o} \right)^2 + \left(\frac{U_{D,o}}{D_o} \right)^2 \right]}$$

Reynold's Number - Fuel

Assume Negligible uncertainty in viscosity

$$\mu_f = \mu \left(Methane, \ \mathrm{P} = P_f, \ \mathrm{T} = T_{f,C} \right)$$

$$Re_f = \frac{\rho_f \cdot V_f \cdot D_f}{\mu_f}$$

$$U_{Re,f} = \sqrt{Re_f^2 \cdot \left[\left(\frac{U_{\rho,f}}{\rho_f} \right)^2 + \left(\frac{U_{V,f}}{V_f} \right)^2 + \left(\frac{U_{D,f}}{D_f} \right)^2 \right]}$$

Momentum Ratio (λ)

$$\lambda = \frac{\dot{m}_f \cdot V_f}{\dot{m}_o \cdot V_o}$$

$$U_\lambda = \sqrt{\lambda^2 \left[\left(\frac{U_{m,f}}{\dot{m}_f} \right)^2 + \left(\frac{U_{V,f}}{V_f} \right)^2 + \left(\frac{U_{m,o}}{\dot{m}_o} \right)^2 + \left(\frac{U_{V,o}}{V_o} \right)^2 \right]}$$

π Criterion

$$\pi^* = \frac{\dot{m}_o}{\dot{m}_f} \sqrt{\frac{\rho_f}{\rho_o}}$$

$$U_{\pi^*} = \sqrt{(\pi^*)^2 \left[\left(\frac{U_{m,o}}{\dot{m}_o} \right)^2 + \left(\frac{U_{m,f}}{\dot{m}_f} \right)^2 + 0.25 \cdot \left(\frac{U_{\rho,f}}{\rho_f} \right)^2 + 0.25 \cdot \left(\frac{U_{\rho,o}}{\rho_o} \right)^2 \right]}$$

Volumetric Flow Rate

$$Q_o = \frac{\dot{m}_o \cdot \left| 0.001 \ \frac{\text{kg}}{\text{g}} \right|}{\rho_o} \cdot \left| 1000000 \ \frac{\text{cm}^3}{\text{m}^3} \right|$$

$$U_{Q,o} = \sqrt{Q_o^2 \left[\left(\frac{U_{m,o}}{\dot{m}_o} \right)^2 + \left(\frac{U_{\rho,o}}{\rho_o} \right)^2 \right]}$$

$$Q_f = \frac{\dot{m}_f \cdot \left| 0.001 \ \frac{\text{kg}}{\text{g}} \right|}{\rho_f} \cdot \left| 1000000 \ \frac{\text{cm}^3}{\text{m}^3} \right|$$

$$U_{Q,f} = \sqrt{Q_f^2 \left[\left(\frac{U_{m,f}}{\dot{m}_f} \right)^2 + \left(\frac{U_{\rho,f}}{\rho_f} \right)^2 \right]}$$

CHAMBER NATURAL FREQUENCY CALCULATIONS

$$R = .1016 \ \text{[m]}$$

$$f_{T1} = \left(\frac{c_{avg}}{2}\right) \cdot \left(\frac{0.586}{R}\right)$$

$$f_{R1} = \left(\frac{c_{avg}}{2}\right) \cdot \left(\frac{1.22}{R}\right)$$

$$f_{T1R1} = \left(\frac{c_{avg}}{2}\right) \cdot \left(\frac{1.697}{R}\right)$$

$$f_{T2} = \left(\frac{c_{avg}}{2}\right) \cdot \left(\frac{0.972}{R}\right)$$

$$f_{R2} = \left(\frac{c_{avg}}{2}\right) \cdot \left(\frac{2.233}{R}\right)$$

$$f_{T1R2} = \left(\frac{c_{avg}}{2}\right) \cdot \left(\frac{2.714}{R}\right)$$

$$f_{T2R1} = \left(\frac{c_{avg}}{2}\right) \cdot \left(\frac{2.135}{R}\right)$$

$$T_{\alpha} = \text{ConvertTemp}(C,\ K,\ T_{\alpha,C})$$

$$T_{\beta} = \text{ConvertTemp}(C,\ K,\ T_{\beta,C})$$

$$T_{\gamma} = \text{ConvertTemp}(C,\ K,\ T_{\gamma,C})$$

$$T_{\delta} = \text{ConvertTemp}(C,\ K,\ T_{\delta,C})$$

$$T_{\epsilon} = \text{ConvertTemp}(C,\ K,\ T_{\epsilon,C})$$

$$Gas, \alpha = 1$$

$$Gas, \beta = 0.6$$

$$Gas, \gamma = 0.3$$

$$Gas, \delta = 0.1$$

$$Gas, \epsilon = 0.05$$

$$\gamma_{air} = 1.4$$

$$\gamma_{prod} = 1.59891 - 0.415495 \cdot OF + 0.189413 \cdot OF^2 - 0.0454315 \cdot OF^3$$

$$+0.00598729 \cdot OF^4 - 0.00040905 \cdot OF^5 + 0.0000113004 \cdot OF^6$$

$$\gamma_{\alpha} = Gas_{\alpha} \cdot \gamma_{prod} + (1 - Gas_{\alpha}) \cdot \gamma_{air}$$

$$\gamma_{\beta} = Gas_{\beta} \cdot \gamma_{prod} + (1 - Gas_{\beta}) \cdot \gamma_{air}$$

$$\gamma_{\gamma} = Gas_{\gamma} \cdot \gamma_{prod} + (1 - Gas_{\gamma}) \cdot \gamma_{air}$$

$$\gamma_{\delta} = Gas_{\delta} \cdot \gamma_{prod} + (1 - Gas_{\delta}) \cdot \gamma_{air}$$

$$\gamma_{\epsilon} = Gas_{\epsilon} \cdot \gamma_{prod} + (1 - Gas_{\epsilon}) \cdot \gamma_{air}$$

$$MW_{air} = 28.85 \ \ [\text{kg/kmol}]$$

$$MW_{prod} = 9.48499 \ \ [\text{kg/kmol}] + (3.70457 \ \ [\text{kg/kmol}]) \cdot OF - (0.1902 \ \ [\text{kg/kmol}]) \cdot OF^2$$

$$MW_{\alpha} = Gas_{\alpha} \cdot MW_{prod} + (1 - Gas_{\alpha}) \cdot MW_{air}$$

$$MW_{\beta} = Gas_{\beta} \cdot MW_{prod} + (1 - Gas_{\beta}) \cdot MW_{air}$$

$$MW_{\gamma} = Gas_{\gamma} \cdot MW_{prod} + (1 - Gas_{\gamma}) \cdot MW_{air}$$

$$MW_{\delta} = Gas_{\delta} \cdot MW_{prod} + (1 - Gas_{\delta}) \cdot MW_{air}$$

$$MW_{\epsilon} = Gas_{\epsilon} \cdot MW_{prod} + (1 - Gas_{\epsilon}) \cdot MW_{air}$$

$$c_{\alpha} = \sqrt{\gamma_{\alpha} \cdot \left(\frac{R\#}{MW_{\alpha}}\right) \cdot T_{\alpha}}$$

$$c_{\beta} = \sqrt{\gamma_{\beta} \cdot \left(\frac{R\#}{MW_{\beta}}\right) \cdot T_{\beta}}$$

$$c_{\gamma} = \sqrt{\gamma_{\gamma} \cdot \left(\frac{R\#}{MW_{\gamma}}\right) \cdot T_{\gamma}}$$

$$c_{\delta} = \sqrt{\gamma_{\delta} \cdot \left(\frac{R\#}{MW_{\delta}}\right) \cdot T_{\delta}}$$

$$c_{\epsilon} = \sqrt{\gamma_{\epsilon} \cdot \left(\frac{R\#}{MW_{\epsilon}}\right) \cdot T_{\epsilon}}$$

$$split = (1/9)$$

$$c_{avg} = 2 \cdot split \cdot c_{\beta} + 2 \cdot split \cdot c_{\gamma} + 2 \cdot split \cdot c_{\delta} + 2 \cdot split \cdot c_{\epsilon} + split \cdot c_{\alpha}$$

APPENDIX E

TEST MATRIX

Table E.1: Test Matrix 1.0-2.0

Test	Set Point	$\dot{m}_{CH4}$ [g/s]	$\dot{m}_{CH4\,FMA}$ SLPM	$\dot{m}_{O2}$ [g/s]	$\dot{m}_{O2\,FMA}$ SLPM	$\frac{O}{F}$	Φ
1.0	1	0.1095	10	0.2184	10.01	1.995	2
1.0	2	0.1095	10	0.2426	11.12	2.216	1.8
1.0	3	0.1095	10	0.273	12.51	2.493	1.6
1.0	4	0.1095	10	0.312	14.3	2.849	1.4
1.0	5	0.1095	10	0.364	16.68	3.324	1.2
1.0	6	0.1095	10	0.4368	20.02	3.989	1
1.0	7	0.1095	10	0.4853	22.25	4.432	0.9
1.0	8	0.1095	10	0.5459	25.03	4.986	0.8
1.0	9	0.1095	10	0.6239	28.6	5.699	0.7
1.0	10	0.1095	10	0.6719	30.8	6.137	0.65
1.0	11	0.1095	10	0.7279	33.37	6.649	0.6
1.0	12	0.1095	10	0.7941	36.4	7.253	0.55
1.0	13	0.1095	10	0.8735	40.04	7.978	0.5
1.5	1	0.1642	15	0.3276	15.02	1.995	2
1.5	2	0.1642	15	0.364	16.68	2.216	1.8
1.5	3	0.1642	15	0.4095	18.77	2.493	1.6
1.5	4	0.1642	15	0.4679	21.45	2.849	1.4
1.5	5	0.1642	15	0.5459	25.03	3.324	1.2
1.5	6	0.1642	15	0.6551	30.03	3.989	1
1.5	7	0.1642	15	0.7279	33.37	4.432	0.9
1.5	8	0.1642	15	0.8189	37.54	4.986	0.8
1.5	9	0.1642	15	0.9359	42.9	5.699	0.7
1.5	10	0.1642	15	1.008	46.2	6.137	0.65
1.5	11	0.1642	15	1.092	50.05	6.649	0.6
1.5	12	0.1642	15	1.191	54.61	7.253	0.55
1.5	13	0.1642	15	1.31	60.07	7.978	0.5
2.0	1	0.219	20	0.4368	20.02	1.995	2
2.0	2	0.219	20	0.4853	22.25	2.216	1.8
2.0	3	0.219	20	0.5459	25.03	2.493	1.6
2.0	4	0.219	20	0.6239	28.6	2.849	1.4
2.0	5	0.219	20	0.7279	33.37	3.324	1.2
2.0	6	0.219	20	0.8735	40.04	3.989	1
2.0	7	0.219	20	0.9706	44.49	4.432	0.9
2.0	8	0.219	20	1.092	50.05	4.986	0.8
2.0	9	0.219	20	1.248	57.21	5.699	0.7
2.0	10	0.219	20	1.344	61.61	6.137	0.65
2.0	11	0.219	20	1.456	66.74	6.649	0.6
2.0	12	0.219	20	1.588	72.81	7.253	0.55
2.0	13	0.219	20	1.747	80.09	7.978	0.5

Table E.2: Test Matrix 2.5-3.5

Test	Set Point	$\dot{m}_{CH4}$ [g/s]	$\dot{m}_{CH4\,FMA}$ SLPM	$\dot{m}_{O2}$ [g/s]	$\dot{m}_{O2\,FMA}$ SLPM	$\frac{O}{F}$	Φ
2.5	1	0.2737	25	0.5459	25.03	1.995	2
2.5	2	0.2737	25	0.6066	27.81	2.216	1.8
2.5	3	0.2737	25	0.6824	31.28	2.493	1.6
2.5	4	0.2737	25	0.7799	35.75	2.849	1.4
2.5	5	0.2737	25	0.9099	41.71	3.324	1.2
2.5	6	0.2737	25	1.092	50.05	3.989	1
2.5	7	0.2737	25	1.213	55.62	4.432	0.9
2.5	8	0.2737	25	1.365	62.57	4.986	0.8
2.5	9	0.2737	25	1.56	71.51	5.699	0.7
2.5	10	0.2737	25	1.68	77.01	6.137	0.65
2.5	11	0.2737	25	1.82	83.42	6.649	0.6
2.5	12	0.2737	25	1.985	91.01	7.253	0.55
2.5	13	0.2737	25	2.184	100.1	7.978	0.5
3.0	1	0.3285	30	0.6551	30.03	1.995	2
3.0	2	0.3285	30	0.7279	33.37	2.216	1.8
3.0	3	0.3285	30	0.8189	37.54	2.493	1.6
3.0	4	0.3285	30	0.9359	42.9	2.849	1.4
3.0	5	0.3285	30	1.092	50.05	3.324	1.2
3.0	6	0.3285	30	1.31	60.07	3.989	1
3.0	7	0.3285	30	1.456	66.74	4.432	0.9
3.0	8	0.3285	30	1.638	75.08	4.986	0.8
3.0	9	0.3285	30	1.872	85.81	5.699	0.7
3.0	10	0.3285	30	2.016	92.41	6.137	0.65
3.0	11	0.3285	30	2.184	100.1	6.649	0.6
3.0	12	0.3285	30	2.382	109.2	7.253	0.55
3.0	13	0.3285	30	2.621	120.1	7.978	0.5
3.5	1	0.3832	35	0.7643	35.04	1.995	2
3.5	2	0.3832	35	0.8492	38.93	2.216	1.8
3.5	3	0.3832	35	0.9554	43.8	2.493	1.6
3.5	4	0.3832	35	1.092	50.05	2.849	1.4
3.5	5	0.3832	35	1.274	58.4	3.324	1.2
3.5	6	0.3832	35	1.529	70.08	3.989	1
3.5	7	0.3832	35	1.698	77.86	4.432	0.9
3.5	8	0.3832	35	1.911	87.6	4.986	0.8
3.5	9	0.3832	35	2.184	100.1	5.699	0.7
3.5	10	0.3832	35	2.352	107.8	6.137	0.65
3.5	11	0.3832	35	2.548	116.8	6.649	0.6
3.5	12	0.3832	35	2.779	127.4	7.253	0.55
3.5	13	0.3832	35	3.057	140.2	7.978	0.5

Table E.3: Test Matrix 4.0-5.0

Test	Set Point	$\dot{m}_{CH4}$ [g/s]	$\dot{m}_{CH4\,FMA}$ SLPM	$\dot{m}_{O2}$ [g/s]	$\dot{m}_{O2\,FMA}$ SLPM	$\frac{O}{F}$	Φ
4.0	1	0.4379	40	0.8735	40.04	1.995	2
4.0	2	0.4379	40	0.9706	44.49	2.216	1.8
4.0	3	0.4379	40	1.092	50.05	2.493	1.6
4.0	4	0.4379	40	1.248	57.21	2.849	1.4
4.0	5	0.4379	40	1.456	66.74	3.324	1.2
4.0	6	0.4379	40	1.747	80.09	3.989	1
4.0	7	0.4379	40	1.941	88.99	4.432	0.9
4.0	8	0.4379	40	2.184	100.1	4.986	0.8
4.0	9	0.4379	40	2.496	114.4	5.699	0.7
4.0	10	0.4379	40	2.688	123.2	6.137	0.65
4.0	11	0.4379	40	2.912	133.5	6.649	0.6
4.0	12	0.4379	40	3.176	145.6	7.253	0.55
4.0	13	0.4379	40	3.494	160.2	7.978	0.5
4.5	1	0.4927	45	0.9827	45.05	1.995	2
4.5	2	0.4927	45	1.092	50.05	2.216	1.8
4.5	3	0.4927	45	1.228	56.31	2.493	1.6
4.5	4	0.4927	45	1.404	64.36	2.849	1.4
4.5	5	0.4927	45	1.638	75.08	3.324	1.2
4.5	6	0.4927	45	1.965	90.1	3.989	1
4.5	7	0.4927	45	2.184	100.1	4.432	0.9
4.5	8	0.4927	45	2.457	112.6	4.986	0.8
4.5	9	0.4927	45	2.808	128.7	5.699	0.7
4.5	10	0.4927	45	3.024	138.6	6.137	0.65
4.5	11	0.4927	45	3.276	150.2	6.649	0.6
4.5	12	0.4927	45	3.573	163.8	7.253	0.55
4.5	13	0.4927	45	3.931	180.2	7.978	0.5
5.0	1	0.5474	50	1.092	50.05	1.995	2
5.0	2	0.5474	50	1.213	55.62	2.216	1.8
5.0	3	0.5474	50	1.365	62.57	2.493	1.6
5.0	4	0.5474	50	1.56	71.51	2.849	1.4
5.0	5	0.5474	50	1.82	83.42	3.324	1.2
5.0	6	0.5474	50	2.184	100.1	3.989	1
5.0	7	0.5474	50	2.426	111.2	4.432	0.9
5.0	8	0.5474	50	2.73	125.1	4.986	0.8
5.0	9	0.5474	50	3.12	143	5.699	0.7
5.0	10	0.5474	50	3.36	154	6.137	0.65
5.0	11	0.5474	50	3.64	166.8	6.649	0.6
5.0	12	0.5474	50	3.97	182	7.253	0.55
5.0	13	0.5474	50	4.368	200.2	7.978	0.5

Table E.4: Test Session Schedule

January						
Sunday	Monday	Tuesday	Wednesday	Thursday	Friday	Saturday
7	8	9	10	11	12	13
				Imp30 (P)	Imp60 (P)	
14	15	16	17	18	19	20
	2O Swirl Delta 2	Imp 45 (P)				

February						
Sunday	Monday	Tuesday	Wednesday	Thursday	Friday	Saturday
4	5	6	7	8	9	10
	Imp45 (1) Imp30 (1) Imp60 (1)	Imp30 (2)	Imp45 (2) Imp60 (2) Imp30 (3)	Imp60 (3) Imp45R (3) Sxox	Imp60R (4) Sxf Imp30 (4) Imp45 (4)	

Sx	Mass flow fluctuation video taken
R	Random test matrix
( )	Corresponding naming scheme

APPENDIX F

INSTRUMENTATION SPECIFICATIONS

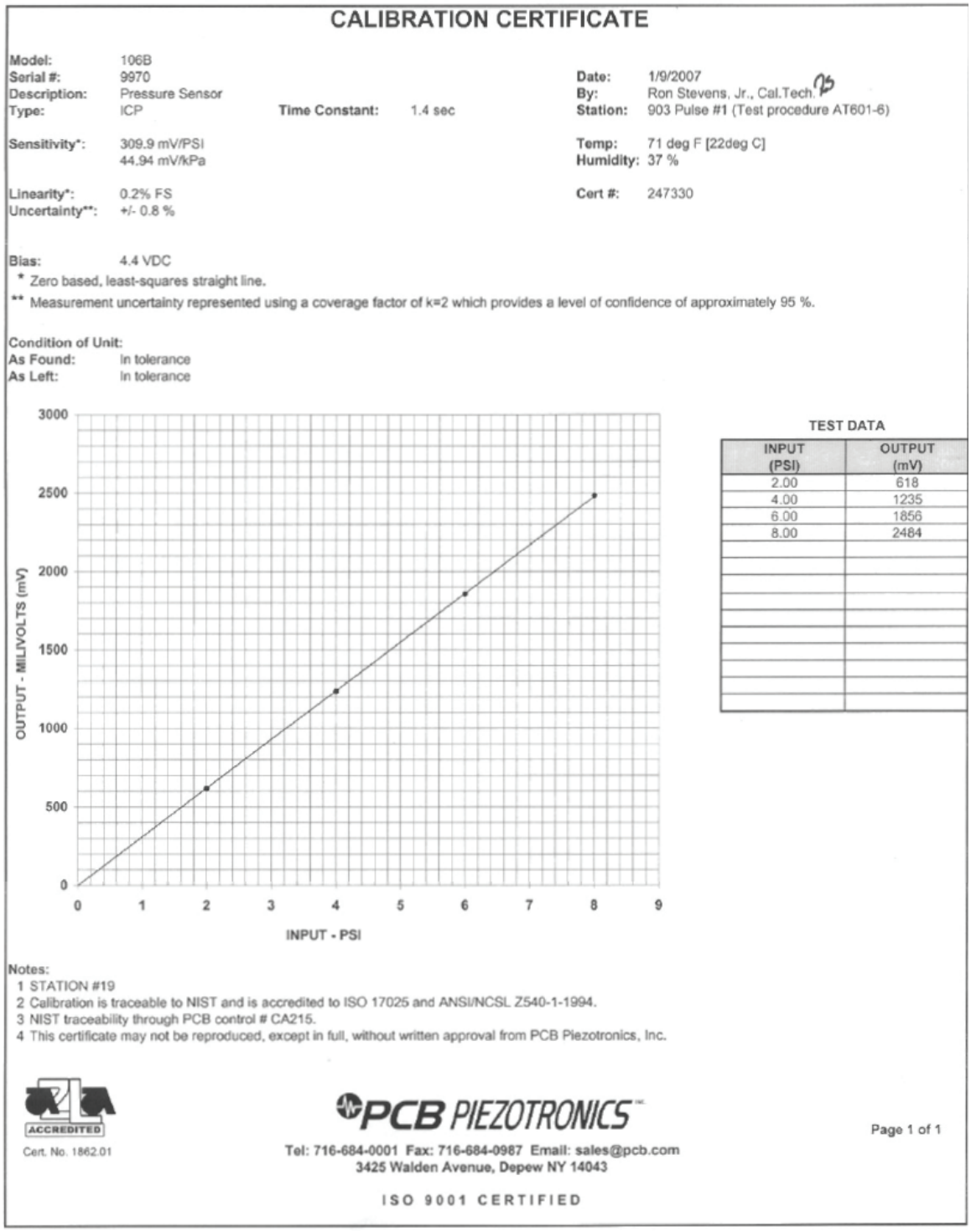

CALIBRATION CERTIFICATE

Model:	106B			**Date:**	1/9/2007
Serial #:	9970			**By:**	Ron Stevens, Jr., Cal.Tech.
Description:	Pressure Sensor				
Type:	ICP	**Time Constant:**	1.4 sec	**Station:**	903 Pulse #1 (Test procedure AT601-6)
Sensitivity*:	309.9 mV/PSI 44.94 mV/kPa			**Temp:** **Humidity:**	71 deg F [22deg C] 37 %
Linearity*:	0.2% FS			**Cert #:**	247330
Uncertainty:**	+/- 0.8 %				

Bias: 4.4 VDC

* Zero based, least-squares straight line.

** Measurement uncertainty represented using a coverage factor of k=2 which provides a level of confidence of approximately 95 %.

Condition of Unit:
As Found: In tolerance
As Left: In tolerance

TEST DATA

INPUT (PSI)	OUTPUT (mV)
2.00	618
4.00	1235
6.00	1856
8.00	2484

Notes:
1 STATION #19
2 Calibration is traceable to NIST and is accredited to ISO 17025 and ANSI/NCSL Z540-1-1994.
3 NIST traceability through PCB control # CA215.
4 This certificate may not be reproduced, except in full, without written approval from PCB Piezotronics, Inc.

ACCREDITED
Cert. No. 1862.01

PCB PIEZOTRONICS

Tel: 716-684-0001 Fax: 716-684-0987 Email: sales@pcb.com
3425 Walden Avenue, Depew NY 14043

ISO 9001 CERTIFIED

Page 1 of 1

Figure F.1: PCB 106B Calibration Sheet 1/2

~ Calibration Certificate ~

per ISA-S37.10

Model Number: 106B

Serial Number: 9970

Description: ICP® Microphone

Manufacturer: PCB Method: Sinusoidal Excitation (Pistonphone)

Calibration Data

Output @124 dB SPL 4.09 mV (pk/pk) Reference Freq.: 250 Hz.

Sensitivity: 314.7 mV/psi 45.64 mV/kPa

Acceleration Sens.: 0.0039 psi/g 0.0027 kPa/ms^{-2} Dev. @ 10 kHz: 0.275 dB

Temperature: 71 °F 22 °C Relative Humidity: 37 %

Electrostatic Frequency Response

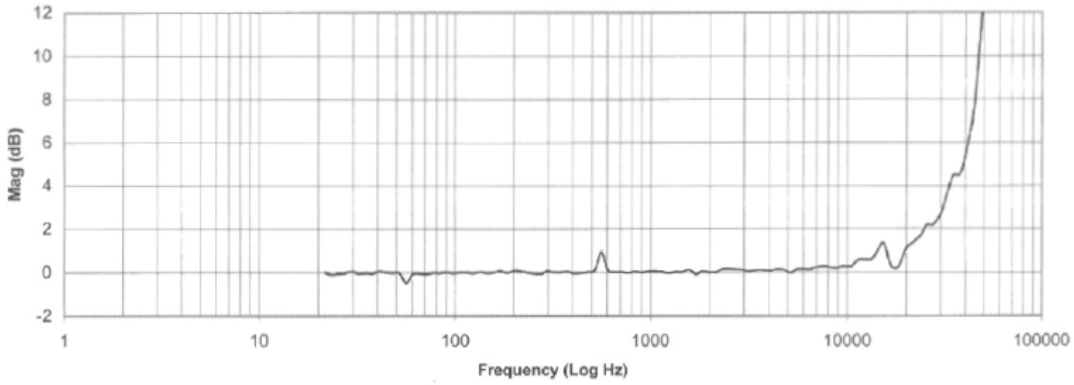

Condition of Unit

As Found: Out of Tolerance, High Acceleration Sensitivity

As Left: Out of Tolerance, High Acceleration Sensitivity, Customer Accepts As Is.

Notes

1. Calibration is N.I.S.T. Traceable through Control No. CA322
2. Reference 0 dB = 20 µPa.
3. This certificate shall not be reproduced, except in full, without written approval from PCB Piezotronics, Inc.
4. Calibration is performed in compliance with ISO 9001, ISO 10012-1, ANSI/NCSL Z540-1-1994 and ISO 17025.
5. See Manufacturer's Specification Sheet for a detailed listing of performance specifications.
6. Measurement uncertainty (95% confidence level with coverage factor of 2) for reference frequency is +/-0.45 dB.

Technician: R. Stevens, Jr. Date: 1/9/2007

ACCREDITED

PCB PIEZOTRONICS
PRESSURE DIVISION

3425 Walden Avenue
Depew, New York 14043

Page 1 of 1 TEL: 888-684-0011 FAX: 716-686-9129 www.pcb.com

Figure F.2: PCB 106B Calibration Sheet 2/2

MASS AND VOLUMETRIC GAS FLOW CONTROLLERS

FMA-2617A
Starts at
$1392

- 20+ Gas Calibrations, Including He, O_2, Neon, N_2O, N_2, Air, Argon, CO, CO_2, Methane, Ethane, H_2, Propane, Butane, iso-Butane, Ethylene, Acetylene, Krypton, Xenon, Sulfur Hexafluoride
- Pressure, Temperature, and Volumetric and Mass Flow Simultaneously Displayed (FMA-2600A Series)
- Easy-to-Use Pushbutton Interface
- NIST Traceability Standard
- Full Scale Ranges from 0.5 SCCM to 1500 LPM
- Response Time of 50 to 100 ms Typical
- Turndown Ratio of 100:1 Typical
- Position Insensitive
- ±0.8% Reading Accuracy
- RS232 Standard

FMA-2601A, $2100, shown smaller than actual size.

The FMA-2600 and FVL-2600 Series mass and volumetric flow controllers use the principle of differential pressure within a laminar flow field to determine and control mass flow rate. A laminar flow element (LFE) inside the meter forces the gas into laminar (streamlined) flow. Inside this region, the Poiseuille equation dictates that the volumetric flow rate be linearly related to the pressure drop. A differential pressure sensor is used to measure the pressure drop along a fixed distance of the LFE. This, along with the viscosity of the gas, is used to accurately determine the volumetric flow rate. Separate absolute temperature and pressure sensors are incorporated and correct the volumetric flow rate to a set of standard conditions. This standardized flow rate is commonly called the mass flow rate and is reported in units such as standard cubic feet per minute (SCFM) or standard liters per minute (SLM).

The controller uses a true proportional valve coupled to the flow body to control flow using the integral PID loop controller. Standard units include a 0 to 5 V output (4 to 20 mA optional) and RS232 communications. The gas-select feature and the setpoints can be adjusted from the front keypad or via RS232 communications. Volumetric flow, mass flow, absolute pressure, and temperature can all be viewed or recorded through the RS232 connection. It is also possible to multi-drop up to 26 units on the same serial connection to a distance of 150'.

The FVL-2600 Series comprises volumetric flow controllers only. They do not measure or correct for absolute pressure or temperature. The FMA-2600 Series is recommended if operating pressure is above 15 psig or if there is any restriction or backpressure in the application.

SPECIFICATIONS

Accuracy: ±0.8% of reading
Repeatability:
FMA-2600A: ±0.5% FS
FVL-2600A: ±1% FS
Turndown Ratio: 100:1
Control Response Time: 100 ms
Input Control Signal: 0 to 5 Vdc, RS232
Output Signal: 0 to 5 Vdc, RS232
Optional Input/Outputs: 4 to 20 mA, 0 to 10 Vdc
Operating Temperature: -10 to 50°C (14 to 122°F)
Zero Shift: 0.02%/ATM FS/°C
Span Shift: 0.02%/ATM FS/°C
Humidity Range: 0 to 100% RH, non-condensing
Excess Flow Rate: 2.4% FS
Maximum Pressure: 125 psig, typical
Mass Flow Controllers: 125 psig
Volumetric Flow Controllers: Near atmosphere†, 15 psig recommended maximum
Minimum Differential Pressure Required:
5 LPM and under: 5 psid; 10 to 250 LPM: 15 psid; 500 LPM: 5 psid; 1500 LPM: 10 psid
Supply Current: 0.250 A for 20 (S) LPM and under; 0.75 A for 50 (S) LPM and above (typical)
Supply Voltage: Less or equal to 20 (S) LPM: 12 to 25 V; Less or equal to 50 (S) LPM: 24 to 30 V
Electrical Connections: 8-pin circular mini DIN
Wetted Materials: 303 and 302 SS, Viton®, silicone RTV (rubber), glass-reinforced nylon, aluminum, brass, 410 SS; >250 (S) LPM: add 416 SS and nickel

† Volumetric flowmeters and controllers not certified for accuracy at mass flow rates above the rated flow range of the meter. They are designed for near atmospheric pressure conditions only. The recommended maximum operating pressure is 15 psig.

Figure F.3: Omega FMA Series Specification Sheet

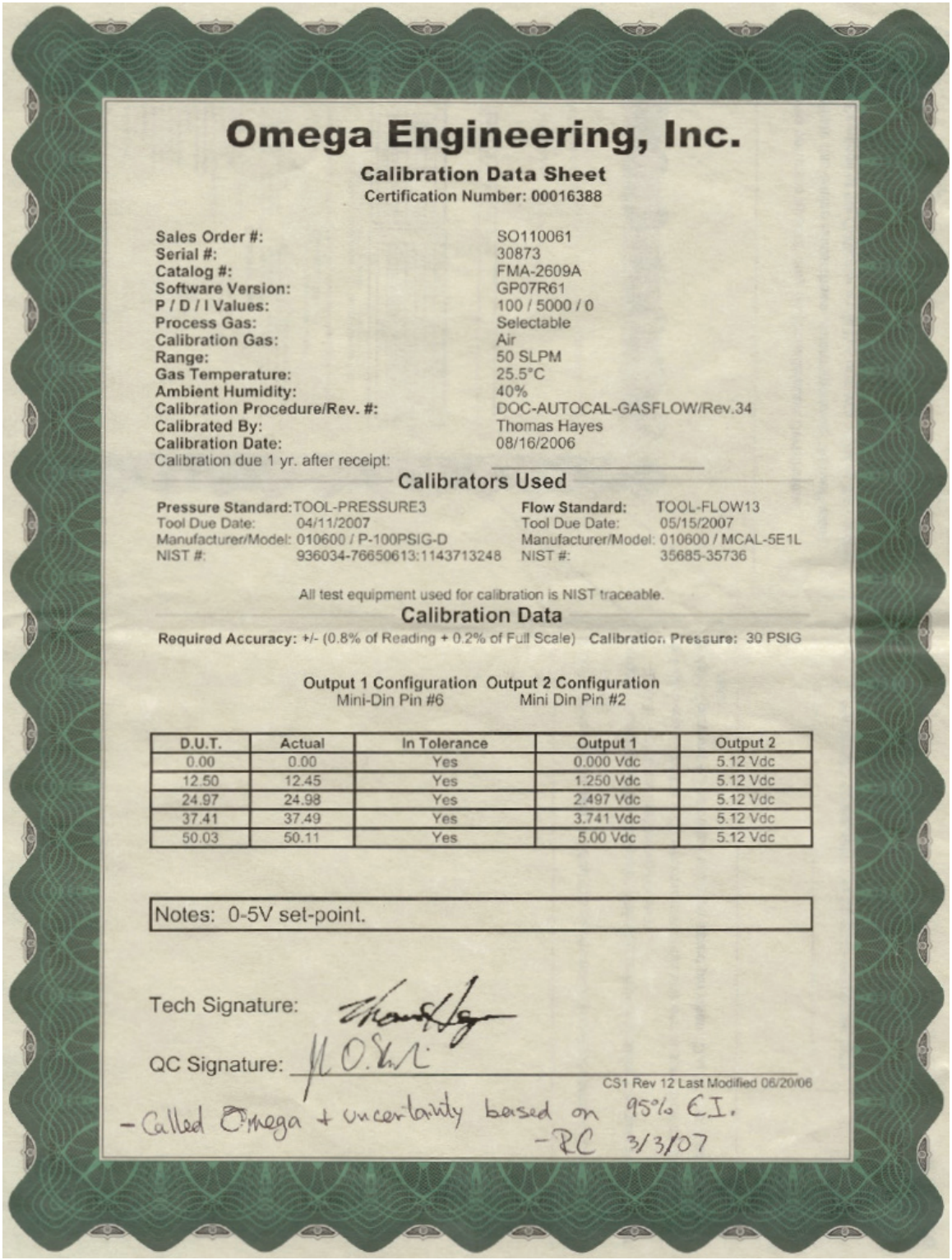

Omega Engineering, Inc.

Calibration Data Sheet

Certification Number: 00016388

Sales Order #:	SO110061
Serial #:	30873
Catalog #:	FMA-2609A
Software Version:	GP07R61
P / D / I Values:	100 / 5000 / 0
Process Gas:	Selectable
Calibration Gas:	Air
Range:	50 SLPM
Gas Temperature:	25.5°C
Ambient Humidity:	40%
Calibration Procedure/Rev. #:	DOC-AUTOCAL-GASFLOW/Rev.34
Calibrated By:	Thomas Hayes
Calibration Date:	08/16/2006
Calibration due 1 yr. after receipt:	

Calibrators Used

Pressure Standard:	TOOL-PRESSURE3	**Flow Standard:**	TOOL-FLOW13
Tool Due Date:	04/11/2007	Tool Due Date:	05/15/2007
Manufacturer/Model:	010600 / P-100PSIG-D	Manufacturer/Model:	010600 / MCAL-5E1L
NIST #:	936034-76650613:1143713248	NIST #:	35685-35736

All test equipment used for calibration is NIST traceable.

Calibration Data

Required Accuracy: +/- (0.8% of Reading + 0.2% of Full Scale) **Calibration Pressure:** 30 PSIG

Output 1 Configuration Mini-Din Pin #6 **Output 2 Configuration** Mini Din Pin #2

D.U.T.	Actual	In Tolerance	Output 1	Output 2
0.00	0.00	Yes	0.000 Vdc	5.12 Vdc
12.50	12.45	Yes	1.250 Vdc	5.12 Vdc
24.97	24.98	Yes	2.497 Vdc	5.12 Vdc
37.41	37.49	Yes	3.741 Vdc	5.12 Vdc
50.03	50.11	Yes	5.00 Vdc	5.12 Vdc

Notes: 0-5V set-point.

Tech Signature:

QC Signature:

CS1 Rev 12 Last Modified 06/20/06

- Called Omega + uncertainty based on 95% CI.
-RC 3/3/07

Figure F.4: FMA-2609 Methane Calibration Sheet

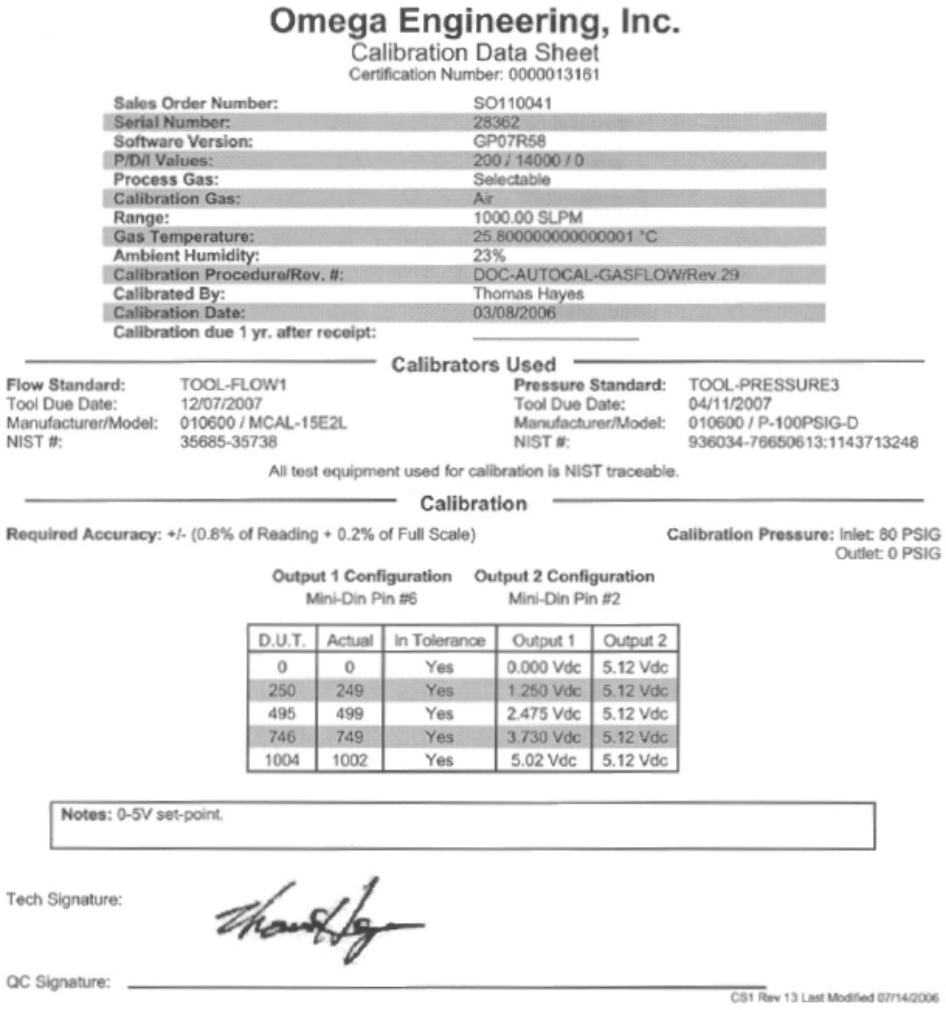

Omega Engineering, Inc.

Calibration Data Sheet

Certification Number: 0000013161

Sales Order Number:	SO110041
Serial Number:	28362
Software Version:	GP07R58
P/D/I Values:	200 / 14000 / 0
Process Gas:	Selectable
Calibration Gas:	Air
Range:	1000.00 SLPM
Gas Temperature:	25.800000000000001 °C
Ambient Humidity:	23%
Calibration Procedure/Rev. #:	DOC-AUTOCAL-GASFLOW/Rev.29
Calibrated By:	Thomas Hayes
Calibration Date:	03/08/2006
Calibration due 1 yr. after receipt:	

Calibrators Used

Flow Standard:	TOOL-FLOW1	**Pressure Standard:**	TOOL-PRESSURE3
Tool Due Date:	12/07/2007	Tool Due Date:	04/11/2007
Manufacturer/Model:	010600 / MCAL-15E2L	Manufacturer/Model:	010600 / P-100PSIG-D
NIST #:	35685-35738	NIST #:	936034-76650613:1143713248

All test equipment used for calibration is NIST traceable.

Calibration

Required Accuracy: +/- (0.8% of Reading + 0.2% of Full Scale)

Calibration Pressure: Inlet: 80 PSIG
Outlet: 0 PSIG

	Output 1 Configuration Mini-Din Pin #6		**Output 2 Configuration** Mini-Din Pin #2	
D.U.T.	Actual	In Tolerance	Output 1	Output 2
0	0	Yes	0.000 Vdc	5.12 Vdc
250	249	Yes	1.250 Vdc	5.12 Vdc
495	499	Yes	2.475 Vdc	5.12 Vdc
746	749	Yes	3.730 Vdc	5.12 Vdc
1004	1002	Yes	5.02 Vdc	5.12 Vdc

Notes: 0-5V set-point.

Tech Signature:

QC Signature:

CS1 Rev 13 Last Modified 07/14/2006

– Uncertainty based on 95% C.I.
–RC 3/3/07

Figure F.5: FMA-2613 Oxygen Calibration Sheet

"T" TYPE AIR PROCESS HEATERS

For In-Line Air and Gas Heating

- ⅜", ½" or ¾" Diameters
- Exit Air or Gas Temperatures to 540°C (1000°F)
- Inlet Air or Gas Temperatures to 121°C (250°F)
- For Horizontal Mounting
- With or Without NPT Fittings*

AHP Series
$59
Basic Unit

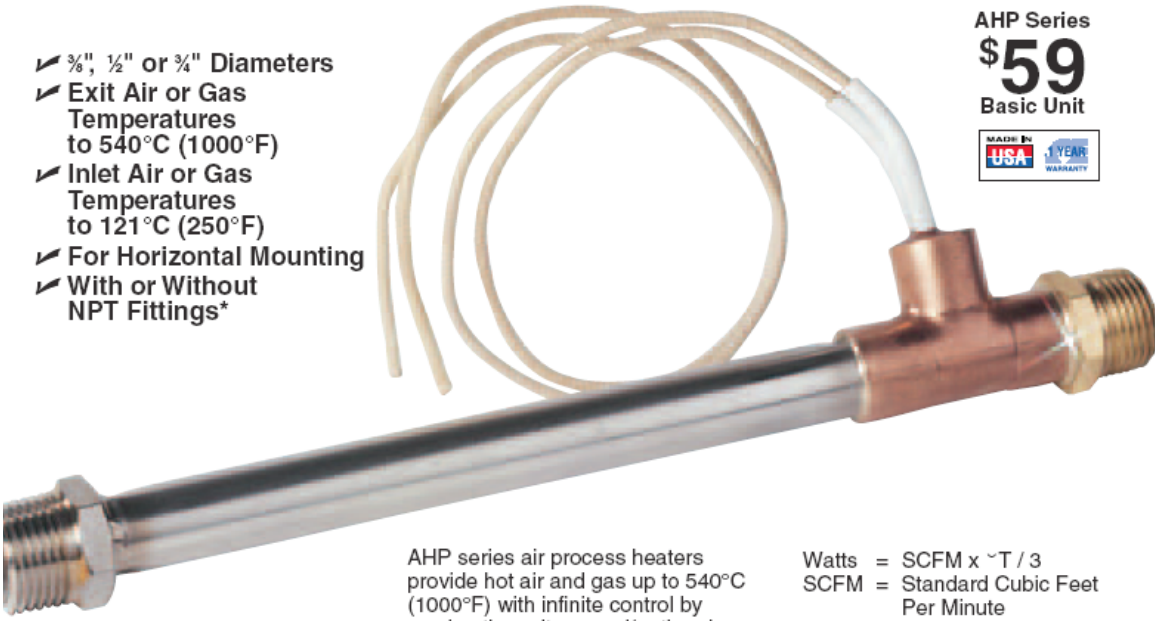

APPLICATIONS

The AHP Series in-line air heaters are used to heat clean, dry air or gas for baking, drying, laminating, metal working, packaging, plastic welding, preheating, sealing, soldering, shrink fitting and synthetic fabric sewing.

AHP series air process heaters provide hot air and gas up to 540°C (1000°F) with infinite control by varying the voltage and/or the air flow. Closed loop control can also be achieved with temperature controllers (section P) and "T" fittings to mount thermocouples. Calculate the flow rate, temperature rise, or power requirement as follows:

Watts = SCFM x ˘T / 3
SCFM = Standard Cubic Feet Per Minute
˘T = Temperature Rise in Degrees F from the Inlet to the Outlet

Maximum flow rates are given in the table below. For minimum flow rates, see table on page J-18.

MOST POPULAR MODELS HIGHLIGHTED!

To Order *(Specify Model Number)*

Model Number	Volts	Watts	Heated Length mm (in)	Watts/ Inch†	Maximum CFM	Diameter mm (in)	NPT Fitting	Price	Weight g (lb)
120 Vac Models									
AHP-3741	120	200	89 (3½)	57	8	10 (⅜)	¼"	$59	82 (0.18)
AHP-5051	120	400	114 (4½)	88	10	13 (½)	⅜"	70	113 (0.25)
AHP-7561	120	700	140 (5½)	136	20	19 (¾)	¾"	93	308 (0.68)
120/240 Vac Models**									
AHP-3742	120 240	50 200	89 (3½) 89 (3½)	14 57	8 8	10 (⅜)	¼"	59	82 (0.18)
AHP-5052	120 240	100 400	11 (4½) 11 (4½)	22 80	10 10	13 (½)	⅜"	70	113 (0.25)
AHP-7562	120 240	190 750	14 (5½) 14 (5½)	34 136	20 20	19 (¾)	¾"	93	308 (0.68)

** Note: To order heaters without NPT fittings add suffix "-NF" to Model no. Price for heaters without fittings is $42 for AHP-374 Series, $51 for AHP-505 Series, and $64 for AHP-756 Series.*

*** These air heaters can be operated on either 120 or 240 Volts. Specifications are shown for operation on both 120 and 240 Volts.*

† Indicates Watts per inch of heated length. Use the table above to determine minimum required flow rates. The Watts per inch of heated length can be changed by reducing the operating voltage or by ordering a custom made heater.

***Ordering Example:** Model AHP-3741/120, 200 W, 120 Vac "T" Type in-line air/gas heater, $59.*

Figure F.6: Omega FMA Inline Heater Specification Sheet

iSeries ⅛ DIN Temperature, Process, & Strain Meters & PID Controllers

i/8

MONOGRAM

- High Quality
- 5-Year Warranty
- High Accuracy ±0.5°C (±0.9°F), 0.03% Reading
- User-Friendly, Simple to Configure
- Free Software
- Full Autotune PID Control
- Universal Inputs: Thermocouple, RTD, Process Voltage/Current, Strain
- Totally Programmable Color Displays, Standard
- Built-in Excitation, Standard
- 2 Control or Alarm Outputs, Choice of dc Pulse, Mechanical Relays, Analog Voltage and Current.
- Embedded Internet Connectivity

$240 ⅛ DIN meter

$310 with 2 control outputs

Embedded Internet Connectivity!

The OMEGA® DPi8/CNi8 is a ⅛ DIN size (96 x 48 mm [3.7 x 1.9"]) Digital Panel Meter featuring the big iSeries color-changing display. The digits are twice the size of typical ⅛ DIN panel meters. The iSeries meters feature the only LED displays that can be programmed to change color between GREEN, AMBER, and RED at any setpoint or alarm point. The "DPi8/CNi8" model is available as an extremely accurate programmable digital panel meter with no outputs or with dual outputs for controlling or alarming functions. Other options include isolated programmable analog output, serial communications, Modbus and Ethernet. The user can easily program the CNi8 for any control or alarming requirement from simple on-off to full autotune PID with a choice of Form C SPDT relays, Solid State Relays, DC pulse, and Analog (voltage and current) outputs.

Fully Isolated Analog Output for retransmission of the process value is available in addition to the control and alarm relays (specify model CNi8A33).

The DPi8/CNi8 covers a broad selection of transducer and transmitter inputs with two input models:

The UNIVERSAL TEMPERATURE & PROCESS instrument (model "i") handles ten common types of thermocouples, multiple RTD's, and several Process (DC) Voltage and Current ranges. This model also features built-in excitation, 24 Vdc @ 25 mA. With its wide choice of signal inputs, this model is an excellent choice for measuring or controlling temperature with a thermocouple, RTD, or 4 to 20 mA transmitter.

The STRAIN & PROCESS instrument (model "iS") measures inputs from Load Cells, Pressure Transducers, and most any strain gage sensor as well as Process Voltage and Current ranges. The "iS" has built-in 5 or 10 Vdc excitation for bridge transducers, 5 Vdc @ 40 mA or 10 Vdc @ 60 mA. (Any excitation voltage between 5 and 24 Vdc is available by special order.) This "iS" model supports 4- and 6-wire bridge configurations, ratiometric and non-ratiometric measurements. The "iS" features fast and easy "in process" calibration/scaling of the signal inputs to any engineering units. And this model also features 10 Point Linearization which allows the user to linearize the signal input from extremely nonlinear transducers of all kinds. The OMEGA® DPi8/CNi8 ⅛ DIN enclosure has a NEMA-4 (IP65) rated front bezel and removable rear connectors for easy installation and wiring.

	Input Type	Range	Accuracy
	Process Voltage	0 to 100 mV, 0 to 1 V, 0 to 10 Vdc	0.03% rdg
	Process Current	0 to 20 mA (4 to 20 mA)	0.03% rdg
J	Iron-Constantan	-210 to 760°C/-346 to 1400°F	0.4°C/0.7°F
K	CHROMEGA®-ALOMEGA®	-270 to -160°C/-160 to 1372°C -454 to -256°F/-256 to 2502°F	1.0°C/0.4°C 1.8°F/0.7°F
T	Copper-Constantan	-270 to -190°C/-190 to 400°C -454 to -310°F/-310 to 752°F	1.0°C/0.4°C 1.8°F/0.7°F
E	CHROMEGA®-Constantan	-270 to -220°C/-220 to 1000°C -454 to -364°F/-364 to 1832°F	1.0°C/0.4°C 1.8°F/0.7°F
R	Pt/13%Rh-Pt	-50 to 40°C/40 to 1768°C -58 to 104°F/104 to 3214°F	1.0°C/0.5°C 1.8°F/0.9°F
S	Pt/10%Rh-Pt	-50 to 100°C/100 to 1768°C -58 to 212°F/212 to 3214°F	1.0°C/0.5°C 1.8°F/0.9°F
B	30%Rh-Pt/6%Rh-Pt	100 to 640°C/640 to 1820°C 212 to 1184°F/1184 to 3308°F	1.0°C/0.5°C 1.8°F/0.9°F
C	5%Re-W/26%Re-W	0 to 2320°C/32 to 4208°F	0.4°C/0.7°F
N	Nicrosil-Nisil	-250 to -100°C/-100 to 1300°C -418 to -148°F/-148 to 2372°F	1.0°C/0.4°C 1.8°F/0.7°F
L	J DIN	-200 to 900°C/-328 to 1652°F	0.4°C/0.7°F
RTD	Pt, 0.00385, 100, 500, 1000 Ω	-200 to 900°C/-328 to 1652°F	0.4°C/0.7°F
RTD	Pt, 0.00392, 100, 500, 1000 Ω	-200 to 850°C/-328 to 1562°F	0.4°C/0.7°F

Figure F.7: Omega CNi Series Heater Control Specification Sheet

SCR Power Controllers For Electrical Resistance Heaters

NEW

SCR19 Series
$249
Basic Unit


SCR19Z-24-060 shown without fuse, $263, shown smaller than actual size.

- Zero Crossing or Phase Angle Fired
- Single or Three Phase Load Switching
- Extends Heater Life. Reduces Thermal Shock
- No Maintenance. All Solid State Components
- Close Control of Low Mass Heaters
- Phase Angle with Soft Start for High Inrush Heaters
- No Relay Noise. Contact Arc Noise Eliminated
- Semiconductor I^2T Fusing
- Optically Isolated Control Signal Input

The SCR19 Series Power Controllers are designed to proportion electric power to resistive loads only, such as ovens, furnaces, heat sealers, etc. (NOTE: They are not designed to drive transformers or any inductive load.) The controllers consist of power semi-conductors (SCRs), properly-sized heat sinks, trigger circuitry, and fuses supplied on panels for surface mounting.

The power controller accepts a 4 to 20 mA dc output from a temperature controller or can be supplied with manual option using a remote potentiometer.

Operation

The SCR19 Series controllers offers two methods of proportional control – Zero-voltage-switched and Phase-angled fired. With the Zero voltage switching mode, the controller switches on complete cycles of the ac supply voltage. The trigger circuit is designed to turn on the SCRs as close as possible to the point where the ac sine wave crosses through zero. In effect, the line voltage is turned on and off and applied to the heaters in whole cycles. With an input of 4 to 20 mA, the output will be off below 4 mA and full on at 20 mA. Proportioning action is obtained by varying the number of cycles on to the number of cycles off. The output will vary from one cycle on and nine cycles off at low input, to all cycles on at maximum input. This output is integrated by the heaters which produce a smoothly proportioning heat output that varies directly with the input signal. With the Phase-angle-fired mode, the power to the load is controlled by governing the point of turn on (firing) of each half cycle of the full ac sine wave.

Features

- Designed to allow the operation of multiple units by a single temperature controller.
- Unique circuitry in the three-phase units allows any phase connection – phases cannot be incorrectly wired resulting in partial output power on or off.
- Optical coupler ensures the elimination of ground loops, high voltage potentials, or damage to drive controller of the SCR Power Controller.
- Completely solid-state, SCR19 Series SCRs have no moving parts to wear out. They are as effective as new, even after 100,000,000 operations.
- SCR19 Series SCRs offer smooth, rapid, proportional heating action. SCR control proportions only the power required to maintain exact temperature.
- SCR19 Series SCRs eliminate high/low cycling and, because the temperature of the heating element is constant, thermal shock is eliminated. Heater life may be increased by up to 7 times.

Specifications

Supply Voltage: 24 to 600 Vac
Frequency: 50 to 60 Hz
Current Rating: 40, 60, and 80 A
Control Signal Isolation: 2500 Vac
Transient Voltage Protection: MOV and RC suppression
Ambient Temperature Range: 0 to 50°C (32 to 122°F) for listed current rating
Load: Resistive, 3-phase, 3 wire Delta or Ungrounded Wye SCR19Z/ SCR19P -1 phase, 1 line control SCR39Z -3 phase, 2 lines controlled SCR39P -3 phase, 3 lines controlled
Diagnostic Indicators: Shorted or open SCR reversed signal input (mA/V)

Figure F.8: Omega Phase Angle Fired Rectifier Specification Sheet

APPENDIX G

DIADEM V10.0 AND MATLAB V6.1 CODE

The following four script files are run in conjunction with a dialog box with inputs for minimum frequency, maximum frequency and the test date. The scripts are written in Visual Basic code, therefore, the single quote syntax is the comment syntax. Also, to format to thesis margins ... signified a position where the code needed to be wrapped.

LOAD DATA SCRIPT

```
'This algorithm loads all of the data files to a single data set
Dim This : Set This = BUTTON2
EditBox1.Text=100
EditBox2.Text=20000
Dim FileToBeImported
Dim STPFile
Dim Counter
Counter=1
'this loop deletes each group before loading any data
If groupcount>0 Then
  Do
    Call GROUPDEL(groupcount)
  Loop Until (groupcount=0)
Else
End If
'this is for the folders
```

```
'msgbox("Please select the chamber data to be analyzed.
'You can select multiple files to be loaded by using CTRL
'+ the files you would like to load.")
Call FileNameGet("ANY", "FileRead", DataDrvUser, "TDM data...
 (*.tdm),*.tdm", "All.lst", True, "Data selection")
MyFileNames = Split(FileDlgFileName,"|")
Msgbox(FileDlgFileName)
For iCount = 0 To Ubound(MyFileNames)
  Call DataFileLoad(MyFileNames(iCount))
Next
  'this sets each group to the name of the original file that
  'the data was
  'loaded from.
  'call groupppropset(groupcounter,"name",chnpropget("[" &...
  groupcounter  & "]/[" & groupcounter & "]","sourcedatafilename"))
  'increments the group counter until all groups have been selected.
  'groupcounter=groupcounter+1
button2.ForeColor=button3.ForeColor
button3.ForeColor=1322987
End Sub
```

FAST FOURIER TRANSFORM SCRIPT

```
Sub BUTTON3_EventClick()
Dim This : Set This = BUTTON3
'This Script Does the FFT of each set point
OriginalGroupCount=Groupcount
FFTINTERVUSER    ="all"
FFTINTERVPARA(1) =1
FFTINTERVPARA(2) =4096
FFTINTERVPARA(3) =1
FFTINTERVOVERL   =0
FFTWNDFCT        ="Rectangle"
FFTWNDPARA       =10
FFTWNDCHN        ="[1]/Time"
FFTWNDCORRECTTYP ="No"
FFTAVERAGETYPE   ="No"
FFTAMPLFIRST     ="Amplitude"
FFTAMPL          =1
FFTAMPLTYPE      ="Ampl.Peak"
FFTCALC          =0
```

```
FFTAMPLEXT       ="No"
FFTPHASE         =0
FFTCEPSTRUM      =0
FFTINdexChn=true
'original data group counter is used to increment through...
'all of the odd channels the even channels will be all of...
'the fft And waterfall data the odd channels will be all...
'of the original data
originaldatagroupcounter=1
'total counter is used to loop through the indices of the chans
totalcounter=1
'this code will perform an fft on all group 1 Transducer data
If OriginalGroupCount >= 1 Then
Do
'this will set the default group to the next original data group
    Call GroupDefaultSet(originaldatagroupcounter)
    'defines new group for waterfall plot 1
    Call GroupCreate("Waterfall " & ChnPropGet("[" &...
     originaldatagroupcounter & "]/Transducer","sourcedatafilename"...
     ) ,GroupCount + 1)
    'defines this as the new default group
    Call GroupDefaultSet(GroupIndexGet("Waterfall " & ChnPropGet...
    ("[" & originaldatagroupcounter & "]/Transducer",...
    "sourcedatafilename")))
    'allocates memory for channels
    Call ChnAlloc("FuelMassFlowRates",1000,1,DataTypeFloat64...
    ,"Numeric")
    Call ChnAlloc("OxMassFlowRates",1000,1,DataTypeFloat64...
    ,"Numeric")
    Call ChnAlloc("Amplitude",1000,1,DataTypeFloat64,"Numeric")
    'sets the group name to the file name
    Call GroupPropSet(originaldatagroupcounter,"name",...
    ChnPropGet("[" & originaldatagroupcounter & "]/...
    Transducer","sourcedatafilename"))
    'allocates memory for loop counter
    intcounter=1
    'stores total length of channel and assumes...
    'that the time channel Is the standard
    intlength=chnpropget("[" & originaldatagroupcounter...
    & "]/Time","length")
    'typecasts string to integer
    length=int(intlength)
    intampchannelnumber=1
    totalcounter=1
    Do Until intcounter-1 = length
```

```
FFTINTERVPARA(3) =intcounter ' resets starting point of fft
'this code performs an fft on the original data
Call CHNFFT1("[" & originaldatagroupcounter & "]...
/Time","[" & originaldatagroupcounter & "]/Transducer")
'sets the channel /Fuel Mass Flow Rates/ values to
'their respective values
CHD(totalcounter,"Waterfall " & ChnPropGet("[" & ...
originaldatagroupcounter & "]/Transducer",...
"sourcedatafilename") & "/FuelMassFlowRates" )=CHD...
(intcounter,"[" & originaldatagroupcounter & "]/CH4 ...
Mass Flow Rate")
'sets the channel /Ox Mass Flow Rates/ values to their
'respective values
CHD(totalcounter,"Waterfall " & ChnPropGet("[" & ...
originaldatagroupcounter & "]/Transducer",...
"sourcedatafilename") & "/OxMassFlowRates" )=CHD...
(intcounter,"[" & originaldatagroupcounter & "]/O2...
Mass Flow Rate")
'sets the channel /Amplitude/ to the max amplitude
'from the ffts found For Each of the ox mass flow rates
CHD(totalcounter,"Waterfall " & ChnPropGet("[" &...
originaldatagroupcounter & "]/Transducer",...
"sourcedatafilename") & "/Amplitude" )=ChnPropGet...
("Waterfall " & ChnPropGet("[" & originaldatagroupcounter...
& "]/Transducer","sourcedatafilename") &...
"/Ampl_Peak","Maximum")
'this renames the frequency data to /Transducer_Freq/
'and concatenates the ox mass flow rate
Call ChnPropSet( "Waterfall " & ChnPropGet("[" & ...
originaldatagroupcounter & "]/Transducer",..
"sourcedatafilename") & "/Frequency","name",...
"Transducer_Freq_"...
 & CHD(intcounter,"[" & originaldatagroupcounter & "]...
 /O2 Mass Flow Rate") )
'this renames the amplitude data to /Transducer_Ampl/ and
'concatenates the ox mass flow rate
Call ChnPropSet( "Waterfall " & ChnPropGet("[" &...
originaldatagroupcounter & "]/Transducer",...
"sourcedatafilename") & "/Ampl_Peak","name",...
"Transducer_Ampl_" & CHD(intcounter,"[" &...
originaldatagroupcounter & "]/O2 Mass Flow Rate"))
'increments the total counter variable which is used
'to Set the channel index values. ex. index 1,2,3,4 etc.
totalcounter=totalcounter+1
intampchannelnumber=intampchannelnumber+1
```

```
        'here the code assumes that the pieces of data will
        'be In chunks of 5000 and hence increments by 5000
        intcounter = intcounter + 5000
     Loop
'now must reset the originaldatacounter To Next original data
originaldatagroupcounter=originaldatagroupcounter + 1
loop until (originaldatagroupcounter-1=OriginalGroupCount)
Else
'the individual must not have selected any data to load
msgbox("You must load data in order to perform an analysis!!")
End If
'this code will reorder the channels
'this code finds the first waterfall group number
groupcounter=(groupcount/2) + 1
Do
    'this will get the total number of channels
    'in the oxmassflowrates
    'channel.  It is assumed that the number of
    oxmassflowrate incidces'
    'will be the same as the number of transducer
    'ampl channels
    channelmax = chnpropget("[" & groupcounter & "]/[2]","length")
    'channel max is decremented to stop the loop
    channelmax = channelmax - 1
    'channel incrementer is 4 b/c want to start at first fft
    'frequency channel in the active group
    channelincrementer=4
    'loop counter is set to zero to account for the first
    'fft frequency channel
    loopcounter= 0
    do
        'this code moves the channel frequency to the top and
        'hence in turn leaves the bottom of the channel indices
        'to be only amplitudes, which is required by the waterfall
        'graphs
        Call ChnMove("[" & groupcounter & "]/[" & ...
        channelincrementer & "]", groupcounter, channelincrementer...
        -loopcounter)
        'increments the channelincrementer by two so that
        'it grabs the Next
        'frequency channel and not the amplitude channel
        channelincrementer=channelincrementer + 2
        'increments the loopcounter variable
        loopcounter=loopcounter + 1
        call chnrenumber()
```

```
    loop until (loopcounter  = channelmax)
    'this last channel move is to move the last frequency
    'to the top.
    'it is done this way b/c it could not be done inside
    'the Loop
    'without receiving an error.
    Call ChnMove("[" & groupcounter & "]/[" & ...
    channelincrementer  & "]", groupcounter, ...
    channelincrementer-loopcounter)
    'this simply renumbers the channels
    call chnrenumber()
    'increments the groupcounter variable.
    groupcounter=groupcounter + 1
loop until(groupcounter-1 = groupcount)
'this will reset the channel numbers to move the
'amplitude channels to the bottom of the group
'Call ChnPropSet((TargetChn, PropName, PropValue)
button3.ForeColor=button4.ForeColor
button4.ForeColor=1322987
End Sub
```

INDIVIDUAL FFT AND WATERFALL PLOT

```
Sub BUTTON4_EventClick()
Dim This : Set This = BUTTON4
testdate=EditBox3.Text
ntestdate=Len(testdate)
If ntestdate=0 Then
msgbox("Put in the date, moron!")
Else
'this code will create a New folder
'For the jpegs To be stored In
 originalgroupcounter=1
   Dim fso, f
   Set fso = CreateObject("Scripting.FileSystemObject")
   Set f = fso.CreateFolder("D:\Hookitup")
   CreateFolderDemo = f.Path
groupcounter=0
'need to create the proper number of sheets
groupcounter=(groupcount/2)
sheetcounter=1
```

```
'do
  'Call GRAPHSHEETNEW("Sheet " & sheetcounter)
  '... GraphSheetName
 ' sheetcounter=sheetcounter+1
'loop until (groupcounter=sheetcounter-1)
'Call WndOpen("VIEW")'opens the sheets so that each
'one can be activated says to loop through each sheet
'In the Set of sheets. it starts out with one sheets
'and creates a New sheet Until the variable groupcounter
'Is equal To the total group count. At this point
' no more sheets are created And hence the code should stop
'this line of code finds the group number where the
'waterfall plots data begins and sets the variable
'groupcounter To this value
groupcounter=(groupcount/2) + 1
Do
Call PICLOAD("C:\Program Files\National Instruments...
\Diadem 10.0\Demo\Custom Analysis\WATERFALL_TEMPLATE.TDR")
Call PICUPDATE()
Call GRAPHObjOpen("3DAxis1")
  sCurveName= D3CurveObj(1)         'gets the curve name
  'msgbox("groupcounter " & groupcounter & "/groupcount "
  '& groupcount )
  'msgbox(sCurveName)
  Call GraphObjOpen(sCurveName)     'opens the particular
  'curve For altering
    'get the length of the oxmass flow rates channel and
    'stores into variable
     NumberOfAmps=    chnpropget( "[" & groupcounter & ...
     "]/OxMassFlowRates","length") '%%%%%%%%%%%%%%%%%%%%
     'this function updates the characteristic values,
     'such As channel min, channel max And
     'other properties.  This action must be performed
     'in order To Get a value of min Or max from a channel.
     '  If this Is Not performed the user will Get a NO
     'VALUE For the string.
     ChnCharacter("[" & groupcounter & "]/OxMassFlowRates")
     minimumflowrate = chnpropget( "[" & groupcounter &...
     "]/OxMassFlowRates","Minimum") '%%%%%%%%%%%%%%%%%%%%
    'the last part of this code gets the lowest oxmass flow
    'rate And uses it To Call out the channel
    D3CCHNXNAME      ="[" & groupcounter & "]/...
    Transducer_Freq_" & chnpropget("[" & groupcounter...
     & "]/OxMassFlowRates","Minimum")
    D3CCHNYNAME      ="[" & groupcounter & "]/....
```

```
    OxMassFlowRates"
    D3CCHNZNAME      =[" & groupcounter & "]/...
    Transducer_Ampl_" & CHD(1,"[" & groupcounter...
     & "]/OxMassFlowRates")
    D3CCURVETYPE     ="Waterfall"
    D3CCURVESTRUC    ="Matrix"
    D3CCURVEISOTYPE  ="XY"
    D3CCURVEISONO    =0
    D3CCURVEVTYPE    ="Vector4D"
    D3CCURVEVPLANETY ="XY-plane"
    D3CURVECOLOR     ="Palette"
    D3CURVECOLORRGB  =50266112
    D3CURVESPECCOLOR ="blue"
    D3CURVESPECCRGB  =50266112
    D3CURVEISOCOLOR  ="green"
    D3CURVEISOCOLRGB =33619712
    D3CURVEVCOLOR    ="black"
    D3CURVEVCOLORRGB =33554432
    D3CURVESYMCOLOR  ="black"
    D3CURVESYMCOLRGB =33554432
    Call GraphObjClose(sCurveName)
    'closes the particular curve for altering
 Call GRAPHObjClose("3DAxis1")
If checkbox1.Value=1 Then
'need to read in the string and seperate the string
'string that holds all of the original information
originalstring=GroupPropGet(originalgroupcounter,...
"description")
delimiter="*"
MyArray = Split(originalstring, delimiter, -1, 1)
Call GraphObjOpen("Text4")
   '------------------- Text --------------------------
  TXTTXT           =MyArray(0)
  TXTFONT          =""
  TXTSIZE          =3.12
  TXTCOLOR         ="black"
  TXTCOLORRGB      =33554432
  TXTBOLD          =1
  TXTITAL          =0
  TXTUNDL          =0
  TXTSTROUT        =0
  TXTFRAME         =0
  TXTBACKCOLOR     =""
  TXTBACKRGB       =0
  '------------------- Position ----------------------
```

```
  TXTPOSX          =20.16938
  TXTPOSY          =14.80876
  TXTANG           =0
  TXTRELPOS        ="r-bot."
Call GraphObjClose("Text4")
'*************************************************
'this sets the injector type
Call GraphObjOpen("Text9")
TXTTXT="Injector: " & MyArray(2)
Call GraphObjClose("Text9")
'this sets the injector distance
Call GraphObjOpen("Text10")
TXTTXT=MyArray(3)
Call GraphObjClose("Text10")
'this sets the test date
Call GraphObjOpen("Text14")
TXTTXT=testdate
Call GraphObjClose("Text14")
'this sets the fuel mass flow rates
Call GraphObjOpen("Text12")
TXTTXT=MyArray(5)
Call GraphObjClose("Text12")
'this sets the ox mass flow rates
Call GraphObjOpen("Text11")
TXTTXT=myarray(4)
Call GraphObjClose("Text11")
'this sets the experimentalist
Call GraphObjOpen("Text13")
TXTTXT=myarray(1)
Call GraphObjClose("Text13")
Else
  'this sets the injector type
Call GraphObjOpen("Text9")
TXTTXT="Injector:"
Call GraphObjClose("Text9")
'this sets the injector distance
Call GraphObjOpen("Text10")
TXTTXT="rrrr"
Call GraphObjClose("Text10")
'this sets the fuel mass flow rates
Call GraphObjOpen("Text12")
TXTTXT="rrr"
Call GraphObjClose("Text12")
'this sets the ox mass flow rates
Call GraphObjOpen("Text11")
```

```
TXTTXT="rrr"
Call GraphObjClose("Text11")
'this sets the experimentalist
Call GraphObjOpen("Text13")
TXTTXT="rrr"
Call GraphObjClose("Text13")
End If
'*******************************************************
Call PicUpdate()        'refreshes the screen and graph
'this will export the files as jpeg files
Call PICEXPORT("D:\Hookitup\Waterfall " & MyArray(2) &...
 " " & MyArray(0) ,"BMP",1,768,1024,"RGB 32",75,..
 "NoCompression",0)
 '... EXFILENAME,EXTYPE,EXUSERATIO,EXHEIGHT,EXWIDTH,
 'EXBITSPERPIXELX,EXQUALITY,EXCOMPRESSTYPEX,EXPROGRESSIVE
Call PicSaveAs(chnpropget("[" & groupcounter & "]/["...
 & groupcounter & "]","groupname"),"")
'CAll picture1.refresh()
'Call PICSAVEAS("somepic","")  '... PICFILE,PICFILECODE
'this code creates a new sheet
groupcounter=groupcounter+1'groupcounter +1 to pick up
'the Next waterfall group this increments through the
'groups While getting the description info In the string
'format *
originalgroupcounter=originalgroupcounter + 1
Loop Until (groupcounter-1=groupcount)
groupcounter=(groupcount/2)+1
channelcounter=1
If checkBox2.Value=1 Then
'Make all FFT plots
do
channelcounter=1
numberOfChannels=ChnPropGet("[" & groupcounter & "]...
/OxMassFlowRates", "length")
'msgbox("GROUPNAME: " & ChnPropGet("[" & groupcounter
'& "]/OxMassFlowRates", "groupname") & "NUMBER OF CHANNELS
': " & numberOfChannels)
numberofChannels=Cint(numberOfChannels)
  do
  'this will load the graph
  Call PICLOAD("C:\Program Files\National Instruments\DIAdem...
   10.0\Demo\Custom Analysis\FFT_TEMPLATE.TDR")'... PICFILE
  'Call PICUPDATE()
  '------------------- Curve and axis definition -----------
    Call GraphObjOpen("2DAxis1")
```

```
    '------------------- Curve list -----------------------
    Call GraphObjOpen("2DObj13_Curve1")
    D2CCHNEXPAND     =1
    D2CCHNXNAME      ="[" & groupcounter & "]/...
    Transducer_Freq_" & chd(channelcounter,"[...
    & groupcounter & "]/OxMassFlowRates")
    D2CCHNYNAME      ="[" & groupcounter & "]/...
    Transducer_Ampl_" & chd(channelcounter,"[...
    & groupcounter & "]/OxMassFlowRates")
    D2CCHNY1NAME     =""
    D2CCHNXFILTER    =""
    D2CCHNYFILTER    =""
    D2CCHNY1FILTER   =""
    D2CCONSTXNAME    =""
    D2CCONSTYNAME    =""
    D2CCONSTY1NAME   =""
    D2CAXISPAIRNO    =1
    D2CCURVETYPE     ="Line"
    D2CURVECOLOR     ="red"
    D2CURVECOLORRGB  =33554687
    D2CURVESPECCOLOR ="red"
    D2CURVESPECCORGB =33554687
  Call GraphObjClose("2DObj13_Curve1")
Call GraphObjClose("2DAxis1")
'Set the Title'
Call GraphObjOpen("Text4")
  '------------------- Text -------------------------
  TXTTXT           =MyArray(0)
  TXTFONT          =""
  TXTSIZE          =3.12
  TXTCOLOR         ="black"
  TXTCOLORRGB      =33554432
  TXTBOLD          =1
  TXTITAL          =0
  TXTUNDL          =0
  TXTSTROUT        =0
  TXTFRAME         =0
  TXTBACKCOLOR     =""
  TXTBACKRGB       =0
  '------------------- Position -----------------------
  TXTPOSX          =20.16938
  TXTPOSY          =14.80876
  TXTANG           =0
  TXTRELPOS        ="r-bot."
Call GraphObjClose("Text4")
```

```
'msgbox((groupcounter - (groupcount/2)))
'Load the Group Description
originalstring=GroupPropGet((groupcounter - (groupcount/2))...
 , "description")
delimiter="*"
MyArray = Split(originalstring, delimiter, -1, 1)
'Fill in the text boxes
'--------------------------------------
  'this sets the injector type
  Call GraphObjOpen("Text9")
  TXTTXT="Injector: " & MyArray(2)
  Call GraphObjClose("Text9")
  'this sets the injector distance
  Call GraphObjOpen("Text10")
  TXTTXT=MyArray(3)
  Call GraphObjClose("Text10")
  'this sets the test date
  Call GraphObjOpen("Text15")
  TXTTXT=testdate
  Call GraphObjClose("Text15")
  'this sets the fuel mass flow rate
  Call GraphObjOpen("Text12")
  TXTTXT="CH4 = " & Round(CHD(channelcounter,"[" & ...
  groupcounter & "]/FuelMassFlowRates"),3) & " g/s"
  Call GraphObjClose("Text12")
  'this sets the ox mass flow rate
  Call GraphObjOpen("Text11")
  TXTTXT="O2 = " & Round(CHD(channelcounter,"[" & ...
  groupcounter & "]/OxMassFlowRates"),3) & " g/s"
  Call GraphObjClose("Text11")
  'this sets the experimentalist
  Call GraphObjOpen("Text13")
  TXTTXT=MyArray(1)
  Call GraphObjClose("Text13")
  'Create OF Ratio
  Call GraphObjOpen("Text14")
  TXTTXT="Mixture Ratio = " & Round((CHD(channelcounter...
  ,"[" & groupcounter & "]/OxMassFlowRates")/CHD(channelcounter...
  ,"[" & groupcounter & "]/FuelMassFlowRates")),2)
  Call GraphObjClose("Text14")
'need to save the report
Call PicUpdate()       'refreshes the screen And graph
'this will export the files as jpeg files
Call PICEXPORT("D:\Hookitup\FFT " & MyArray(2) & " " & ...
MyArray(0) & " " & Round(CHD(channelcounter,"[" & groupcounter...
```

```
 & "]/OxMassFlowRates"),3) & ".O2 " & Round(CHD(channelcounter...
 ,"[" & groupcounter & "]/FuelMassFlowRates"),3) & ".CH4 ",...
 "BMP",1,768,1024,"RGB 32",75,"NoCompression",0)
 '... EXFILENAME,EXTYPE,EXUSERATIO,EXHEIGHT,EXWIDTH,EXBITSPERPIXELX
 ',EXQUALITY,EXCOMPRESSTYPEX,EXPROGRESSIVE
'msgbox(channelcounter & " " & numberOfChannels)
channelcounter=channelcounter+1
loop Until (numberOfChannels=channelcounter-1)
groupcounter=groupcounter+1
'msgbox("counter = " & groupcounter & " Groupcount
'= " & (groupcount))
loop until ((groupcounter-1)=(groupcount))
'*******************************************************
Else
End If
button4.ForeColor=button5.ForeColor
button5.ForeColor=1322987
msgbox("Your plots have been saved on the desktop in a
folder named Hookitup.  Please rename the folder now.")
End If
End Sub
```

PEAK AMPLITUDE SEARCH

```
Sub BUTTON5_EventClick() Dim This : Set This = BUTTON5
button5.ForeColor=button2.ForeColor
button2.ForeColor=1322987
'************************************************** '--
Comment: this code assumes that the other 'analysis has already
been run. '-- In turn this assumes that the first half of ' the
channels are test data channels '-- and that the last half of
the channels are FFT ' data channels.  This also assumes '--
that the first three channels in all of the groups ' are flow
rate And amplitude '-- channels.  With this assumption comes
the assumption ' that the first Is a '-- fuel mass flow rates
channel.  This channel could 'also be an oxmass flow rates '--
channel as long as the number of values represent 'the number
of ffts performed. '-- Assumptions: (1) 4th channel in each
group is a 'frequency channel '--              (2) 1st channel
length is the same 'as the number of ffts performed '--
(3) last half of the groups are all 'fft data
```

```
'****************************************************** 'this
string holds the output values outputstring="Min Frequency" &
Chr(9) & "Max Frequency" &...
 Chr(9) & "Amplitude" & Chr(13)
'this is the lower input frequency lower_input_frequency =100
'this is the upper input frequency upper_input_frequency = 1500
'this variable is to loop through the groups
groupcounter=(groupcount/2)+1 'this variable is to hold the
amount of offset to find 'the first frequency channel
channeloffset=4 'this variable is to loop through the frequency
channels channelfreqcounter=channeloffset-1 'this variable is
to loop through the channels channelIncrementer=1 'this is to
store the lower input frequency that is found 'in the group
found_lower_input_frequency=0 'this is to store the upper input
frequency that is found 'in the group
found_upper_input_frequency=0 'this is store the index of the
lower input frequency Index_lower_input_frequency=0 'this
variable is used to store the maximum amplitude 'found within a
range maxamplitude=0 'this variable is used to loop through the
channel amplitudes channelampcounter=chnpropget("[" &
groupcounter & "]/... [1]","length") + channeloffset-1
channelampcounter=Cint(channelampcounter) 'this is to loop
through the outer channel loop outerchannelcounter=0 'this dims
an array to hold the amplitudes Dim amplitudes(1000) 'this is
for the array counter arraycounter=0 Dim MinFreq (1000) Dim
MaxFreq(1000) Dim Amp(1000)
'******************************************************** If
isempty(editbox1.Text) Or IsEmpty(editbox2.Text) Then ' do not
process the data msgbox("YOU MUST FIRST SET A FREQUENCY
RANGE.")

Else  tempholder=editbox1.text
lower_input_frequency =INT(tempholder)
tempholder=editbox2.text  upper_input_frequency =
INT(tempholder)
'msgbox(typename(lower_input_frequency))  'this code will
check to see what the minimum and max  'frequency possible
Is  'this is to save the lowest maximum frequency
max_possible_frequency=chnpropget("[" & groupcounter...
& "]/[" & channeloffset & "]","maximum")  'this is to
save the largest minimum frequency
min_possible_frequency=chnpropget("[" & groupcounter...
& "]/[" & channeloffset & "]","minimum")  If
lower_input_frequency > upper_input_frequency Then  'in
this case cannot process the data.......
```

```
msgbox("Surely you are smarter than this Mr....
Wisconsin!!!!")  Else  'this goes through each
of the groups  Do
     '*****************************
     'reinitialize variables
     channelampcounter=chnpropget("[" & groupcounter...
      & "]/[1]","length") + channeloffset-1
     channelampcounter=Cint(channelampcounter)
     channelfreqcounter=channeloffset-1
     outerchannelcounter=0
     numberofchannels=chnpropget("[" & groupcounter...
      & "]/OxMassFlowRates","length")
     numberofchannels=Cint(numberofchannels)
     '*****************************
     'this goes through each channel in the group
     Do
     '*****************************
     'initialize variables for loop
     channelIncrementer=1
     channelfreqcounter=channelfreqcounter+1
     channelampcounter=channelampcounter+1
     outerchannelcounter=outerchannelcounter+1
     outerchannelcounter=Cint(outerchannelcounter)
     '*****************************
         'msgbox("I went again cause I am stupid")
         'this loop will search through and find the
         'frequency that closest matches the lower
         'input frequency
         Do
           'this will increment the channel counter
           channelIncrementer= channelIncrementer + 1
         Loop Until (lower_input_frequency < chd(....
         channelIncrementer,"[" & groupcounter & "]/["...
          & channelfreqcounter & "]"))
'this will put the lower found frequency
into the  'variable
         found_lower_input_frequency=chd(...
         channelIncrementer-2,"[" & groupcounter & "]/["...
          & channelfreqcounter & "]")
         'this will set the index of the lower input
         'frequency into a variable
         Index_lower_input_frequency=channelIncrementer-1
         'sets the channel incrementer back to one
         channelincrementer=1
         'this loop finds the frequency that closest
```

```
        'matches the upper input frequency
        Do
          channelIncrementer=channelIncrementer+1
        Loop Until (upper_input_frequency < chd(...
        channelIncrementer,"[" & groupcounter & "]/...
        [" & channelfreqcounter & "]"))
        'this stores the frequency that is found that
        'closest matches the upper input frequency
        found_upper_input_frequency=chd(channelIncrementer...
        ,"[" & groupcounter & "]/[" & channelfreqcounter & "]")
'this will set the max amplitude to the
first amplitude
        maxamplitude=chd(Index_lower_input_frequency,...
        "[" & groupcounter & "]/[" & channelampcounter & "]")
        'this loop will look through and find the maximum
        'input amplitude between two specified frequencies
        Do
          If maxamplitude < chd(Index_lower_input_frequency...
          ,"[" & groupcounter & "]/[" & channelampcounter &...
           "]") Then
            'sets the maximum amplitude if it is not yet
            'the max
            maxamplitude=chd(Index_lower_input_frequency,...
            "[" & groupcounter & "]/[" & channelampcounter...
             & "]")
          End If
          Index_lower_input_frequency= Index_lower_...
          input_frequency + 1
        Loop Until (  Index_lower_input_frequency-1=...
        channelIncrementer-1)
        'this will store the max amplitudes into an array
        amplitudes(arraycounter)=maxamplitude
        'increment the array counter
        MinFreq(arraycounter)=found_lower_input_frequency
        MaxFreq(arraycounter)=found_upper_input_frequency
        Amp(arraycounter)=maxamplitude
        arraycounter=arraycounter+1
        outputstring=outputstring & found_lower_input_frequency...
         & Chr(9) & found_upper_input_frequency & Chr(9)...
          & maxamplitude & Chr(13)
        'msgbox(outerchannelcounter & "   " & numberofchannels
        '& "     " & channelampcounter & "     " &
        'channelfreqcounter)
    Loop Until (outerchannelcounter = (numberofchannels))
    groupcounter=groupcounter+1
```

```
     'msgbox(chnpropget("[" & groupcounter-1 & "]/" &
     '"OxMassFlowRates","groupname"))
Loop Until (groupcounter-1=groupcount)  counter=0  Do
'msgbox(counter)  table1.Cells(counter+1,1).value =
MinFreq(counter)  table1.Cells(counter+1,2).value =
MaxFreq(counter)  table1.Cells(counter+1,3).value =
Amp(counter)  counter=counter+1  Loop Until (counter-1=
arraycounter)
'*********************************************************
'this will store the values in the string into their
'respective channels 'defines new group to store the surface
plot channels into Call GroupCreate("Surface Plot
Data",GroupCount + 1) 'defines this as the new default group
Call GroupDefaultSet(GroupIndexGet("Surface Plot Data"))
'allocates memory for a channel to store the data into Call
ChnAlloc("Min Frequency",1000,1,DataTypeFloat64,... "Numeric")
Call ChnAlloc("Max Frequency",1000,1,DataTypeFloat64,...
"Numeric") Call
ChnAlloc("Amplitudes",1000,1,DataTypeFloat64,... "Numeric")
Call ChnAlloc("Ox mass flow rates",1000,1,DataTypeFloat64...
,"Numeric") Call ChnAlloc("Fuel mass flow
rates",1000,1,DataTypeFloat64... ,"Numeric") CHD(1, "[" &
groupcount & "]/Min Frequency")=... found_lower_input_frequency
CHD(1, "[" & groupcount & "]/Max Frequency")=...
found_upper_input_frequency 'store all of the ox mass flow
rates into a single channel 'this variable is used to store the
number of waterfall groups
waterfall_groupcount=(groupcount-1)/2 loop_counter=1 do
  'this code will concatenate two channels together
  'this one is for the ox mass flow rates
  Call ChnConcat("[" & ((groupcount-1)/2) + loop_counter...
   & "]/OxMassFlowRates","[" & groupcount & "]/Ox mass...
   flow rates")
  'this is for the fuel mass flow rates
  Call ChnConcat("[" & ((groupcount-1)/2) + loop_counter...
  & "]/FuelMassFlowRates","[" & groupcount & "]/Fuel...
  mass flow rates")
  loop_counter=loop_counter+1
loop until (loop_counter-1=waterfall_groupcount) 'this loop
will put the amplitudes into a channel loop_counter=0 do
    CHD(loop_counter + 1,"[" & groupcount & "]/Amplitudes")
    '= amplitudes(loop_counter)
    loop_counter=loop_counter + 1
loop until (loop_counter = arraycounter) end if 'this is to
convert from a triplet to an x,y and z matrix... Call
```

```
ChnMatConvert("[" & groupcount & "]/Ox mass flow rates... ","["
& groupcount & "]/Fuel mass flow rates" , "[" & ... groupcount
& "]/Amplitudes" ,"[" & groupcount & "]/Plot X... " , "[" &
groupcount & "]/Plot Y", "relative",10, 10, 10, "mean")
'D3StrucOut ="Matrix" 'D3GridGen(1) ="calculated"
'D3GridCalc(1) ="automatic" 'D3GridNo(1) =20 'D3GridGen(2)
="calculated" 'D3GridCalc(2) ="automatic" 'D3GridNo(2) =25
'D3GridCalcAll =0 'D3GridPolyg ="convex hull" 'D3NodeMeth ="n
neigh. pts" 'D3NodeNo =5 'D3InterpMethChn ="ThinPlate" 'Call
ChnD3Interp("[" & groupcount & "]/Ox mass flow rates", '"[" &
groupcount & "]/Fuel mass flow rates","[" & groupcount '&
"]/Amplitudes","[" & groupcount & "]/Plot X","[" & groupcount '
& "]/Plot Y")
'*****************************************************************
'***THIS IS THE SECTION TO THAT PLOTS THE SURFACE
GRAPH*********
'*****************************************************************
Call PICLOAD("C:\Program Files\National Instruments\DIAdem
10.0... \Demo\Custom Analysis\SURFACE_PLOT.TDR")
'... PICFILE Call PICUPDATE() Call GRAPHObjOpen("3DAxis1")
  Call GRAPHObjOpen("3DObj8_Curve1")
    D3CCHNXNAME      ="[" & groupcount & "]/Plot X"
    D3CCHNYNAME      ="[" & groupcount & "]/Plot Y"
    D3CCHNZNAME      ="[" & groupcount & "]/ConvMatr_Z1"
    'D3CCHNZNAME      ="[" & groupcount & "]/D3Interp_Z1"
    D3CCHNXFILTER    =""
    D3CCHNYFILTER    =""
    D3CCHNZFILTER    =""
    D3CCHNX1NAME     ="[10]/Plot X"
    D3CCHNY1NAME     ="[10]/Plot Y"
    D3CCHNZ1NAME     ="[9]/ConvMatr_Z1"
    'D3CCHNZ1NAME     ="[9]/D3Interp_Z1"
    D3CCHNX1FILTER   =""
    D3CCHNY1FILTER   =""
    D3CCHNZ1FILTER   =""
    D3CCURVETYPE     ="Surface"
    D3CCURVESTRUC    ="Matrix"
    D3CCURVEISOTYPE  ="XY"
    D3CCURVEISONO    =0
    D3CCURVEVTYPE    ="Vector4D"
    D3CCURVEVPLANETY ="XY-plane"
    D3CURVECOLOR     ="Palette"
    D3CURVECOLORRGB  =50266112
    D3CURVESPECCOLOR ="blue"
    D3CURVESPECCRGB  =50266112
```

```
    D3CURVEISOCOLOR  ="green"
    D3CURVEISOCOLRGB =33619712
    D3CURVEVCOLOR    ="black"
    D3CURVEVCOLORRGB =33554432
    D3CURVESYMCOLOR  ="black"
    D3CURVESYMCOLRGB =33554432
    D3LEGDRAW        =0
    D3LEGPDRAW       =0
  Call GRAPHObjClose("3DObj8_Curve1")
Call GRAPHObjClose("3DAxis1") Call PicUpdate()   'refreshes the
screen and graph End If End Sub
```

OPERATING CONDITION AVERAGING AND DEVIATION

```
Dim Endpoints
Dim points
Dim interval
Dim lower
'%%%%%%%%%%%%%%%%%%%%%%%%%%%%%%%%%%%%%%%%%%%%%%%%%%%%%%%%%%%%
'Find the gaps where to take data
indy=ChnAlloc("Indicies",100)
indicies = ChnLength("Time")
past=ChD(1,"Time")
counter=2
gapcounter=1
loopy=1
Do
  present=Chd(counter,"Time")
  difference = present - past
If difference > 1 Then
gapcounter=gapcounter + 1
Else
End If
If gapcounter=2 Then
  'msgbox("gap found at " & counter)
  ChD(loopy,"Indicies") = (counter - 1)
  loopy=loopy+1
  gapcounter=0
Else
End If
    counter = counter + 1
```

```
  past = present
Loop Until (counter=(indicies -1))
points= ChnLength("Indicies")
'250 indicies = 1 second
interval=50
'Arithmetic Mean
StatSel(6) = "Yes"
'Standard Deviation
StatSel(14) = "Yes"
StatResChn = "No"
'%%%%%%%%%%%%%%%%%%%%%%%%%%%%%%%%%%%%%%%%%%%%%%%%
'Calculate all Fuel Pressure Values
FuelMean = ChnAlloc("Fuel Mean",50)
FuelDev = ChnAlloc("Fuel Dev",50)
'Get Mean Ambient Pressure
Call StatBlockCalc("Channel","1-100","Fuel Inj")
ambientpf=StatArithMean
counter=1
Do
  lower=chd(counter,"Indicies") - interval + 1
  Call StatBlockCalc("Channel",lower & "-" & chd...
  (counter,"Indicies"),"Fuel Inj")
  ChD(counter,"Fuel Mean") = (StatArithMean - ambientpf)
  ChD(counter,"Fuel Dev") = StatDeviation
  counter=counter+1
Loop Until (counter=(points+1))
'%%%%%%%%%%%%%%%%%%%%%%%%%%%%%%%%%%%%%%%%%%%%%%%%
'Calculate all Ox Pressure Values
OxMean = ChnAlloc("Ox Mean",50)
OxDev = ChnAlloc("Ox Dev",50)
'Get Mean Ambient Pressure
Call StatBlockCalc("Channel","1-100","Ox Inj")
ambientpox=StatArithMean
counter=1
Do
  lower=chd(counter,"Indicies") - interval + 1
  Call StatBlockCalc("Channel",lower & "-" &...
  chd(counter,"Indicies"),"Ox Inj")
  ChD(counter,"Ox Mean") = (StatArithMean - ambientpox)
  ChD(counter,"Ox Dev") = StatDeviation
  counter=counter+1
Loop Until (counter=(points+1))
'%%%%%%%%%%%%%%%%%%%%%%%%%%%%%%%%%%%%%%%%%%%%%%%%
'Calculate Fuel Temp Values
TFuelMean = ChnAlloc("Temp Fuel Mean",50)
```

```
TFuelDev = ChnAlloc("Temp Fuel Dev",50)
counter=1
Do
  lower=chd(counter,"Indicies") - interval + 1
  Call StatBlockCalc("Channel",lower & "-" &...
   chd(counter,"Indicies"),"Ox Collector")
  ChD(counter,"Temp Fuel Mean") = StatArithMean
  ChD(counter,"Temp Fuel Dev") = StatDeviation
  counter=counter+1
loop Until (counter=(points+1))
'%%%%%%%%%%%%%%%%%%%%%%%%%%%%%%%%%%%%%%%%%%%%%%%%
'Calculate Ox Temp Values
TOxMean = ChnAlloc("Temp Ox Mean",50)
TOxDev = ChnAlloc("Temp Ox Dev",50)
counter=1
Do
  lower=chd(counter,"Indicies") - interval + 1
  Call StatBlockCalc("Channel",lower & "-" &...
   chd(counter,"Indicies"),"Fuel Collector")
  ChD(counter,"Temp Ox Mean") = StatArithMean
  ChD(counter,"Temp Ox Dev") = StatDeviation
  counter=counter+1
Loop Until (counter=(points+1))
'%%%%%%%%%%%%%%%%%%%%%%%%%%%%%%%%%%%%%%%%%%%%%%%%
'Calculate Alpha Temp Values
TOxMean = ChnAlloc("Alpha Mean",50)
TOxDev = ChnAlloc("Alpha Dev",50)
counter=1
Do
  lower=chd(counter,"Indicies") - interval + 1
  Call StatBlockCalc("Channel",lower & "-" &...
  chd(counter,"Indicies"),"Alpha Chamber")
  ChD(counter,"Alpha Mean") = StatArithMean
  ChD(counter,"Alpha Dev") = StatDeviation
  counter=counter+1
Loop Until (counter=(points+1))
'%%%%%%%%%%%%%%%%%%%%%%%%%%%%%%%%%%%%%%%%%%%%%%%%
'Calculate Beta Temp Values
TOxMean = ChnAlloc("Beta Mean",50)
TOxDev = ChnAlloc("Beta Dev",50)
counter=1
Do
  lower=chd(counter,"Indicies") - interval + 1
  Call StatBlockCalc("Channel",lower & "-" &...
  chd(counter,"Indicies"),"Beta Chamber")
```

```
  ChD(counter,"Beta Mean") = StatArithMean
  ChD(counter,"Beta Dev") = StatDeviation
  counter=counter+1
Loop Until (counter=(points+1))
%%%%%%%%%%%%%%%%%%%%%%%%%%%%%%%%%%%%%%%%%%%%%%%%%%%%
'Calculate Gamma Temp Values
TOxMean = ChnAlloc("Gamma Mean",50)
TOxDev = ChnAlloc("Gamma Dev",50)
counter=1
Do
  lower=chd(counter,"Indicies") - interval + 1
  Call StatBlockCalc("Channel",lower & "-" &...
  chd(counter,"Indicies"),"Gamma Chamber")
  ChD(counter,"Gamma Mean") = StatArithMean
  ChD(counter,"Gamma Dev") = StatDeviation
  counter=counter+1
Loop Until (counter=(points+1))
'%%%%%%%%%%%%%%%%%%%%%%%%%%%%%%%%%%%%%%%%%%%%%%%%%%%%
'Calculate Delta Temp Values
TOxMean = ChnAlloc("Delta Mean",50)
TOxDev = ChnAlloc("Delta Dev",50)
counter=1
Do
  lower=chd(counter,"Indicies") - interval + 1
  Call StatBlockCalc("Channel",lower & "-" &...
  chd(counter,"Indicies"),"Delta Chamber")
  ChD(counter,"Delta Mean") = StatArithMean
  ChD(counter,"Delta Dev") = StatDeviation
  counter=counter+1
Loop Until (counter=(points+1))
'%%%%%%%%%%%%%%%%%%%%%%%%%%%%%%%%%%%%%%%%%%%%%%%%%%%%
'Calculate Alpha Temp Values
TOxMean = ChnAlloc("Epsilon Mean",50)
TOxDev = ChnAlloc("Epsilon Dev",50)
counter=1
Do
  lower=chd(counter,"Indicies") - interval + 1
  Call StatBlockCalc("Channel",lower & "-" &...
  chd(counter,"Indicies"),"Epsilon Chamber")
  ChD(counter,"Epsilon Mean") = StatArithMean
  ChD(counter,"Epsilon Dev") = StatDeviation
  counter=counter+1
Loop Until (counter=(points+1))
```

POWER DENSITY CALCULATIONS AND PEAK SEARCHING

```
'------------------------------------------------
'-- Created on 02/17/2007 23:48:05
'-- Author: Ryan Cavitt
'-- Comment: This code is wicked
'------------------------------------------------
'%%%%%%%%%%%%%%%%%%%%%%%%%%%%%%%%%%%%%%%%%%%%%%%%%%%%%%%%%%%%%%%%%%%%%%%
'The input data must be a first set of chamber data, the
'next groups must be
'the waterfall groups from RUSKIE Analysis (by Erik "VB
'Master" Lee).  The
'threshold of noise must be input in Pa.
threshold = 207 'Pa
'The code goes through each FFT and creates the following
'outputs
'   -peak frequency (1)
'   -Total energy below the cutoff frequency [kW/m^3] (2)
'   -The amount of energy confined in the peaks [kW/m^3] (3)
'   -The percentage of confined energy to total energy (
'4)=(3)/(2)
'   -The number of peaks found above the threshold (5)
'   -The lower limit of each peak (6)
'   -The upper limit of each peak (7)
'   -The corresponding fuel mass flow rate (8)
'   -The corresponding oxygen mass flow rate (9)
'The algorithm for peak identification is based on
'incrementing through every
'FFT index.  At each index, the loop looks at the
'previous point and the next
'two points to enable boolean operation conditions
'that create the beginning
'of the peak, as well as the end of a peak. (see below
'for wicked details)
'The conditioning enables the absence narrow spikes as
'well as correctly
'defining broad peaks in the spectrum.
'%%%%%%%%%%%%%%%%%%%%%%%%%%%%%%%%%%%%%%%%%%%%%%%%%%%%%%%%%%%%%%%%%%%%%%%
Groups=groupcount
groupnow=Groups/2+1
groupcounter=1
'Loop through each group
```

```
Do Until (Groups/2)+1 = groupcounter
   'Get the group properties from the data set - not waterfall
   originalstring=GroupPropGet(groupcounter, "description")
   delimiter="*"
   MyArray = Split(originalstring, delimiter, -1, 1)
   'Create new group for integration sets
   Call Groupcreate(MyArray(0) & " Integration Data",...
   groupcount +1)
   'Make the new group the default
   Call GroupDefaultSet(GroupIndexGet(MyArray(0) & " ...
   Integration Data"))
   wisconsin=1
     channelindex=1
     'Loop through each channel
     Do until channelindex = chnlength("[" & groupnow & ...
     "]/OxMassFlowRates") + 1
        'msgbox(channelindex & "    " & chnlength("[" &...
         groupnow & "]/OxMassFlowRates"))
        'Find the Ox Mass Flow Rate that corresponds to ...
        the frequency and amplitude
        OxMassFlowRate = chd(channelindex, "[" & groupnow...
         & "]/OxMassFlowRates")
        FuelMassFlowRate = chd(channelindex, "[" & groupnow...
         & "]/FuelMassFlowRates")
        'Set the variables as channel names
        XChannel="Transducer_Freq_" & OxMassFlowRate
        'Find index where frequency is 20,000
        Cutoffindex = PNo(XChannel, 20000)
        YChannel="Transducer_Ampl_" & OxMassFlowRate
        'Convert psi amplitudes to Pa
        Call matscalmul(YChannel, 6894.757, "No")
        Convert="MatSkalMul_Z1"
        'Integrate across the whole channel
        Call CHNINTEGRATE(XChannel,Convert,"[" & groupcount...
         & "]/Total Energy Density " & OxMassFlowRate)
            'Create channels for the upper and lower limits
            If channelindex = 1 Then
              Call chnalloc(MyArray(0) & " Upper Limit", 500)
              Call chnalloc(MyArray(0) & " Lower Limit", 500)
            Else
            End if
                bump=0
                index=2
                peaks=0
                summedenergy=0
```

```
'Find the energy above a certain threshhold
Do until index=Cutoffindex
  h = chd((index-1), Convert)
  i = chd(index, Convert)
  j = chd((index+1), Convert)
  k = chd((index+2), Convert)
  If bump=0 Then
    If h < threshold and i > threshold and ...
    (j > threshold or k > threshold) Then
      If index = 0 Then
        startindex = 0
      Else
        startindex = index - 1
      End if
     bump = 1
      'msgbox("startindex = " & startindex...
       & "  h = " & h & "i = " & i & "j = ...
       " & j & "k = " & k)
    Else
      bump = 0
    End if
  Else
    If h > threshold and  i < threshold ...
    and j < threshold and k < threshold Then
      endindex = index + 1
      upper=chd(endindex, "[" & groupcount ...
      & "]/Total Energy Density " & ...
      OxMassFlowRate)
      lower=chd(startindex, "[" & groupcount...
      & "]/Total Energy Density " & ...
      OxMassFlowRate)
      intervalenergy=(upper-lower)
      summedenergy = summedenergy + ...
      intervalenergy
      bump = 0
      peaks=peaks+1
      lowerfreq = chd(startindex, XChannel)
      upperfreq = chd(endindex, XChannel)
      'Populate channels
      chd(wisconsin, MyArray(0) & " Lower...
       Limit") = lowerfreq
      chd(wisconsin, MyArray(0) & " Upper...
       Limit") = upperfreq
      wisconsin=wisconsin+1
    Else
```

```
            End if
          End if
         index = index+1
        Loop
'Find the peak frequency
index=4
maxamp=0
Do Until index = Cutoffindex
  value = chd(index, Convert)
    If value > maxamp Then
      maxamp = value
      maxindex = index
    Else
    End if
  index=index+1
Loop
maxfreq=chd(maxindex, XChannel)
'msgbox(maxfreq)
'msgbox(maxindex)
'Delete converted Pa amplitudes and Integration Chan
Call ChnDel(Convert)
totalenergy=chd(Cutoffindex, "[" & groupcount...
& "]/Total Energy Density " & OxMassFlowRate)
Call ChnDel("Total Energy Density " & OxMassFlowRate)
'Create other channels
If channelindex = 1 Then
    Call chnalloc(MyArray(0) & " Total Energy ...
    Density", 50)
    Call chnalloc(MyArray(0) & " OxMassFlowRates"...
    , 50)
    Call chnalloc(MyArray(0) & " FuelMassFlowRates...
    ", 50)
    Call chnalloc(MyArray(0) & " Energy above ...
    threshold", 50)
    Call chnalloc(MyArray(0) & " Percent above ...
    threshold", 50)
    Call chnalloc(MyArray(0) & " Number of Peaks", 50)
    Call chnalloc(MyArray(0) & " Peak Frequency", 50)
Else
End if
'Populate other channels
chd(channelindex, MyArray(0) & " Percent above ...
threshold") = (summedenergy/totalenergy)*100
chd(channelindex, MyArray(0) & " Total Energy Density")...
 = totalenergy/1000
```

```
 chd(channelindex, MyArray(0) & " OxMassFlowRates")...
  = OxMassFlowRate
 chd(channelindex, MyArray(0) & " FuelMassFlowRates")...
  = FuelMassFlowRate
 chd(channelindex, MyArray(0) & " Energy Above ...
 Threshold") = summedenergy/1000
 chd(channelindex, MyArray(0) & " Number of Peaks") ...
 = peaks
 chd(channelindex, MyArray(0) & " Peak Frequency") = ...
 maxfreq
 channelindex=channelindex+1
Loop
   If groupnow=Groups/2+1 Then
     Call Groupcreate("All Integration Data",...
     groupcount +1)
     'Make the new group the default
     Call GroupDefaultSet(GroupIndexGet("All ...
     Integration Data"))
     Call chnalloc("All Total Energy Density", 1000)
     Call chnalloc("All OxMassFlowRates", 1000)
     Call chnalloc("All FuelMassFlowRates", 1000)
     Call chnalloc("All Energy above threshold", 1000)
     Call chnalloc("All Percent above threshold", 1000)
     Call chnalloc("All Number of Peaks", 1000)
     Call chnalloc("All Peak Frequency", 1000)
     Call ChnCopy(MyArray(0) & " Percent above ...
     threshold", "All Percent above threshold")
     Call ChnCopy(MyArray(0) & " Total Energy ...
     Density","All Total Energy Density")
     Call ChnCopy(MyArray(0) & " OxMassFlowRates...
     ","All OxMassFlowRates")
     Call ChnCopy(MyArray(0) & " FuelMassFlowRates...
     ","All FuelMassFlowRates")
     Call ChnCopy(MyArray(0) & " Energy Above...
      Threshold","All Energy above threshold")
     Call ChnCopy(MyArray(0) & " Number of Peaks...
     ","All Number of Peaks")
     Call ChnCopy(MyArray(0) & " Peak Frequency"...
     ,"All Peak Frequency")
   Else
     Call ChnConcat(MyArray(0) & " Percent above ...
     threshold", "All Percent above threshold")
     Call ChnConcat(MyArray(0) & " Total Energy ...
     Density","All Total Energy Density")
     Call ChnConcat(MyArray(0) & " OxMassFlowRates...
```

```
            ","All OxMassFlowRates")
            Call ChnConcat(MyArray(0) & " FuelMassFlowRates...
            ","All FuelMassFlowRates")
            Call ChnConcat(MyArray(0) & " Energy Above...
             Threshold","All Energy above threshold")
            Call ChnConcat(MyArray(0) & " Number of ...
            Peaks","All Number of Peaks")
            Call ChnConcat(MyArray(0) & " Peak Frequency...
            ","All Peak Frequency")
          End if
'msgbox(groupcounter & "   " & Groups/2)
groupcounter=groupcounter+1
groupnow=groupnow+1
Loop
```

MATLAB STABILITY MAPPING CODE

This m-file is compatible with MATLAB v6.1. As such, the comment syntax is the percent symbol %.

```
clc
clear all
%*********************************************************
%Input Test Date i.e. Feb.05.2007
Date='All Dates ';
%Input Injector Type
injector='60 Degree Impinging Jet';
%Amplitude file to read
amplfile=dlmread('D:\Engineering\Research\Final Analysis\...
Imp60 Overall\CSV Sheets\Imp60 Overall Amplitude ...
Maximum.csv',',',3,0);
%Operating Conditions file to read
OC=dlmread('D:\Engineering\Research\Final Analysis\Imp60...
Overall\CSV Sheets\Imp60 Overall O.C. Uncertainty...
Average.csv',',',1,0);
%[highlabel,lowlabel,radialf,combf,allf]=Amptitles...
('D:\Engineering\Research\Final Analysis\Imp30 Feb....
05.2007\CSV Sheets\Imp30 Feb.05.2007 Amplitude.csv')
%Set the mesh size
mesh=500;
```

```
%************************************************************
%All high subscripts correlate to thresholds = 0.05 psi
%Total Energy Density [KW/m^3]
E_high=amplfile(:,1);
%Oxygen Mass Flow Rate
m_ohigh=amplfile(:,2);
%Fuel Mass Flow Rate
m_fhigh=amplfile(:,3);
%Amount of energy above the threshold
E_uphigh=amplfile(:,4);
%Percent of energy above the threshold
Percent_high=amplfile(:,5);
%Number of Peaks found
Peaks_high=amplfile(:,6);
%Peak Frequency
Peakf_high=amplfile(:,7);
%All low subscripts correlate to thresholds = 0.03 psi
E_low=amplfile(:,8);
m_olow=amplfile(:,9);
m_flow=amplfile(:,10);
E_uplow=amplfile(:,11);
Percent_low=amplfile(:,12);
Peaks_low=amplfile(:,13);
Peakf_low=amplfile(:,14);
%FFT Amplitudes between 2000 and 3000 Hz
amp_R=amplfile(:,15);
m_oR=amplfile(:,16);
m_fR=amplfile(:,17);
%FFT Amplitudes between 3300 and 4300 Hz
amp_comb=amplfile(:,18);
m_ocomb=amplfile(:,19);
m_fcomb=amplfile(:,20);
%FFT Amplitudes between 100 and 20,000 Hz
amp_all=amplfile(:,21);
m_oall=amplfile(:,22);
'True=I love you Keri
m_fall=amplfile(:,23);
%Oxygen mass flow rate
m_o=OC(:,1);
%Fuel mass flow rate
m_f=OC(:,2);
%Fuel manifold pressure
P_f=OC(:,3);
%Standard Deviation of fuel manifold pressure
sigma_Pf=OC(:,4);
```

```
%Oxygen manifold pressure
P_o=OC(:,5);
%Standard deviation of oxygen manifold pressure
sigma_Po=OC(:,6);
%Fuel manifold temperature
T_f=OC(:,7);
%Standard deviation of fuel manifold temperature
sigma_Tf=OC(:,8);
%Oxygen manifold temperature
T_o=OC(:,9);
%Standard Deviation of the manifold temperature
sigma_o=OC(:,10);
%Alpha temperature
T_alpha=OC(:,11);
%Beta temperature
T_Beta=OC(:,12);
%gamma temperature
T_gamma=OC(:,13);
%delta temperature
T_delta=OC(:,14);
%Epsilon temperature
T_Epsilon=OC(:,15);
%Uncertainty in oxygen mass flow rate
U_mo=OC(:,16);
%Uncertainty in fuel mass flow rate
U_mf=OC(:,17);
%Oxidizer to fuel ratio
OF=OC(:,18);
%Uncertainty in oxidizer to fuel ratio
U_OF=OC(:,19);
%Total mass flow rate
m_total=OC(:,20);
%Uncertainty in total mass flow rate
U_mtotal=OC(:,21);
%Oxidizer velocity
V_o=OC(:,22);
%Uncertainty in oxidizer velocity
U_Vo=OC(:,23);
%Fuel velocity
V_f=OC(:,24);
%Uncertainty in fuel velocity
U_Vf=OC(:,25);
%Velocity Ratio (F/O)
V_ratio=OC(:,26);
%Uncertainty in velocity ratio
```

```
U_Vratio=OC(:,27);
%Oxidizer Reynolds number
Re_o=OC(:,28);
%Uncertainty in Oxidizer Reynolds number
U_Reo=OC(:,29);
%Fuel Reynolds number
Re_f=OC(:,30);
%Uncertainty in Fuel Reynolds number
U_Ref=OC(:,31);
%Momentum ratio
lambda=OC(:,32);
%Uncertainty in momentum ratio
U_lambda=OC(:,33);
%Pi star criterion
Pi_star=OC(:,34);
%Uncertainty in Pi star criterion
U_Pistar=OC(:,35);
%Calculated 1st tangential mode
f_T=OC(:,36);
%Calculated 2nd tangential mode
f_TT=OC(:,37);
%Calculated 1st radial mode
f_R=OC(:,38);
%Calculated 2nd radial mode
f_RR=OC(:,39);
%Calculated 1st tangential/1st radial mode
f_TR=OC(:,40);
%Calculated 1st tangential/2nd radial mode
f_TRR=OC(:,41);
%Calculated 2nd tangential/1st radial mode
f_TTR=OC(:,42);
%Fuel Volumetric Flow Rate
Q_f=OC(:,43);
%Uncertainty in fuel volumetric flow rate
U_Qf=OC(:,44);
%Oxygen Volumetric Flow Rate
Q_o=OC(:,45);
%Uncertainty in oxygen volumetric flow rate
U_Qo=OC(:,46);
%*********************************************************
%Assign variables to plot axes
x=m_total;
U_x=U_mtotal;
y=OF;
U_y=U_OF;
```

```
z=E_low;
%Set the x axis label with units ie. Oxygen Mass Flow Rate...
[g/s]
xlab='Total Mass Flow Rate [g/s]';
%Set the y axis label with units ie. Methane Mass Flow...
Rate [g/s]
ylab='Mixture Ratio';
%If the y-axis needs to be logarithmic set logscale=1
logscale=0;
%To autoscale the axes autoscale=1, otherwise
%autoscale=0 and input maximums
autoscale=0;
%To make the colormap grayscale blackandwhite=1
blackandwhite=0;
if autoscale == 1
    %Find Minimums and Maximums
    minx=min(x);
    maxx=max(x);
    miny=min(y);
    maxy=max(y);
else
    minx=0;
    maxx=5.5;
    miny=1;
    maxy=9;
    cmaxi=2700;
    cmini=-.0010;
end
%*********************************************************
vert=0;
if z==amp_comb;
    note='[3300-4300] Hz';
    scale='psi';
elseif z==amp_all;
    note='[100-20,000] Hz';
    scale='psi';
elseif z==amp_R;
    note='[2000-3000] Hz';
    scale='psi';
elseif z==E_low
    note=' ';
    scale='KW/m^3';
elseif z==E_uplow
    note='Threshold = 0.03 psi';
    scale='KW/m^3';
```

```
elseif z==Percent_low
    note='Threshold = 0.03 psi';
    scale='% Above Threshold';
    vert=1;
elseif z==E_high
    note='Threshold = 0.05 psi';
    scale='KW/m^3';
elseif z==E_uphigh
    note=' ';
    scale='KW/m^3';
elseif z==Percent_high
    note='Threshold = 0.05 psi';
    scale='% Above Threshold';
    vert=1;
end
% Frequency Stuff
% minfreq=a(:,2);
% maxfreq=a(:,3);
% minf=max(minfreq);
% maxf=max(maxfreq);
% minfstr=int2str(minf);
% maxfstr=int2str(maxf);
% freqrange=strcat('Freq. Range = [',[minfstr '-' maxfstr...
],']  Hz');
%Grid Generation
xincrement=(maxx-minx)/mesh;
yincrement=(maxy-miny)/mesh;
dx = (minx-(minx*.2)):xincrement:(maxx+(minx*.2));
dy = (miny-(miny*.2)):yincrement:(maxy+(miny*.2));
[XI,YI] = meshgrid(dx,dy);
ZI = griddata(x,y,z,XI,YI,'linear');
%Customize Plot Text
maptitle=strcat(injector,' Stability Map');
fourtitle=strcat(injector,' Stability Surface');
%Plot 3D Stability Map
figure
poo = axes('Position',[0.09 0.12 .93 .85]);
surf(XI,YI,ZI,'EdgeColor','none'),hold
errorbar(x,y,U_y,'.k'),hold on
herrorbar(x,y,U_x,'.k'),hold on
shading interp
    if autoscale==0
        %set(cbar,'cLim', [cmini, cmaxi])
        %xlim(cbar,[cmini, cmaxi])
         caxis([cmini cmaxi])
```

```
end
apple=colorbar;
old_bar = findobj('tag','Colorbar');
delete(old_bar);
cbar=colorbar('vert');
cpos=get(cbar,'Position');
cpos(3)=cpos(3)/1.5;
cpos(1) = cpos(1)*.94;
set(cbar,'Position',cpos);
view(0, -90)
axis([minx maxx miny maxy]);
set(gca,'YDir','reverse')
if blackandwhite==1
    colormap(gray)
end
if logscale==1
    set(gca,'YScale', 'log')
end
h = axes('Position',[0 0 1 1],'Visible','off');
if scale=='KW/m^3'
    text(.902,.08,'KW','FontSize',12,'HorizontalAlignment...
    ','center', 'FontWeight', 'bold');
    text(.902,.076,'___','FontSize',12,'...
    HorizontalAlignment','center', 'FontWeight', 'bold');
    text(.902,.03,'m^{3}','FontSize',12,'...
    HorizontalAlignment','center', 'FontWeight', 'bold');
end
text(.47,.04,xlab,'FontWeight','bold','FontSize',15,'...
HorizontalAlignment','center');
text(.03,.54,ylab,'FontWeight','bold','FontSize',15,'...
HorizontalAlignment','center', 'Rotation',90);
set(gcf,'PaperPositionMode','auto')
print -dbmp StabilityMap
```

APPENDIX H

EXPERIMENTAL DATA

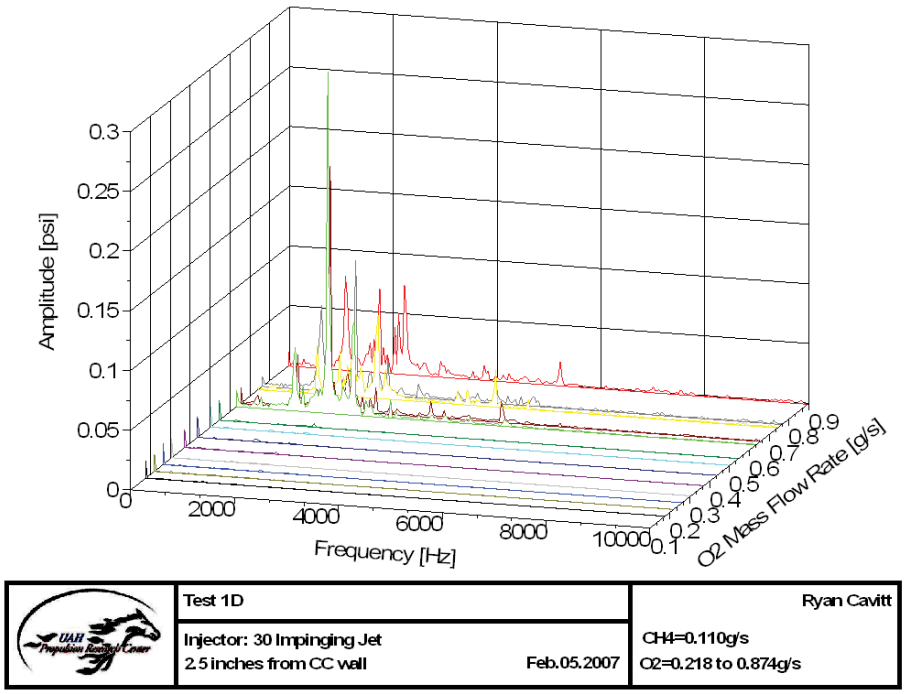

Figure H.1: 30-1-1 Waterfall Plot

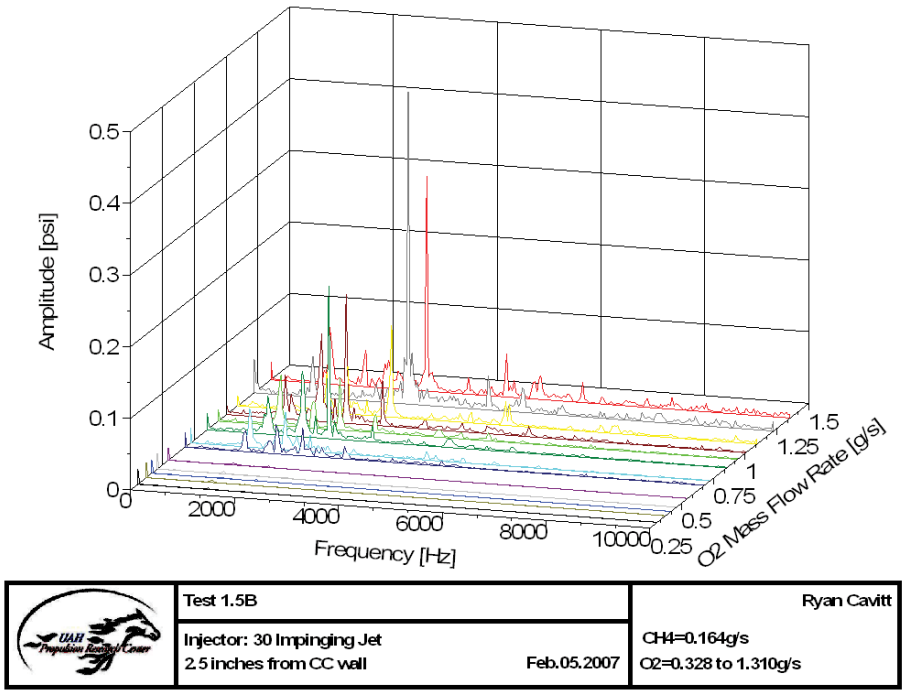

Figure H.2: 30-1-1.5 Waterfall Plot

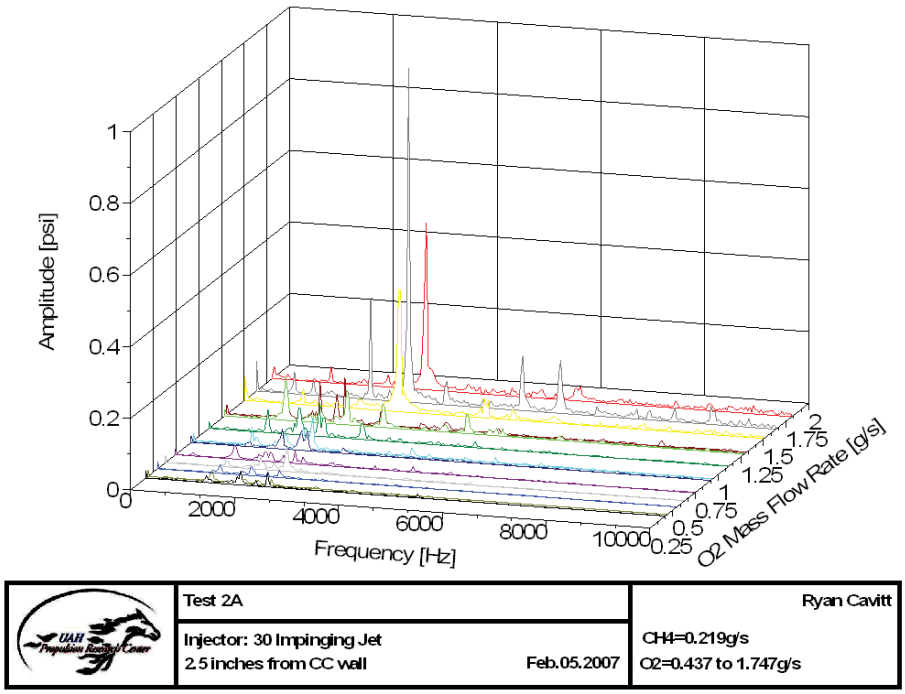

Figure H.3: 30-1-2 Waterfall Plot

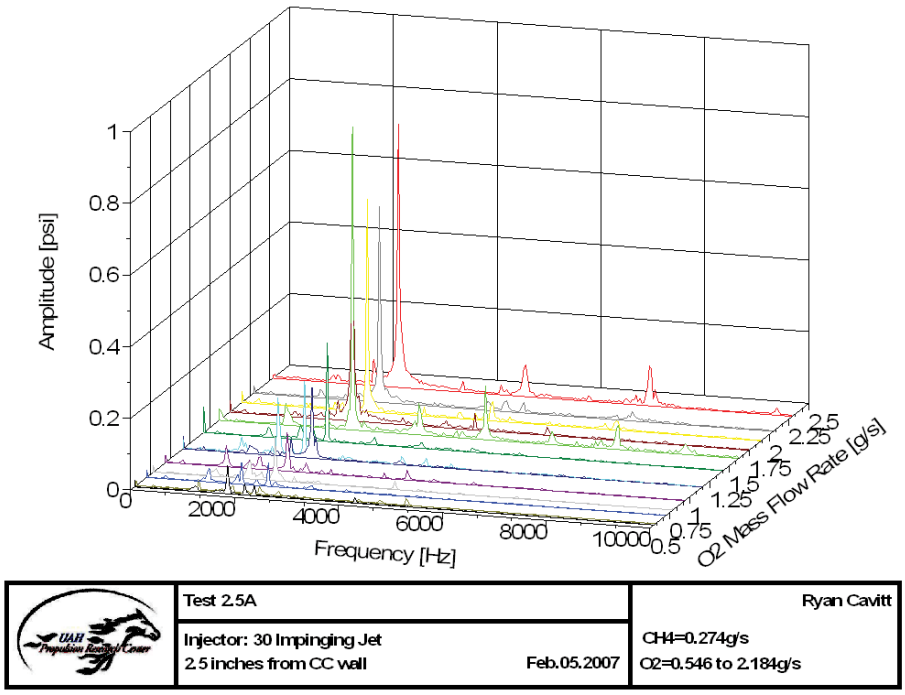

Figure H.4: 30-1-2.5 Waterfall Plot

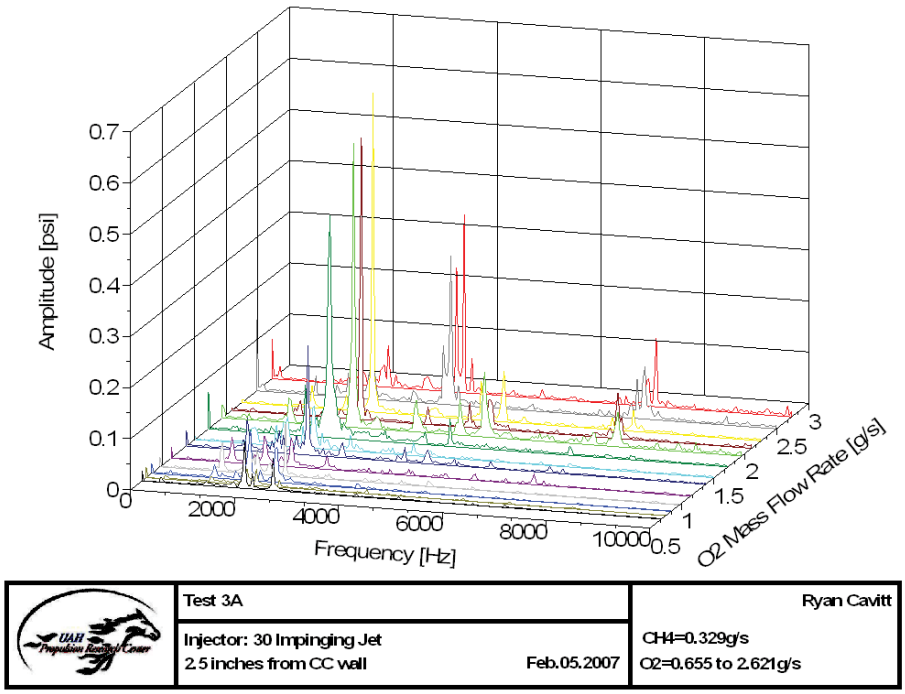

Figure H.5: 30-1-3 Waterfall Plot

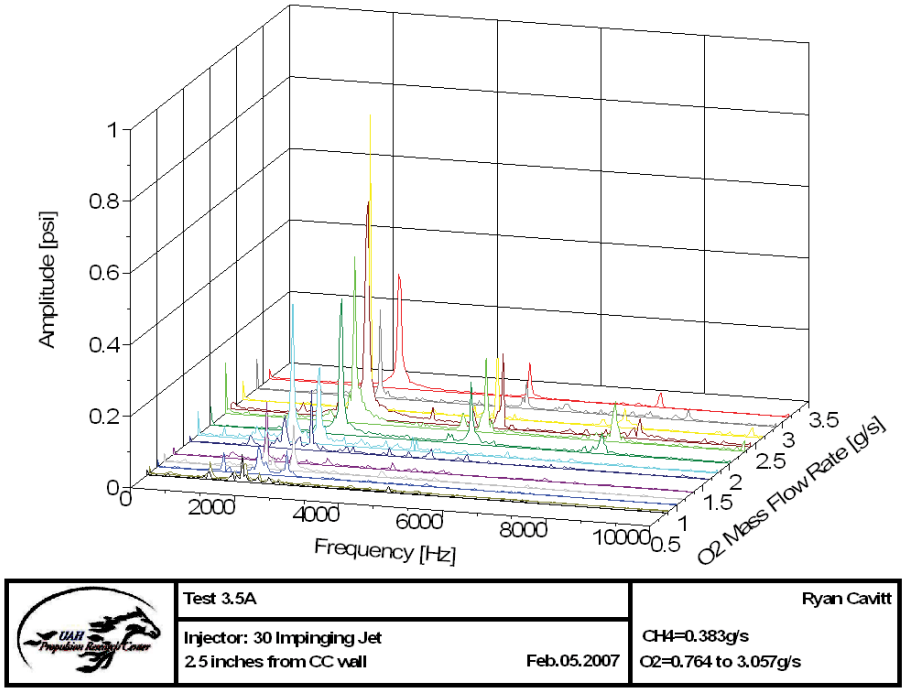

Figure H.6: 30-1-3.5 Waterfall Plot

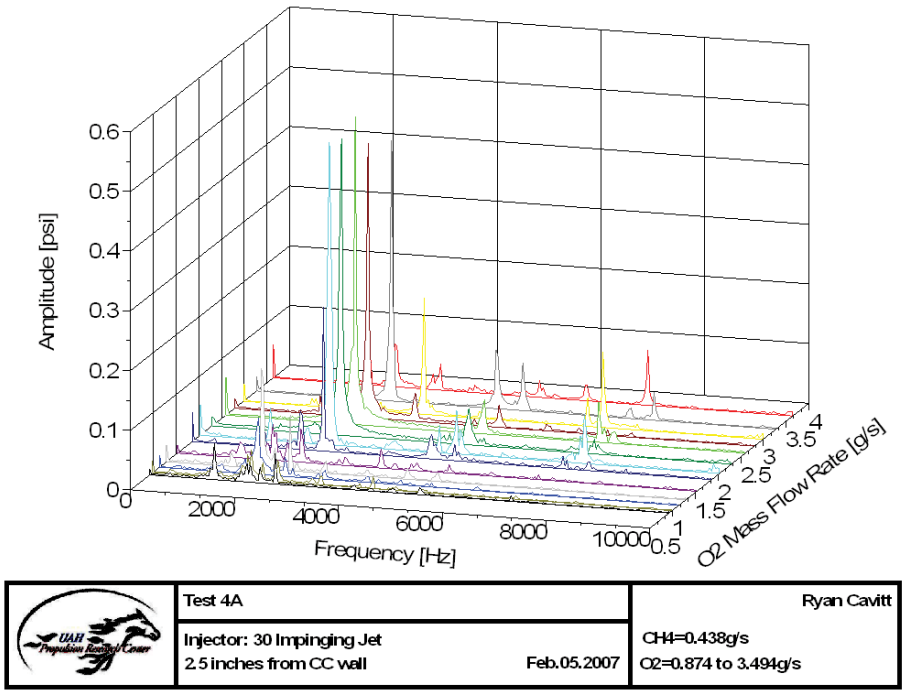

Figure H.7: 30-1-4 Waterfall Plot

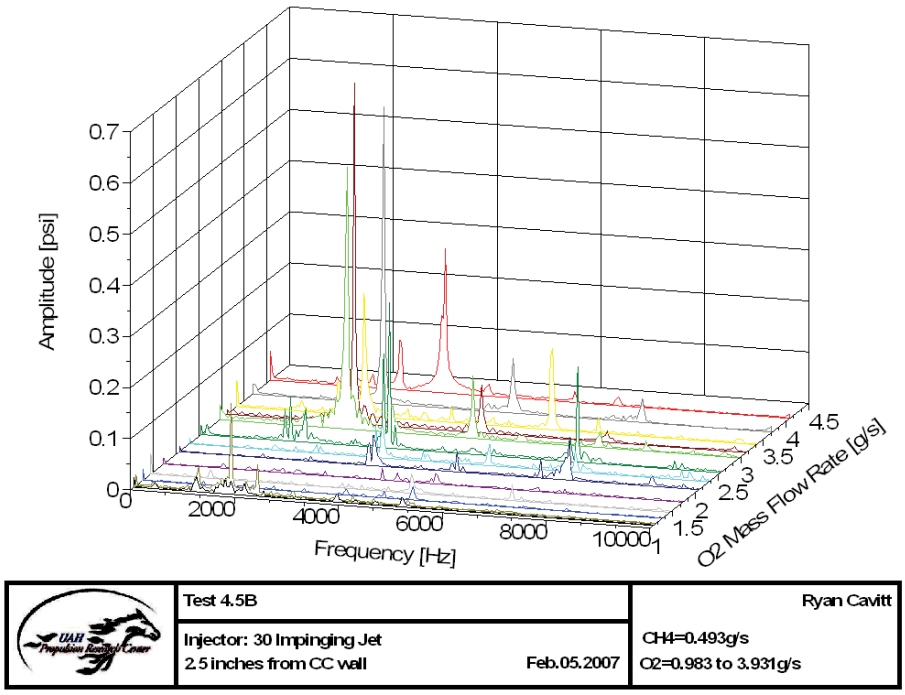

Figure H.8: 30-1-4.5 Waterfall Plot

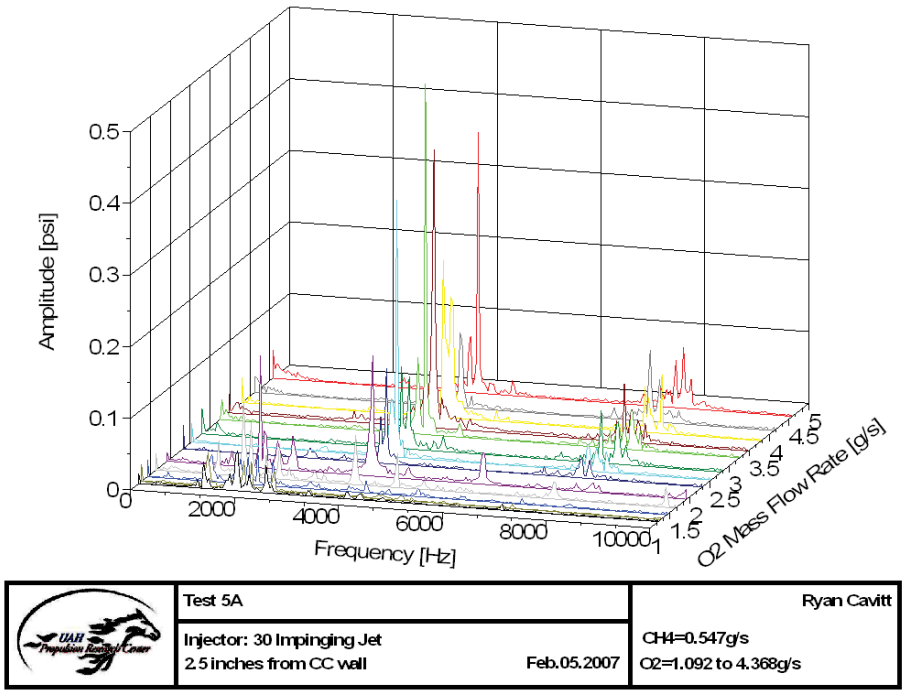

Figure H.9: 30-1-5 Waterfall Plot

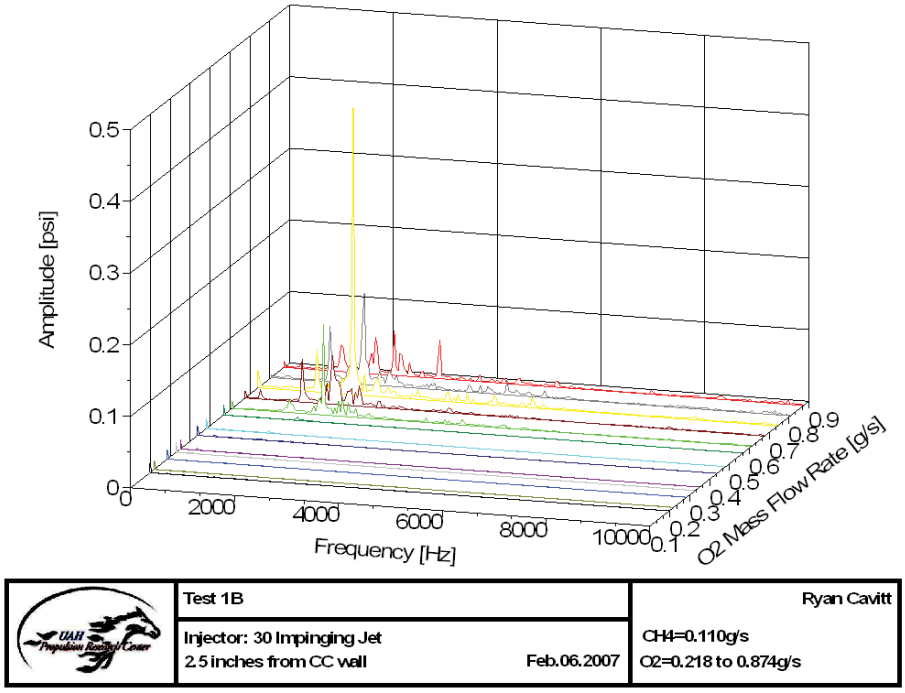

Figure H.10: 30-2-1 Waterfall Plot

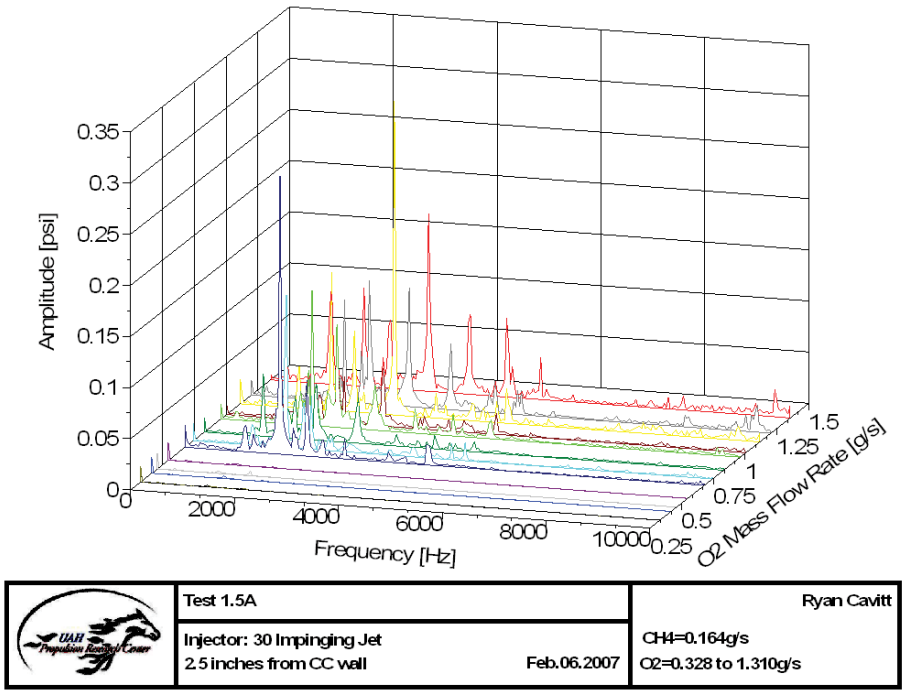

Figure H.11: 30-2-1.5 Waterfall Plot

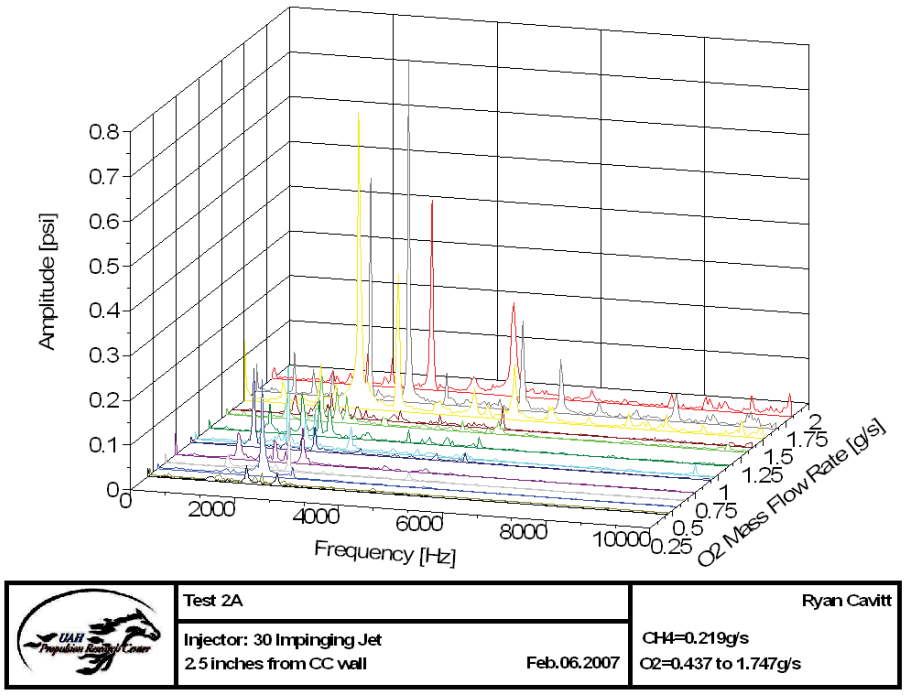

Figure H.12: 30-2-2 Waterfall Plot

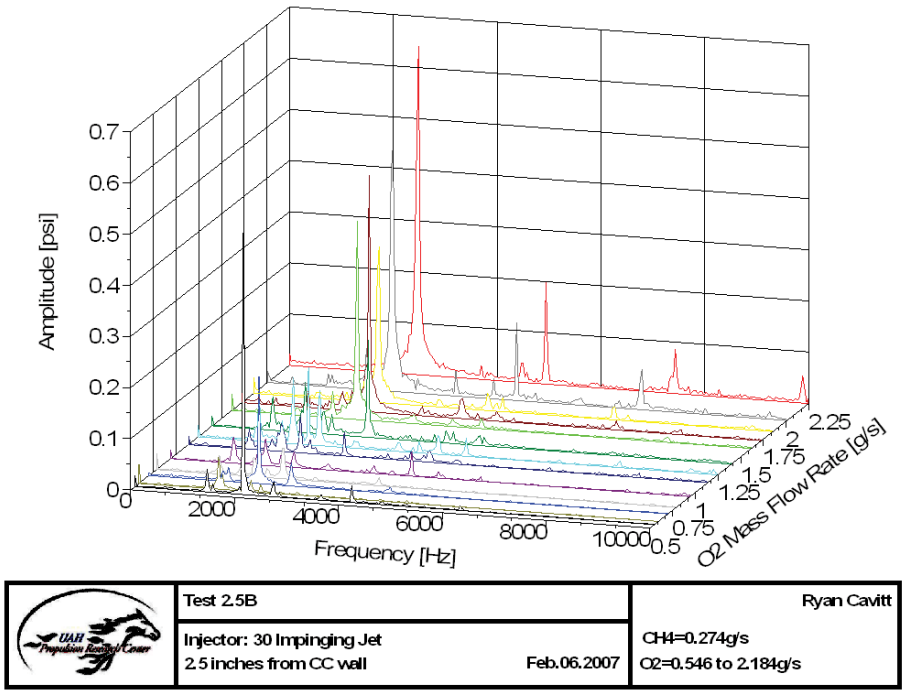

Figure H.13: 30-2-2.5 Waterfall Plot

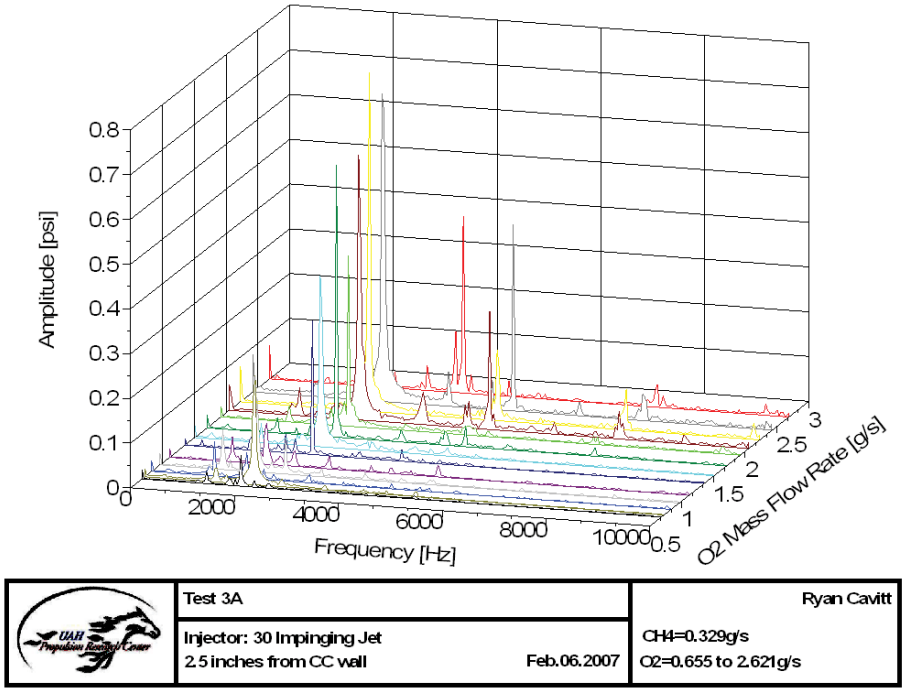

Figure H.14: 30-2-3 Waterfall Plot

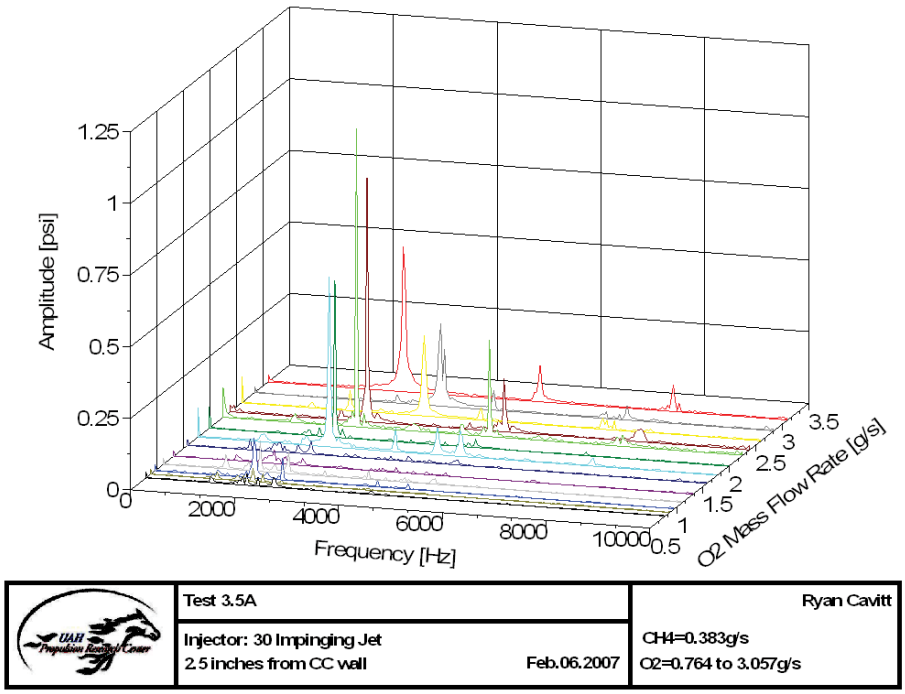

Figure H.15: 30-2-3.5 Waterfall Plot

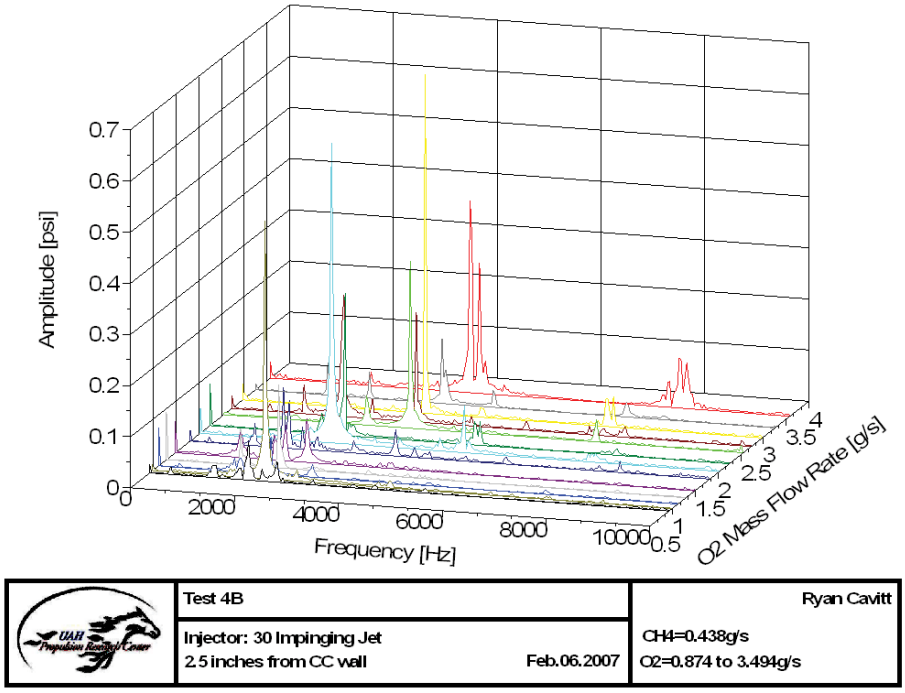

Figure H.16: 30-2-4 Waterfall Plot

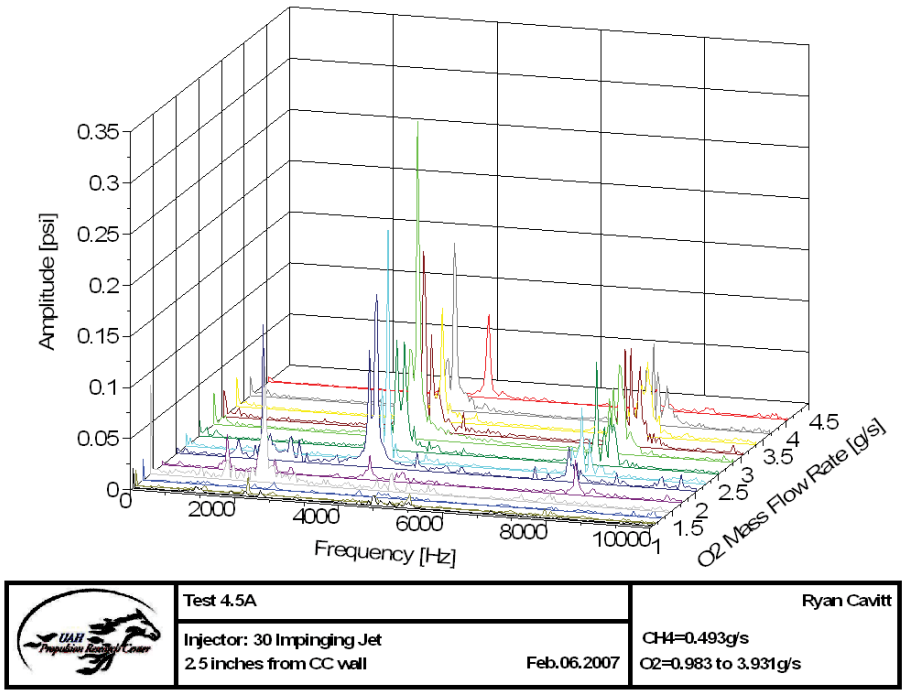

Figure H.17: 30-2-4.5 Waterfall Plot

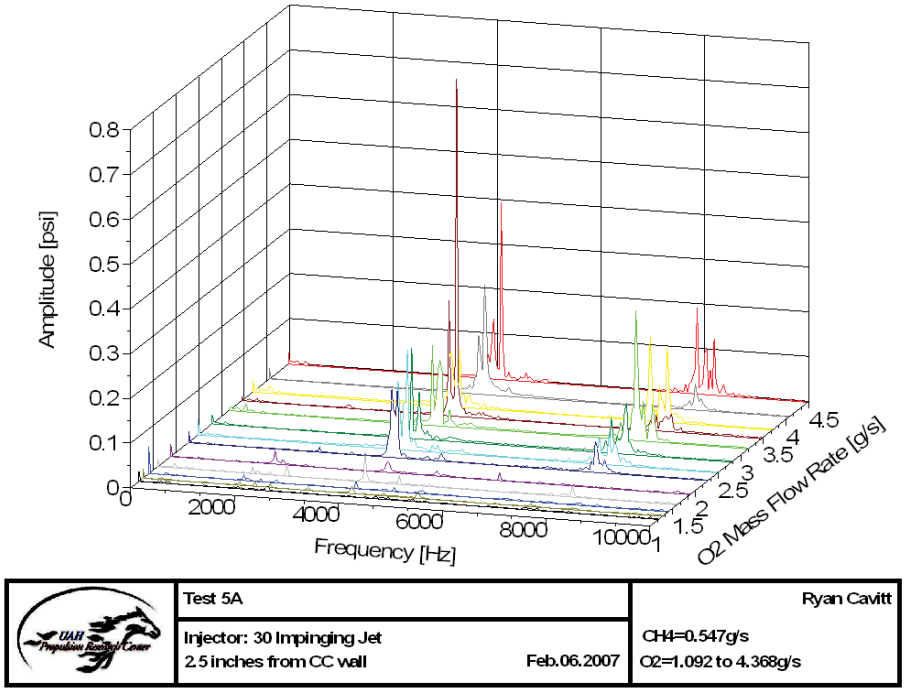

Figure H.18: 30-2-5 Waterfall Plot

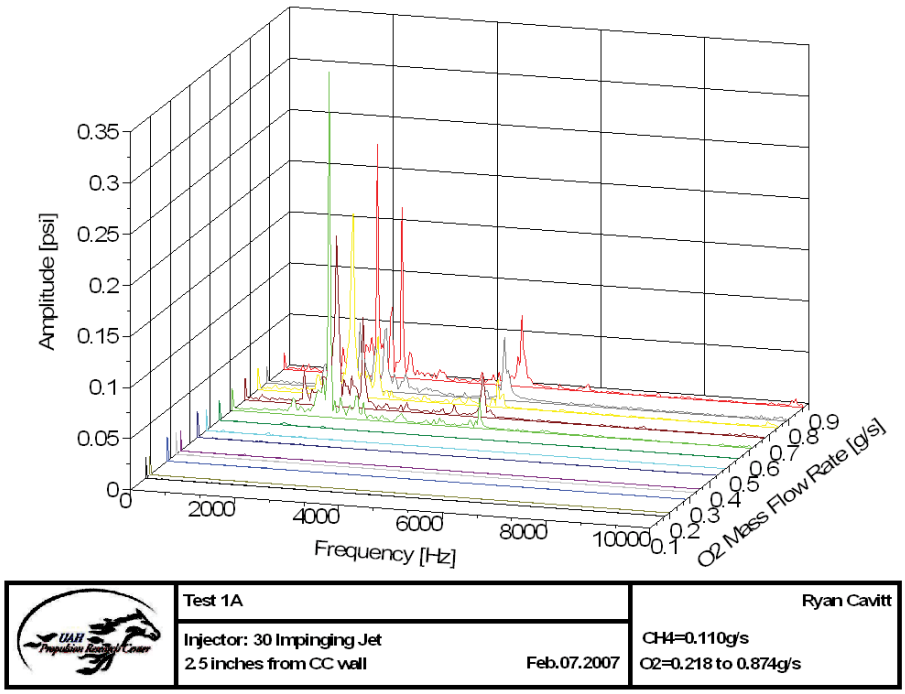

Figure H.19: 30-3-1 Waterfall Plot

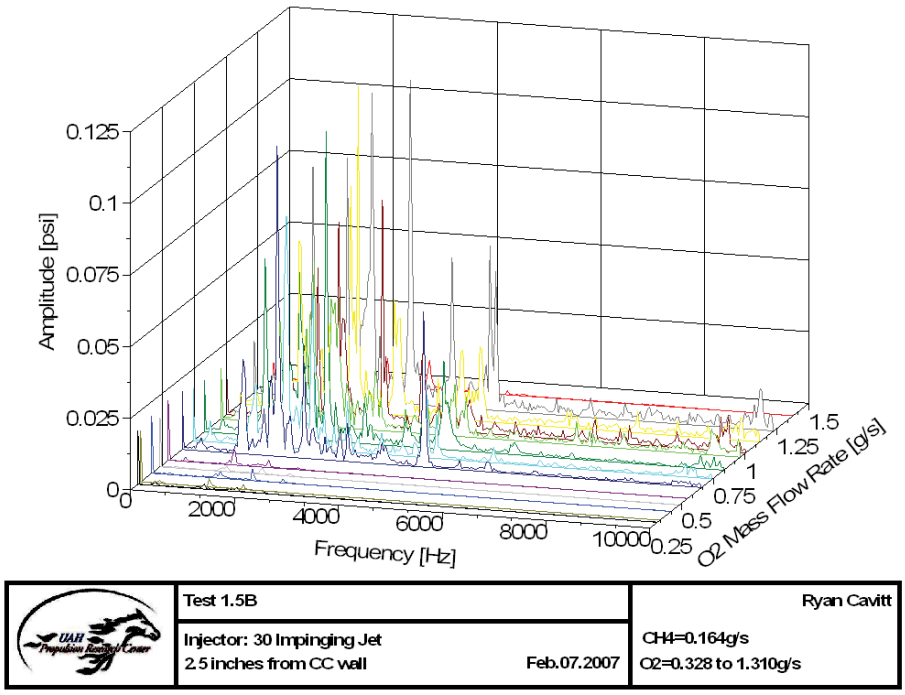

Figure H.20: 30-3-1.5 Waterfall Plot

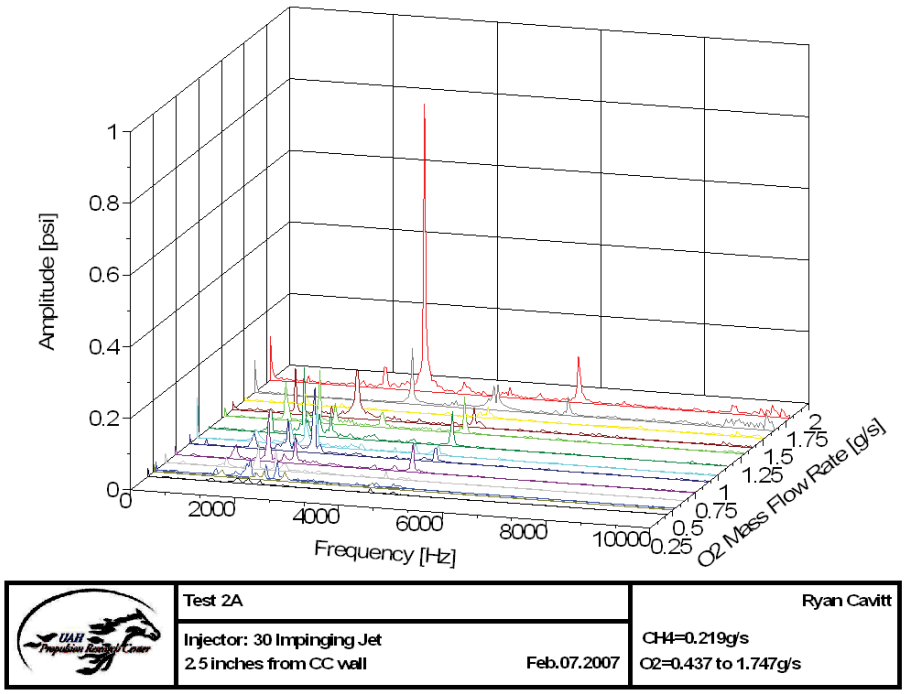

Figure H.21: 30-3-2 Waterfall Plot

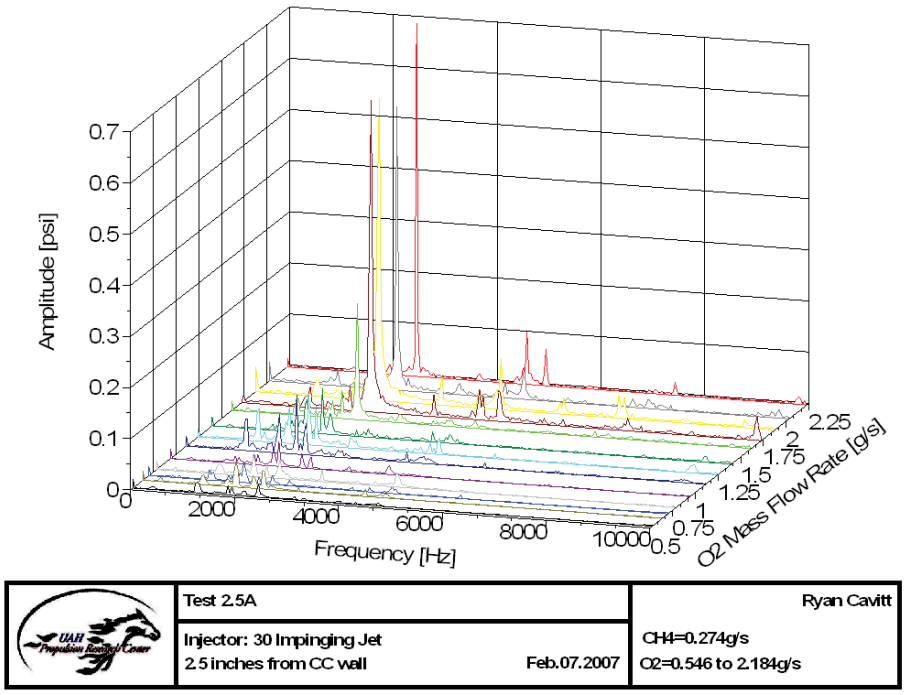

Figure H.22: 30-3-2.5 Waterfall Plot

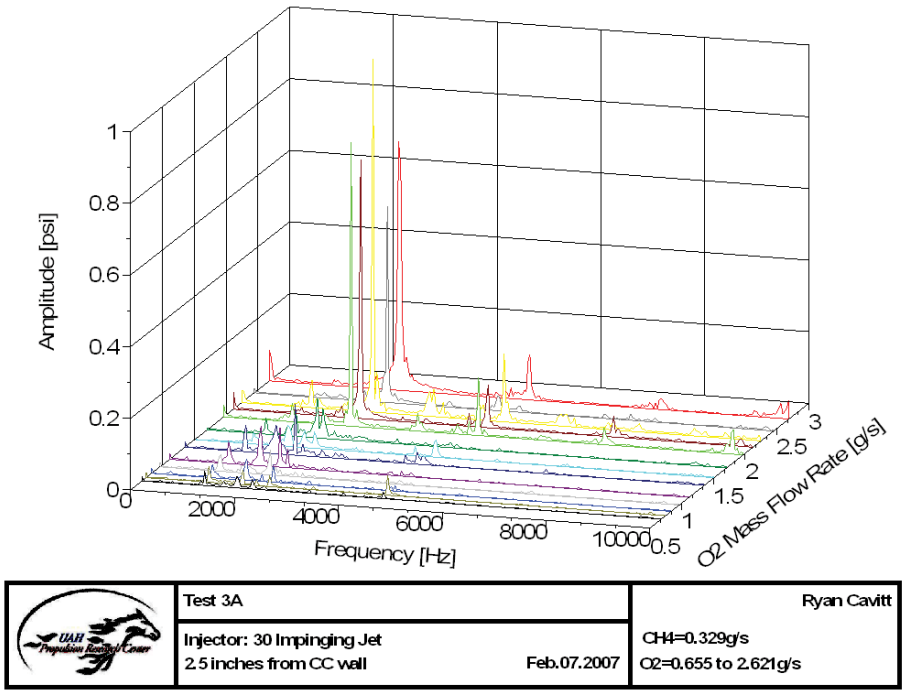

Figure H.23: 30-3-3 Waterfall Plot

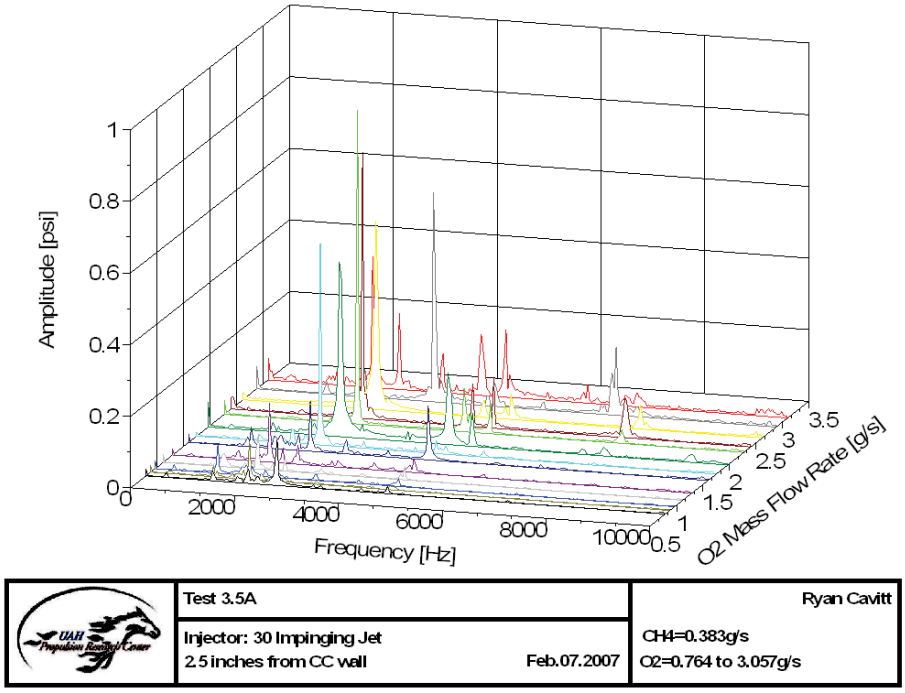

Figure H.24: 30-3-3.5 Waterfall Plot

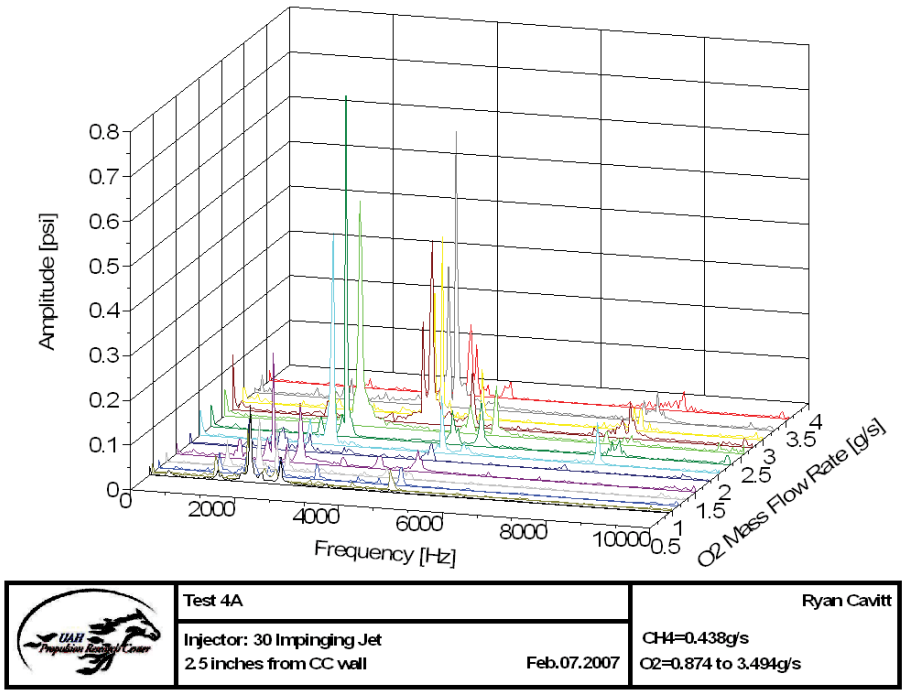

Figure H.25: 30-3-4 Waterfall Plot

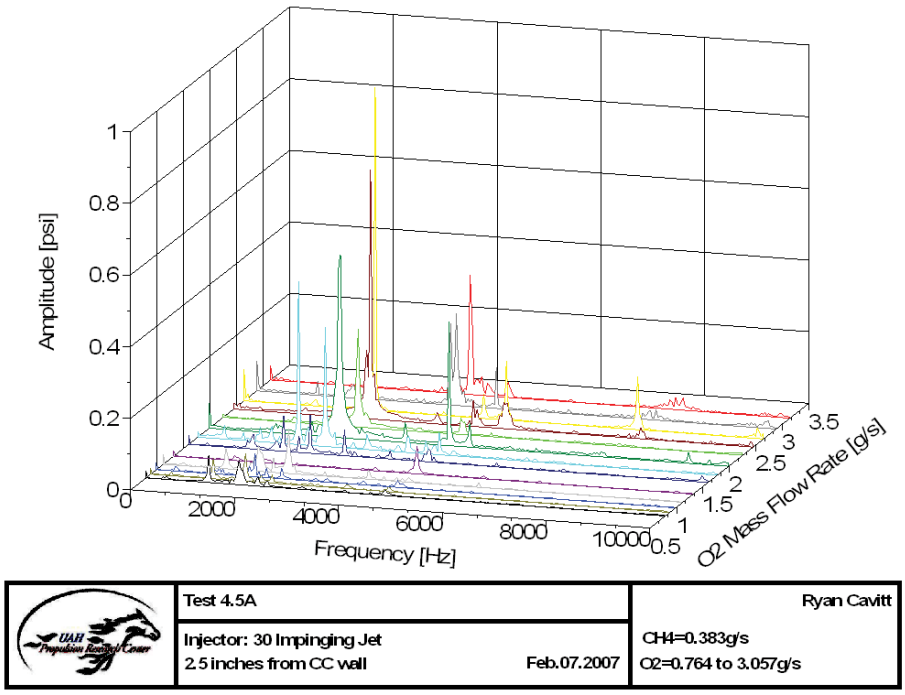

Figure H.26: 30-3-4.5 Waterfall Plot

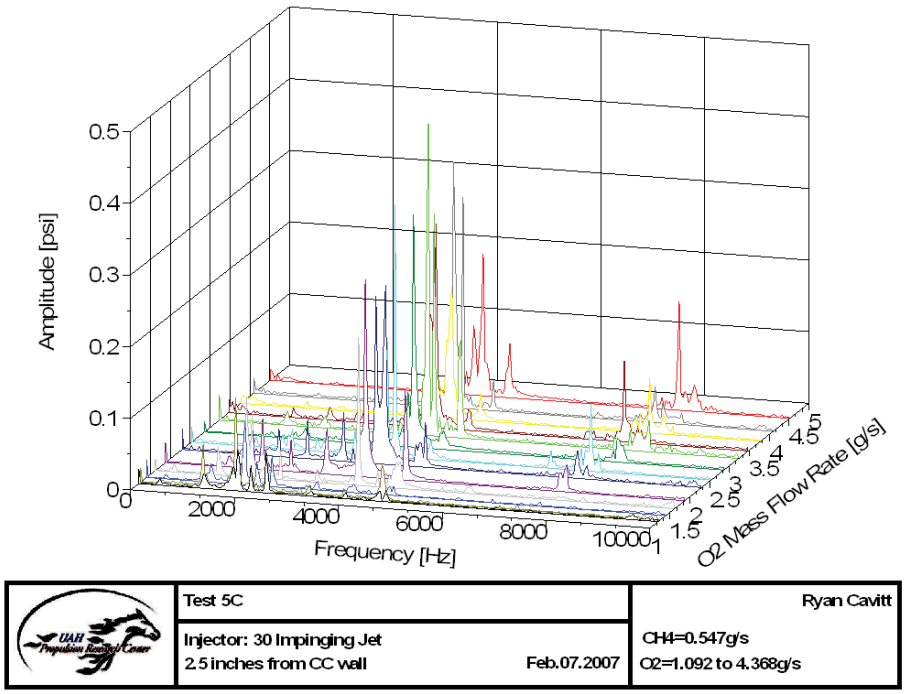

Figure H.27: 30-3-5 Waterfall Plot

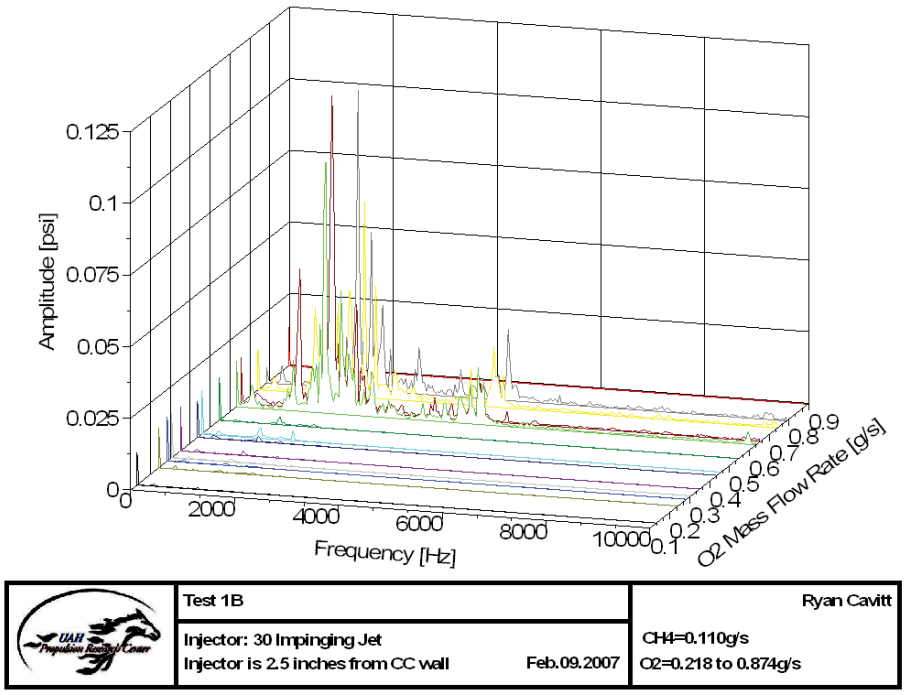

Figure H.28: 30-4-1 Waterfall Plot

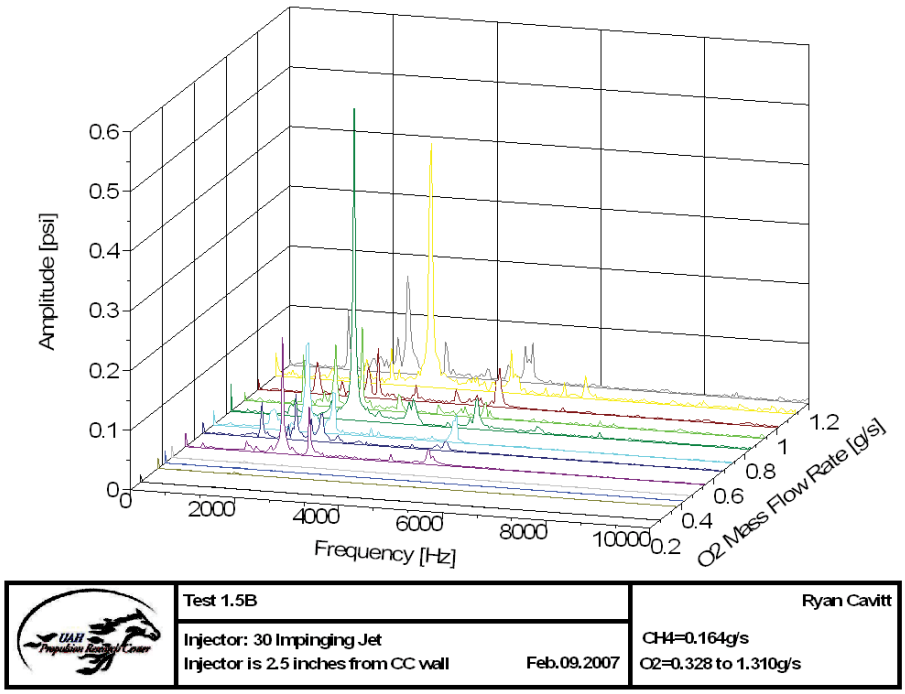

Figure H.29: 30-4-1.5 Waterfall Plot

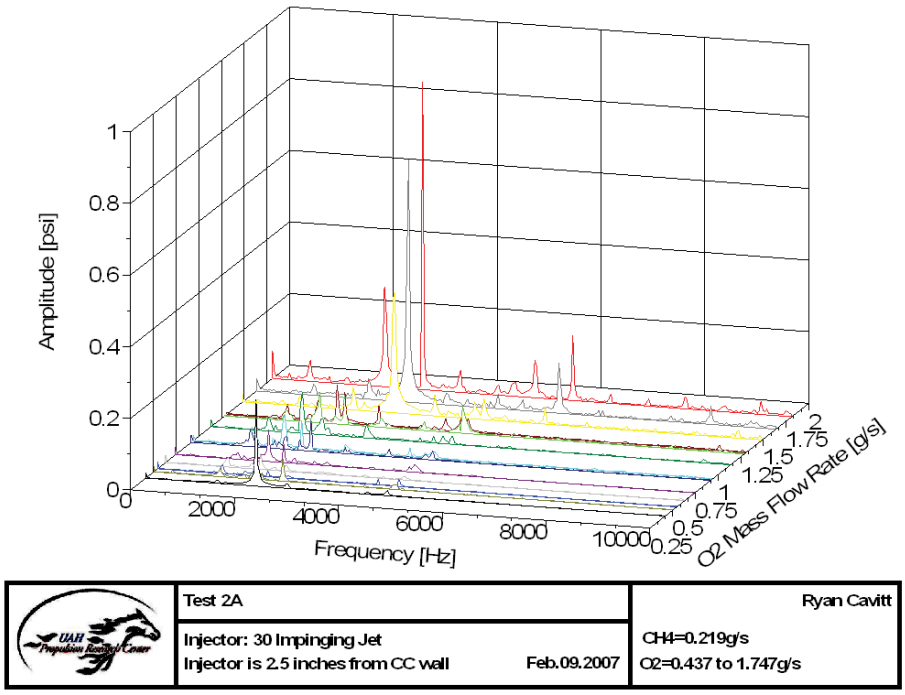

Figure H.30: 30-4-2 Waterfall Plot

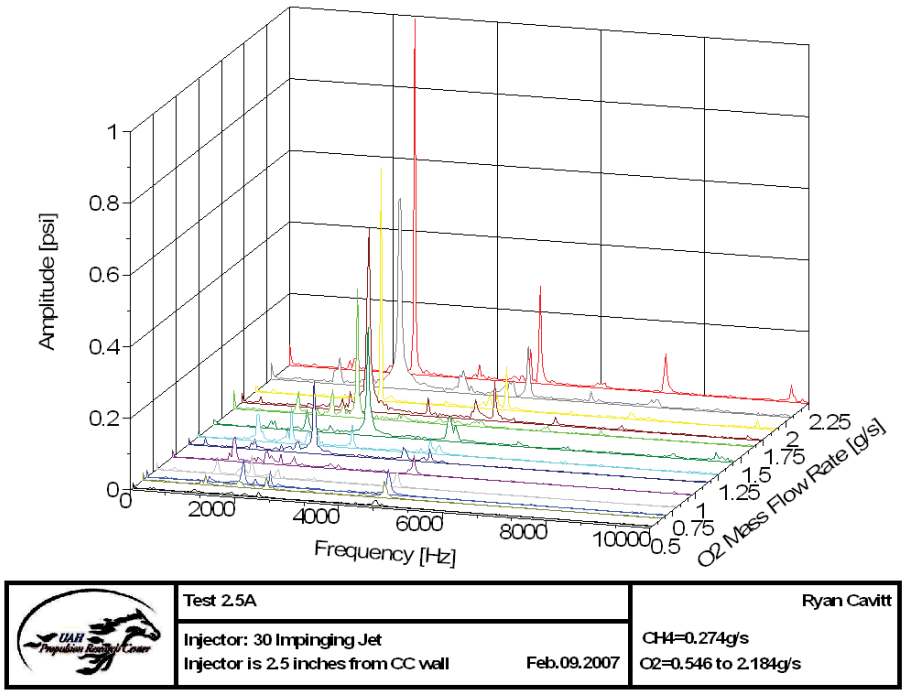

Figure H.31: 30-4-2.5 Waterfall Plot

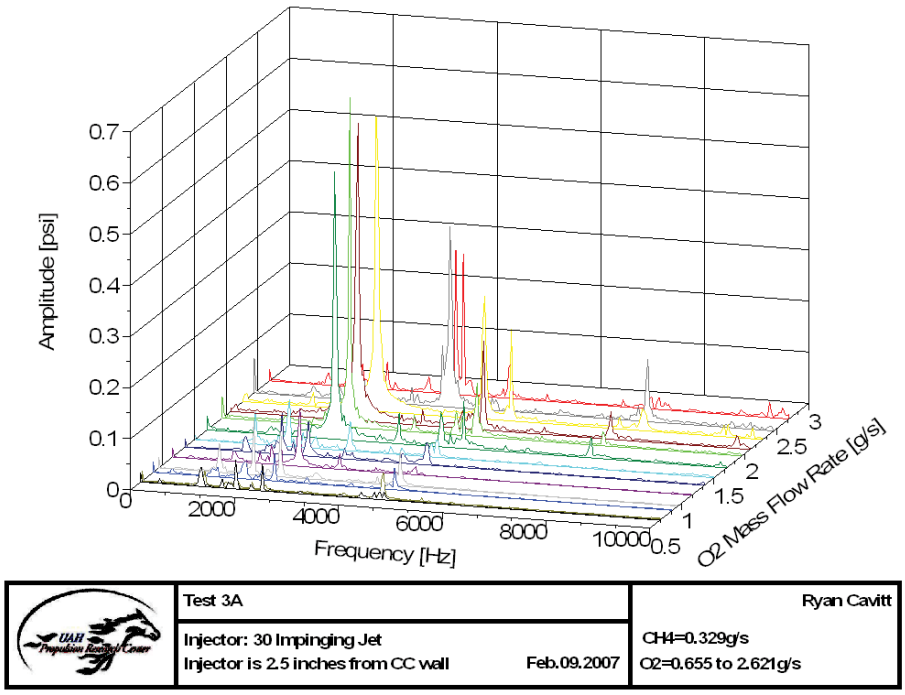

Figure H.32: 30-4-3 Waterfall Plot

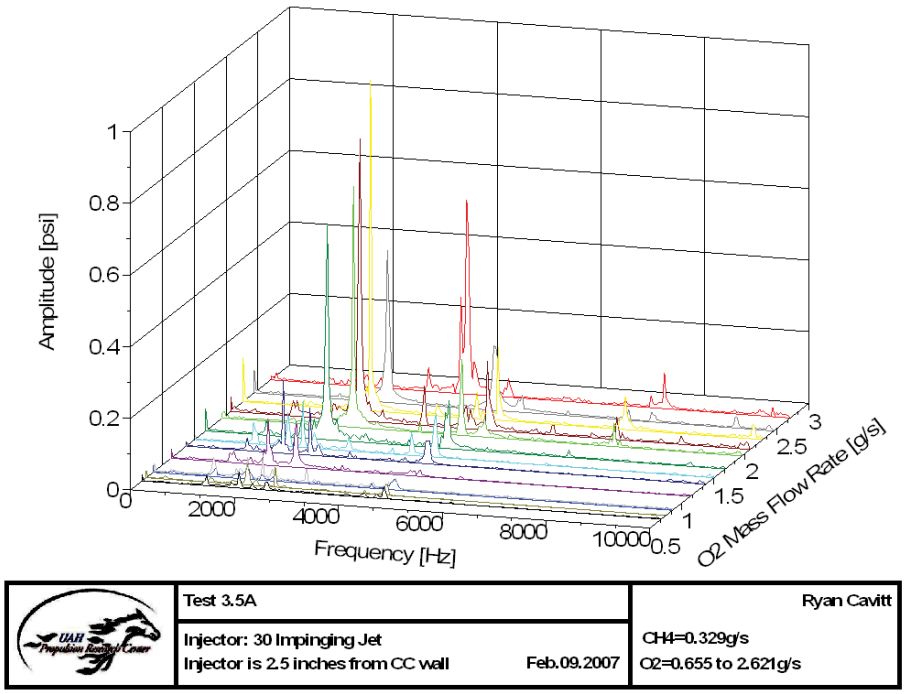

Figure H.33: 30-4-3.5 Waterfall Plot

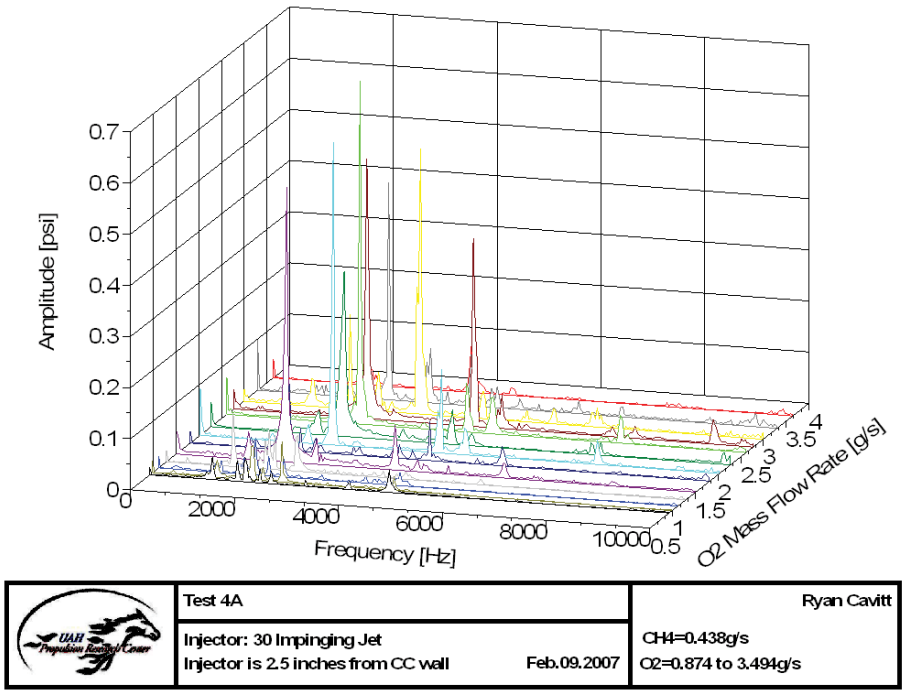

Figure H.34: 30-4-4 Waterfall Plot

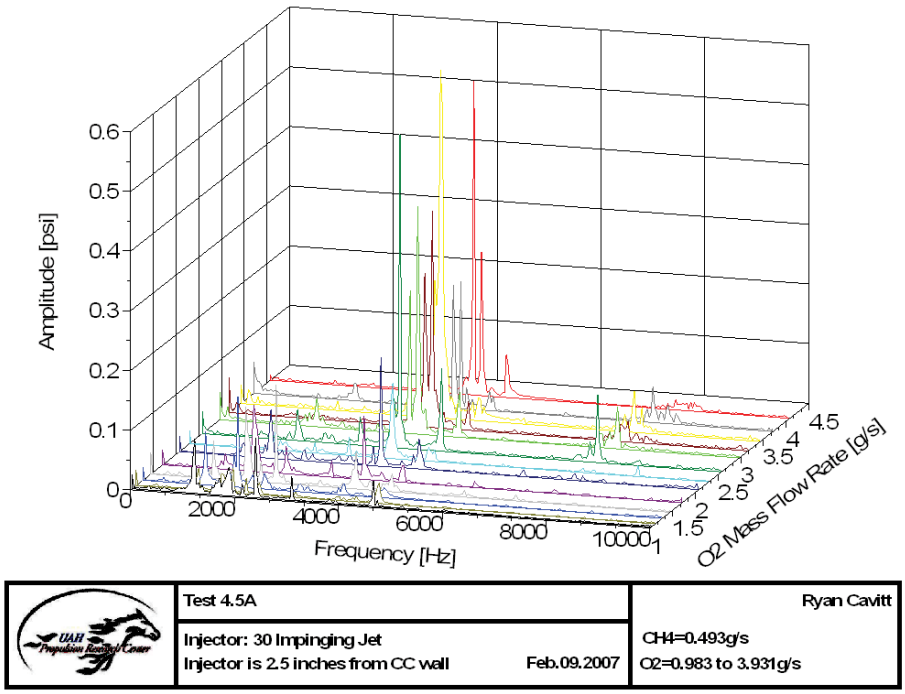

Figure H.35: 30-4-4.5 Waterfall Plot

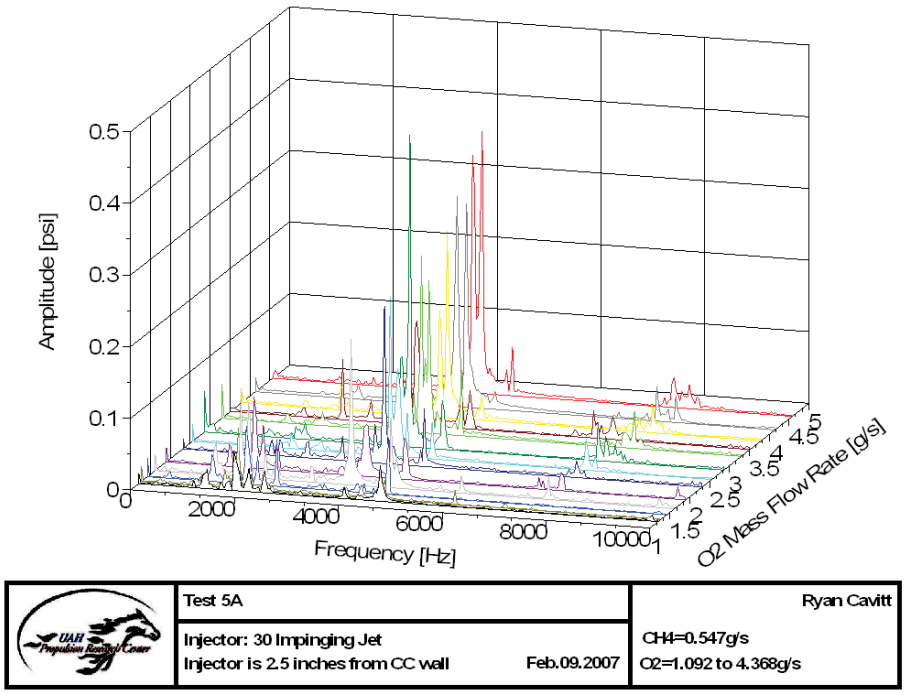

Figure H.36: 30-4-5 Waterfall Plot

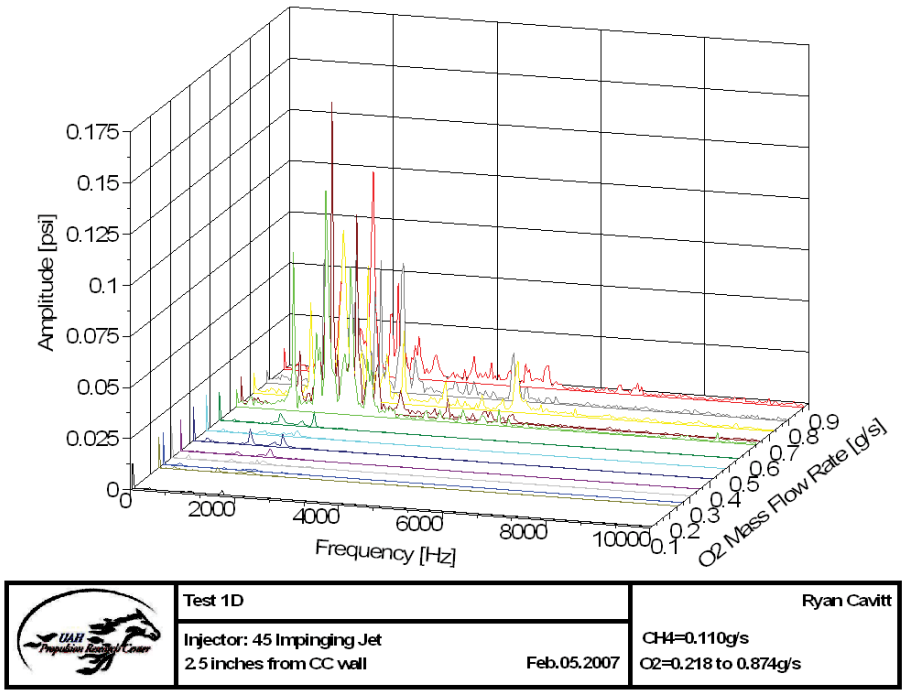

Figure H.37: 45-1-1 Waterfall Plot

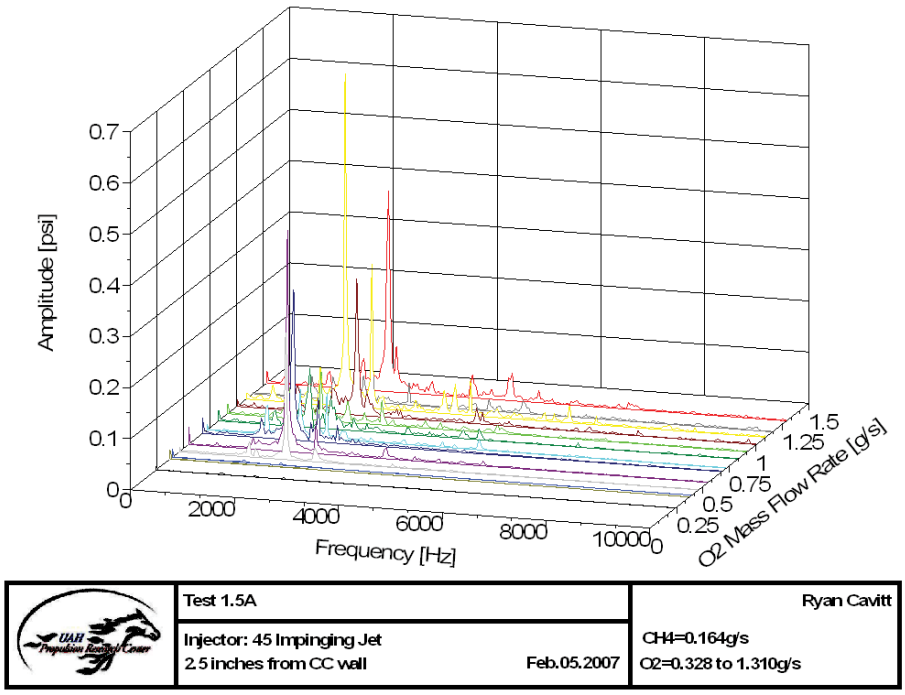

Figure H.38: 45-1-1.5 Waterfall Plot

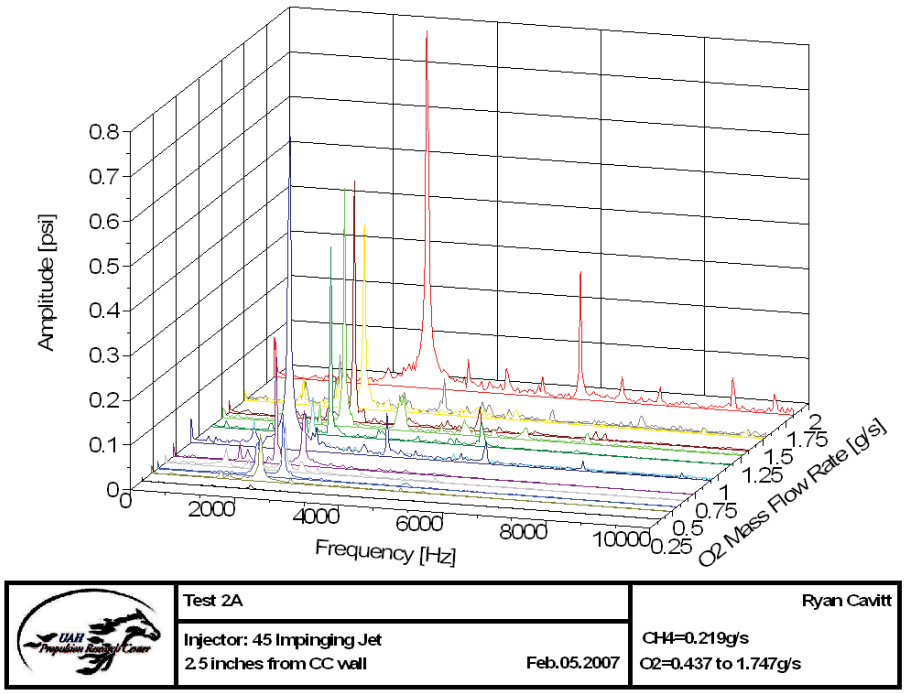

Figure H.39: 45-1-2 Waterfall Plot

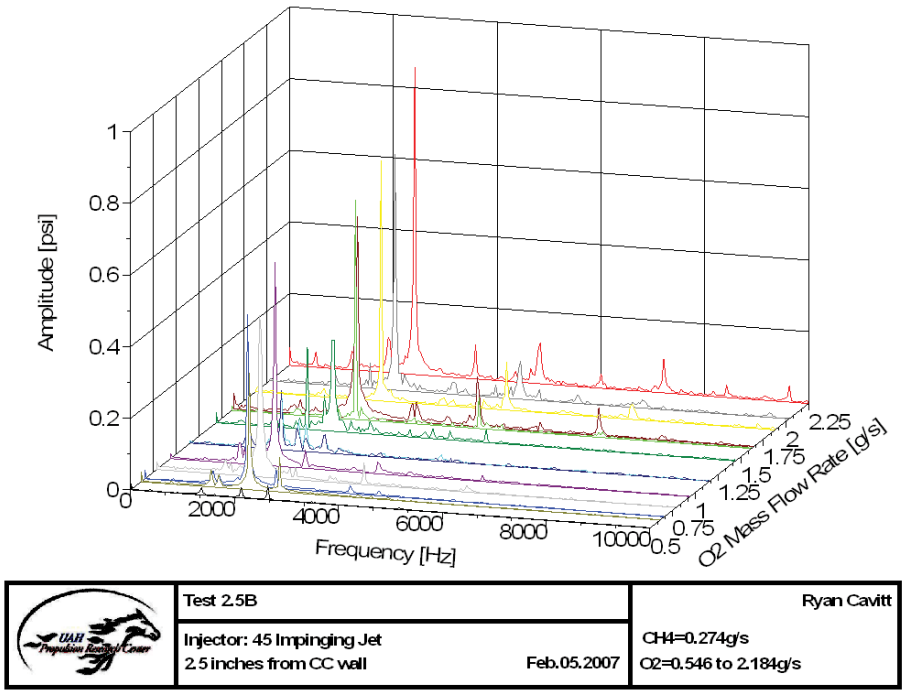

Figure H.40: 45-1-2.5 Waterfall Plot

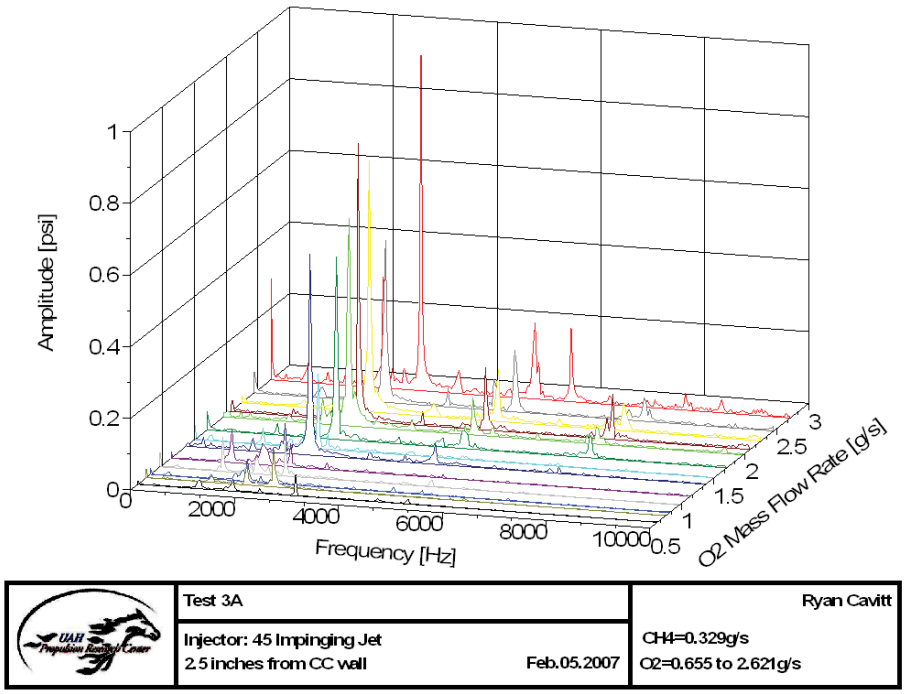

Figure H.41: 45-1-3 Waterfall Plot

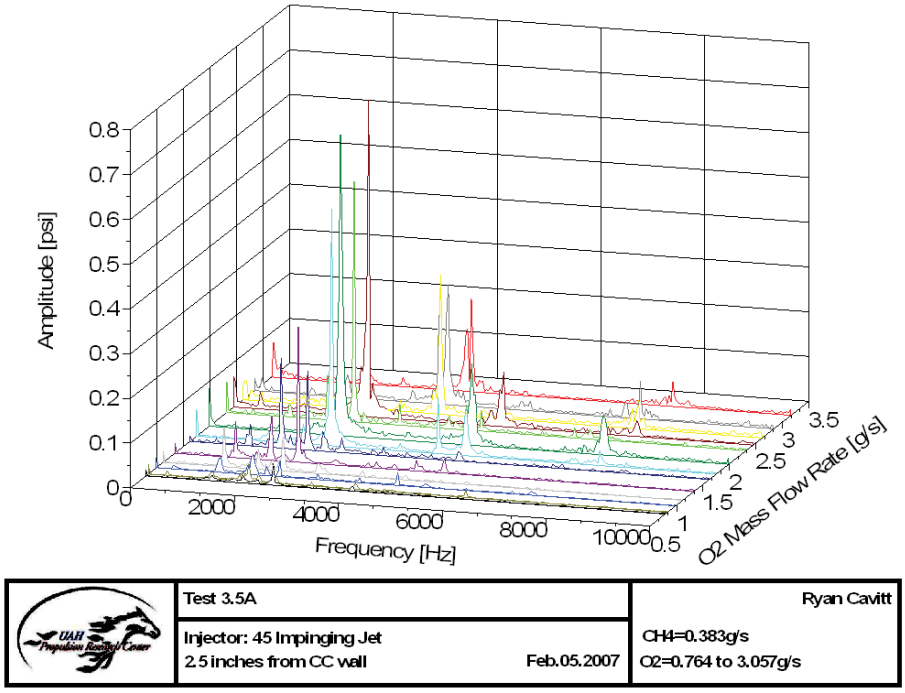

Figure H.42: 45-1-3.5 Waterfall Plot

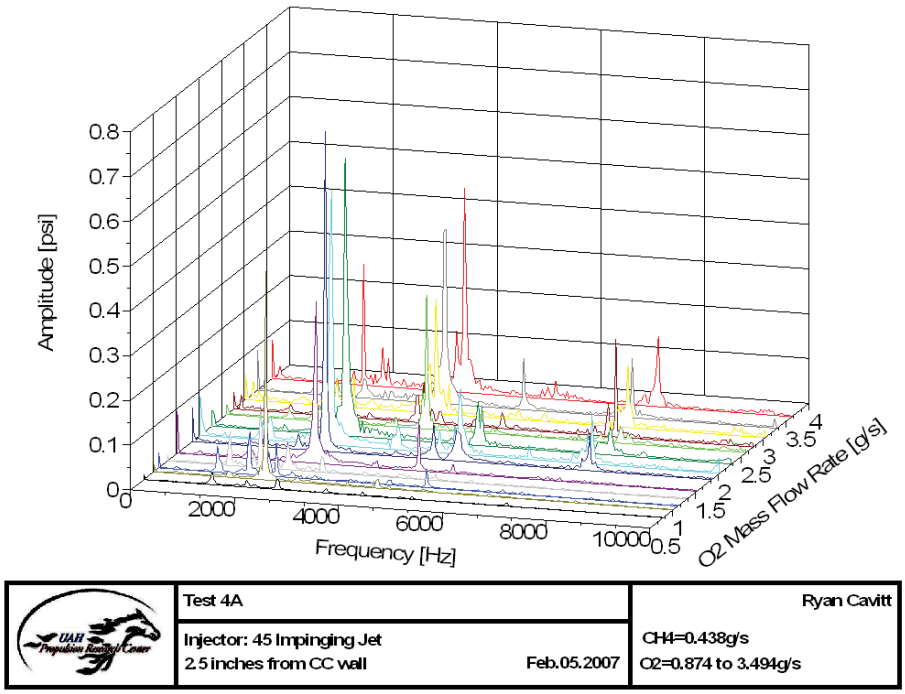

Figure H.43: 45-1-4 Waterfall Plot

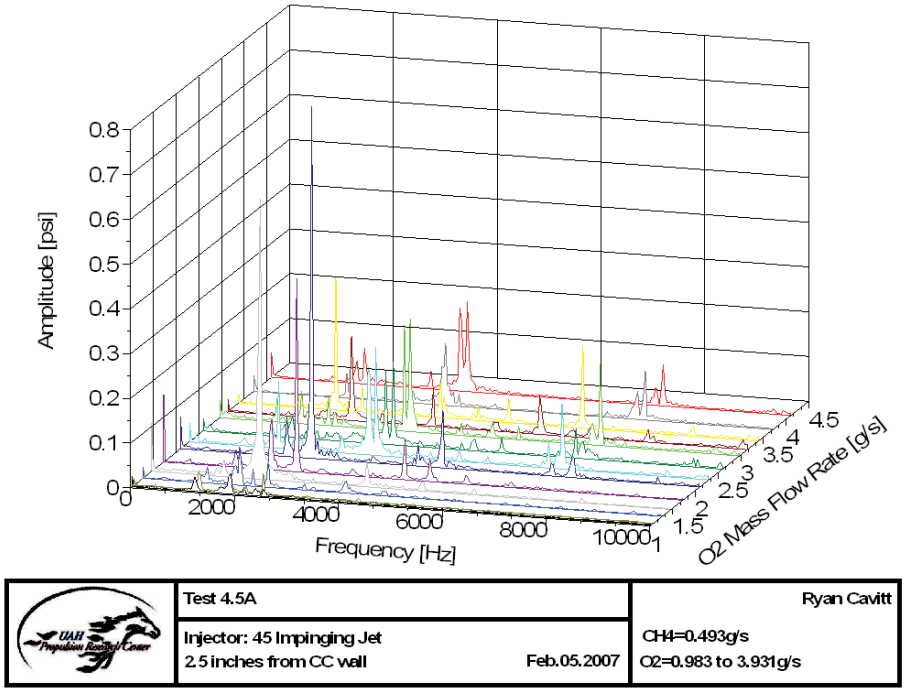

Figure H.44: 45-1-4.5 Waterfall Plot

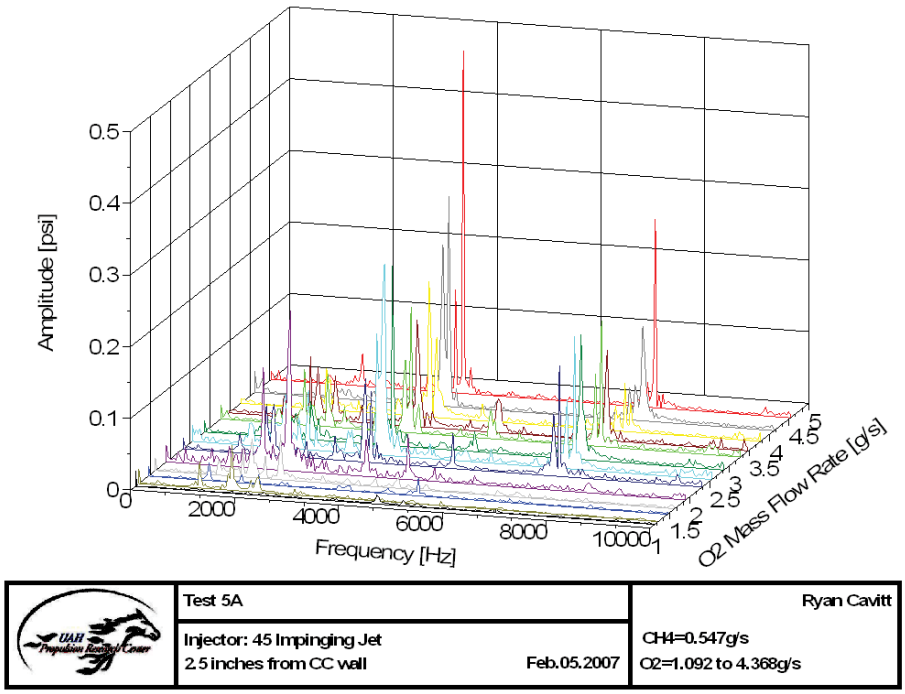

Figure H.45: 45-1-5 Waterfall Plot

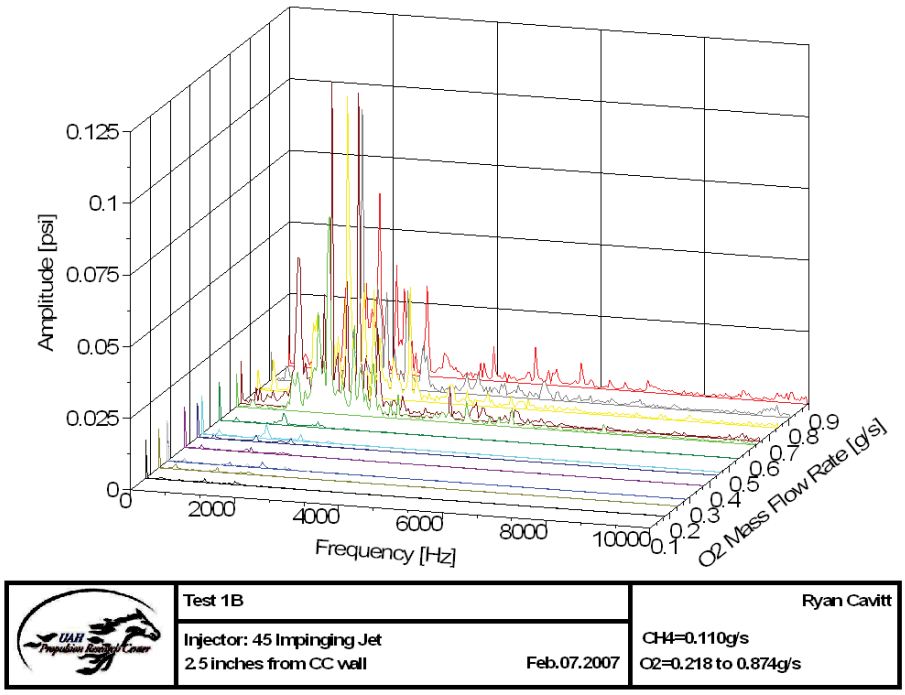

Figure H.46: 45-2-1 Waterfall Plot

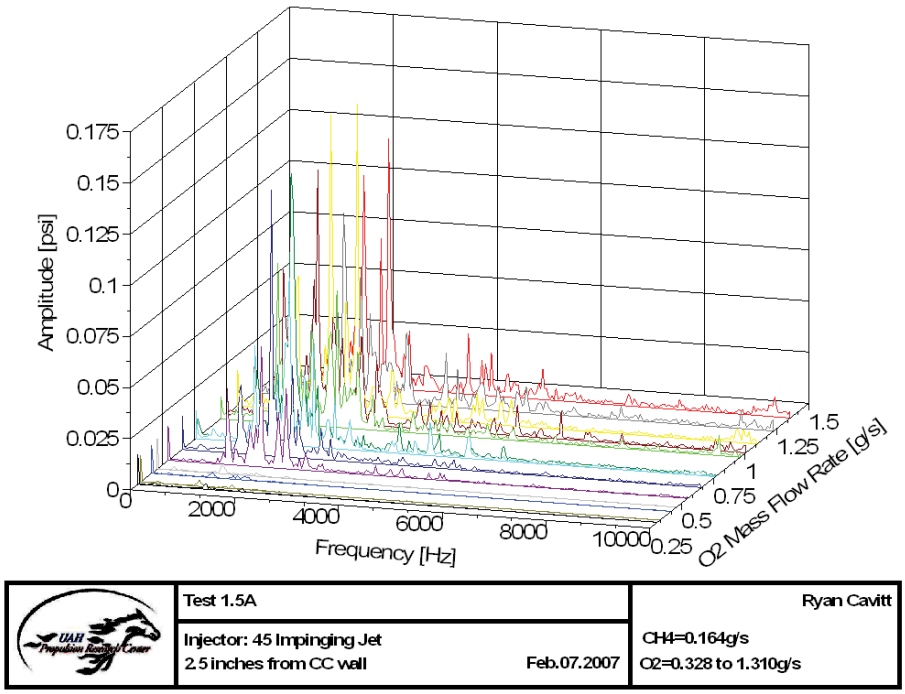

Figure H.47: 45-2-1.5 Waterfall Plot

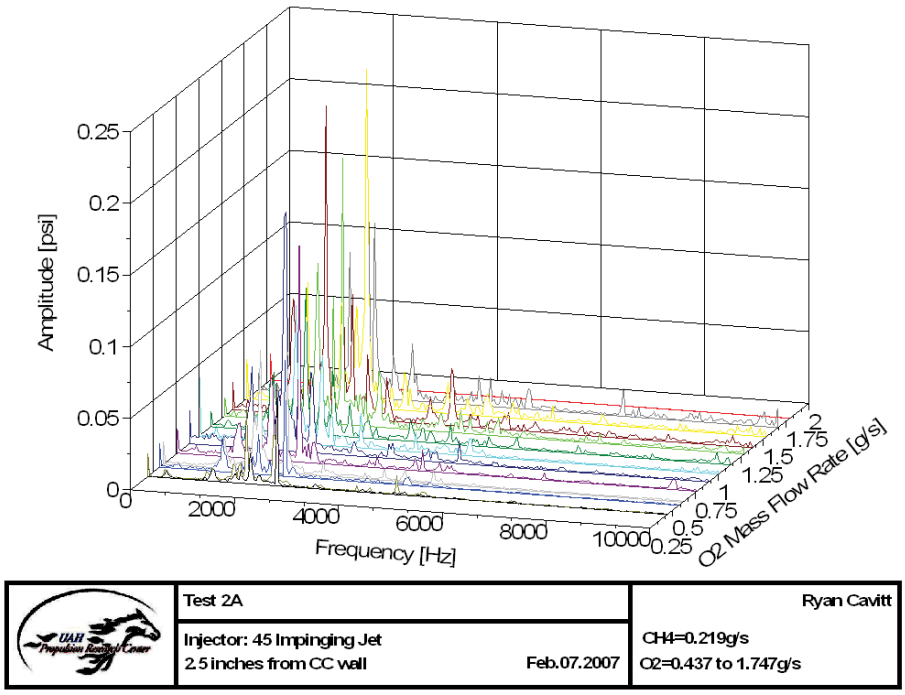

Figure H.48: 45-2-2 Waterfall Plot

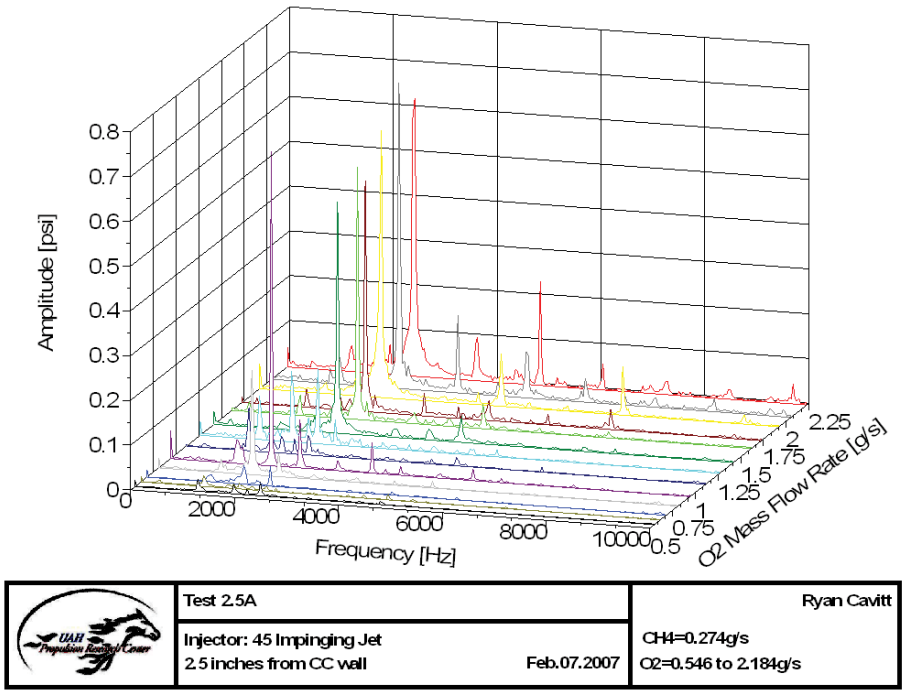

Figure H.49: 45-2-2.5 Waterfall Plot

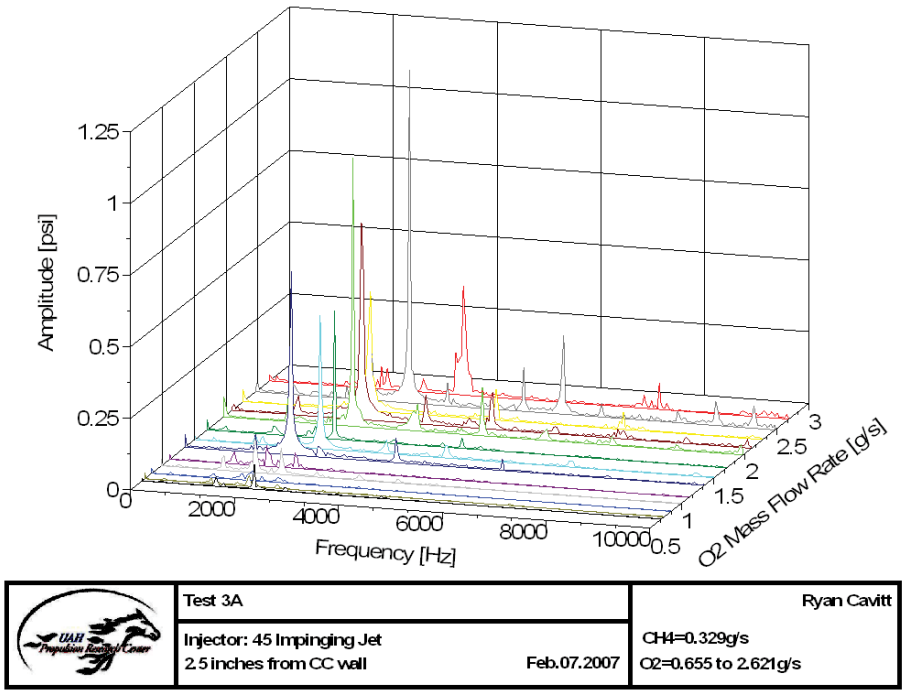

Figure H.50: 45-2-3 Waterfall Plot

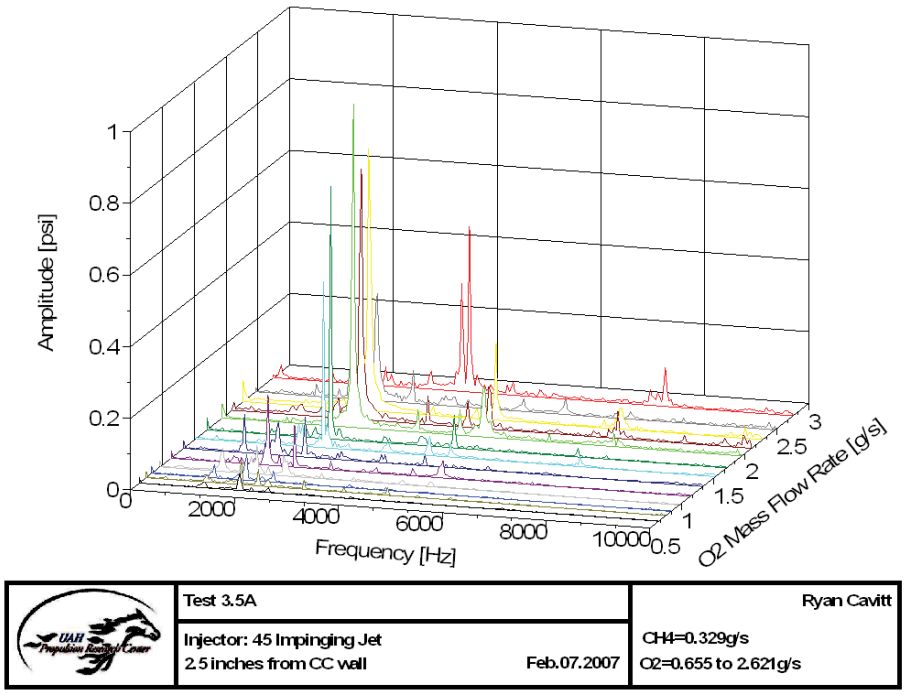

Figure H.51: 45-2-3.5 Waterfall Plot

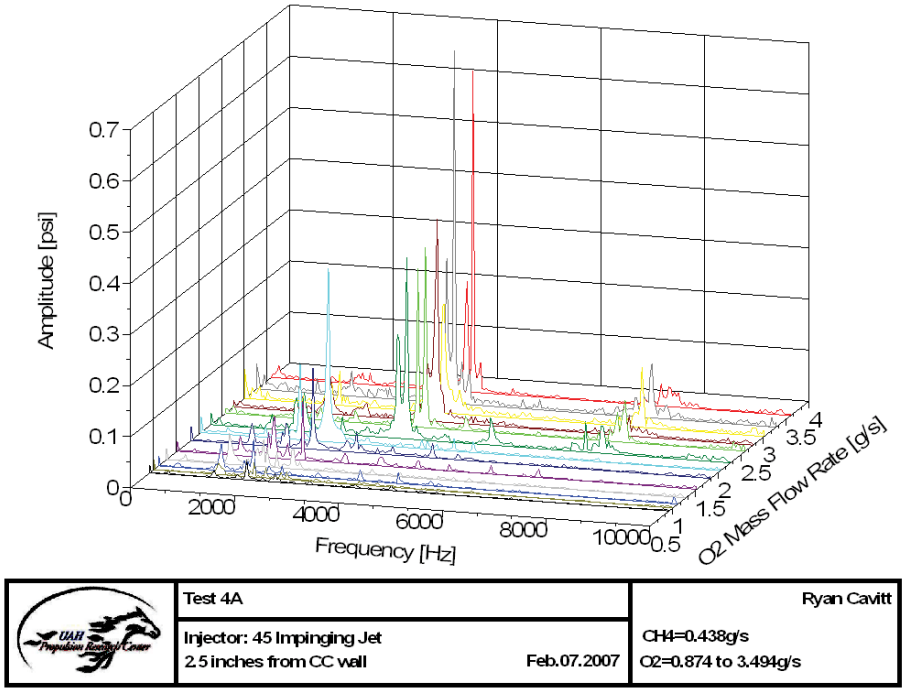

Figure H.52: 45-2-4 Waterfall Plot

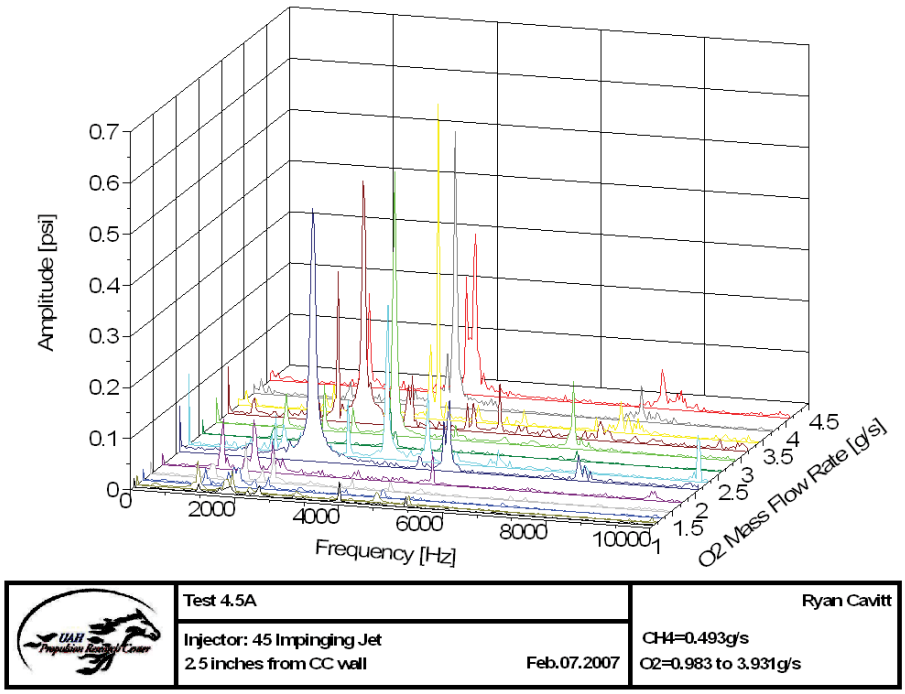

Figure H.53: 45-2-4.5 Waterfall Plot

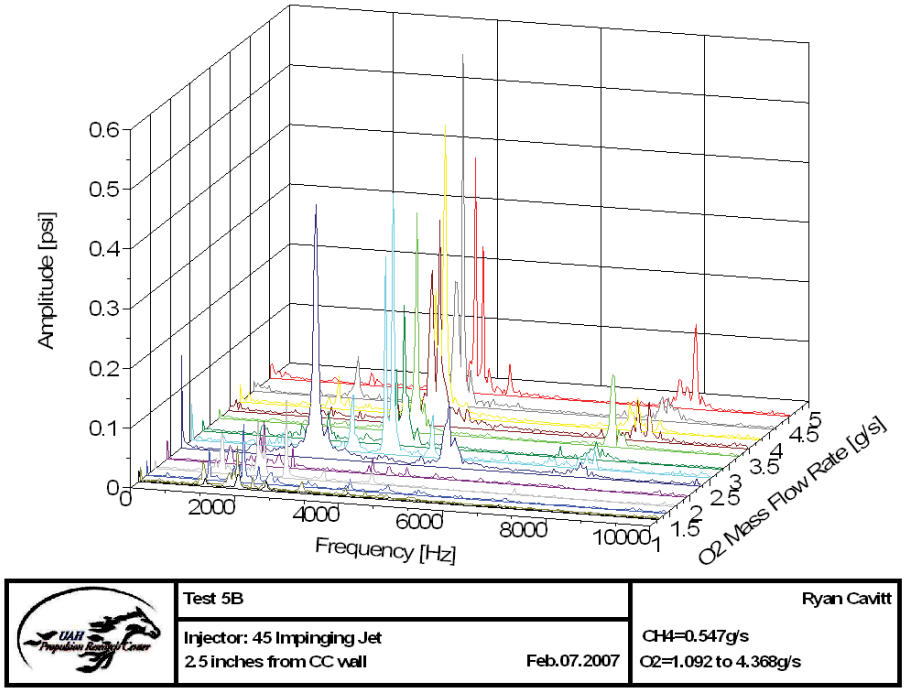

Figure H.54: 45-2-5 Waterfall Plot

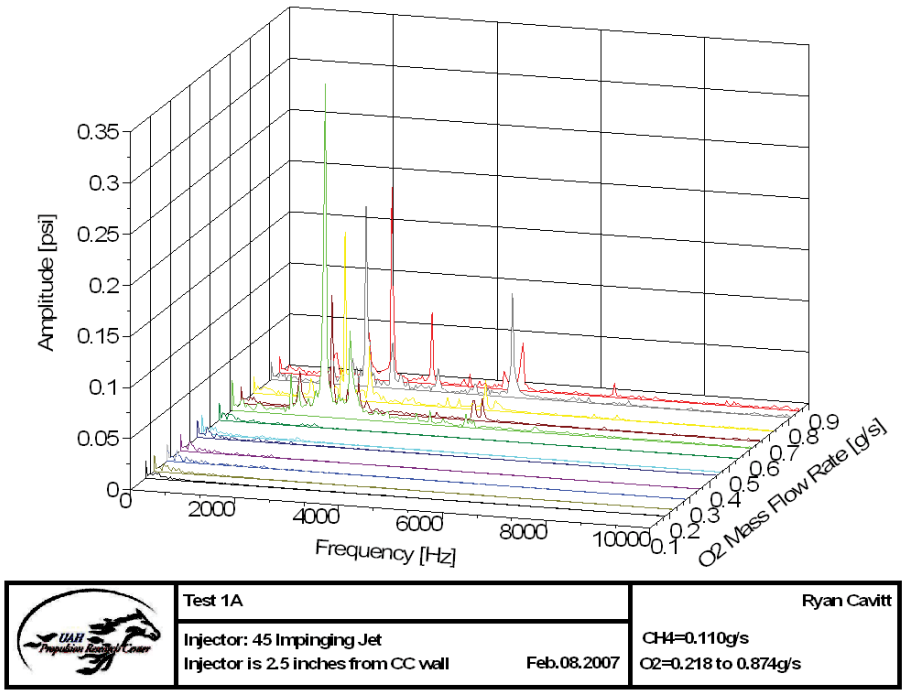

Figure H.55: 45-3-1 Waterfall Plot

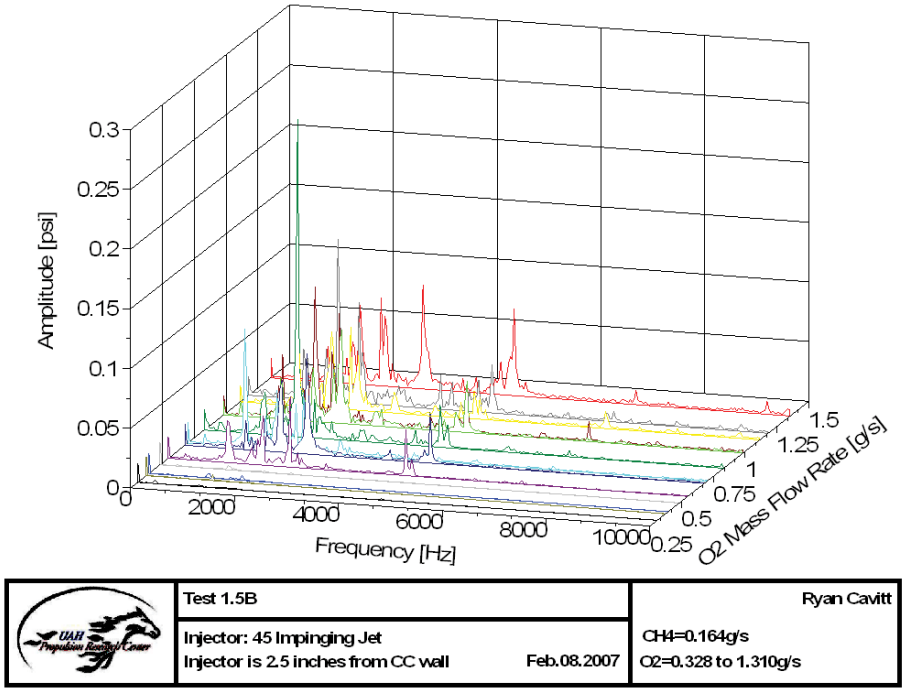

Figure H.56: 45-3-1.5 Waterfall Plot

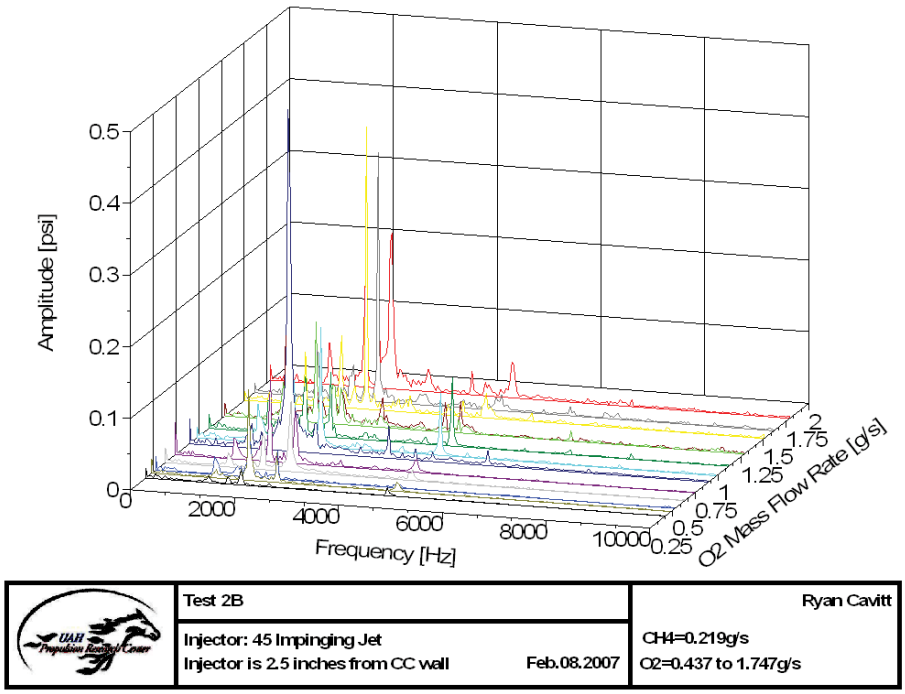

Figure H.57: 45-3-2 Waterfall Plot

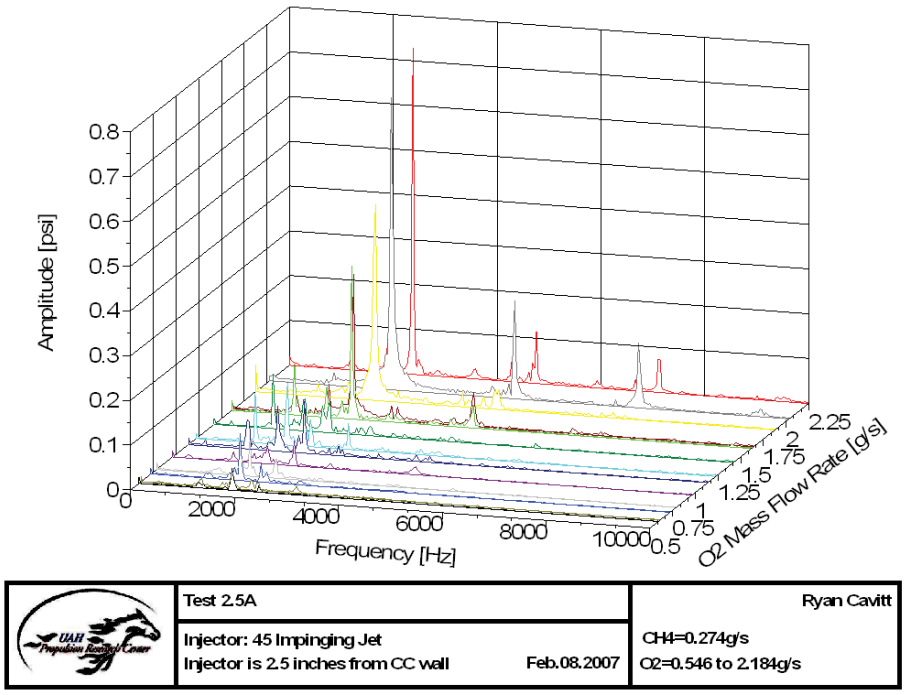

Figure H.58: 45-3-2.5 Waterfall Plot

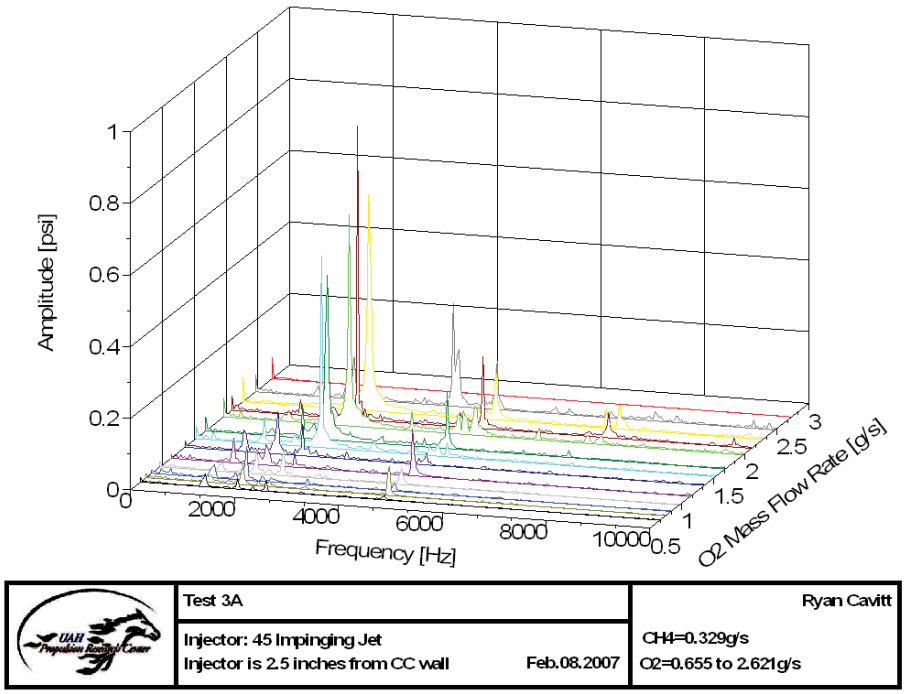

Figure H.59: 45-3-3 Waterfall Plot

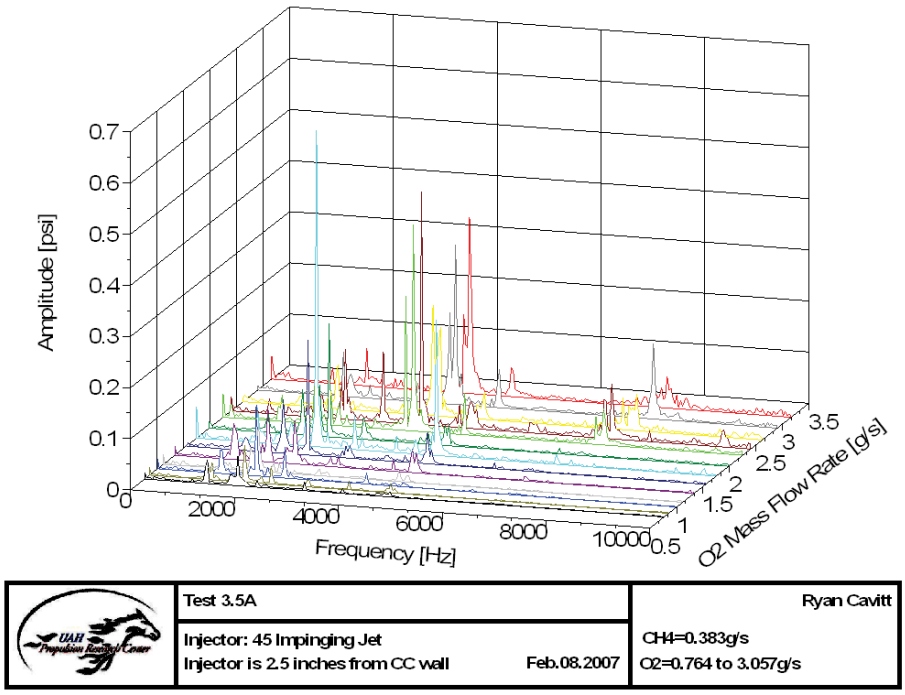

Figure H.60: 45-3-3.5 Waterfall Plot

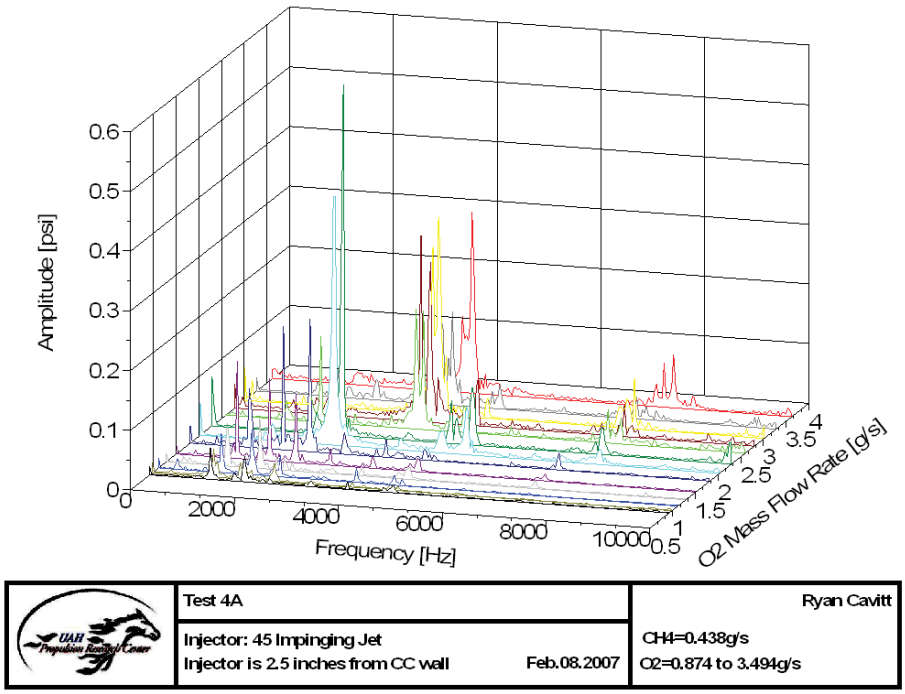

Figure H.61: 45-3-4 Waterfall Plot

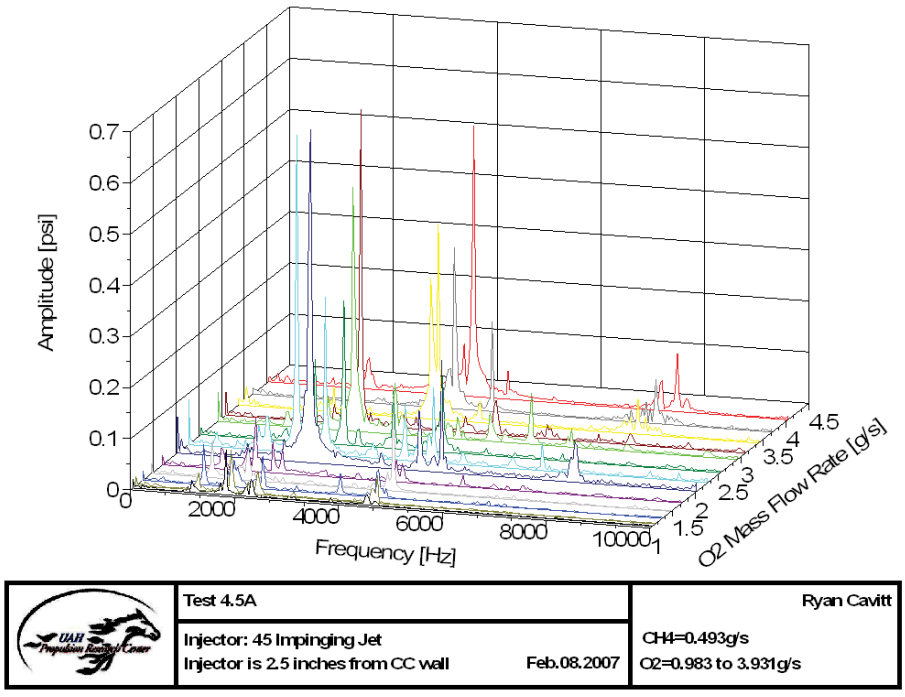

Figure H.62: 45-3-4.5 Waterfall Plot

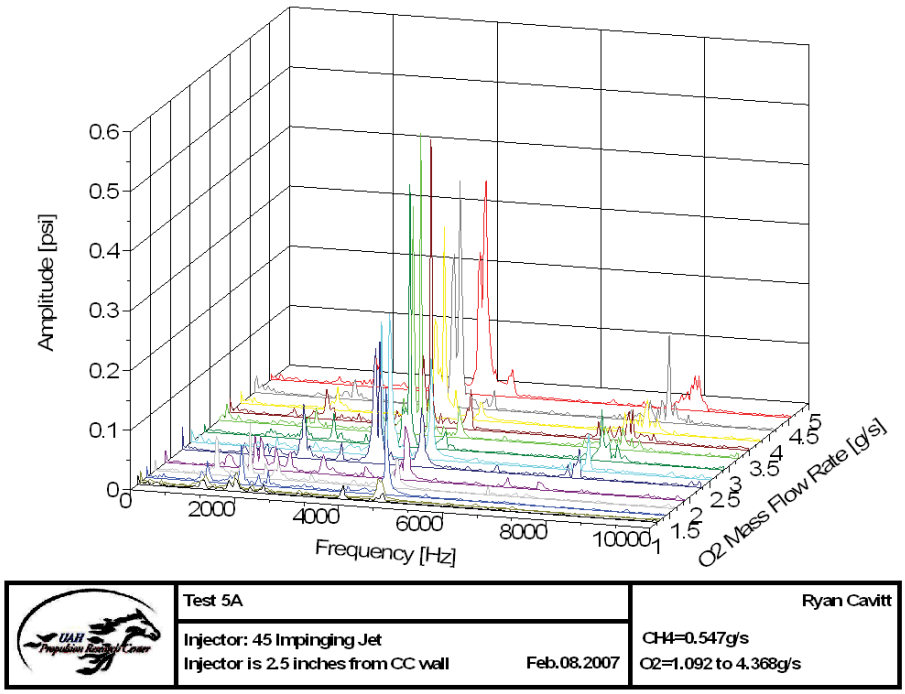

Figure H.63: 45-3-5 Waterfall Plot

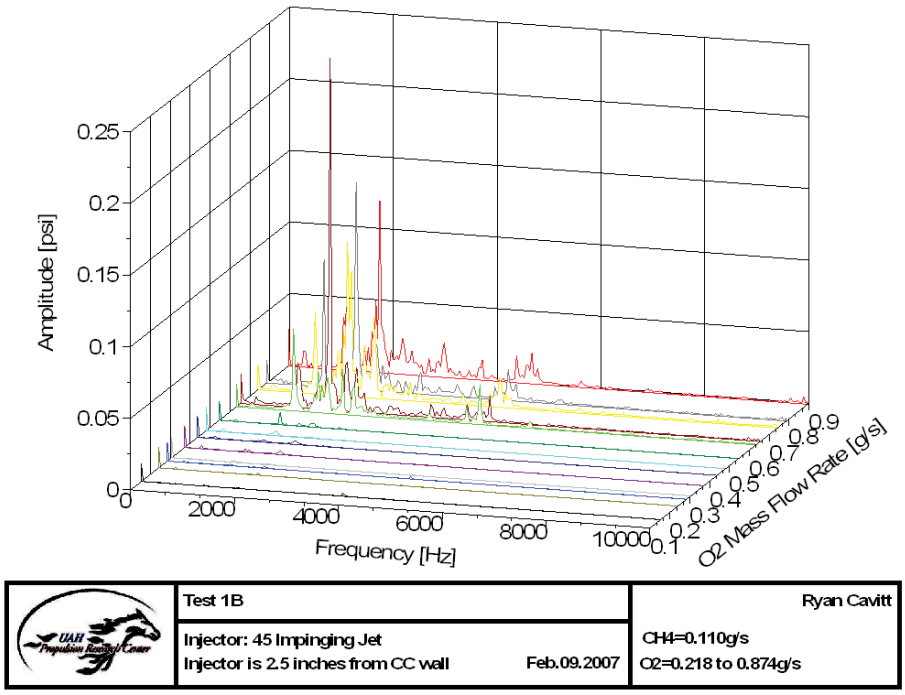

Figure H.64: 45-4-1 Waterfall Plot

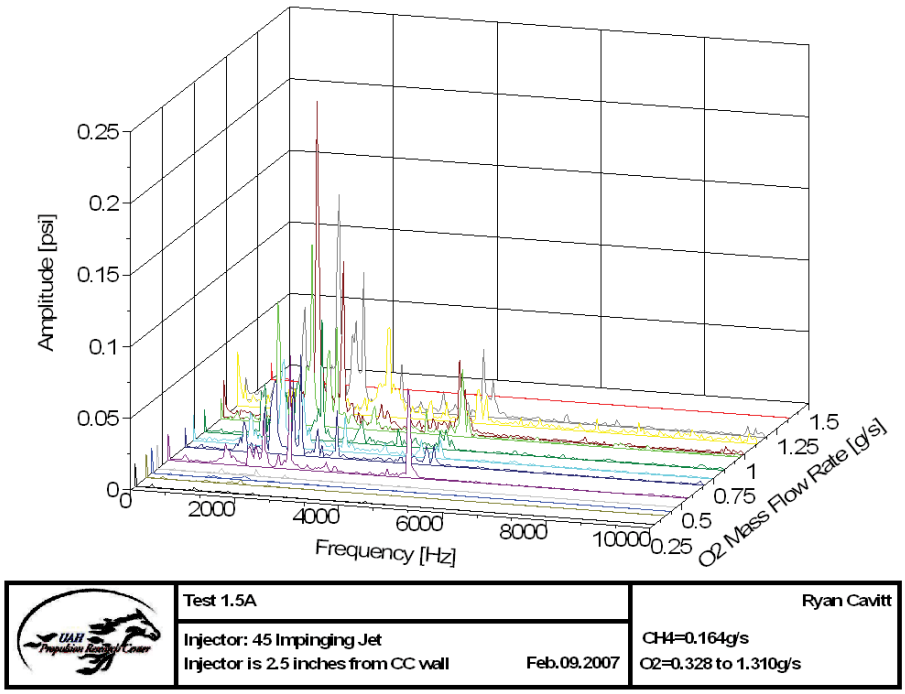

Figure H.65: 45-4-1.5 Waterfall Plot

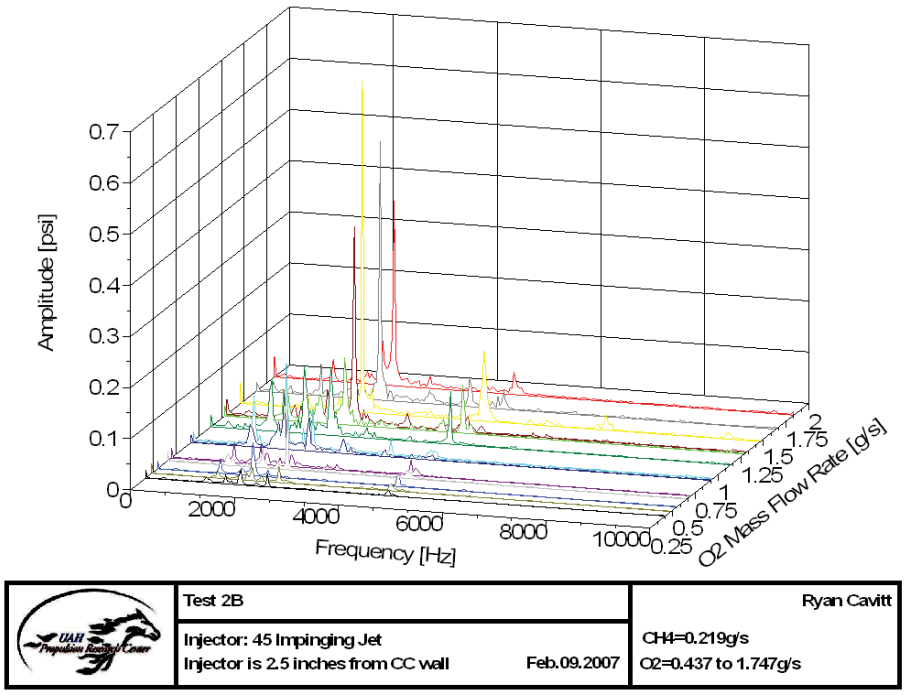

Figure H.66: 45-4-2 Waterfall Plot

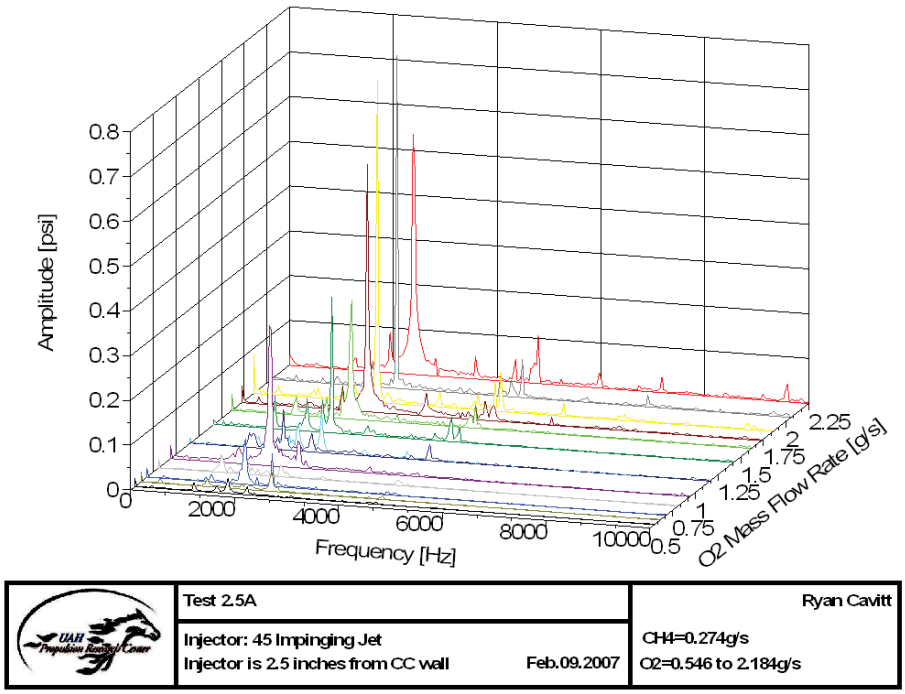

Figure H.67: 45-4-2.5 Waterfall Plot

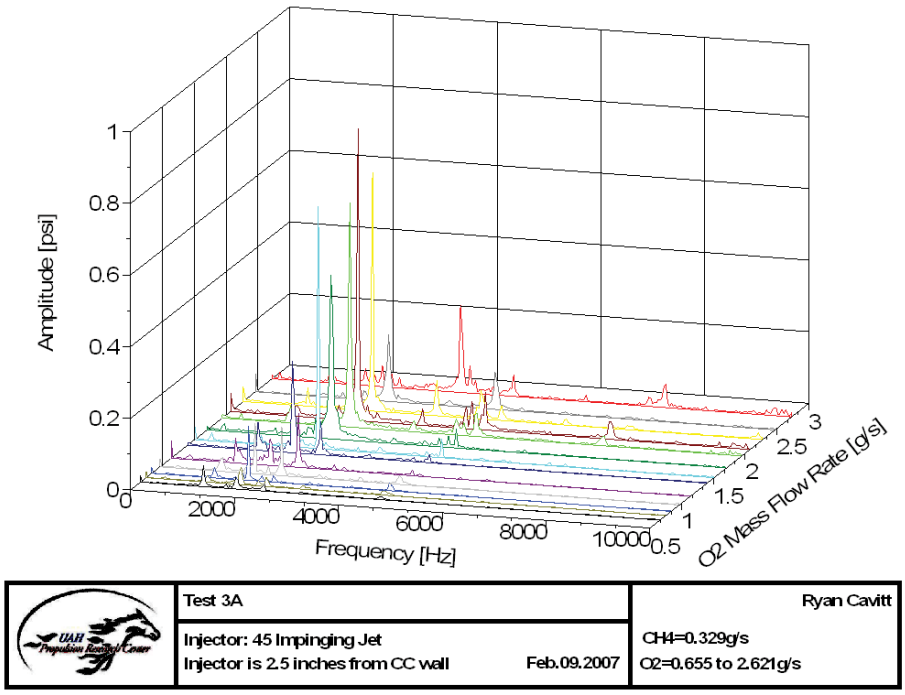

Figure H.68: 45-4-3 Waterfall Plot

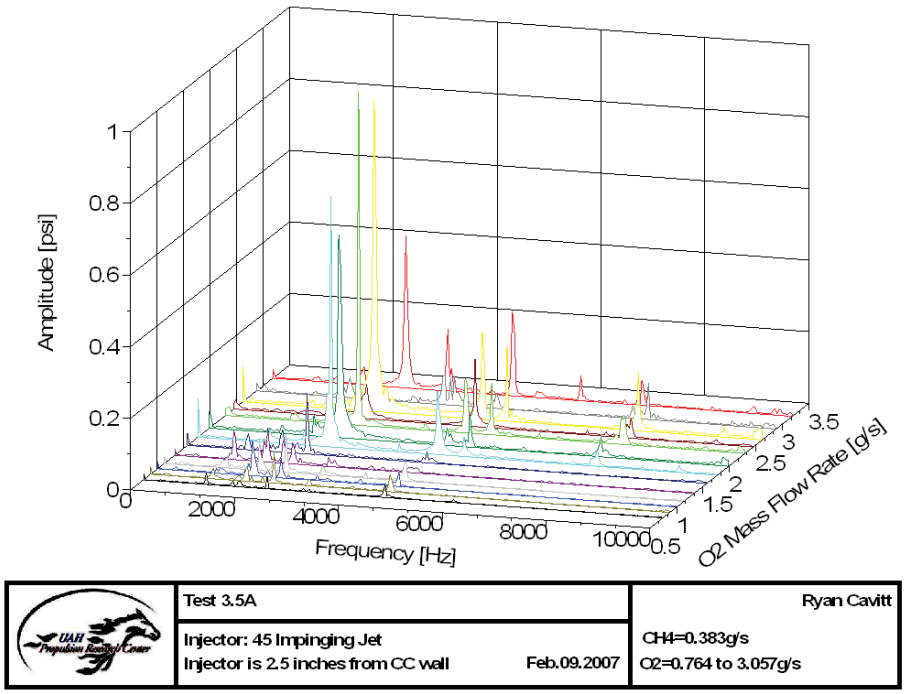

Figure H.69: 45-4-3.5 Waterfall Plot

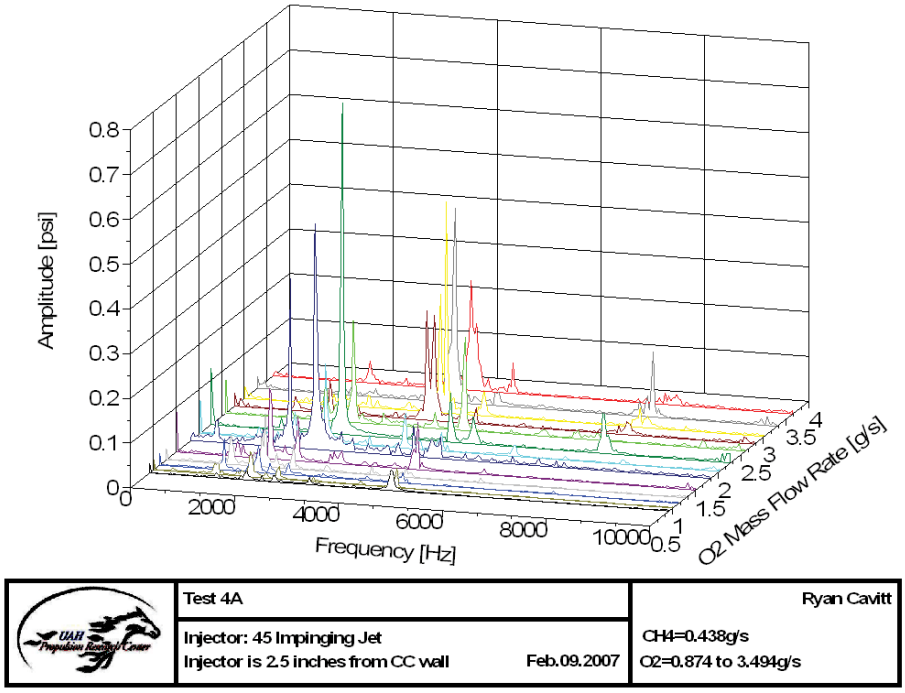

Figure H.70: 45-4-4 Waterfall Plot

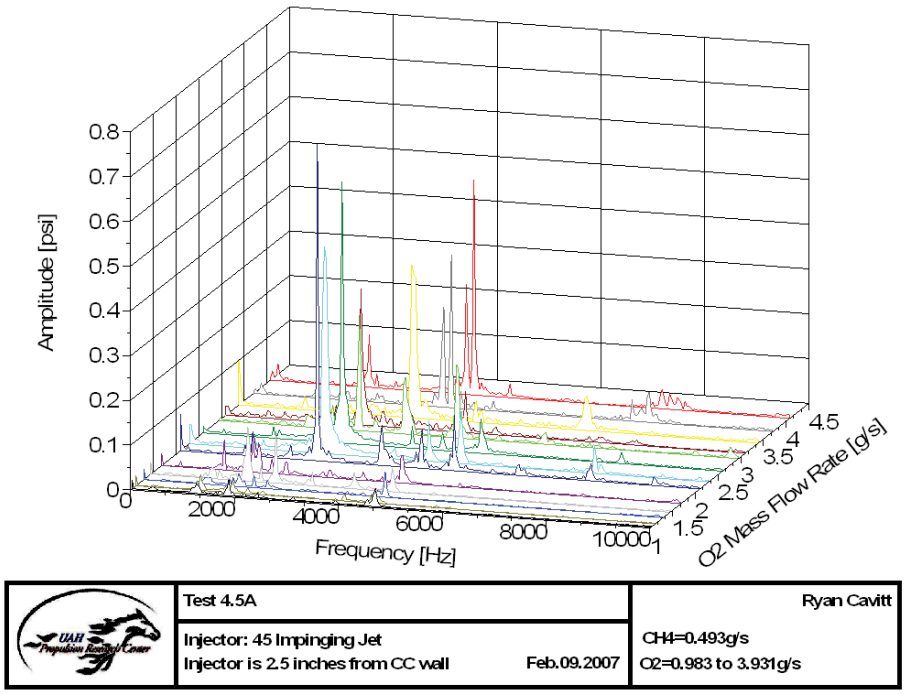

Figure H.71: 45-4-4.5 Waterfall Plot

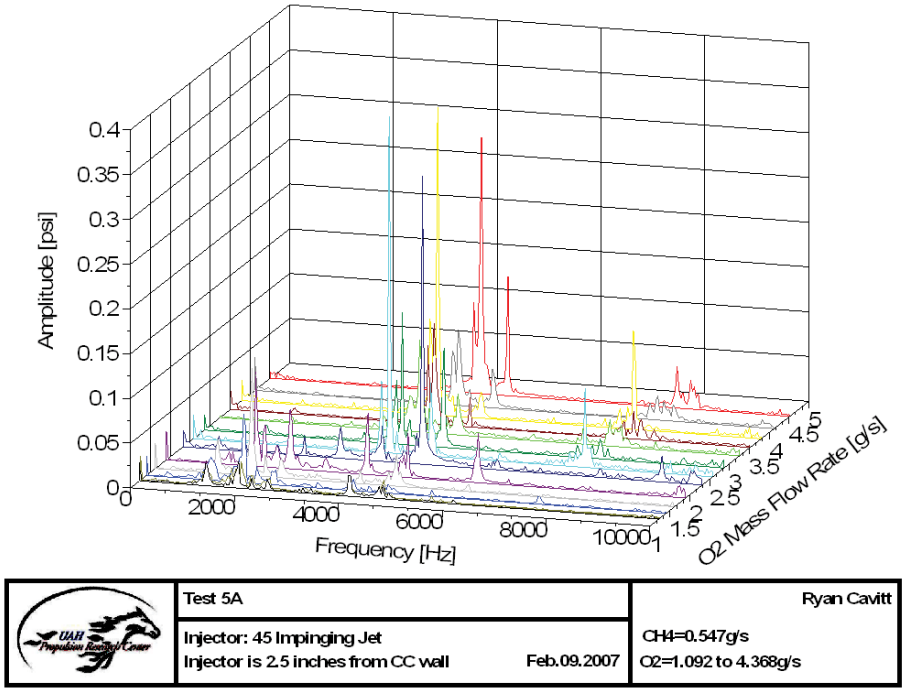

Figure H.72: 45-4-5 Waterfall Plot

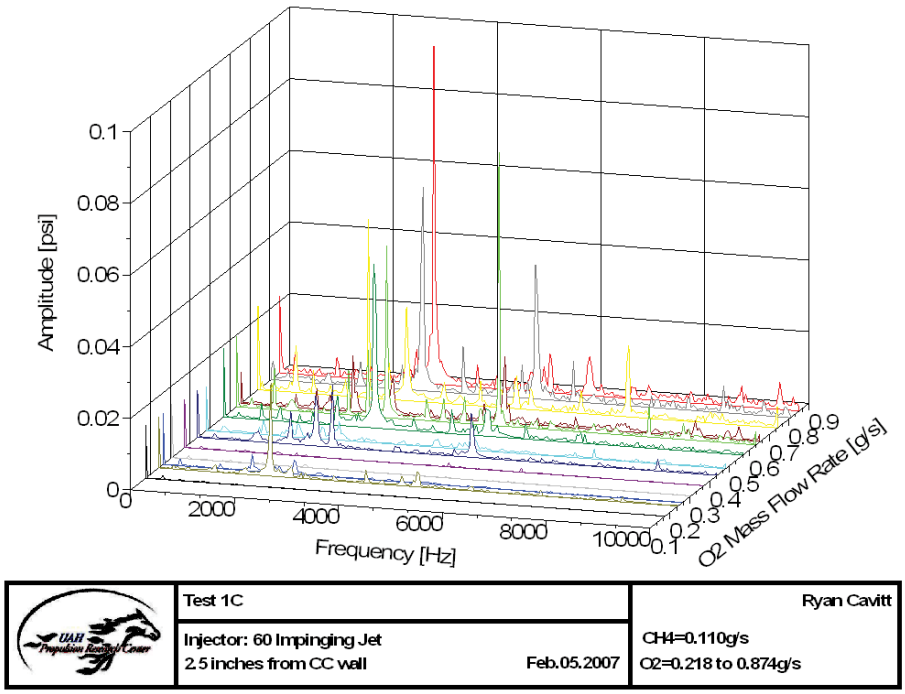

Figure H.73: 60-1-1 Waterfall Plot

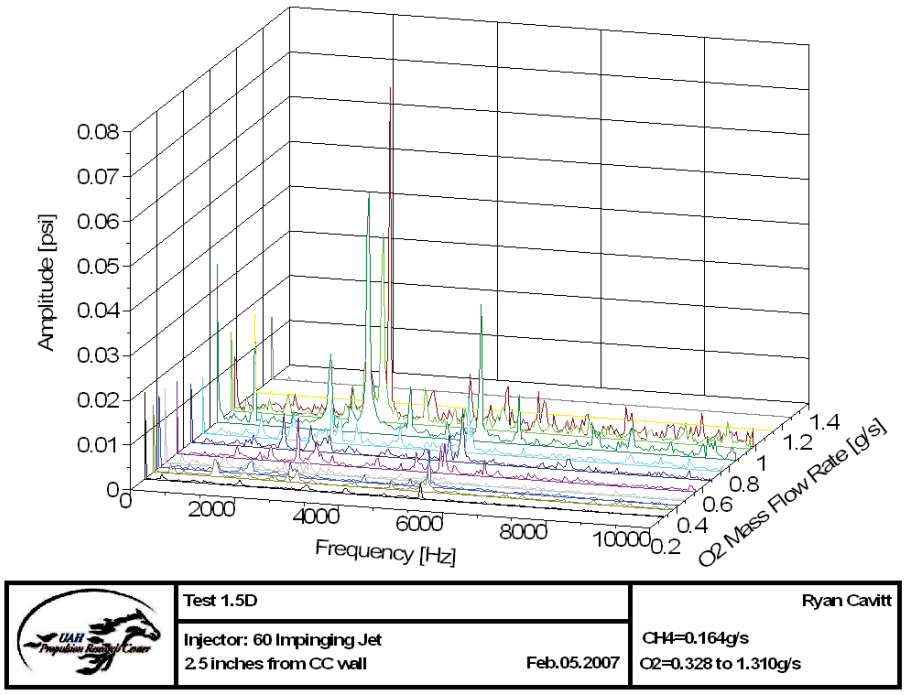

Figure H.74: 60-1-1.5 Waterfall Plot

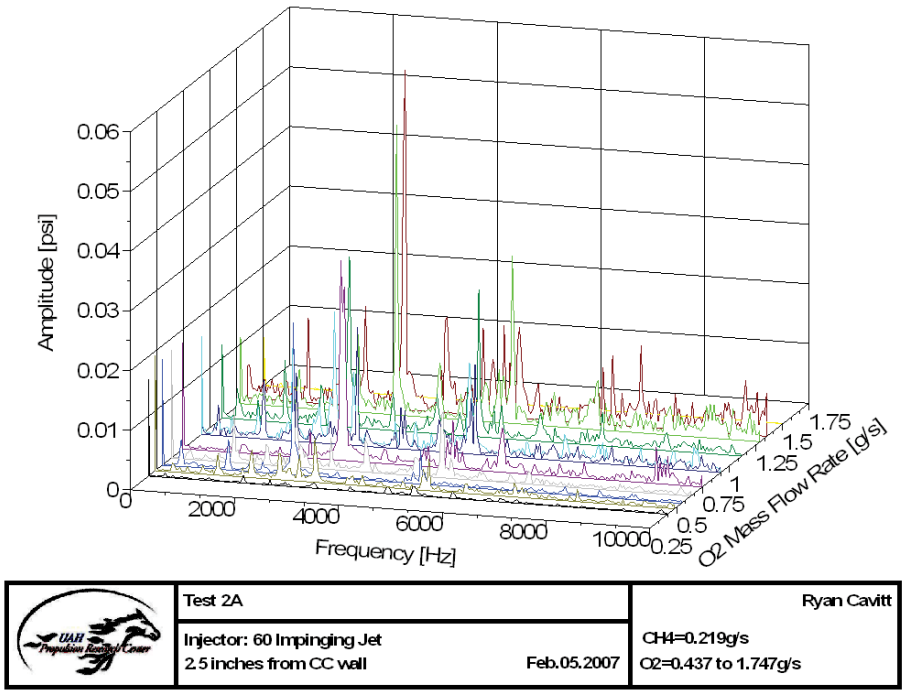

Figure H.75: 60-1-2 Waterfall Plot

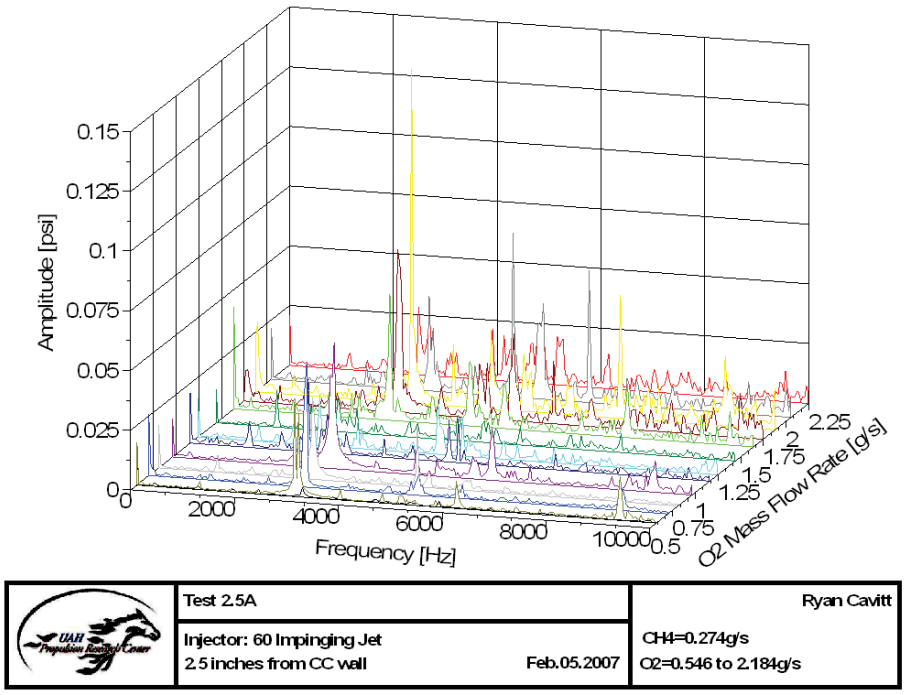

Figure H.76: 60-1-2.5 Waterfall Plot

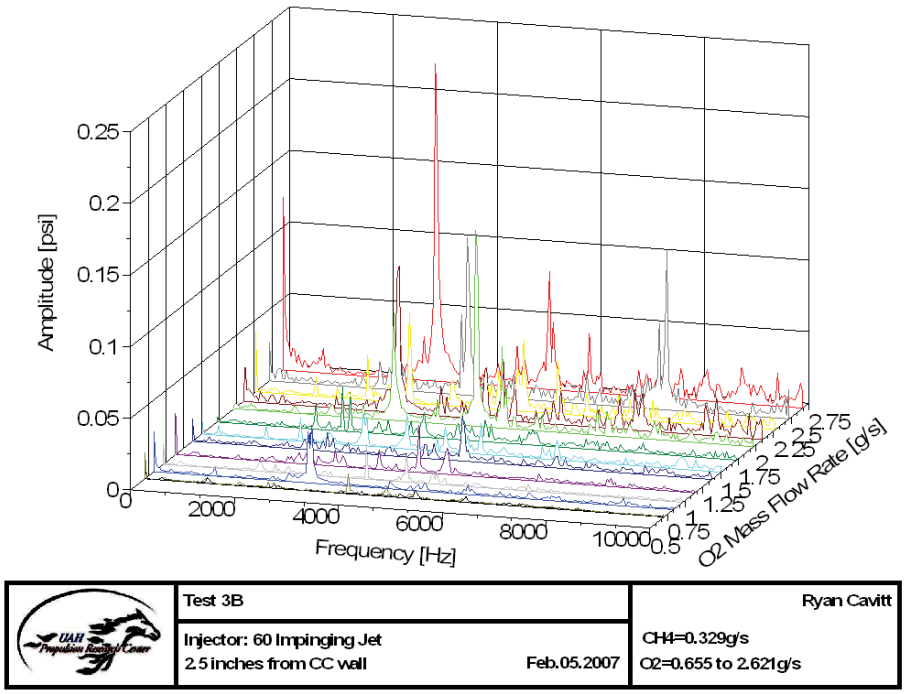

Figure H.77: 60-1-3 Waterfall Plot

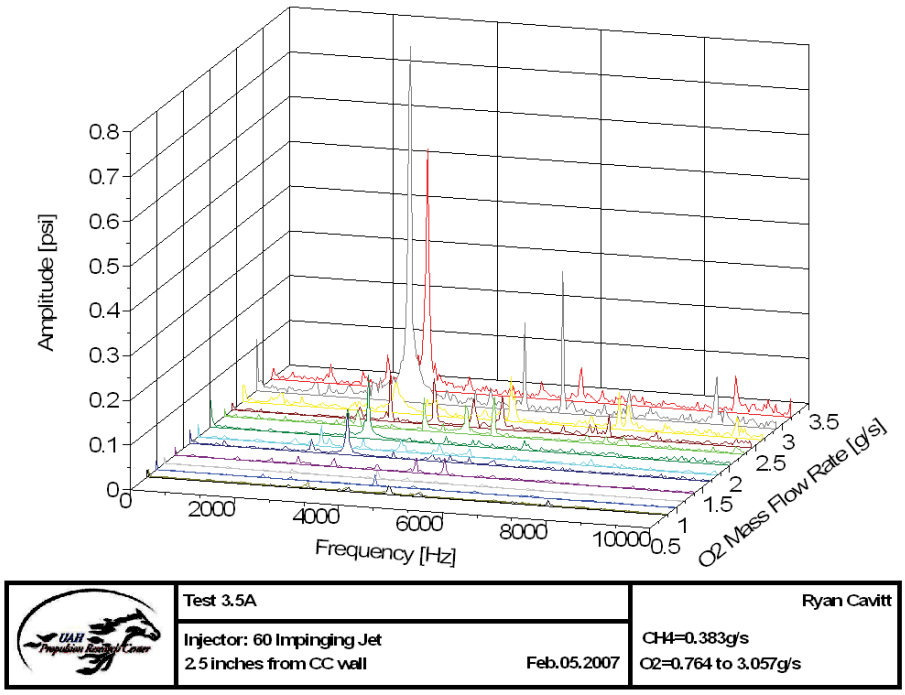

Figure H.78: 60-1-3.5 Waterfall Plot

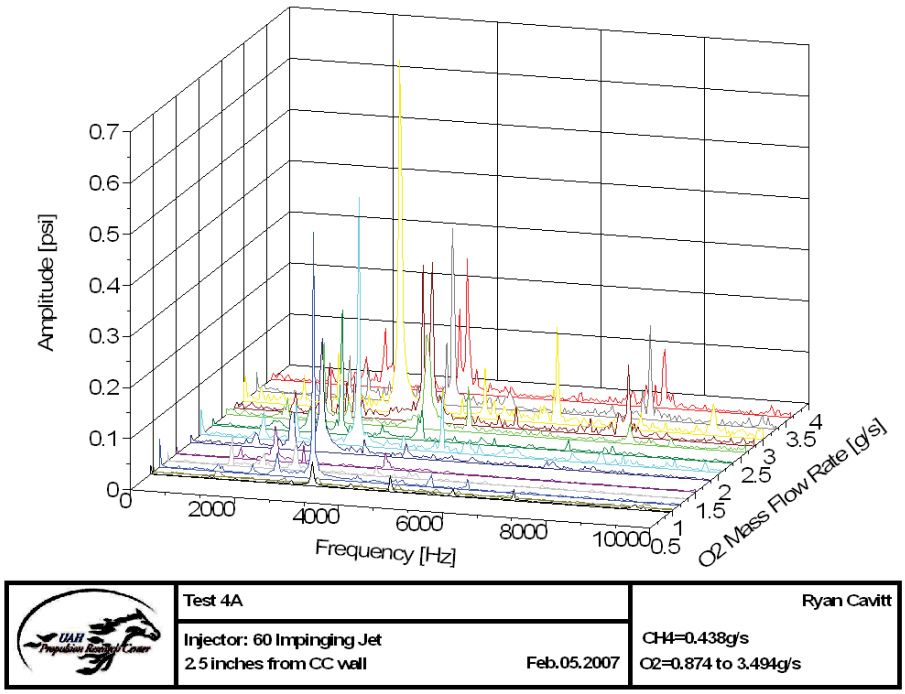

Figure H.79: 60-1-4 Waterfall Plot

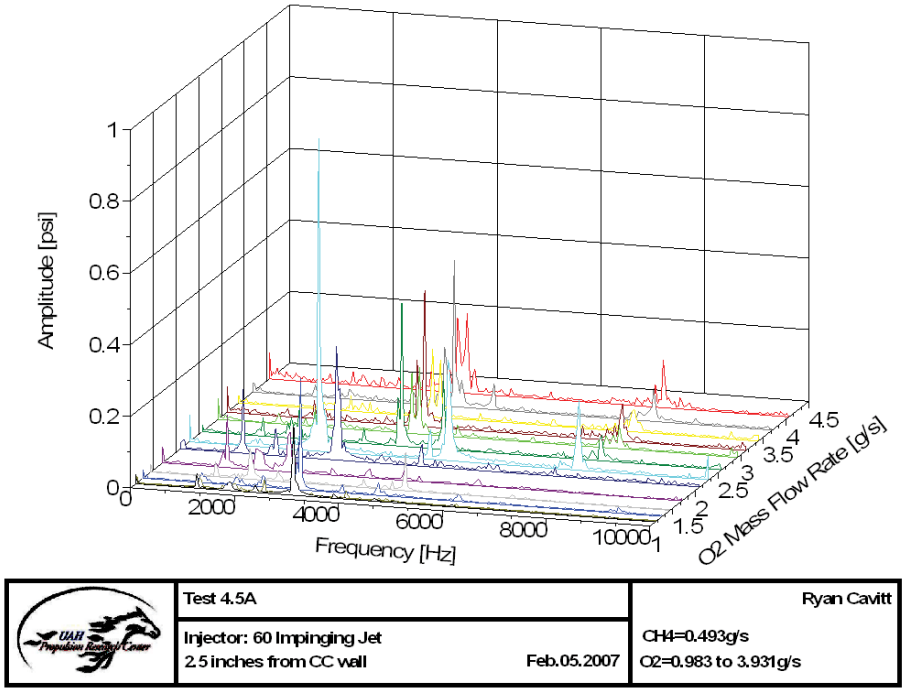

Figure H.80: 60-1-4.5 Waterfall Plot

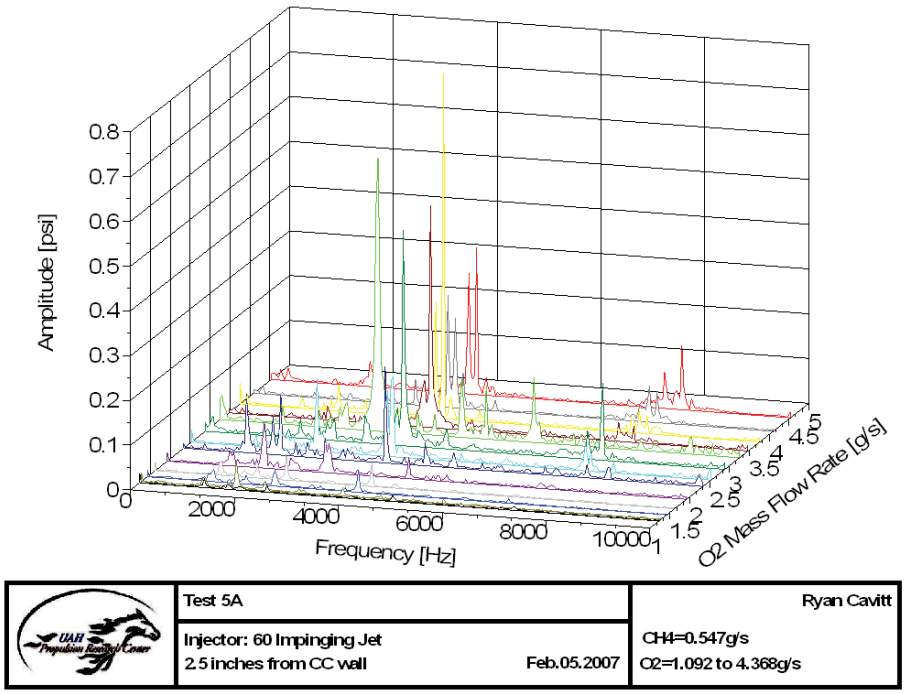

Figure H.81: 60-1-5 Waterfall Plot

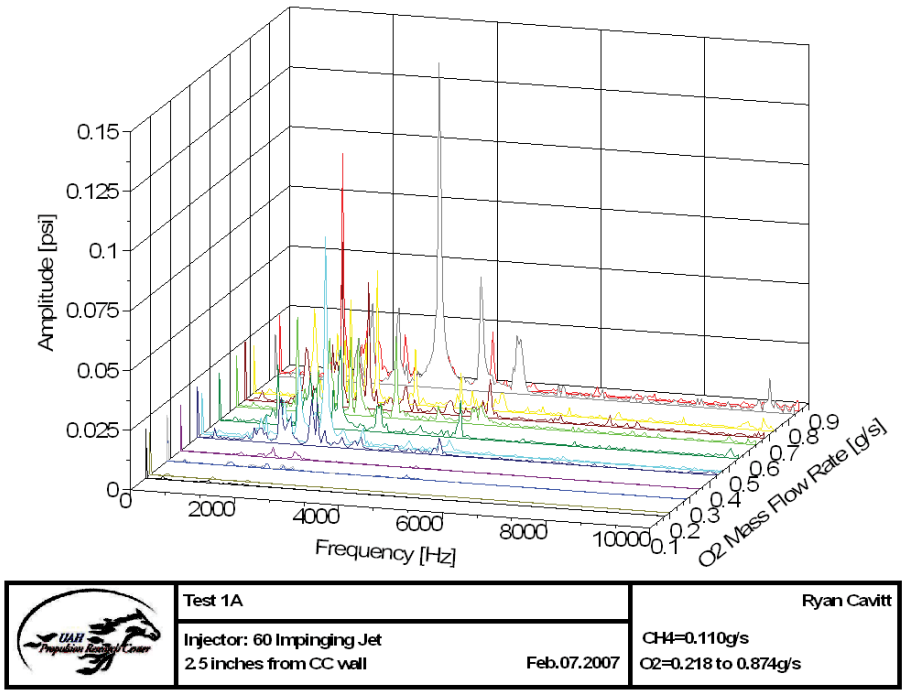

Figure H.82: 60-2-1 Waterfall Plot

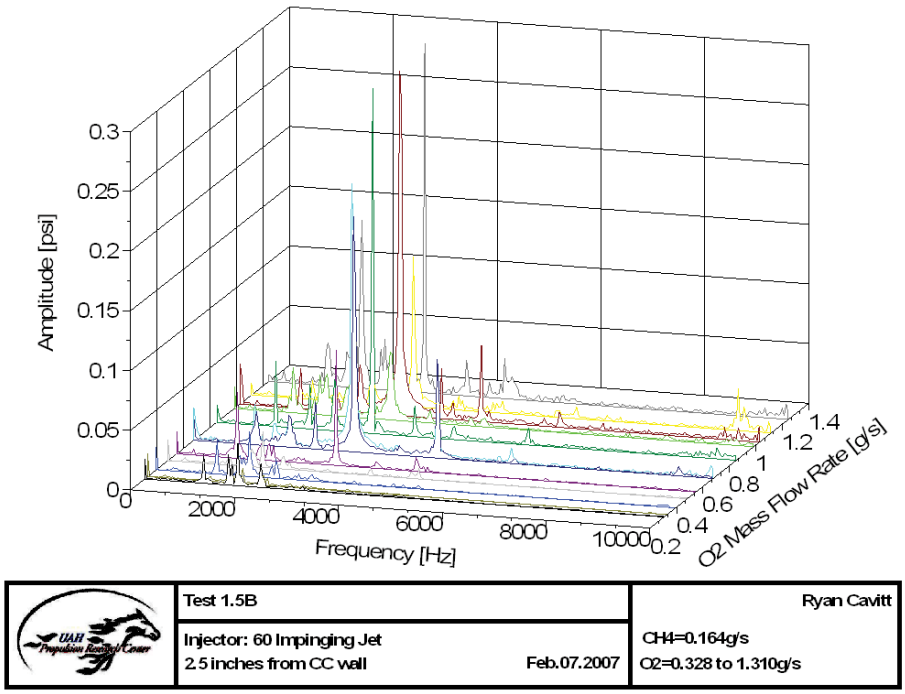

Figure H.83: 60-2-1.5 Waterfall Plot

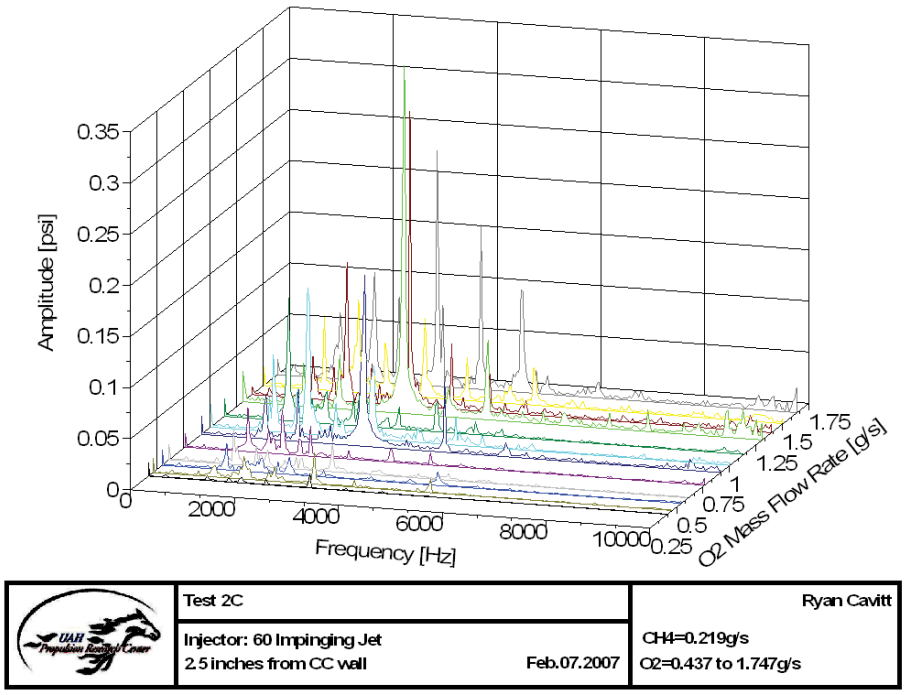

Figure H.84: 60-2-2 Waterfall Plot

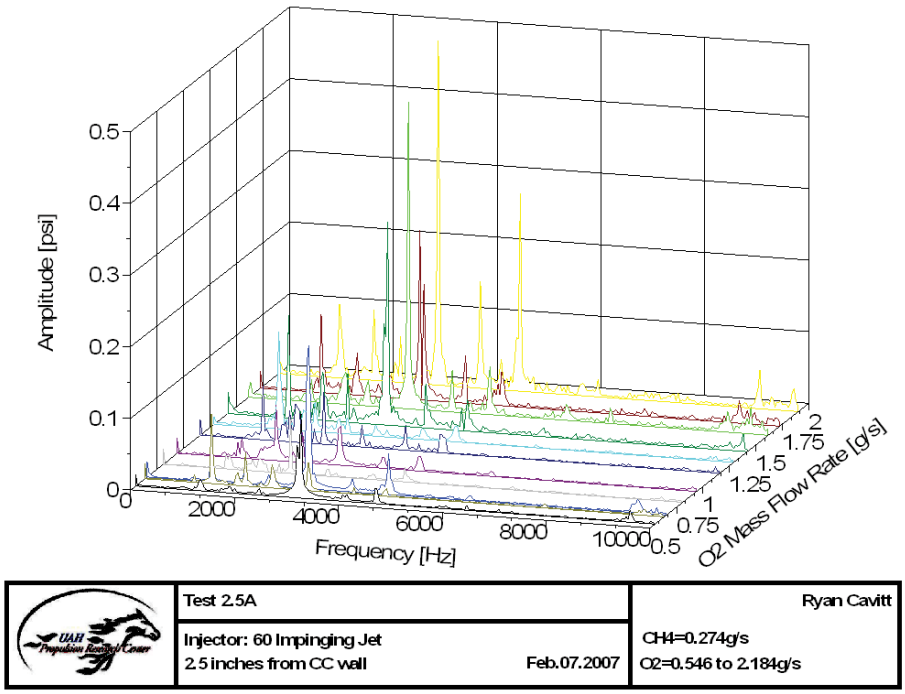

Figure H.85: 60-2-2.5 Waterfall Plot

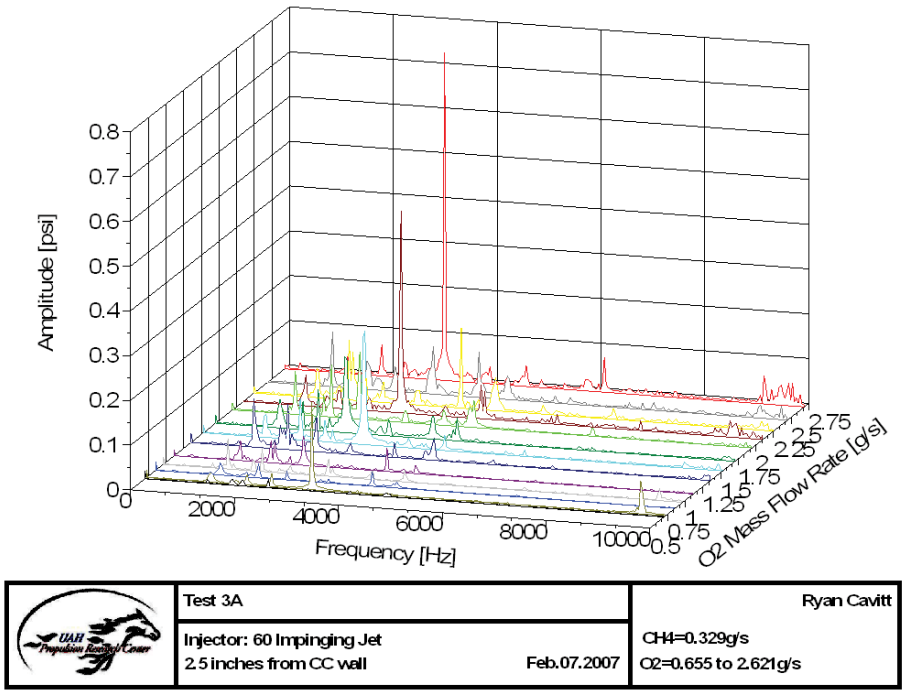

Figure H.86: 60-2-3 Waterfall Plot

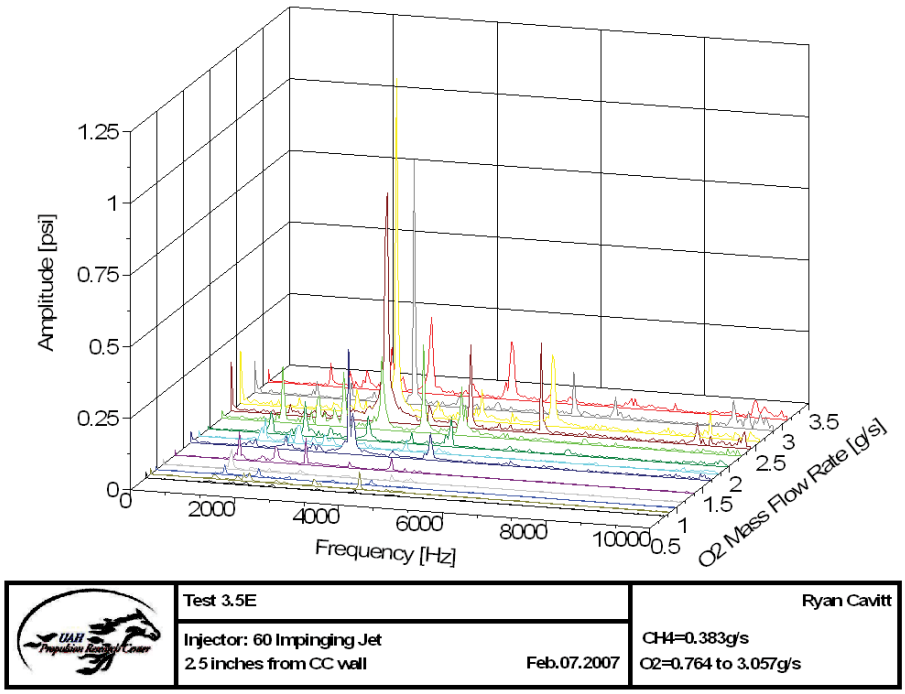

Figure H.87: 60-2-3.5 Waterfall Plot

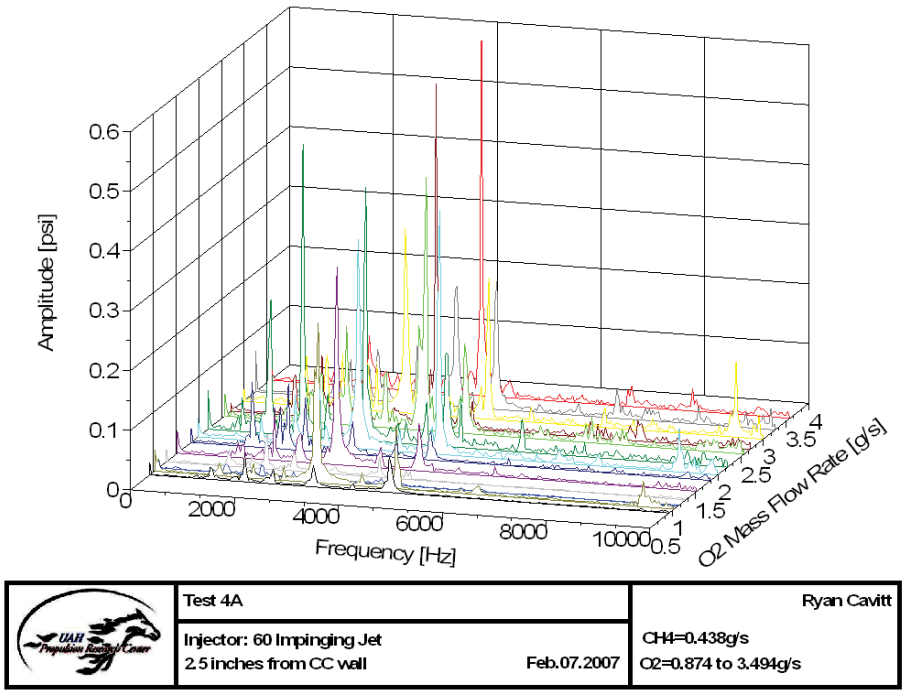

Figure H.88: 60-2-4 Waterfall Plot

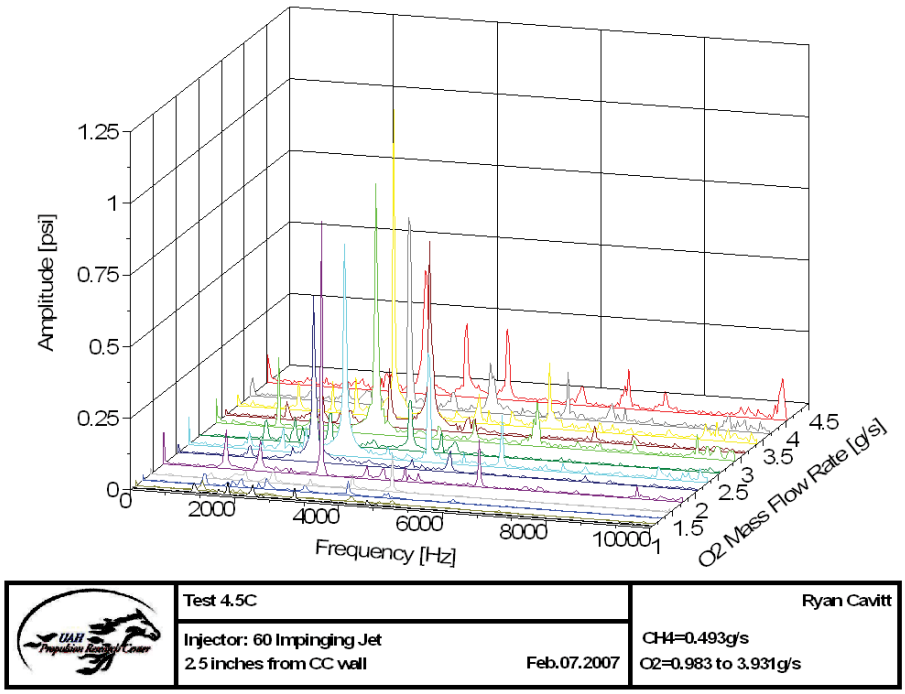

Figure H.89: 60-2-4.5 Waterfall Plot

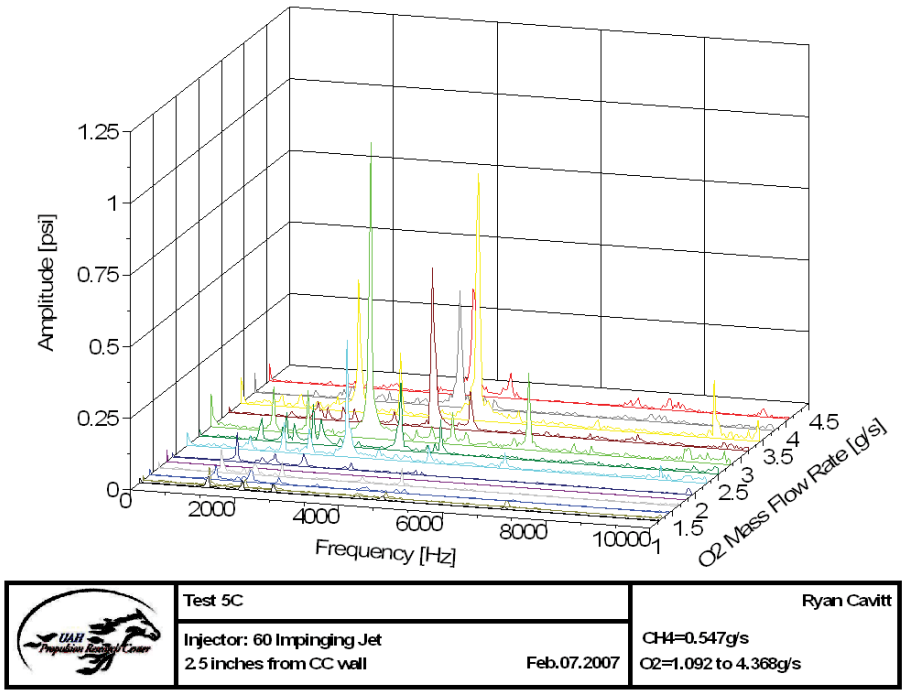

Figure H.90: 60-2-5 Waterfall Plot

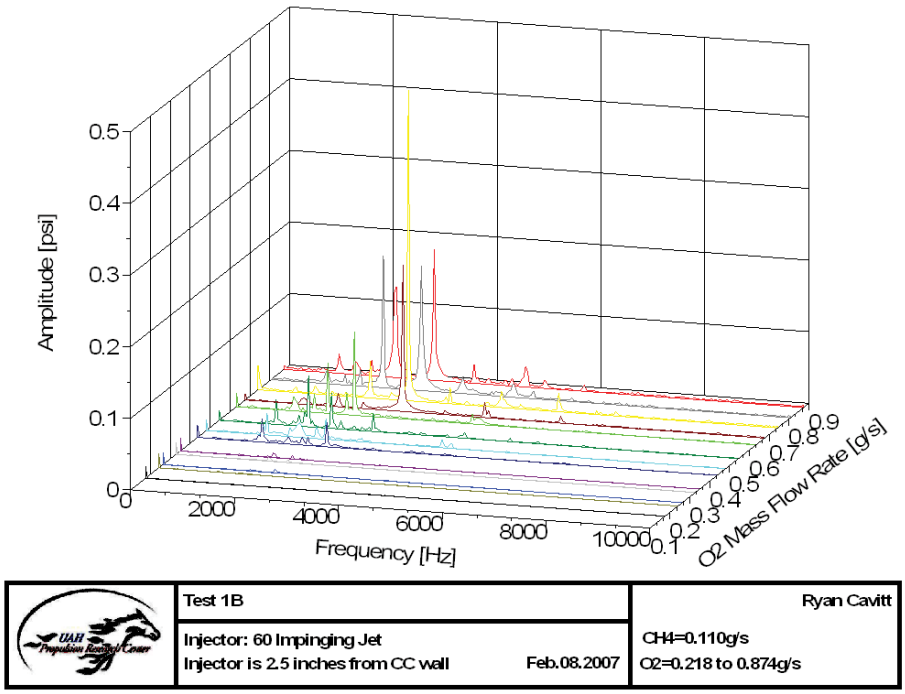

Figure H.91: 60-3-1 Waterfall Plot

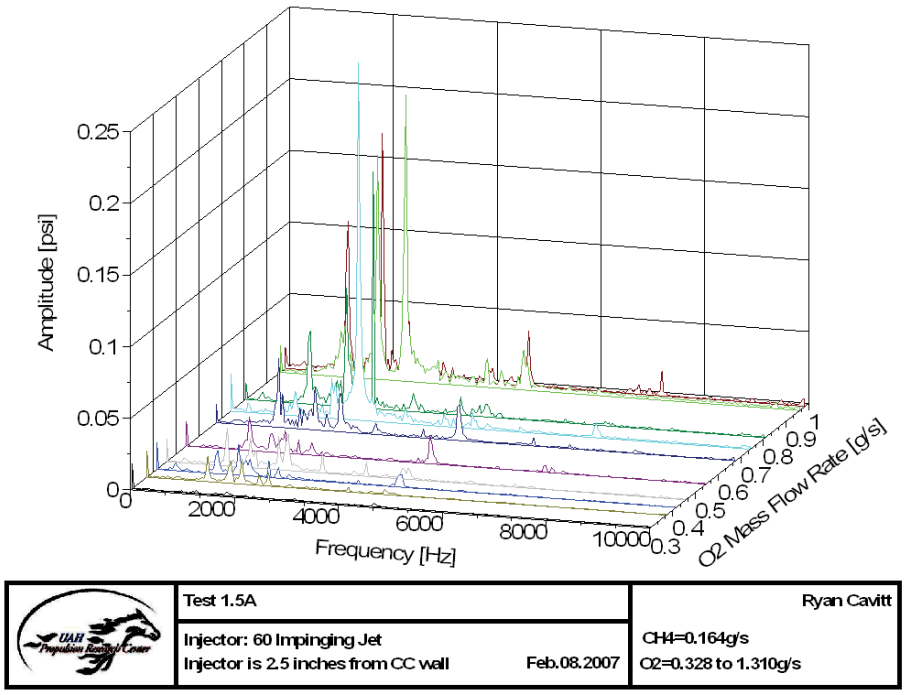

Figure H.92: 60-3-1.5 Waterfall Plot

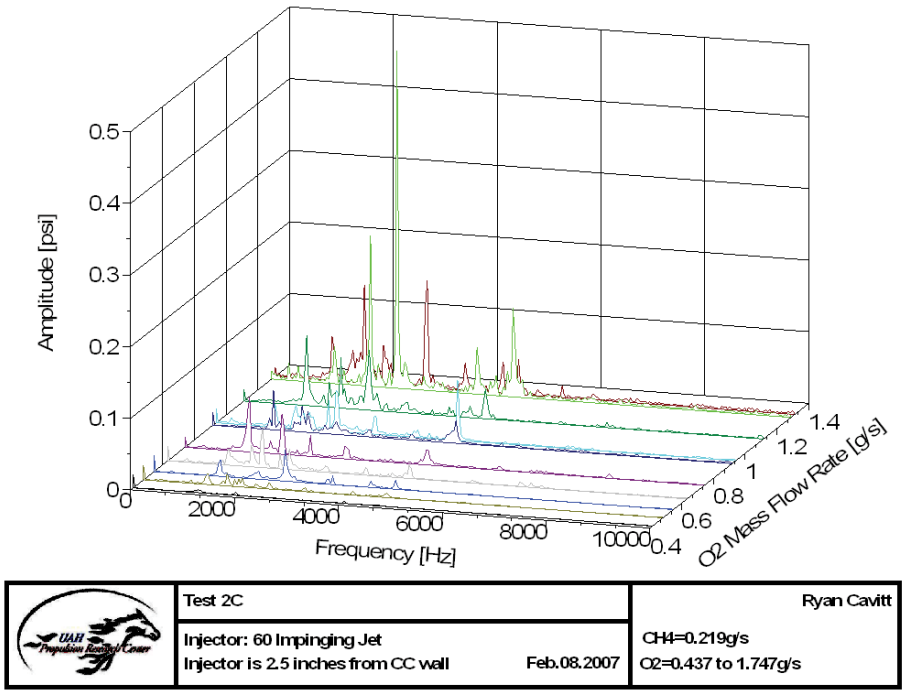

Figure H.93: 60-3-2 Waterfall Plot

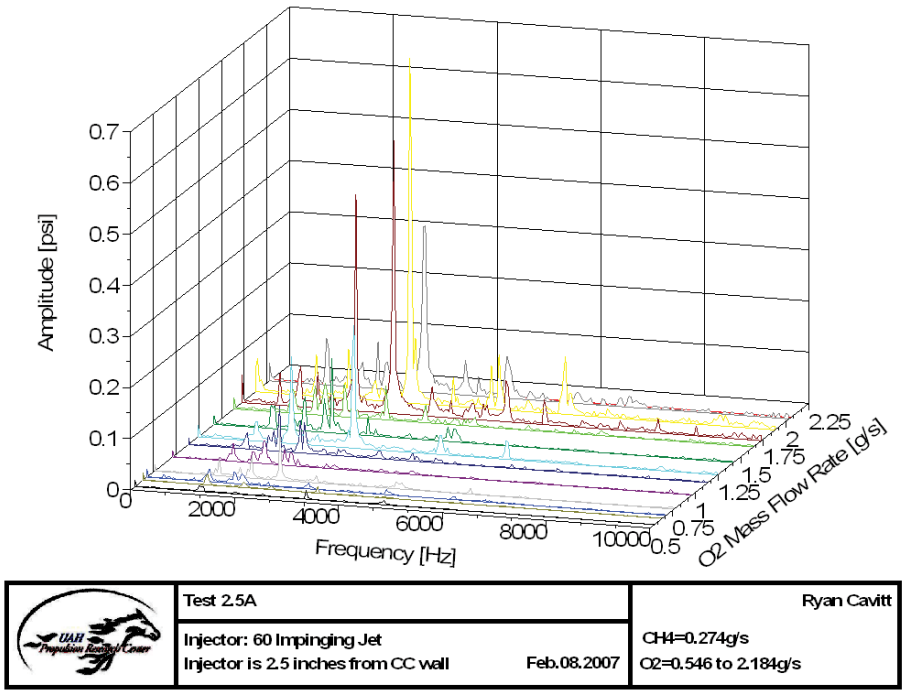

Figure H.94: 60-3-2.5 Waterfall Plot

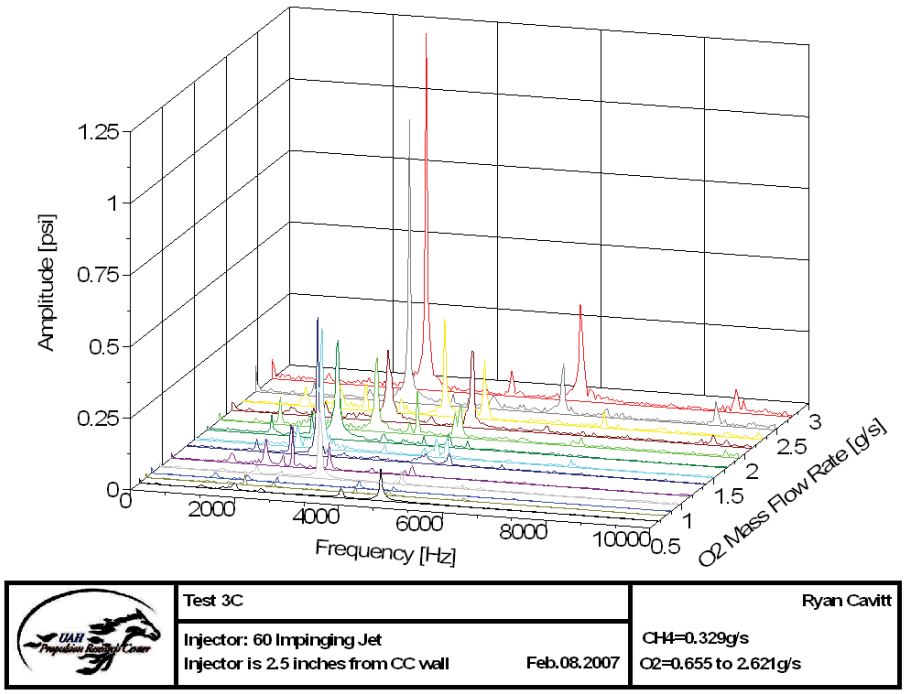

Figure H.95: 60-3-3 Waterfall Plot

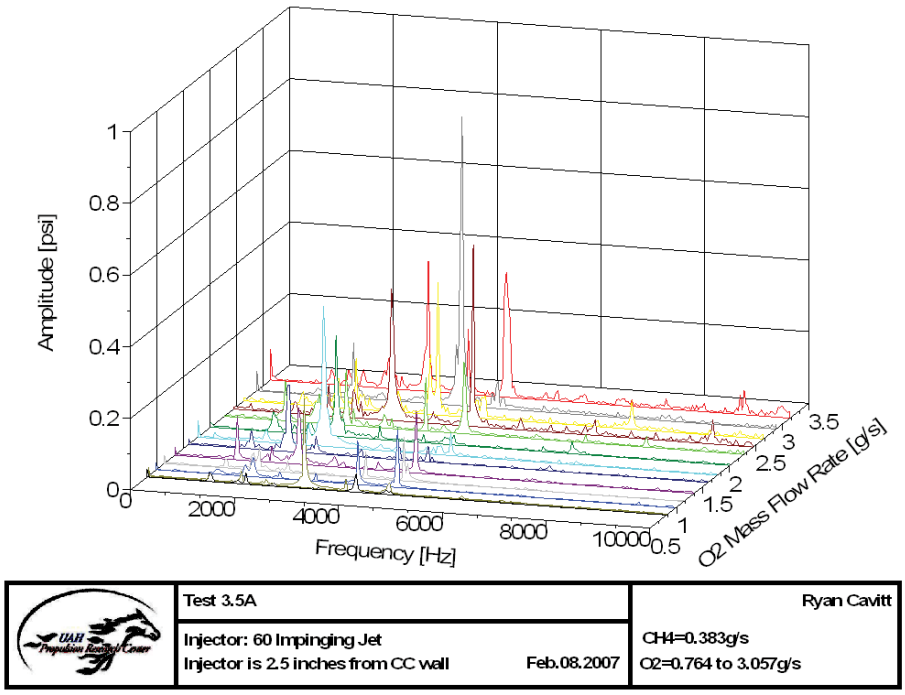

Figure H.96: 60-3-3.5 Waterfall Plot

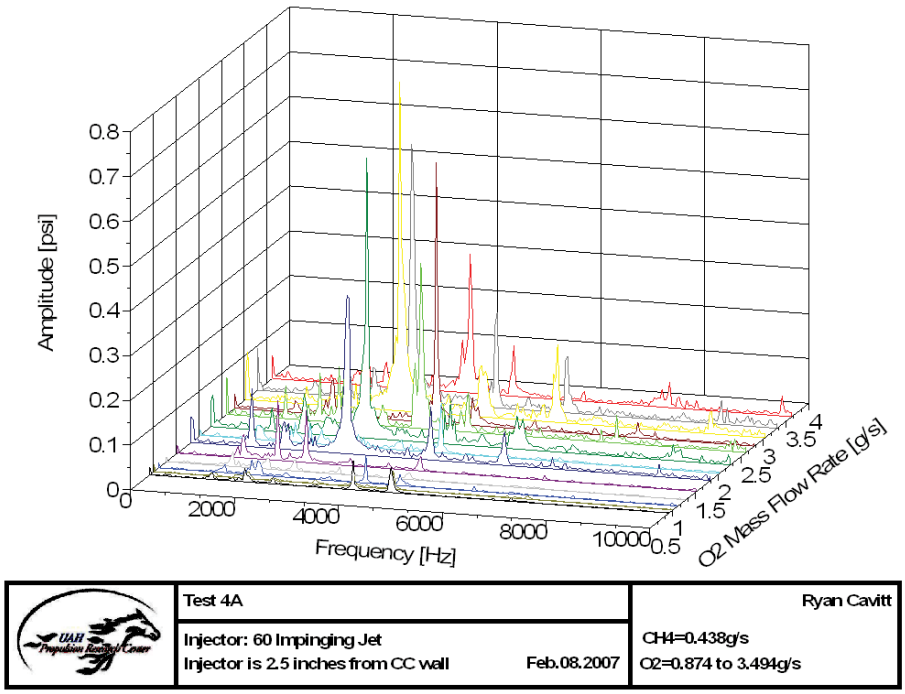

Figure H.97: 60-3-4 Waterfall Plot

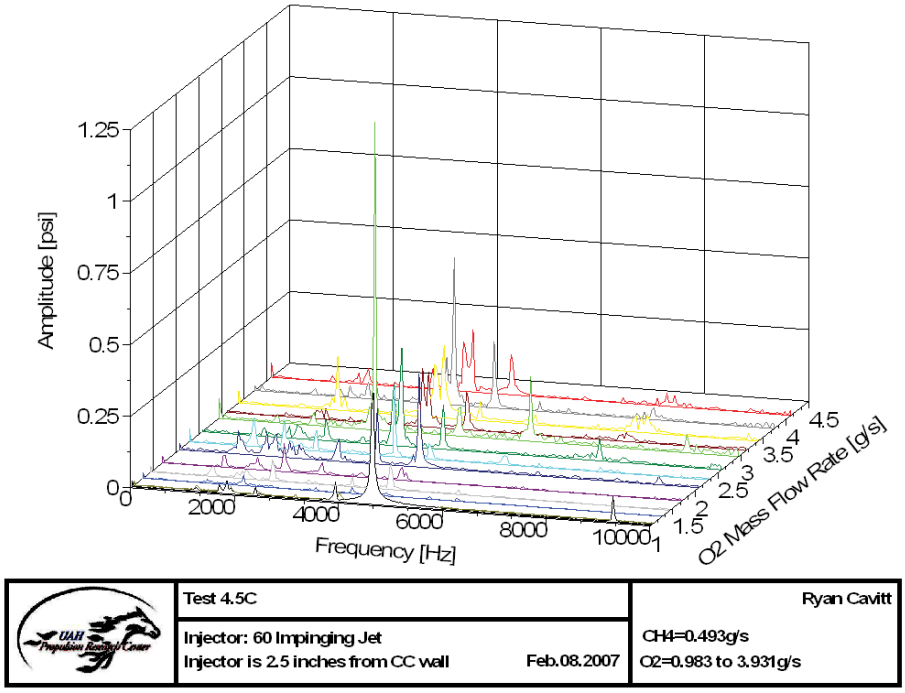

Figure H.98: 60-3-4.5 Waterfall Plot

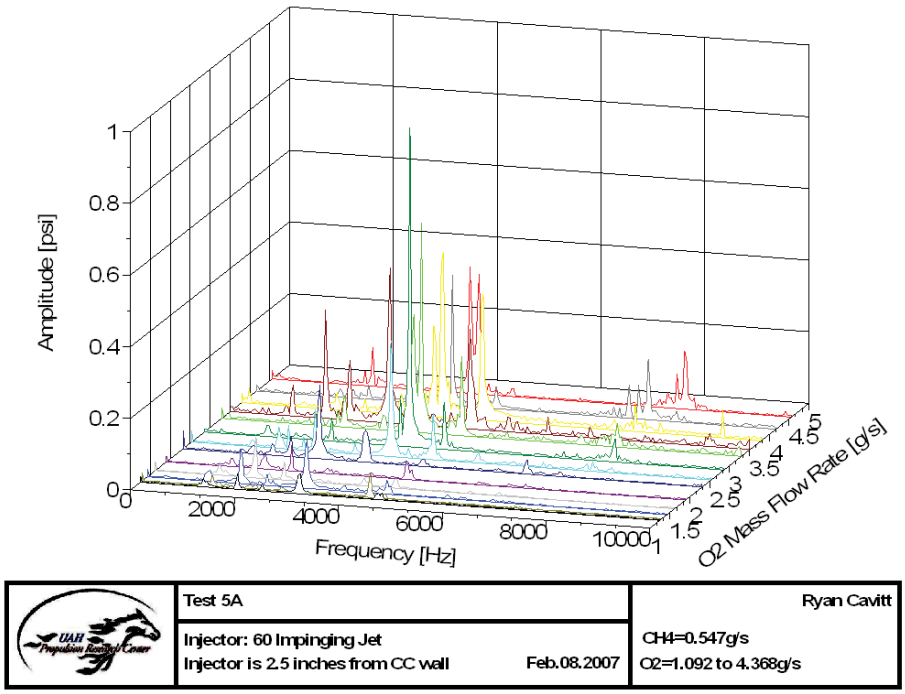

Figure H.99: 60-3-5 Waterfall Plot

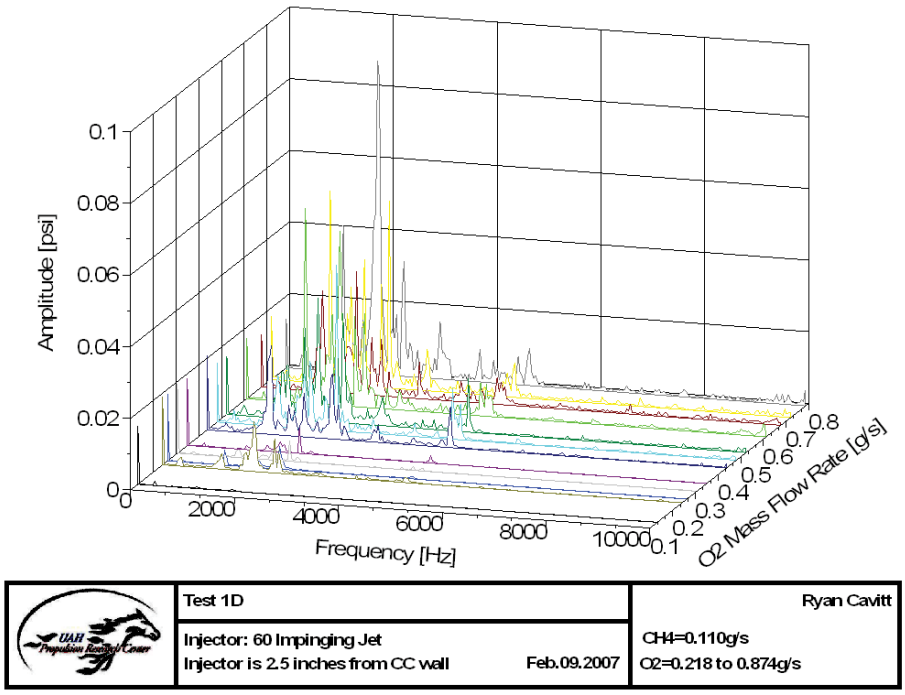

Figure H.100: 60-4-1 Waterfall Plot

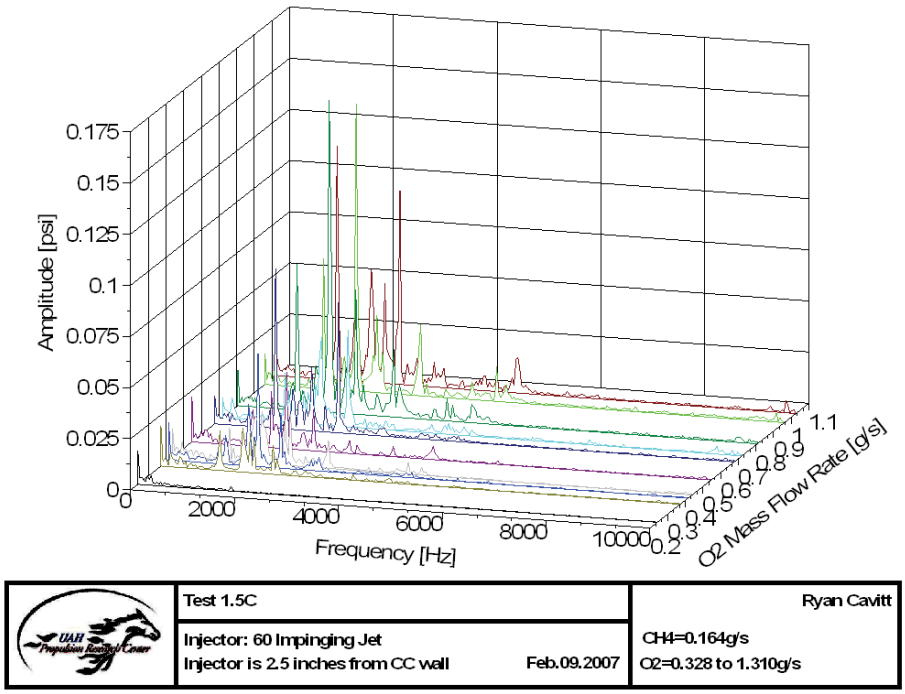

Figure H.101: 60-4-1.5 Waterfall Plot

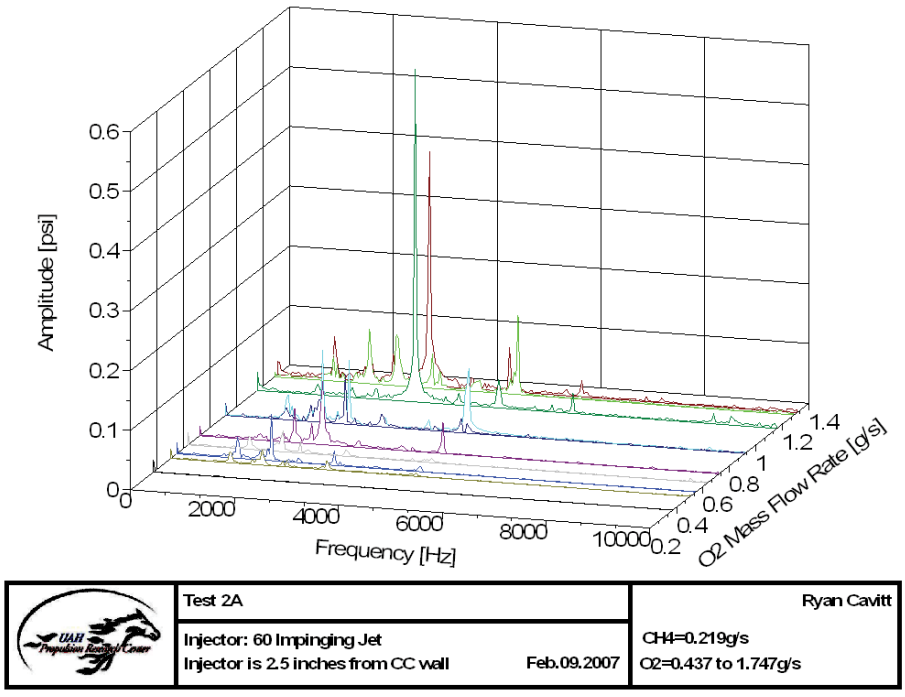

Figure H.102: 60-4-2 Waterfall Plot

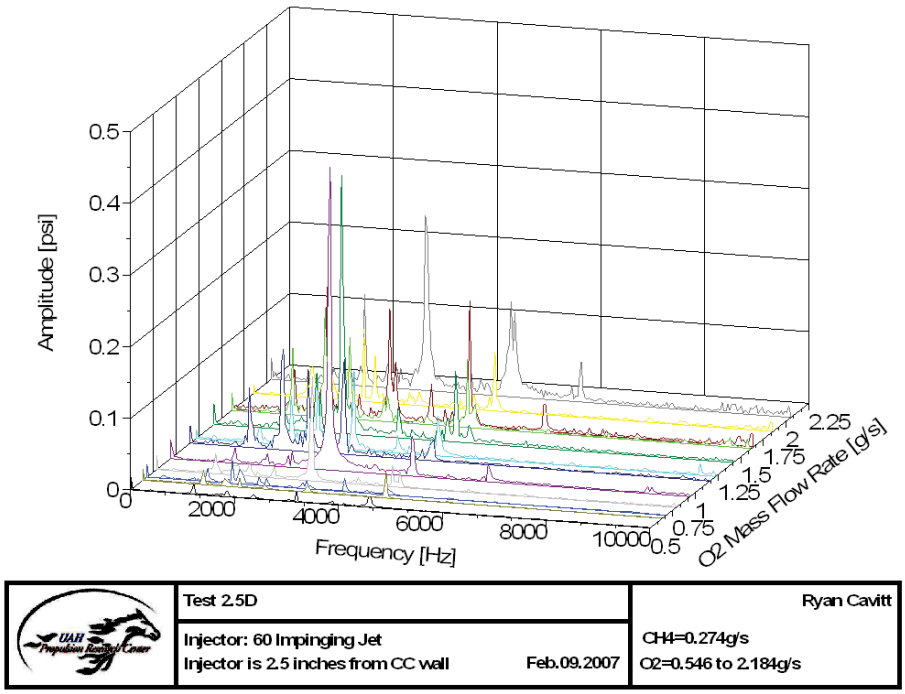

Figure H.103: 60-4-2.5 Waterfall Plot

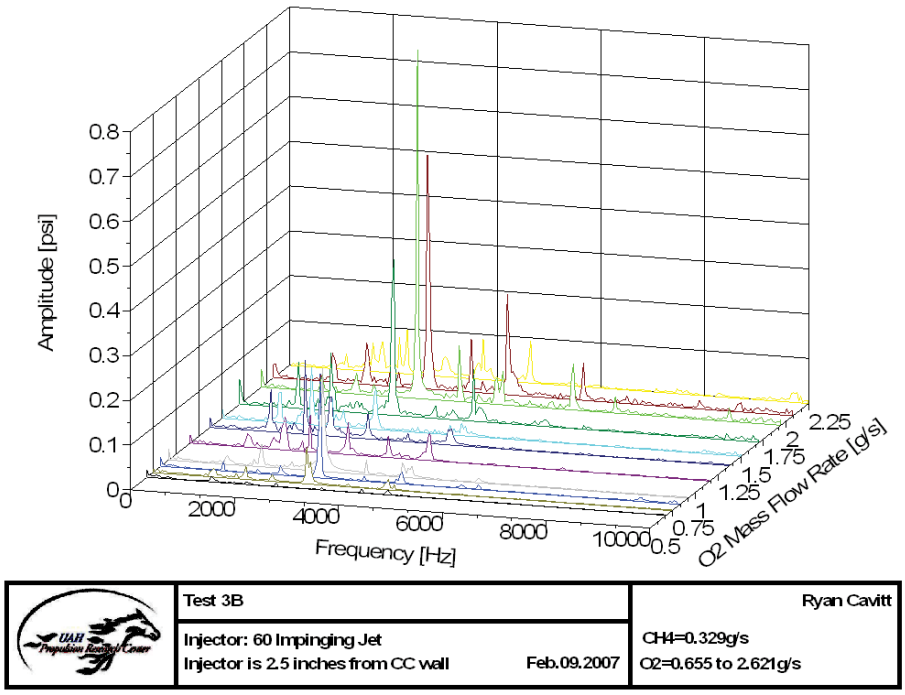

Figure H.104: 60-4-3 Waterfall Plot

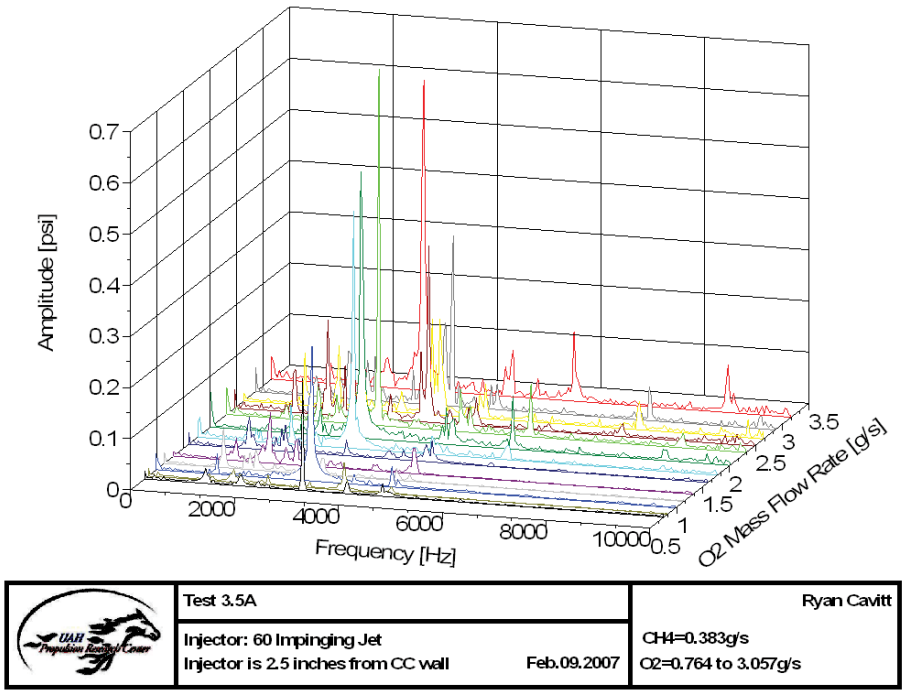

Figure H.105: 60-4-3.5 Waterfall Plot

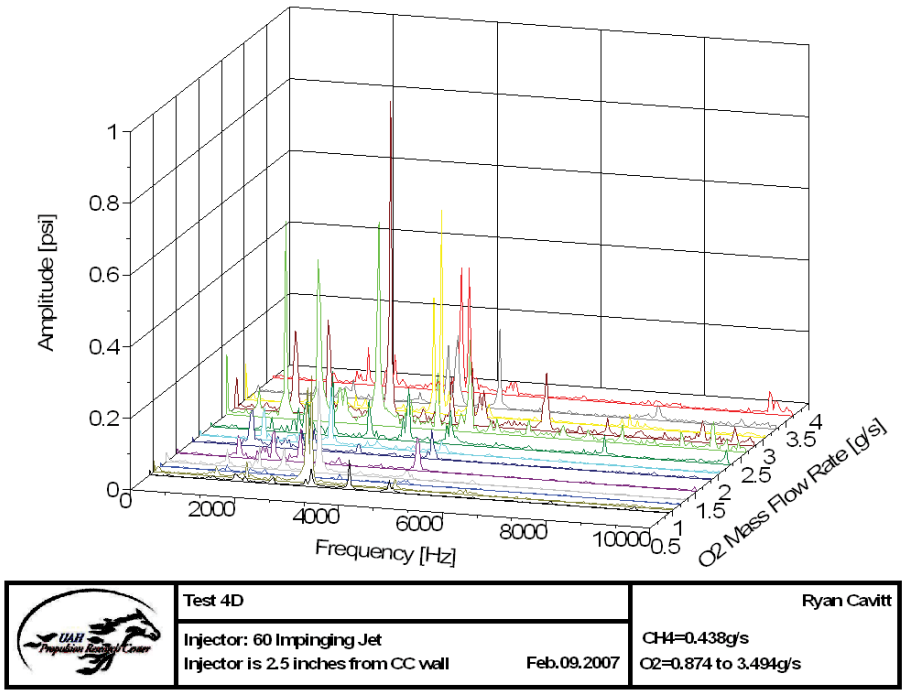

Figure H.106: 60-4-4 Waterfall Plot

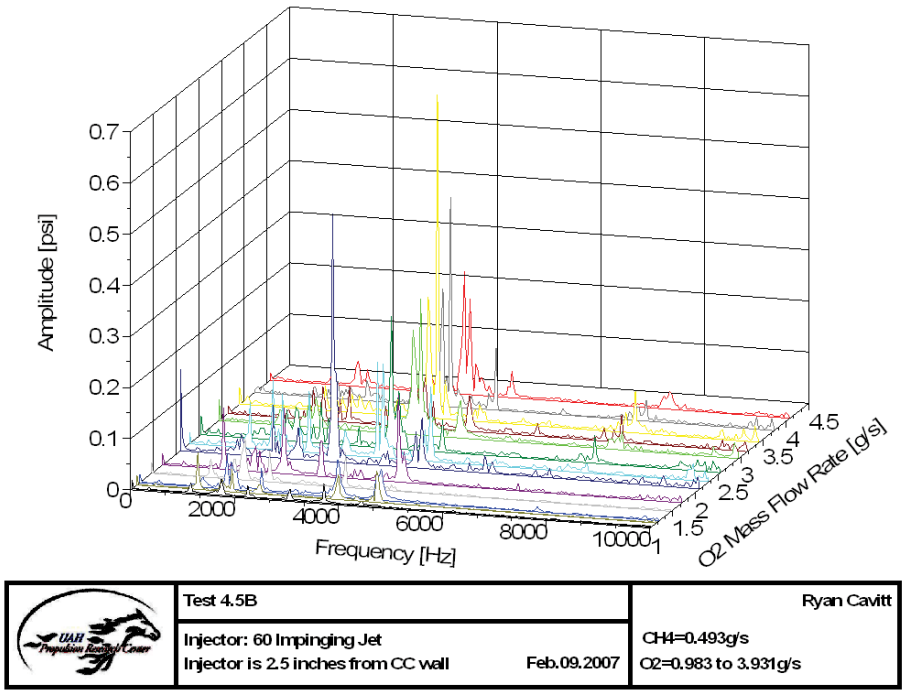

Figure H.107: 60-4-4.5 Waterfall Plot

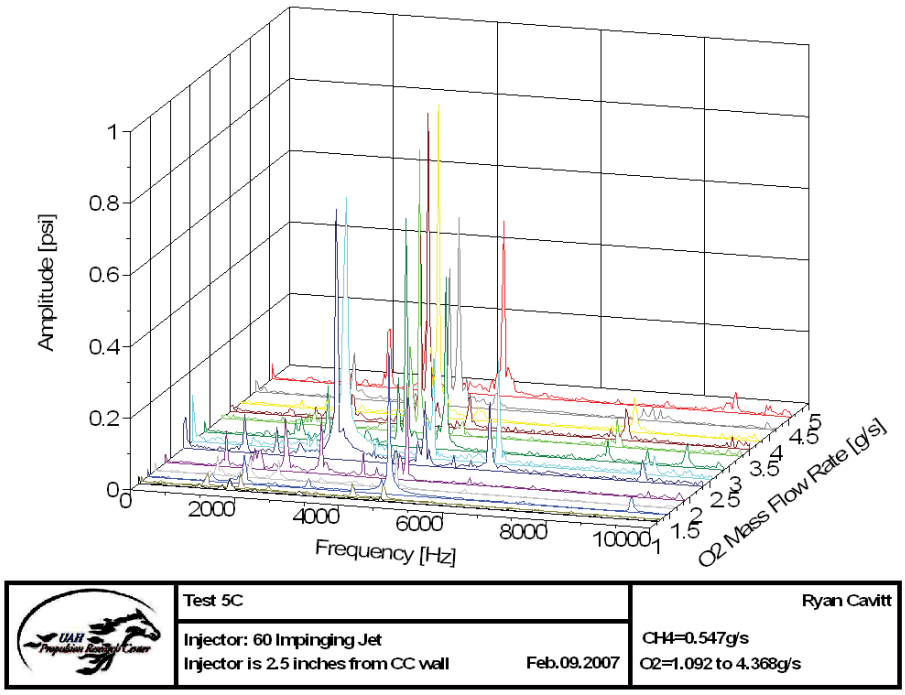

Figure H.108: 60-4-5 Waterfall Plot

Table H.1: 30 Degree Injector Average Stability Map Data [Test 1.0 to 2.0]

$\dot{m}_{O2}$ $\left[\frac{g}{s}\right]$	$\dot{m}_{CH4}$ $\left[\frac{g}{s}\right]$	Energy Density $\left[\frac{KW}{m^3}\right]$	(2 - 3) kHz Amplitude [psi]	(3.3 - 4.3) kHz Amplitude [psi]	(.1 - 20) kHz Amplitude [psi]
0.169	0.108	5.819	0.000	0.000	0.001
0.218	0.109	6.195	0.000	0.000	0.001
0.278	0.110	6.964	0.000	0.000	0.001
0.316	0.109	8.472	0.000	0.000	0.001
0.354	0.109	8.028	0.000	0.000	0.002
0.436	0.109	8.857	0.000	0.000	0.002
0.480	0.109	10.158	0.000	0.000	0.004
0.551	0.109	83.809	0.001	0.000	0.005
0.618	0.109	323.165	0.043	0.007	0.338
0.665	0.109	342.208	0.047	0.010	0.204
0.742	0.109	286.053	0.057	0.012	0.401
0.785	0.109	351.843	0.043	0.009	0.128
0.880	0.109	414.276	0.102	0.012	0.226
0.300	0.165	8.475	0.001	0.000	0.002
0.349	0.165	9.409	0.001	0.000	0.004
0.414	0.163	10.522	0.002	0.000	0.004
0.464	0.164	12.131	0.001	0.000	0.004
0.545	0.164	83.939	0.021	0.003	0.195
0.665	0.164	296.212	0.050	0.008	0.272
0.731	0.164	334.102	0.050	0.007	0.150
0.834	0.164	473.220	0.225	0.018	0.524
0.943	0.164	434.691	0.089	0.017	0.138
1.003	0.164	444.439	0.095	0.019	0.180
1.107	0.164	669.490	0.228	0.021	0.409
1.211	0.165	626.407	0.207	0.042	0.436
1.360	0.165	587.221	0.039	0.035	0.301
0.425	0.218	9.553	0.081	0.006	0.242
0.474	0.219	82.746	0.033	0.008	0.064
0.540	0.220	112.630	0.076	0.008	0.215
0.633	0.219	274.891	0.067	0.008	0.116
0.742	0.220	286.053	0.063	0.010	0.131
0.911	0.219	375.328	0.095	0.011	0.183
0.954	0.219	392.464	0.090	0.024	0.183
1.118	0.218	514.309	0.071	0.017	0.190
1.292	0.218	560.088	0.079	0.017	0.147
1.342	0.218	375.056	0.099	0.023	0.137
1.500	0.220	1067.938	0.337	0.029	0.663
1.631	0.218	803.323	0.599	0.047	0.932
1.805	0.220	1400.487	0.548	0.040	0.858

Table H.2: 30 Degree Injector Average Stability Map Data [Test 2.5 to 3.5]

$\dot{m}_{O2}$ $\left[\frac{g}{s}\right]$	$\dot{m}_{CH4}$ $\left[\frac{g}{s}\right]$	Energy Density $\left[\frac{KW}{m^3}\right]$	(2 - 3) kHz Amplitude [psi]	(3.3 - 4.3) kHz Amplitude [psi]	(.1 - 20) kHz Amplitude [psi]
0.534	0.274	65.106	0.150	0.014	0.526
0.605	0.274	192.493	0.030	0.008	0.067
0.693	0.274	237.483	0.085	0.006	0.210
0.785	0.274	314.102	0.061	0.008	0.121
0.943	0.273	297.336	0.055	0.014	0.110
1.134	0.273	420.354	0.148	0.021	0.203
1.222	0.275	474.500	0.135	0.018	0.215
1.407	0.274	277.461	0.179	0.017	0.304
1.620	0.274	754.947	0.456	0.035	0.849
1.729	0.273	884.263	0.478	0.039	0.610
1.876	0.274	683.549	0.535	0.027	0.651
2.034	0.274	1027.803	0.529	0.037	0.554
2.252	0.274	1110.238	0.766	0.028	0.995
0.671	0.326	329.200	0.047	0.008	0.094
0.720	0.328	320.127	0.080	0.008	0.245
0.834	0.329	316.031	0.049	0.007	0.100
0.954	0.328	390.983	0.089	0.011	0.167
1.129	0.329	469.064	0.079	0.010	0.113
1.358	0.328	580.865	0.182	0.024	0.298
1.505	0.328	929.163	0.137	0.021	0.385
1.707	0.328	763.152	0.420	0.031	0.608
1.941	0.328	1077.424	0.594	0.040	0.793
2.083	0.330	1153.283	0.612	0.038	0.724
2.247	0.328	1152.673	0.736	0.031	0.985
2.449	0.328	1181.328	0.332	0.184	0.687
2.694	0.329	1167.177	0.223	0.260	0.694
0.793	0.381	307.521	0.061	0.006	0.128
0.865	0.384	422.299	0.036	0.007	0.114
0.974	0.383	490.036	0.056	0.013	0.139
1.120	0.382	521.206	0.081	0.019	0.128
1.302	0.383	513.217	0.033	0.019	0.164
1.592	0.384	699.559	0.119	0.021	0.167
1.760	0.384	823.744	0.458	0.045	0.593
1.985	0.383	930.068	0.472	0.018	0.550
2.269	0.383	1186.729	0.794	0.020	1.042
2.392	0.384	1337.253	0.734	0.022	0.852
2.610	0.382	917.661	0.473	0.101	0.821
2.865	0.388	965.829	0.123	0.295	0.583
3.105	0.383	1172.490	0.396	0.064	0.505

Table H.3: 30 Degree Injector Average Stability Map Data [Test 4.0 to 5.0]

$\dot{m}_{O2}$ $\left[\frac{g}{s}\right]$	$\dot{m}_{CH4}$ $\left[\frac{g}{s}\right]$	Energy Density $\left[\frac{KW}{m^3}\right]$	(2 - 3) kHz Amplitude [psi]	(3.3 - 4.3) kHz Amplitude [psi]	(.1 - 20) kHz Amplitude [psi]
0.916	0.435	349.319	0.045	0.011	0.172
0.982	0.437	382.890	0.162	0.011	0.504
1.118	0.437	650.032	0.046	0.010	0.094
1.287	0.440	503.053	0.109	0.015	0.169
1.505	0.438	429.448	0.203	0.040	0.537
1.821	0.438	975.531	0.096	0.024	0.240
2.029	0.437	785.562	0.540	0.012	0.591
2.269	0.435	1184.182	0.466	0.011	0.763
2.585	0.439	917.164	0.437	0.090	0.671
2.759	0.435	1142.165	0.306	0.172	0.507
2.978	0.437	936.906	0.065	0.444	0.662
3.261	0.438	838.280	0.233	0.214	0.618
3.605	0.438	811.780	0.027	0.159	0.376
1.047	0.490	254.156	0.044	0.008	0.101
1.112	0.493	727.576	0.033	0.008	0.176
1.265	0.494	227.279	0.014	0.013	0.152
1.440	0.492	412.488	0.095	0.027	0.164
1.709	0.491	844.282	0.023	0.051	0.113
2.058	0.492	951.022	0.018	0.138	0.183
2.269	0.492	989.735	0.013	0.139	0.226
2.545	0.493	909.345	0.030	0.306	0.526
2.923	0.493	1047.414	0.179	0.249	0.512
3.112	0.492	929.496	0.226	0.183	0.666
3.367	0.492	1046.270	0.085	0.242	0.583
3.679	0.491	904.752	0.205	0.128	0.580
4.065	0.492	662.706	0.036	0.297	0.527
1.194	0.544	250.385	0.035	0.010	0.058
1.260	0.550	257.380	0.023	0.014	0.127
1.407	0.548	277.461	0.041	0.015	0.092
1.614	0.548	522.781	0.042	0.136	0.207
1.892	0.547	566.101	0.039	0.135	0.276
2.296	0.547	661.812	0.026	0.191	0.251
2.525	0.548	906.212	0.012	0.289	0.359
2.825	0.547	914.290	0.006	0.269	0.436
3.234	0.547	1129.680	0.010	0.338	0.490
3.474	0.548	1100.785	0.031	0.393	0.754
3.763	0.545	1133.043	0.009	0.198	0.261
4.106	0.548	1024.415	0.010	0.251	0.343
4.544	0.547	1180.465	0.253	0.436	0.985

Table H.4: 30 Degree Injector Maximum Stability Map Data [Test 1.0 to 2.0]

$\dot{m}_{O2}$ $\left[\frac{g}{s}\right]$	$\dot{m}_{CH4}$ $\left[\frac{g}{s}\right]$	Energy Density $\left[\frac{KW}{m^3}\right]$	(2 - 3) kHz Amplitude [psi]	(3.3 - 4.3) kHz Amplitude [psi]	(.1 - 20) kHz Amplitude [psi]
0.169	0.108	6.271	0.000	0.000	0.001
0.218	0.109	7.041	0.001	0.000	0.001
0.278	0.110	7.707	0.000	0.000	0.001
0.316	0.109	9.410	0.000	0.000	0.001
0.354	0.109	10.705	0.000	0.000	0.002
0.436	0.109	9.477	0.001	0.000	0.002
0.480	0.109	11.382	0.000	0.000	0.004
0.551	0.109	296.389	0.001	0.000	0.005
0.618	0.109	408.510	0.079	0.007	0.338
0.665	0.109	419.629	0.090	0.013	0.204
0.742	0.109	319.385	0.070	0.015	0.401
0.785	0.109	441.214	0.062	0.011	0.128
0.880	0.109	506.020	0.167	0.013	0.226
0.300	0.165	10.032	0.001	0.000	0.002
0.349	0.165	10.705	0.002	0.000	0.004
0.414	0.163	13.150	0.002	0.000	0.004
0.464	0.164	13.533	0.002	0.000	0.004
0.545	0.164	296.389	0.083	0.013	0.195
0.665	0.164	390.087	0.074	0.010	0.272
0.731	0.164	458.608	0.069	0.010	0.150
0.834	0.164	759.041	0.524	0.044	0.524
0.943	0.164	506.996	0.138	0.024	0.138
1.003	0.164	551.033	0.180	0.026	0.180
1.107	0.164	1036.512	0.362	0.025	0.409
1.211	0.165	925.251	0.436	0.064	0.436
1.360	0.165	892.792	0.067	0.078	0.301
0.425	0.218	10.736	0.242	0.012	0.242
0.474	0.219	167.922	0.064	0.015	0.064
0.540	0.220	296.389	0.215	0.016	0.215
0.633	0.219	408.510	0.116	0.021	0.116
0.742	0.220	319.385	0.084	0.015	0.131
0.911	0.219	484.058	0.183	0.021	0.183
0.954	0.219	506.996	0.109	0.030	0.183
1.118	0.218	670.660	0.094	0.029	0.190
1.292	0.218	701.524	0.097	0.025	0.147
1.342	0.218	535.927	0.137	0.033	0.137
1.500	0.220	1735.753	0.663	0.058	0.663
1.631	0.218	1497.755	0.932	0.072	0.932
1.805	0.220	1545.306	0.858	0.063	0.858

Table H.5: 30 Degree Injector Maximum Stability Map Data [Test 2.5 to 3.5]

$\dot{m}_{O2}$ $\left[\frac{g}{s}\right]$	$\dot{m}_{CH4}$ $\left[\frac{g}{s}\right]$	Energy Density $\left[\frac{KW}{m^3}\right]$	(2 - 3) kHz Amplitude [psi]	(3.3 - 4.3) kHz Amplitude [psi]	(.1 - 20) kHz Amplitude [psi]
0.534	0.274	130.262	0.526	0.033	0.526
0.605	0.274	276.444	0.036	0.014	0.067
0.693	0.274	304.711	0.210	0.008	0.210
0.785	0.274	441.214	0.121	0.016	0.121
0.943	0.273	335.634	0.110	0.018	0.110
1.134	0.273	493.268	0.203	0.035	0.203
1.222	0.275	609.333	0.215	0.024	0.215
1.407	0.274	330.112	0.304	0.022	0.304
1.620	0.274	1218.420	0.849	0.089	0.849
1.729	0.273	1050.091	0.610	0.052	0.610
1.876	0.274	805.361	0.651	0.057	0.651
2.034	0.274	1341.068	0.554	0.066	0.554
2.252	0.274	1444.327	0.995	0.041	0.995
0.671	0.326	419.629	0.094	0.012	0.094
0.720	0.328	440.266	0.245	0.010	0.245
0.834	0.329	373.350	0.069	0.010	0.100
0.954	0.328	506.996	0.105	0.015	0.167
1.129	0.329	670.660	0.113	0.014	0.113
1.358	0.328	892.792	0.298	0.028	0.298
1.505	0.328	1735.753	0.385	0.026	0.385
1.707	0.328	1037.052	0.608	0.059	0.608
1.941	0.328	1365.000	0.793	0.063	0.793
2.083	0.330	1547.551	0.724	0.073	0.724
2.247	0.328	1408.938	0.985	0.077	0.985
2.449	0.328	1695.109	0.687	0.352	0.687
2.694	0.329	1505.104	0.694	0.395	0.694
0.793	0.381	441.214	0.128	0.008	0.128
0.865	0.384	506.020	0.046	0.007	0.114
0.974	0.383	551.033	0.078	0.021	0.139
1.120	0.382	670.660	0.128	0.033	0.128
1.302	0.383	535.927	0.052	0.020	0.164
1.592	0.384	1218.420	0.167	0.025	0.167
1.760	0.384	973.311	0.593	0.082	0.593
1.985	0.383	1365.000	0.550	0.029	0.550
2.269	0.383	1444.327	1.042	0.028	1.042
2.392	0.384	1774.608	0.852	0.046	0.852
2.610	0.382	1176.263	0.821	0.280	0.821
2.865	0.388	1338.957	0.246	0.583	0.583
3.105	0.383	1545.532	0.505	0.170	0.505

Table H.6: 30 Degree Injector Maximum Stability Map Data [Test 4.0 to 5.0]

$\dot{m}_{O2}$ $\left[\frac{g}{s}\right]$	$\dot{m}_{CH4}$ $\left[\frac{g}{s}\right]$	Energy Density $\left[\frac{KW}{m^3}\right]$	(2 - 3) kHz Amplitude [psi]	(3.3 - 4.3) kHz Amplitude [psi]	(.1 - 20) kHz Amplitude [psi]
0.916	0.435	484.058	0.062	0.017	0.172
0.982	0.437	608.424	0.504	0.020	0.504
1.118	0.437	1036.512	0.073	0.014	0.094
1.287	0.440	701.524	0.162	0.025	0.169
1.505	0.438	545.414	0.537	0.089	0.537
1.821	0.438	1545.306	0.240	0.052	0.240
2.029	0.437	903.351	0.591	0.020	0.591
2.269	0.435	1444.327	0.763	0.024	0.763
2.585	0.439	1250.989	0.671	0.327	0.671
2.759	0.435	1571.097	0.507	0.412	0.507
2.978	0.437	1212.141	0.184	0.662	0.662
3.261	0.438	1300.216	0.436	0.618	0.618
3.605	0.438	1262.915	0.071	0.376	0.376
1.047	0.490	357.804	0.101	0.016	0.101
1.112	0.493	1036.512	0.058	0.010	0.176
1.265	0.494	277.505	0.027	0.019	0.152
1.440	0.492	521.895	0.164	0.063	0.164
1.709	0.491	1037.052	0.046	0.107	0.113
2.058	0.492	1547.551	0.025	0.183	0.183
2.269	0.492	1310.947	0.018	0.226	0.226
2.545	0.493	1033.468	0.068	0.526	0.526
2.923	0.493	1113.710	0.512	0.382	0.512
3.112	0.492	1127.890	0.666	0.362	0.666
3.367	0.492	1534.637	0.239	0.583	0.583
3.679	0.491	1024.321	0.580	0.213	0.580
4.065	0.492	896.745	0.098	0.527	0.527
1.194	0.544	299.582	0.058	0.016	0.058
1.260	0.550	347.684	0.039	0.019	0.127
1.407	0.548	330.112	0.065	0.017	0.092
1.614	0.548	728.318	0.048	0.207	0.207
1.892	0.547	805.361	0.048	0.276	0.276
2.296	0.547	949.632	0.054	0.251	0.251
2.525	0.548	1036.314	0.019	0.359	0.359
2.825	0.547	1022.324	0.008	0.436	0.436
3.234	0.547	1300.216	0.017	0.490	0.490
3.474	0.548	1431.239	0.084	0.754	0.754
3.763	0.545	1227.484	0.014	0.261	0.261
4.106	0.548	1300.143	0.021	0.343	0.343
4.544	0.547	1256.120	0.985	0.618	0.985

Table H.7: 45 Degree Injector Average Stability Map Data [Test 1.0 to 2.0]

$\dot{m}_{O2}$ $\left[\frac{g}{s}\right]$	$\dot{m}_{CH4}$ $\left[\frac{g}{s}\right]$	Energy Density $\left[\frac{KW}{m^3}\right]$	(2 - 3) kHz Amplitude [psi]	(3.3 - 4.3) kHz Amplitude [psi]	(.1 - 20) kHz Amplitude [psi]
0.153	0.107	13.808	0.000	0.001	0.003
0.234	0.109	16.453	0.000	0.000	0.004
0.278	0.110	17.806	0.001	0.000	0.004
0.294	0.109	16.451	0.001	0.000	0.004
0.360	0.110	18.686	0.001	0.000	0.005
0.431	0.109	20.805	0.001	0.000	0.006
0.469	0.111	21.517	0.001	0.000	0.005
0.545	0.109	280.073	0.001	0.000	0.007
0.627	0.109	339.161	0.055	0.007	0.140
0.654	0.109	293.610	0.068	0.009	0.156
0.731	0.109	293.669	0.055	0.009	0.115
0.796	0.109	356.212	0.044	0.009	0.121
0.878	0.110	370.003	0.075	0.013	0.118
0.284	0.162	13.065	0.002	0.000	0.003
0.360	0.163	13.504	0.001	0.000	0.003
0.404	0.164	16.030	0.002	0.000	0.004
0.464	0.163	78.062	0.071	0.002	0.072
0.545	0.164	280.073	0.060	0.008	0.158
0.671	0.164	337.579	0.072	0.006	0.145
0.731	0.164	295.105	0.057	0.007	0.084
0.813	0.164	395.447	0.053	0.013	0.150
0.954	0.164	419.085	0.066	0.013	0.116
0.993	0.164	512.094	0.131	0.010	0.182
1.096	0.164	603.934	0.142	0.024	0.234
1.178	0.163	426.193	0.077	0.021	0.121
1.331	0.165	658.904	0.200	0.029	0.200
0.409	0.221	53.955	0.028	0.001	0.033
0.469	0.219	14.024	0.054	0.004	0.079
0.545	0.220	262.155	0.069	0.002	0.084
0.633	0.219	272.724	0.110	0.007	0.110
0.731	0.219	313.616	0.131	0.006	0.144
0.905	0.219	507.490	0.101	0.042	0.363
0.965	0.218	603.180	0.106	0.014	0.136
1.129	0.219	460.345	0.172	0.014	0.188
1.282	0.218	571.979	0.226	0.031	0.247
1.325	0.219	607.616	0.265	0.032	0.315
1.500	0.218	661.919	0.423	0.021	0.423
1.609	0.220	592.561	0.258	0.042	0.272
1.818	0.218	1158.645	0.459	0.039	0.459

Table H.8: 45 Degree Injector Average Stability Map Data [Test 2.5 to 3.5]

$\dot{m}_{O2}$ $\left[\frac{g}{s}\right]$	$\dot{m}_{CH4}$ $\left[\frac{g}{s}\right]$	Energy Density $\left[\frac{KW}{m^3}\right]$	(2 - 3) kHz Amplitude [psi]	(3.3 - 4.3) kHz Amplitude [psi]	(.1 - 20) kHz Amplitude [psi]
0.545	0.272	143.192	0.025	0.003	0.038
0.611	0.274	321.956	0.101	0.006	0.108
0.682	0.274	259.094	0.159	0.009	0.183
0.796	0.274	279.271	0.144	0.020	0.202
0.943	0.274	569.429	0.198	0.030	0.410
1.140	0.273	392.783	0.066	0.010	0.117
1.200	0.273	522.542	0.102	0.013	0.139
1.423	0.272	465.504	0.287	0.020	0.300
1.614	0.274	405.149	0.446	0.017	0.446
1.680	0.274	853.313	0.488	0.044	0.488
1.881	0.274	632.331	0.607	0.030	0.607
2.040	0.274	1082.338	0.684	0.061	0.684
2.241	0.274	1311.688	0.687	0.072	0.687
0.649	0.328	300.276	0.038	0.004	0.061
0.736	0.329	235.899	0.047	0.005	0.069
0.823	0.328	285.425	0.022	0.006	0.086
0.965	0.329	343.255	0.100	0.011	0.111
1.129	0.329	453.983	0.077	0.009	0.112
1.369	0.329	539.029	0.387	0.032	0.395
1.511	0.328	709.624	0.472	0.026	0.472
1.696	0.329	799.163	0.469	0.018	0.469
1.958	0.329	1166.442	0.683	0.053	0.683
2.083	0.326	1183.986	0.775	0.051	0.775
2.263	0.330	1257.717	0.597	0.043	0.597
2.459	0.328	1019.351	0.458	0.110	0.522
2.705	0.329	1626.611	0.359	0.230	0.521
0.763	0.384	289.340	0.033	0.008	0.048
0.851	0.382	373.594	0.045	0.013	0.064
0.996	0.385	279.027	0.050	0.015	0.095
1.120	0.383	362.170	0.069	0.011	0.099
1.331	0.383	528.026	0.150	0.016	0.168
1.578	0.383	426.817	0.190	0.013	0.198
1.752	0.384	1026.955	0.616	0.024	0.616
1.985	0.384	1127.779	0.487	0.017	0.487
2.283	0.383	1050.747	0.505	0.157	0.624
2.429	0.382	1117.585	0.314	0.159	0.451
2.618	0.386	1713.181	0.304	0.184	0.465
2.872	0.384	1132.577	0.023	0.222	0.227
3.170	0.381	1286.640	0.155	0.242	0.326

Table H.9: 45 Degree Injector Average Stability Map Data [Test 4.0 to 5.0]

$\dot{m}_{O2}$ $\left[\frac{g}{s}\right]$	$\dot{m}_{CH4}$ $\left[\frac{g}{s}\right]$	Energy Density $\left[\frac{KW}{m^3}\right]$	(2 - 3) kHz Amplitude [psi]	(3.3 - 4.3) kHz Amplitude [psi]	(.1 - 20) kHz Amplitude [psi]
0.883	0.435	281.212	0.016	0.009	0.042
0.998	0.437	456.042	0.136	0.011	0.150
1.118	0.439	358.510	0.038	0.016	0.076
1.292	0.437	516.951	0.044	0.015	0.102
1.516	0.437	601.514	0.176	0.017	0.201
1.832	0.438	673.215	0.400	0.033	0.400
2.034	0.437	1054.778	0.375	0.044	0.375
2.279	0.439	1097.664	0.499	0.100	0.577
2.601	0.439	1234.823	0.077	0.222	0.270
2.781	0.435	1160.955	0.020	0.261	0.293
3.016	0.437	1288.265	0.032	0.318	0.318
3.283	0.439	1402.418	0.029	0.419	0.419
3.621	0.438	1343.344	0.034	0.408	0.408
1.042	0.492	214.511	0.021	0.016	0.053
1.107	0.494	290.015	0.030	0.009	0.055
1.271	0.493	588.911	0.044	0.022	0.066
1.451	0.492	536.886	0.205	0.031	0.256
1.701	0.490	556.539	0.148	0.015	0.181
2.072	0.492	1208.203	0.660	0.037	0.660
2.279	0.493	1297.734	0.321	0.169	0.406
2.579	0.494	798.460	0.237	0.107	0.283
2.928	0.492	1083.516	0.224	0.249	0.379
3.119	0.493	951.833	0.396	0.061	0.396
3.381	0.495	1143.123	0.034	0.358	0.410
3.703	0.492	1127.465	0.014	0.334	0.334
4.074	0.492	1335.914	0.023	0.382	0.382
1.178	0.546	166.315	0.013	0.015	0.023
1.232	0.547	229.260	0.017	0.007	0.050
1.407	0.548	298.573	0.022	0.012	0.094
1.614	0.546	405.149	0.063	0.015	0.102
1.898	0.547	558.968	0.091	0.041	0.125
2.296	0.548	964.236	0.145	0.093	0.277
2.547	0.548	1078.048	0.037	0.344	0.344
2.847	0.548	871.862	0.038	0.270	0.270
3.245	0.547	1007.060	0.026	0.289	0.291
3.485	0.549	1094.012	0.026	0.272	0.272
3.774	0.547	1095.239	0.013	0.336	0.336
4.117	0.548	1069.587	0.025	0.337	0.343
4.526	0.547	1047.610	0.021	0.380	0.380

Table H.10: 45 Degree Injector Maximum Stability Map Data [Test 1.0 to 2.0]

$\dot{m}_{O2}$ $\left[\frac{g}{s}\right]$	$\dot{m}_{CH4}$ $\left[\frac{g}{s}\right]$	Energy Density $\left[\frac{KW}{m^3}\right]$	(2 - 3) kHz Amplitude [psi]	(3.3 - 4.3) kHz Amplitude [psi]	(.1 - 20) kHz Amplitude [psi]
0.153	0.107	32.708	0.000	0.002	0.006
0.234	0.109	36.159	0.001	0.000	0.009
0.278	0.110	39.756	0.001	0.000	0.011
0.294	0.109	38.542	0.001	0.000	0.011
0.360	0.110	39.653	0.001	0.000	0.011
0.431	0.109	41.381	0.001	0.000	0.011
0.469	0.111	40.637	0.001	0.000	0.008
0.545	0.109	547.884	0.001	0.001	0.009
0.627	0.109	542.181	0.086	0.014	0.325
0.654	0.109	334.924	0.111	0.011	0.245
0.731	0.109	321.249	0.067	0.013	0.164
0.796	0.109	404.057	0.064	0.010	0.176
0.878	0.110	405.182	0.189	0.014	0.189
0.284	0.162	14.172	0.004	0.000	0.004
0.360	0.163	14.713	0.002	0.000	0.005
0.404	0.164	17.277	0.005	0.000	0.005
0.464	0.163	262.328	0.277	0.007	0.277
0.545	0.164	547.884	0.079	0.021	0.434
0.671	0.164	575.164	0.088	0.009	0.295
0.731	0.164	321.249	0.089	0.009	0.099
0.813	0.164	458.923	0.085	0.015	0.267
0.954	0.164	475.312	0.078	0.017	0.181
0.993	0.164	604.434	0.267	0.014	0.267
1.096	0.164	1052.090	0.282	0.059	0.652
1.178	0.163	524.666	0.095	0.029	0.148
1.331	0.165	922.791	0.392	0.045	0.392
0.409	0.221	101.256	0.072	0.002	0.072
0.469	0.219	16.822	0.105	0.004	0.127
0.545	0.220	547.884	0.142	0.003	0.142
0.633	0.219	378.781	0.124	0.010	0.124
0.731	0.219	434.174	0.272	0.008	0.272
0.905	0.219	879.099	0.151	0.098	0.699
0.965	0.218	833.907	0.167	0.028	0.167
1.129	0.219	580.373	0.420	0.019	0.420
1.282	0.218	792.510	0.532	0.079	0.532
1.325	0.219	666.412	0.539	0.042	0.539
1.500	0.218	782.669	0.649	0.024	0.649
1.609	0.220	755.315	0.506	0.078	0.506
1.818	0.218	2128.657	0.798	0.071	0.798

Table H.11: 45 Degree Injector Maximum Stability Map Data [Test 2.5 to 3.5]

$\dot{m}_{O2}$ $\left[\frac{g}{s}\right]$	$\dot{m}_{CH4}$ $\left[\frac{g}{s}\right]$	Energy Density $\left[\frac{KW}{m^3}\right]$	(2 - 3) kHz Amplitude [psi]	(3.3 - 4.3) kHz Amplitude [psi]	(.1 - 20) kHz Amplitude [psi]
0.545	0.272	189.268	0.039	0.004	0.048
0.611	0.274	542.181	0.326	0.008	0.326
0.682	0.274	334.924	0.480	0.023	0.480
0.796	0.274	404.057	0.452	0.061	0.452
0.943	0.274	833.907	0.570	0.067	0.702
1.140	0.273	492.181	0.115	0.013	0.166
1.200	0.273	648.284	0.168	0.017	0.168
1.423	0.272	725.142	0.519	0.028	0.519
1.614	0.274	448.100	0.612	0.025	0.612
1.680	0.274	1203.765	0.562	0.056	0.562
1.881	0.274	877.673	0.720	0.037	0.720
2.040	0.274	1309.496	0.744	0.172	0.744
2.241	0.274	1643.962	0.860	0.098	0.860
0.649	0.328	454.046	0.088	0.006	0.088
0.736	0.329	282.005	0.107	0.008	0.107
0.823	0.328	403.408	0.036	0.009	0.150
0.965	0.329	424.517	0.137	0.021	0.142
1.129	0.329	580.373	0.151	0.011	0.151
1.369	0.329	814.579	0.641	0.086	0.641
1.511	0.328	782.669	0.676	0.049	0.676
1.696	0.329	921.407	0.511	0.024	0.511
1.958	0.329	1340.157	0.938	0.097	0.938
2.083	0.326	1455.771	0.819	0.104	0.819
2.263	0.330	1511.486	0.701	0.097	0.701
2.459	0.328	1302.407	1.162	0.288	1.162
2.705	0.329	2319.121	0.939	0.382	0.939
0.763	0.384	404.057	0.049	0.010	0.058
0.851	0.382	458.923	0.082	0.017	0.082
0.996	0.385	297.444	0.060	0.021	0.140
1.120	0.383	580.373	0.113	0.017	0.113
1.331	0.383	666.412	0.303	0.022	0.303
1.578	0.383	490.510	0.225	0.019	0.225
1.752	0.384	1157.248	0.698	0.032	0.698
1.985	0.384	1588.375	0.673	0.021	0.673
2.283	0.383	1280.607	0.931	0.403	0.931
2.429	0.382	1327.285	0.709	0.456	0.709
2.618	0.386	2088.169	0.870	0.311	0.870
2.872	0.384	1270.388	0.025	0.312	0.312
3.170	0.381	1426.849	0.424	0.345	0.424

Table H.12: 45 Degree Injector Maximum Stability Map Data [Test 4.0 to 5.0]

$\dot{m}_{O2}$ $\left[\frac{g}{s}\right]$	$\dot{m}_{CH4}$ $\left[\frac{g}{s}\right]$	Energy Density $\left[\frac{KW}{m^3}\right]$	(2 - 3) kHz Amplitude [psi]	(3.3 - 4.3) kHz Amplitude [psi]	(.1 - 20) kHz Amplitude [psi]
0.883	0.435	404.057	0.025	0.013	0.053
0.998	0.437	604.434	0.465	0.015	0.465
1.118	0.439	580.373	0.075	0.024	0.096
1.292	0.437	550.016	0.061	0.022	0.141
1.516	0.437	755.315	0.362	0.021	0.362
1.832	0.438	1026.240	0.715	0.070	0.715
2.034	0.437	1309.496	0.568	0.079	0.568
2.279	0.439	1354.572	0.742	0.355	0.742
2.601	0.439	1820.394	0.227	0.352	0.352
2.781	0.435	1303.341	0.027	0.396	0.396
3.016	0.437	1476.497	0.068	0.471	0.471
3.283	0.439	1771.872	0.044	0.691	0.691
3.621	0.438	1533.633	0.088	0.629	0.629
1.042	0.492	240.033	0.034	0.040	0.088
1.107	0.494	399.574	0.047	0.013	0.083
1.271	0.493	792.510	0.064	0.041	0.086
1.451	0.492	856.771	0.626	0.057	0.626
1.701	0.490	631.081	0.433	0.019	0.433
2.072	0.492	1543.063	0.786	0.091	0.786
2.279	0.493	1354.572	0.621	0.301	0.621
2.579	0.494	1086.498	0.583	0.185	0.583
2.928	0.492	1221.933	0.477	0.517	0.517
3.119	0.493	1426.250	0.616	0.100	0.616
3.381	0.495	1271.864	0.056	0.618	0.618
3.703	0.492	1423.407	0.020	0.541	0.541
4.074	0.492	1496.535	0.031	0.529	0.529
1.178	0.546	197.609	0.017	0.024	0.031
1.232	0.547	244.994	0.022	0.013	0.069
1.407	0.548	395.356	0.030	0.018	0.178
1.614	0.546	448.100	0.131	0.023	0.131
1.898	0.547	844.301	0.224	0.068	0.224
2.296	0.548	1354.572	0.425	0.205	0.425
2.547	0.548	1415.451	0.083	0.489	0.489
2.847	0.548	1017.617	0.053	0.439	0.439
3.245	0.547	1216.651	0.075	0.506	0.506
3.485	0.549	1451.631	0.063	0.481	0.481
3.774	0.547	1365.479	0.019	0.490	0.490
4.117	0.548	1264.563	0.070	0.590	0.590
4.526	0.547	1253.596	0.053	0.479	0.479

Table H.13: 60 Degree Injector Average Stability Map Data [Test 1.0 to 2.0]

$\dot{m}_{O2}$ $\left[\frac{g}{s}\right]$	$\dot{m}_{CH4}$ $\left[\frac{g}{s}\right]$	Energy Density $\left[\frac{KW}{m^3}\right]$	(2 - 3) kHz Amplitude [psi]	(3.3 - 4.3) kHz Amplitude [psi]	(.1 - 20) kHz Amplitude [psi]
0.164	0.109	7.168	0.000	0.000	0.001
0.229	0.109	25.944	0.009	0.001	0.011
0.267	0.109	18.789	0.004	0.000	0.005
0.305	0.109	17.123	0.003	0.000	0.004
0.354	0.109	26.498	0.004	0.000	0.005
0.436	0.109	113.854	0.022	0.003	0.024
0.474	0.109	132.408	0.042	0.003	0.042
0.545	0.109	158.932	0.040	0.003	0.047
0.627	0.109	206.809	0.056	0.005	0.072
0.671	0.110	231.344	0.027	0.005	0.084
0.731	0.110	236.051	0.148	0.012	0.148
0.807	0.109	316.340	0.077	0.024	0.116
0.858	0.109	403.646	0.099	0.019	0.124
0.289	0.161	42.932	0.006	0.001	0.012
0.360	0.164	73.543	0.009	0.002	0.014
0.409	0.164	102.095	0.014	0.002	0.031
0.458	0.164	116.254	0.017	0.004	0.023
0.545	0.164	137.277	0.012	0.004	0.042
0.671	0.164	231.344	0.034	0.005	0.084
0.720	0.164	308.279	0.086	0.008	0.134
0.829	0.164	332.022	0.089	0.015	0.165
0.965	0.163	369.210	0.079	0.012	0.110
1.003	0.164	420.213	0.050	0.017	0.162
1.112	0.163	439.591	0.021	0.012	0.125
1.243	0.164	629.001	0.043	0.030	0.293
0.420	0.219	77.104	0.004	0.002	0.007
0.496	0.219	121.528	0.015	0.004	0.025
0.567	0.219	169.738	0.020	0.006	0.040
0.654	0.219	153.296	0.016	0.005	0.040
0.785	0.220	236.062	0.044	0.008	0.063
0.916	0.220	313.856	0.036	0.009	0.082
0.993	0.218	384.890	0.056	0.013	0.094
1.172	0.219	421.352	0.045	0.018	0.206
1.309	0.220	541.463	0.153	0.032	0.251
1.338	0.216	704.754	0.194	0.040	0.277
1.505	0.221	560.974	0.050	0.041	0.090
1.636	0.219	954.820	0.085	0.161	0.230

Table H.14: 60 Degree Injector Average Stability Map Data [Test 2.5 to 3.5]

$\dot{m}_{O2}$ $\left[\frac{g}{s}\right]$	$\dot{m}_{CH4}$ $\left[\frac{g}{s}\right]$	Energy Density $\left[\frac{KW}{m^3}\right]$	(2 - 3) kHz Amplitude [psi]	(3.3 - 4.3) kHz Amplitude [psi]	(.1 - 20) kHz Amplitude [psi]
0.540	0.271	112.370	0.005	0.009	0.039
0.616	0.273	168.541	0.013	0.007	0.049
0.676	0.273	267.248	0.014	0.011	0.077
0.791	0.274	246.746	0.082	0.006	0.092
0.949	0.272	481.491	0.036	0.013	0.149
1.151	0.273	376.022	0.075	0.017	0.084
1.249	0.276	367.146	0.082	0.014	0.128
1.423	0.273	441.164	0.147	0.031	0.202
1.625	0.274	442.279	0.060	0.029	0.175
1.707	0.274	958.176	0.174	0.048	0.255
1.876	0.273	1020.884	0.214	0.064	0.349
2.043	0.274	1007.304	0.191	0.037	0.213
2.247	0.274	434.654	0.029	0.022	0.029
0.676	0.327	139.946	0.011	0.013	0.037
0.725	0.328	263.396	0.034	0.012	0.082
0.834	0.329	282.212	0.027	0.019	0.085
0.949	0.330	401.699	0.069	0.023	0.138
1.134	0.328	340.619	0.079	0.033	0.083
1.369	0.328	516.085	0.167	0.018	0.197
1.511	0.329	559.671	0.143	0.023	0.208
1.707	0.329	725.318	0.224	0.033	0.224
1.936	0.329	741.647	0.126	0.083	0.332
2.089	0.332	1186.536	0.195	0.048	0.336
2.258	0.330	910.024	0.076	0.157	0.171
2.458	0.325	1339.907	0.360	0.085	0.425
2.690	0.330	1710.234	0.504	0.027	0.733
0.791	0.381	234.556	0.008	0.024	0.076
0.840	0.382	229.442	0.016	0.039	0.097
0.982	0.383	412.510	0.058	0.048	0.123
1.129	0.383	282.744	0.019	0.028	0.074
1.325	0.383	500.436	0.081	0.024	0.103
1.609	0.383	573.272	0.052	0.024	0.182
1.772	0.383	542.641	0.166	0.026	0.246
1.996	0.384	903.894	0.219	0.024	0.267
2.269	0.386	1071.840	0.271	0.138	0.324
2.432	0.380	1456.706	0.214	0.139	0.441
2.618	0.386	1554.922	0.102	0.169	0.458
2.863	0.383	1635.283	0.234	0.305	0.698
3.141	0.384	1801.469	0.282	0.074	0.445

Table H.15: 60 Degree Injector Average Stability Map Data [Test 4.0 to 5.0]

$\dot{m}_{O2}$ $\left[\frac{g}{s}\right]$	$\dot{m}_{CH4}$ $\left[\frac{g}{s}\right]$	Energy Density $\left[\frac{KW}{m^3}\right]$	(2 - 3) kHz Amplitude [psi]	(3.3 - 4.3) kHz Amplitude [psi]	(.1 - 20) kHz Amplitude [psi]
0.922	0.437	380.807	0.017	0.042	0.064
1.009	0.439	418.735	0.077	0.021	0.156
1.129	0.439	359.909	0.134	0.025	0.145
1.292	0.438	388.109	0.092	0.021	0.103
1.521	0.439	420.131	0.075	0.025	0.157
1.838	0.438	827.670	0.161	0.026	0.196
2.023	0.436	954.488	0.094	0.027	0.296
2.263	0.438	1120.185	0.182	0.078	0.385
2.607	0.446	1946.783	0.235	0.285	0.388
2.770	0.441	1727.991	0.120	0.400	0.589
3.010	0.435	1800.650	0.268	0.177	0.576
3.272	0.437	1565.973	0.185	0.195	0.340
3.610	0.437	1473.541	0.075	0.379	0.379
1.052	0.490	412.154	0.030	0.031	0.168
1.112	0.492	242.206	0.019	0.030	0.045
1.249	0.493	219.904	0.045	0.042	0.118
1.445	0.493	352.001	0.055	0.044	0.102
1.707	0.491	835.454	0.093	0.027	0.328
2.078	0.492	1078.350	0.305	0.070	0.428
2.285	0.491	1473.349	0.323	0.125	0.512
2.558	0.493	1529.831	0.081	0.294	0.294
2.923	0.493	1690.908	0.076	0.135	0.601
3.119	0.494	1428.698	0.039	0.340	0.340
3.381	0.491	1706.785	0.065	0.281	0.539
3.697	0.491	1613.619	0.057	0.349	0.499
4.063	0.490	1765.345	0.047	0.235	0.347
1.216	0.547	202.914	0.020	0.006	0.038
1.271	0.547	237.498	0.020	0.018	0.060
1.418	0.547	447.940	0.029	0.024	0.159
1.614	0.546	359.174	0.054	0.027	0.093
1.903	0.547	564.999	0.074	0.029	0.137
2.307	0.549	1196.373	0.258	0.095	0.383
2.530	0.548	1387.651	0.284	0.205	0.369
2.841	0.549	1855.432	0.095	0.517	0.761
3.250	0.552	1699.695	0.096	0.496	0.637
3.479	0.549	1936.348	0.180	0.365	0.667
3.763	0.547	1629.226	0.037	0.629	0.629
4.117	0.546	1488.268	0.028	0.379	0.379
4.552	0.547	1502.687	0.081	0.242	0.390

REFERENCES

[1] Coultas, T. A., "Combustion Instability," *Liquid Propellant Rocket Combustion Instability, NASA SP-194*, edited by R. F. H. Harrje, D. T., 1972, pp. 14–29.

[2] Fisher, S. C., "Scaling Techniques for Liquid Rocket Combustion Stability Testing," *Liquid Rocket Thrust Chambers: Aspects of Modeling, Analysis and Design*, edited by V. Yang, Progress in Astronautics and Aeronautics, American Institure of Aeronautics and Astronautics, 2004, pp. 545–564.

[3] Hutt, J. J., "High-Frequency Injection-Coupled Combustion Instability," *Liquid Rocket Engine Combustion Instability*, edited by V. Yang and W. Anderson, Progress in Astronautics and Aeronautics, American Institute of Aeronautics and Astronautics, 1995, pp. 345–356.

[4] Culick, F., "Overview of Combustion Instabilities in Liquid-Propellant Rocket Engines," *Liquid Rocket Engine Combustion Instability*, edited by V. Yang and W. Anderson, Progress in Astronautics and Aeronautics, American Institute of Aeronautics and Astronautics, 1995, pp. 1–38.

[5] Harrje, D., "Historical Survey," *Liquid Propellant Rocket Combustion Instability, NASA SP-194*, edited by R. F. H. Harrje, D. T., 1972, pp. 30–36.

[6] Penner, S. S., "On the Development of Rational Scaling Procedure for Liquid-Fuel Rocket Engines," *Jet Propulsion*, 1957, pp. 156–168.

[7] Penner, S. S., "On Generalized Scaling Procedure for Liquid-Fuel Rocket Engines," *Combustion and Flame*, 1957, pp. 229–240.

[8] Crocco, L., *Theory of Combustion Instability in Liquid Propellant Rocket Motors*, Butterworths Scientific, London, 1956.

[9] Oefelein, J. C., "Comprehensive Review of Liquid-Propellant Combustion Instabilities in F-1 Engines," *Journal of Propulsion and Power*, Vol. 9, No. 5, 1993, pp. 657–677.

[10] Sutton, G. P., *Rocket Propulsion Elements*, Wiley-Interscience, New York, seventh ed., 2001.

[11] Hood, C., "On the Interaction of a Premixed Flame with Acoustic Disturbance," *AIAA Joint Propulsion Conference*, No. 2005-4304, American Institute of Astronautics and Aeronautics, Tuscon, AZ, 2005.

[12] Zinn, B., "An Overview of Active Control of Combustion Instabilities," *AIAA Aerospace Sciences Meeting*, No. 1997-461, American Institute of Aeronautics and Astronautics, Reno, NV, 1997.

[13] Cavitt, R., "Experimental Methodology for Measuring Combustion and Injection-Coupled Responses," *AIAA Joint Propulsion Conference*, No. 2006-4527, American Institute of Astronautics and Aeronautics, Sacramento, CA, 2005.

[14] Bazarov, V. G., "Personal Communication: Train whistle process conversation," 2005.

[15] Shibanov, A. A., "Scaling Techniques for Design, Development and Test," *Liquid Rocket Thrust Chambers: Aspects of Modeling, Analysis and Design*, edited by V. Yang, Progress in Astronautics and Aeronautics, American Institute of Aeronautics and Astronautics, 2004, pp. 553–600.

[16] Sohn, C. H., "On the Method for Hot-Fire Modeling of High-Frequency Combustion Instability in Liquid Rocket Engines," *KSME International Journal*, Vol. 18, No. 6, 2004, pp. 1010–1018.

[17] Lee, K., "Combustion Stability Assessment of Double Swirl Coaxial Injectors Using Simulant Propellants," *AIAA Joint Propulsion Conference*, No. 2005-4443, American Institute of Aeronautics and Astronautics, Tucson, AZ, 2005.

[18] Sohn, C. H., "Combustion Stability Boundaries of the Subscale Rocket Chamber with Impinging Jet Injectors," *Journal of Propulsion and Power*, Vol. 23, No. 1, 2007, pp. 131–139.

[19] Anonymous, "Guidelines for Combustion Stability Specifications and Verification Procedures for Liquid Propellant Rocket Engines," 1997.

[20] Zierep, J., *Similarity Laws and Modeling*, Marcel Dekker, New York, 1971.

[21] Katorgin, B. I., "The RD-170, A Different Approach to Launch Vehicle Propulsion," *AIAA Joint Propulsion Conference*, No. 1993-2415, American Institute of Aeronautics and Astronautics, Monterey, CA, 1993.

[22] Vasin, "Liquid-Propellant Rocket Engine Chamber and Its Casing," 2001.

[23] Goertz, C., "A Modular Method for the Analysis of Liquid Rocket Engine Cycles," *AIAA Joint Propulsion Conference*, No. 1995-2966, American Institute of Aeronautics and Astronautics, San Diego, CA, 1995.

[24] Manski, D., "Cycles for Earth-to-Orbit Propulsion," *Journal of Propulsion and Power*, Vol. 14, No. 5, 1998, pp. 588–604.

[25] Jensen, R. J., "LOX/Hydrocarbon Combustion Instability Investigation," 1989.

[26] Coleman, H. W., *Experimentation and Uncertainty Analysis for Engineers*, Wiley-Interscience Publication, New York, 1999.

[27] Barrere, M., *Rocket Propulsion*, Elsevier, New York, 1960.